NOTICES

Disclaimers

The findings in this report are not to be construed as an official Department of the Army position, unless so designated by other authorized documents.

The citation of trade names and names of manufacturers in this report is not to be construed as official Government indorsement or approval of commercial products or services referenced herein.

Disposition

Destroy this report when it is no longer needed. Do not return it to the originator.

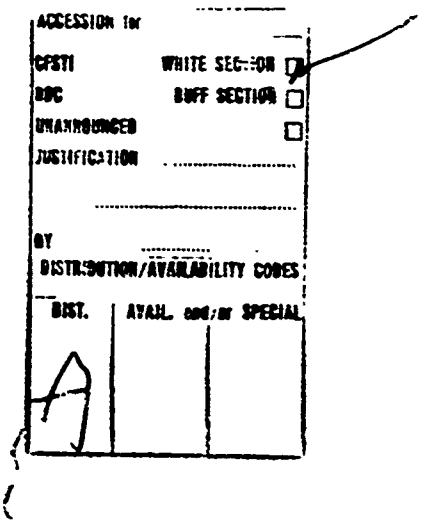

UNCLASSIFIED

Security Classification

DOCUMENT CONTROL DATA - R & D

(Security classification of title, body of abstract and indexing annotation must be entered when the overall report is classified)

1. ORIGINATING ACTIVITY (Corporate author)	2a. REPORT SECURITY CLASSIFICATION
Stanford Research Institute Menlo Park, California 94025	Unclassified
	2b. GROUP N/A

3. REPORT TITLE

SUMMARY OF MEASUREMENTS AND MODELING OF THE RADIATION PATTERNS OF SIMPLE HF FIELD ANTENNAS IN OPEN (LEVEL) TERRAIN, MOUNTAINS, AND FORESTS

4. DESCRIPTIVE NOTES (Type of report and inclusive dates)

Special Technical Report 45

5. AUTHOR(S) (First name, middle initial, last name)

G. E. Barker J. Taylor G. H. Hagn

6. REPORT DATE	7a. TOTAL NO. OF PAGES	7b. NO. OF REFS
December 1971	~~286~~ 239	31

8a. CONTRACT OR GRANT NO.	9a. ORIGINATOR'S REPORT NUMBER(S)
DAAB07-70-C-0220	Special Technical Report 45
b. PROJECT NO. Order No. 5384-PM-63-91	SRI Project 8663
c.	9b. OTHER REPORT NO(S) (Any other numbers that may be assigned this report)
d.	

10. DISTRIBUTION STATEMENT

This document has been approved for public release and sale, its distribution is unlimited.

11. SUPPLEMENTARY NOTES	12. SPONSORING MILITARY ACTIVITY
	U.S. Army Electronics Command Fort Monmouth, New Jersey

13. ABSTRACT

Full-scale measurements of the radiation patterns of simple HF field-expedient antennas (dipoles, monopoles, inverted L's, and slant wires) were conducted while the antennas were situated over open (level) terrain, in a U.S. pine forest, in a tropical forest in Thailand, and (under another contract) in hilly terrain. The results of the measurements at the four sites have been described elsewhere in individual measurement reports. The major results from these measurements are summarized and examples of the measured data are presented in this report.

A computer model of a short dipole antenna in a homogeneous, isotropic forest medium was developed and the calculated results are compared with measured data from short and half-wave resonant dipoles. The six parameters of the model (antenna height, forest height, and permittivity and loss tangent of both the earth and the forest) were varied to determine the sensitivity of the antenna patterns to each of these parameters. This test indicated that the effect of the antenna height is the most significant variable.

The measurements did not readily yield absolute gains of the antennas, but a method is presented for estimating these absolute gains and a table of the estimated absolute gains for many of the antennas measured is presented.

DD FORM 1 NOV 68 1473 (PAGE 1)

S/N 0101-807-6801

UNCLASSIFIED

Security Classification

14 KEY WORDS	LINK A		LINK B		LINK C	
	ROLE	WT	ROLE	WT	ROLE	WT
Field expedient antennas						
Dipole antennas						
Monopole antennas						
Inverted-L antennas						
Slant wire antennas						
Antenna pattern measurements						
Seacore						
Southeast Asia						
Thailand						
Dry evergreen forest						
Jungle						
Tropical forest						
Xeledop						
Antenna directivity						
High frequency (HF)						
Pine forest						
Rough terrain						

Special Technical Report 45 *December 1971*

SUMMARY OF MEASUREMENTS AND MODELING OF THE RADIATION PATTERNS OF SIMPLE HF FIELD ANTENNAS IN OPEN (LEVEL) TERRAIN, MOUNTAINS, AND FORESTS

By: G. E. BARKER J. TAYLOR G. H. HAGN

Prepared for:

U.S. ARMY ELECTRONICS COMMAND
BUILDING 2504, CHARLES WOOD AREA
FORT MONMOUTH, NEW JERSEY 07703

CONTRACT DAAB07-70-C-0220
Order No. 5384-PM-63-91

SRI Project 8663

Approved by:

R. F. DALY, *Director*
Telecommunications Department

E. J. MOORE, *Executive Director*
Engineering Systems Division

Sponsored by

ADVANCED RESEARCH PROJECTS AGENCY
ARPA ORDER 371
AND
U.S. ARMY ELECTRONICS COMMAND

ABSTRACT

Full-scale measurements of the radiation patterns of simple HF field-expedient antennas (dipoles, monopoles, inverted L's, and slant wires) were conducted while the antennas were situated over open (level) terrain, in a U.S. pine forest, in a tropical forest in Thailand, and (under another contract) in hilly terrain. The results of the measurements at the four sites have been described elsewhere in individual measurement reports. The major results from these measurements are summarized and examples of the measured data are presented in this report.

A computer model of a short dipole antenna in a homogeneous, isotropic forest medium was developed and the calculated results are compared with measured data from short and half-wave resonant dipoles. The six parameters of the model (antenna height, forest height, and permittivity and loss tangent of both the earth and the forest) were varied to determine the sensitivity of the antenna patterns to each of these parameters. This test indicated that the effect of the antenna height is the most significant variable.

The measurements did not readily yield absolute gains of the antennas, but a method is presented for estimating these absolute gains and a table of the estimated absolute gains for many of the antennas measured is presented.

PREFACE

This report summarizes the results of an extensive effort on modeling and measuring the performance of HF field-expedient antennas in various terrains. The Thailand phase of the work described in this report was performed as part of the SEACORE program of the U.S. Department of Defense with the support, and using the facilities, of the Military Research and Development Center (MRDC) in Bangkok, Thailand. The MRDC is a joint Thai-U.S. organization established to conduct research and development work in the tropical environment. The overall direction of the U.S. portion of the MRDC has been assigned to the Advanced Research Projects Agency (ARPA) of the U.S. Department of Defense who, in 1962, asked the U.S. Army Electronics Command (USAECOM) and the Stanford Research Institute (SRI) to establish an electronics laboratory in Thailand to facilitate the study of radio communications/electronics in the tropics. The MRDC-Electronics Laboratory (MRDC-EL) began operation in 1963 [under Contract DA 36-039 AMC-00040(E)] and since that time the ARPA has actively monitored and directed the efforts of USAECOM and SRI. In Bangkok, this function is carried out by the ARPA Research and Development Center. The cooperation of the Thai Ministry of Defense and the Thailand and CONUS representatives of the ARPA and USAECOM made possible the work relating to the measurements and computer modeling of HF field-expedient antennas installed in open terrain and in forested areas.

During 1967, a separate program was initiated by the U.S. Department of Defense (under Contract DAHC07-67-C-0144) which involved the measurement of the radiation patterns of HF field-expedient antennas in hilly terrain.

Since these measurements are supplementary to those performed under SEACORE, selected examples are presented in this summary report.

The preparation and printing of this report was supported by USECOM under Contract DAAB07-70-C-0220.

CONTENTS

ILLUSTRATIONS

ILLUSTRATIONS

TABLES

I INTRODUCTION

This report is concerned with the effects of terrain and vegetation on the directivity and gain of HF field-expedient antennas. Interest in these so-called simple antennas has been stimulated by the need for better field communications in jungle and mountainous areas. Whereas the radiation patterns and gains of simple dipoles, etc. over perfect ground have been well documented, relatively little information is available on the performance of these antennas in less than ideal situations--with unbalanced feedlines, over poorly conducting ground, in jungle and mountain environments, and in situations similar to those encountered in actual field use.[1]*

In order to better understand the effects of forest and terrain on the radiation patterns of field-expedient HF antennas, measurements of the radiation patterns of dipoles, monopoles, inverted L's, and slant wires were performed while the antennas were situated over open, flat terrain,[2] in a U.S. pine forest,[3] and in a tropical forest in Thailand,[4] under Contract DA 36-039 AMC-00040(E), and while the antennas were situated in hilly terrain under Contract DAHC07-67-C-0144.[5] The data resulting from the above measurements provided some insight to the problem, but, in the absence of appropriate mathematical models, these data were relevant only to the specific locations measured. In order to interpret these data in a more general sense, a computer model was developed to mathematically predict the radiation patterns of simple antennas when immersed in a forest (as approximated by a lossy dielectric slab).[6]

---

*References are listed at the end of the report.

This model (like any other mathematical model) is potentially only as accurate as its input data (i.e., in this case the ground and vegetation electrical constants and an estimate of the forest and antenna heights). In order to provide information on the electrical constants of ground and vegetation, open-wire transmission-line techniques (discussed elsewhere[7-9]) were devised to perform these measurements. This report summarizes the results of antenna directivity pattern measurements at the various locations, discusses intra-site comparisons of the various antennas, and compares the dipole data from the forested sites with the results predicted by the computer model.

At this point, a few comments on the organization of this report may be useful to the reader. The description of the three measurement sites used under Contract DA 36-039 AMC-00040(E) is presented in Section II. The measurement system and data-acquisition processing and display are discussed in Section III. The measurement antennas are described in Section IV in a sequence that is maintained throughout the report when practical--i.e., dipoles, monopoles, inverted L's, slant wires, loops, and long-wire antennas. Table 1 in Section IV lists all the antennas whose patterns were measured under Contract DA 36-039 AMC-00040(E) and summarizes the pattern data available in the three measurement reports,[2-4] and an inter-site comparison is given in Section V. A description of the measurements over hilly terrain (performed under Contract DAHC07-67-C-0144)--including the site description--is given in Section VI. The forest slab model is described in Section VII and a brief investigation of the sensitivity of this model to the variation of the input parameters is presented in Section VIII. A comparison of the model predictions for dipole antennas at all but the hilly site is given in Section IX. Summaries of measured relative antenna gains and estimated absolute gains (gain relative to an isotropic radiator) are presented and discussed in Section X. A summary of major findings resulting from

this work is presented in Section XI. For convenient reference, the pattern data are provided in appendices at the end of this report. The directivity pattern data from the open (level) and forested sites and in the hilly terrain are presented in Appendices A and B respectively, and the comparison between the computed and measured patterns for the Thailand site is given in Appendix C.

II DESCRIPTION OF MEASUREMENT SITES

Antenna pattern measurements were performed at several sites in California and Thailand (see Figures 1 and 2, respectively). This section briefly describes the sites considered under Contract DA 36-039 AMC-00040(E) in terms of terrain, ground condition, and measured values of ground constants and vegetation constants (where available or applicable). The site considered under Contract DAHC07-67-C-0144 is described in Sec. VI.

For further information, refer to the reports from which the antenna data were obtained, and in the case of the Thailand site, the separate report by the Environmental Sciences Division of the Military Research and Development Center, Bangkok, Thailand.[10] Additional data on ground and vegetation constant measurement techniques and measured ground and vegetation constants in Thailand are given in Refs. 7 through 9 and 11 through 15.

A. Lodi, California

Antenna patterns were measured over open, flat farmland, near Lodi, California during September and October 1964.[2] This site was chosen to keep obstructions at a minimum. The nearest obstruction was a fence, consisting of a few strands of barbed wire 2 to 3 ft high, several hundred feet south of the antennas. Otherwise, the ground was clear and very gently rolling for at least a half mile in all directions, with no terrain or obstruction higher than a degree or two in elevation relative to the test site. The weather before and during the antenna measurements was hot and dry.

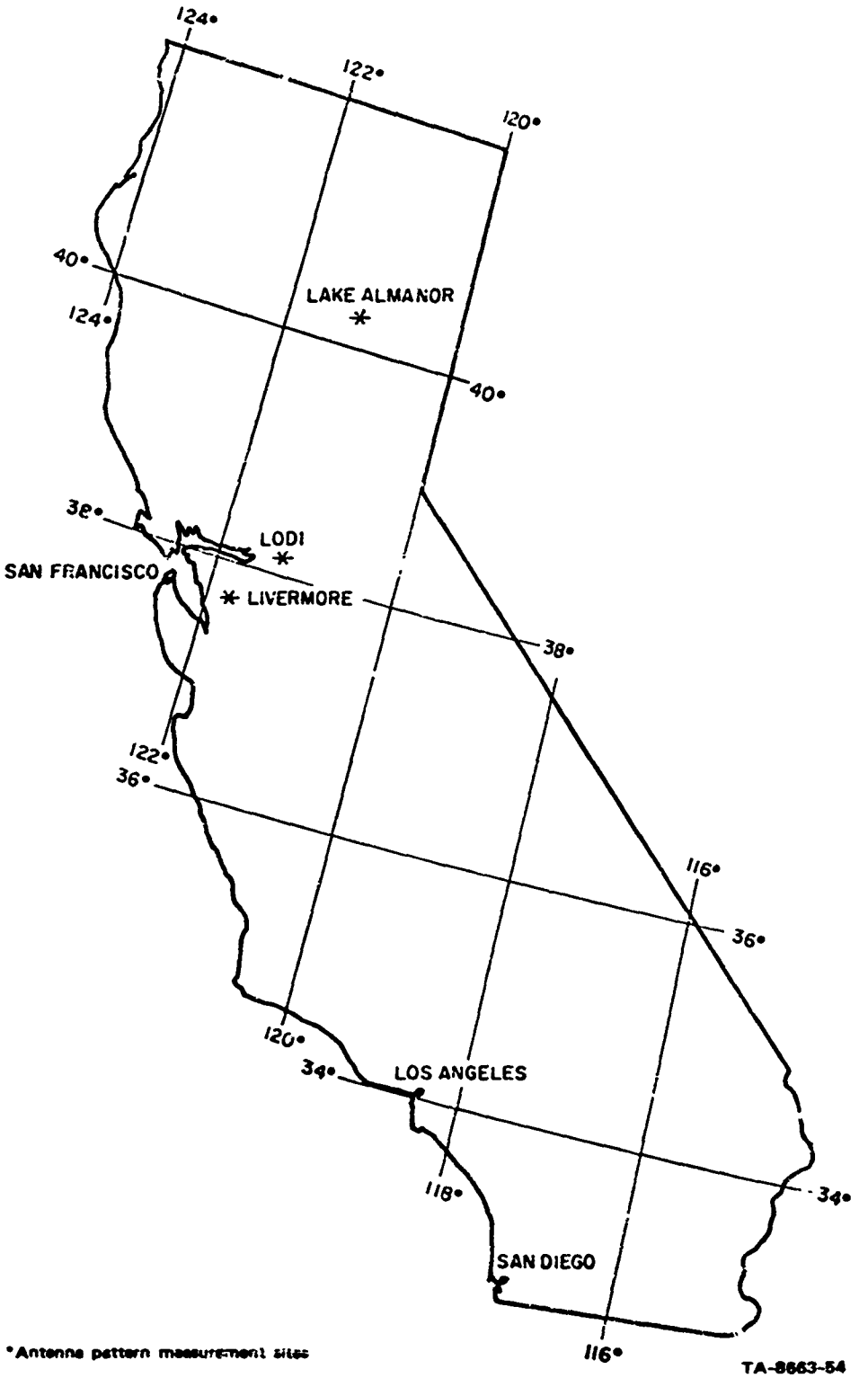

FIGURE 1 MAP SHOWING ANTENNA PATTERN MEASUREMENT SITES—CALIFORNIA

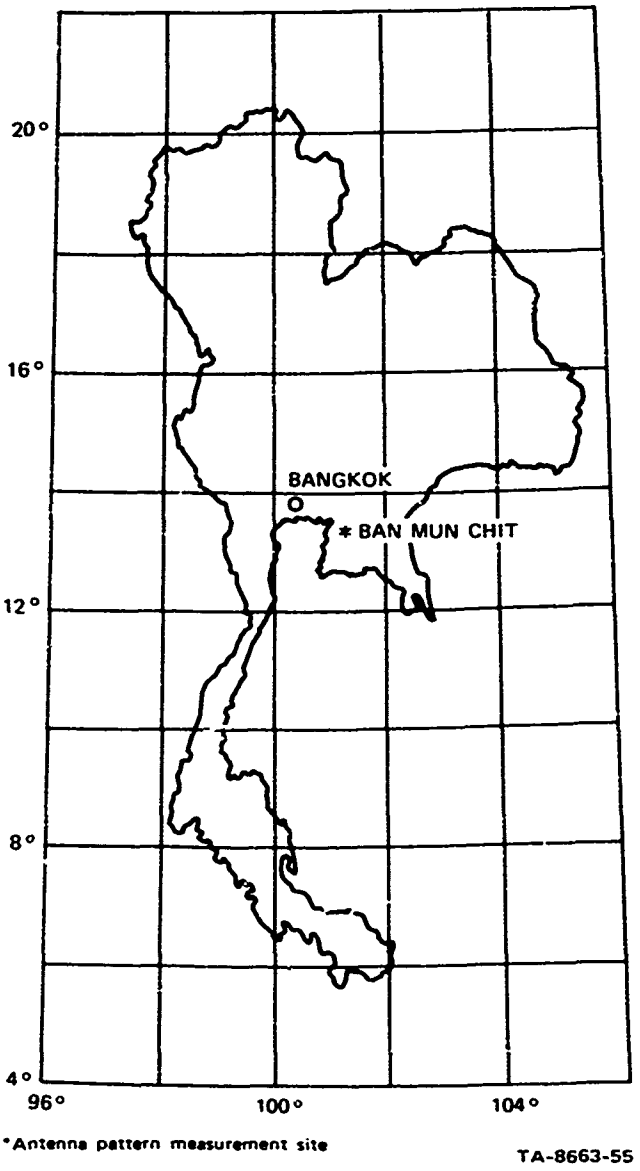

FIGURE 2 MAP SHOWING ANTENNA PATTERN MEASUREMENT SITE—THAILAND

No RF ground-constant measurements were made at this site; however, the dc ground conductivity was sampled as a function of depth using the Schlumberger method as described in the Appendix of Refs. 2 and 12. Unfortunately, even these measurements could not be made until two months later than the antenna pattern measurements--after a rainy period. The survey found two distinct layers within several skin depths of the surface (35 ft). The dc conductivity of the 2-ft, plowed surface layer was about 10^{-2} mhos/meter. Beneath this, the conductivity increased considerably. In spite of the uncertainty introduced by the ground wetting, it appeared that the dc conductivity was about 5×10^{-2} mhos/meter, somewhat higher than that normally associated with farmland. The dc resistance measurements do not yield the relative dielectric constant, but it is estimated to have been approximately 12 in the surface layer and 30 below it. No other significant discontinuities were found by the survey or a search of geological records.

B. Almanor, California

Measurements in a conifer forest were conducted during May and June 1965.[3] The forest was a pine farm located near Almanor in northern California. The trees varied in height from 50 to 100 ft and in diameter from 1 to 13 ft. They were randomly spaced and approximately 10 ft apart. Undergrowth was sparse and consisted primarily of pine saplings. The density of the trees can be seen in the photograph showing a typical antenna installation (Figure 3). The receiving and recording equipment van and tracking unit were situated in a small clearing near a highway and small lake. Most of the antennas duplicated those measured at Lodi, California, over open, flat terrain, so that a comparison could be made of directivity patterns of the antennas in the forest at Almanor and in the open at Lodi. The antennas were placed in the forest at least 200 ft from the edge of the clearing used for the receiving van and were erected in open spaces among the trees.

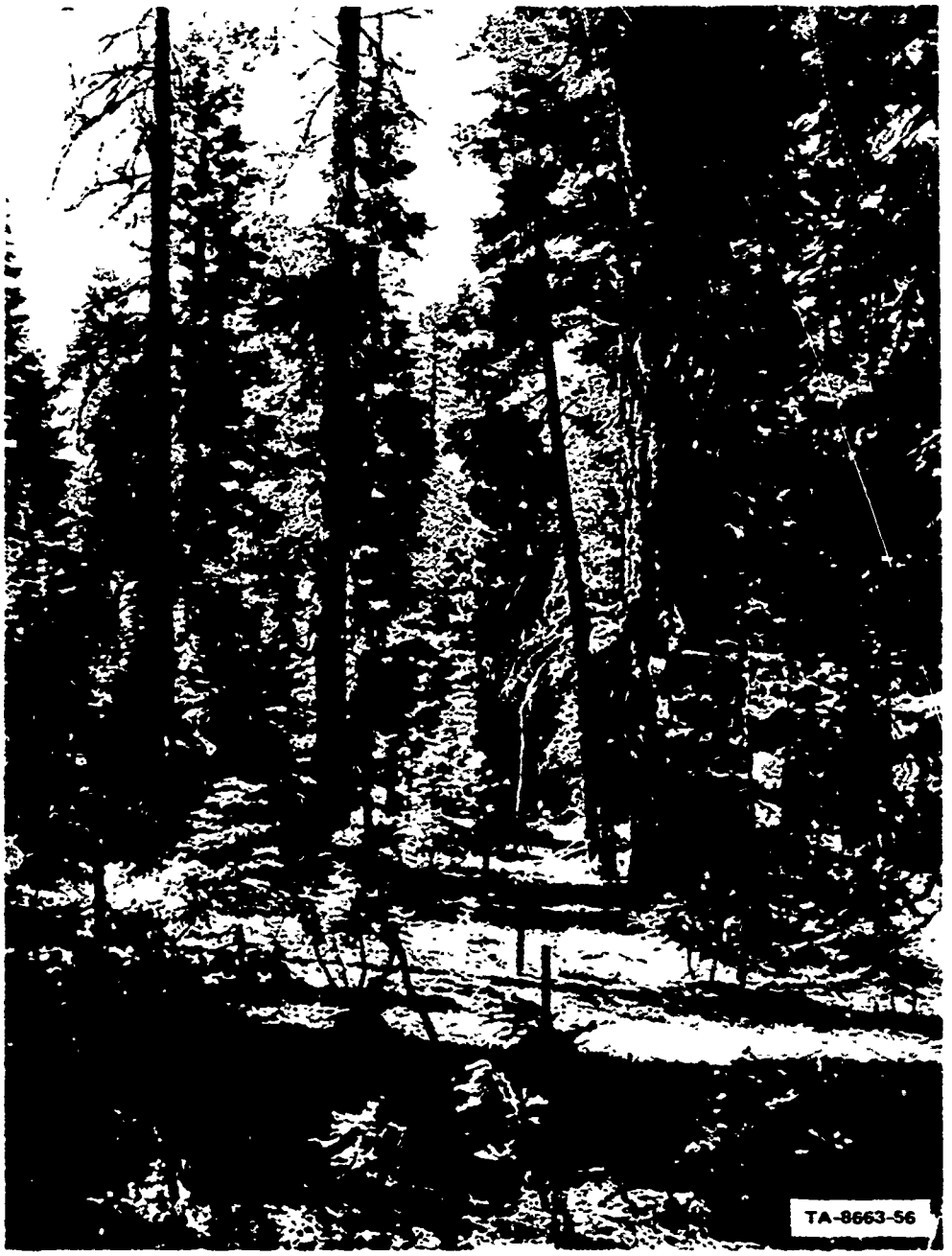

FIGURE 3 PHOTOGRAPH OF 2-FOOT-HIGH UNBALANCED DIPOLE ANTENNA AT ALMANOR

No measured data are available on the ground or foliage constants at this site.

C. Ban Mun Chit, Thailand

During June and July 1966, measurements were performed in a tropical forest near the village of Ban Mun Chit, Thailand.[4] This site lies approximately 90 km southeast of Bangkok in Cholburi Province. It lies in the middle of gently rolling hill country about 30 km due east of Siricha which is on the east coast of the Gulf of Thailand.

Measurements at this site included the same antennas that were previously measured at Lodi and Almanor, in addition to an antenna of each type designed for 6 MHz. Selected dipoles and monopoles also were measured while located in, and out of, the dry-evergreen tropical forest.

The area originally had been heavily forested, but much of the forest had been removed previously for commercial and agricultural purposes. Consequently, much of the forest area consisted of second growth. The site itself was comprised of a clear area free of undergrowth adjacent to a moderately heavily forested area. Tree heights were estimated to be 50 to 75 ft, with a moderately dense but uneven and broken canopy. There was a considerable amount of undergrowth to a height of 20 to 25 ft.

The ground was sandy and dry, with good drainage--little standing water remained shortly after heavy rains.

Figure 4 shows a general view of the site. In the foreground is the cleared area with a new growth of cultivated tapioca. The forest is in the background.

Measured values of ground constants show the dielectric constant and conductivity to be low, as seen in Figure 5.[9] Therefore, the ground could be classified as "electrically poor ground." The dashed lines indicate the trend of the data as a function of frequency. The measured

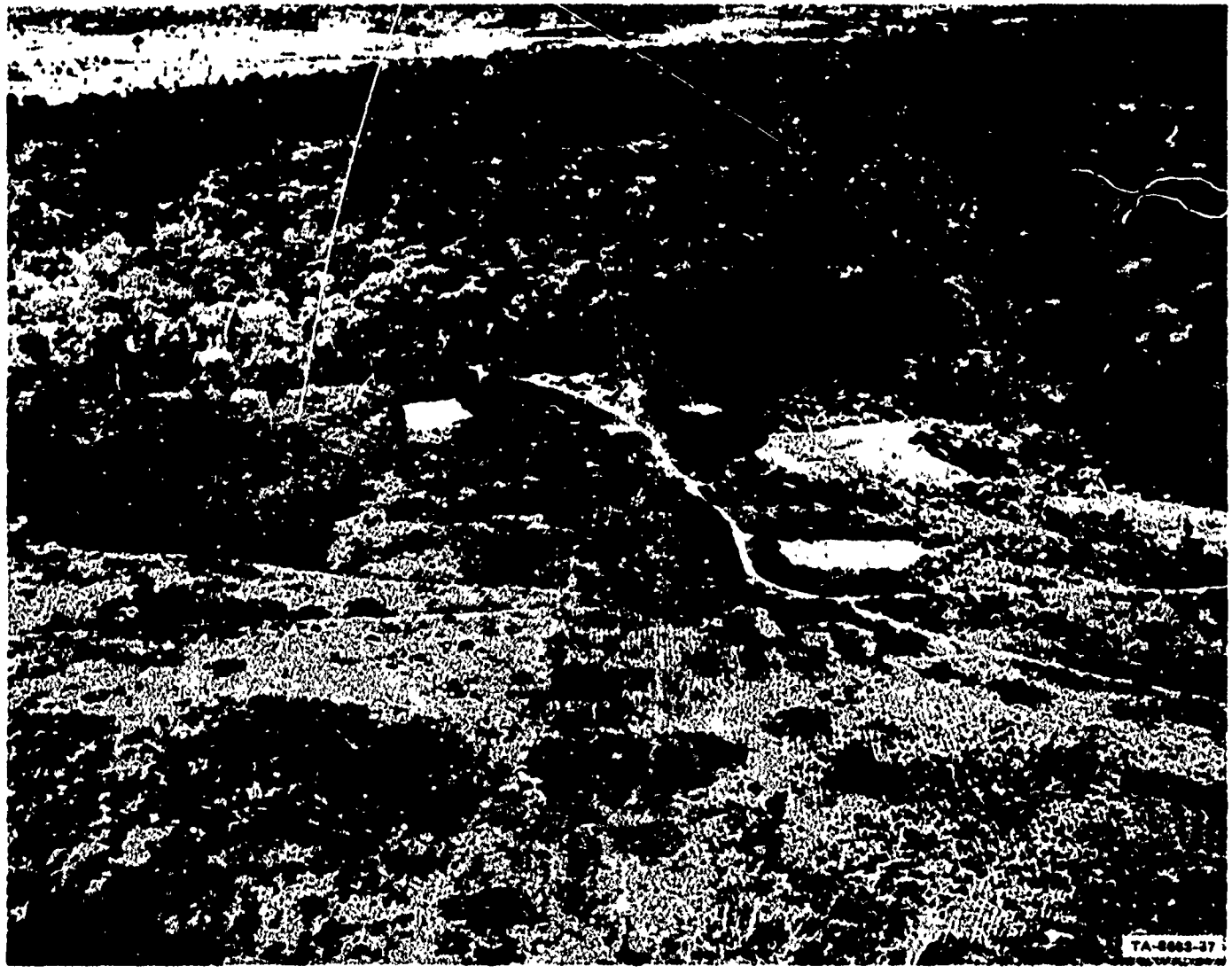

FIGURE 4 PHOTOGRAPH OF BAN MUN CHIT MEASUREMENT SITE

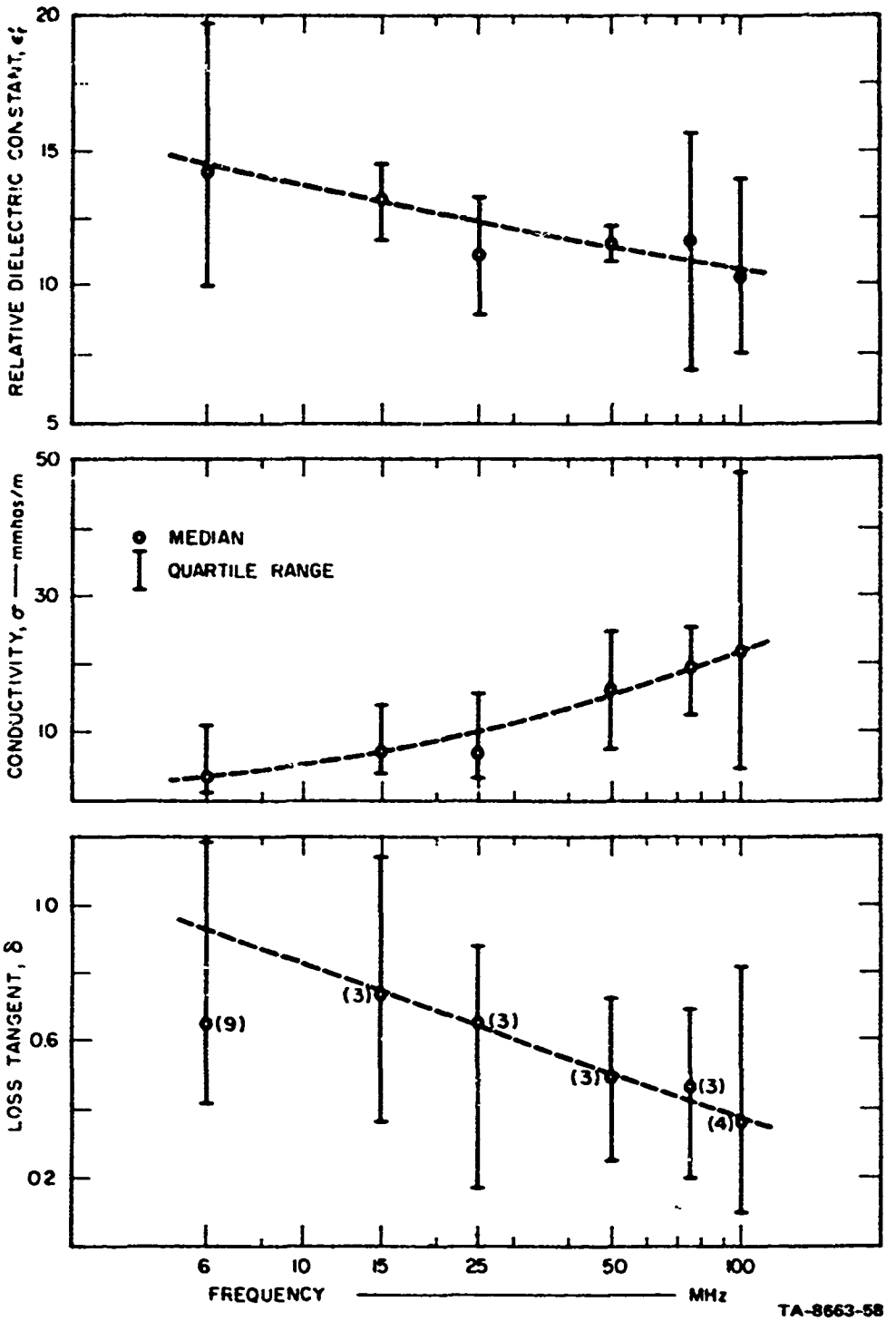

FIGURE 5 SURFACE GROUND CONSTANTS MEASURED IN FOREST AT BAN MUN CHIT

values of foliage constants are given in Figure 6.[9] The data for undergrowth sample I were obtained in one of the most dense parts of the site. Indeed, these data represent the highest complex dielectric constants measured in living vegetation at any site surveyed during this contract. The data for undergrowth sample II were probably more typical of "undisturbed" undergrowth at the site. The tapioca data were obtained in the cultivated area visible in the foreground of Figure 4.

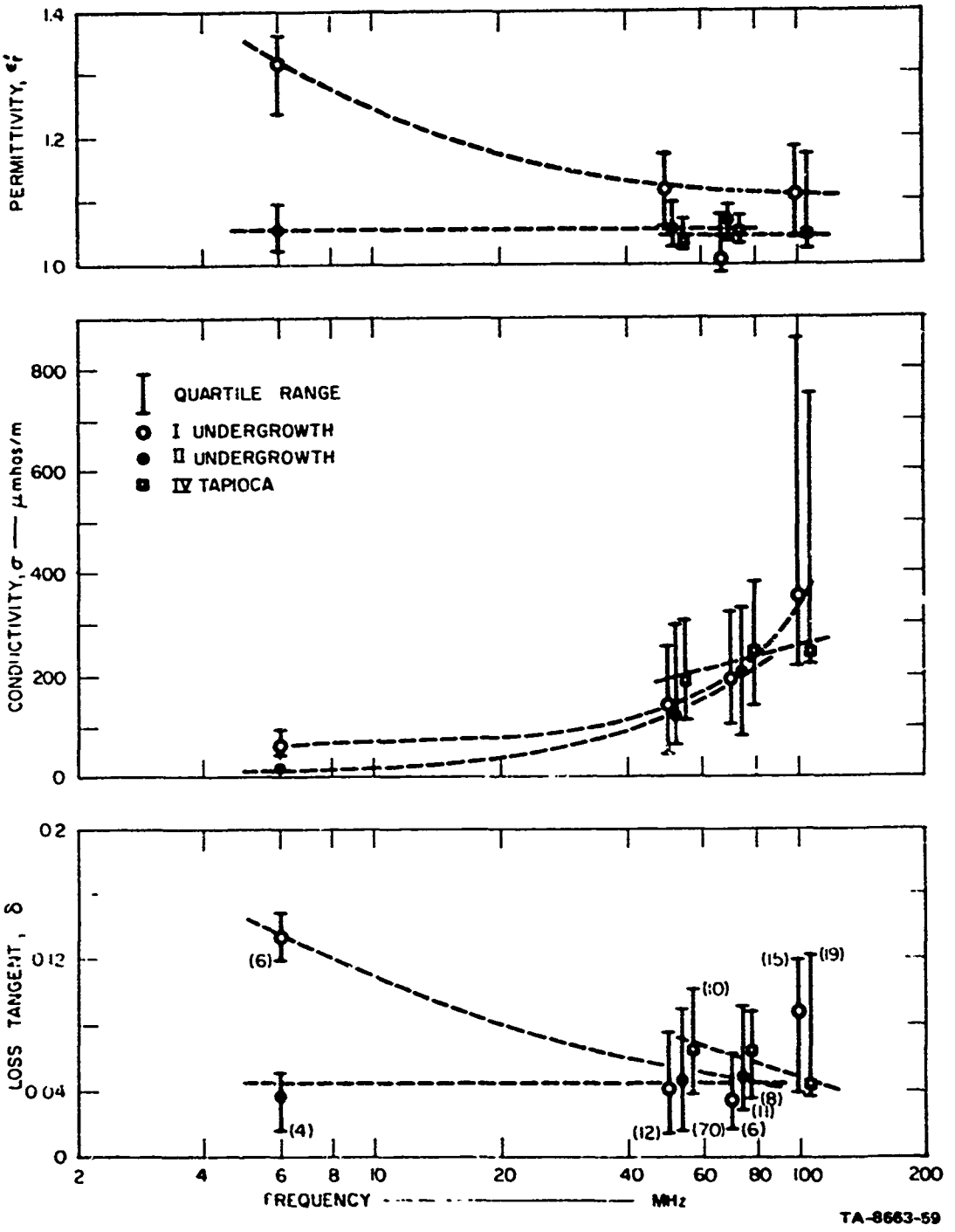

FIGURE 6 FOLIAGE CONSTANTS MEASURED AT BAN MUN CHIT

III MEASUREMENT OF ANTENNA RADIATION PATTERNS

The radiation patterns of HF field-expedient antennas discussed in this report were measured by towing a special transmitter (Xeledop*) on specified courses (orbits and linear passes) around the measurement antennas with an aircraft modified especially for this purpose. The signals received by the measurement antennas on the ground were recorded on strip-charts, together with the position of the towing aircraft. Later, these analog data were scaled and punched onto IBM cards and processed using digital computers to produce contour maps of the received signal strength, each of which shows the response of one antenna to one frequency and one polarization.[16]

The instrumentation and data-processing techniques are briefly described in this chapter. More details can be found in the reports describing the individual measurements,[2-4] and in Ref. 16 and in the open literature.[17]

A. The Xeledop

The Xeledop is a sequentially keyed transmitter operating on eight frequencies between 2 and 30 MHz. It is towed behind an aircraft on approximately 300 ft of dielectric rope. All the electronics and batteries are contained in a central sphere. Arms extending out from the sphere are fed as a balanced dipole antenna, whose total length is always less than one-half wavelength for the frequencies used. Thus, the directivity pattern of the Xeledop is approximately that of a Hertzian dipole for

---

*An acronym denoting Transmitting Elementary Dipole with Optional Polarization.

all the measurement frequencies. The Xeledop can be towed to transmit either horizontally (E_ϕ) or vertically (E_θ, when corrected for the transmitting dipole pattern) polarized waves. The electrical symmetry of the Xeledop is such that the radiated polarization depends only upon its physical orientation, and its radiated power remains constant for either polarization.

B. Aircraft Tracking and Guidance

In addition to towing the Xeledop transmitter, the aircraft carried a low-power radio beacon transmitter and a modified AN/APX-6 (IFF) transponder unit. Both are used for position information: the beacon is tracked by ground equipment, which provides azimuth and elevation information for data processing; the airborne transponder works with a similar unit on the ground to indicate slant range to the pilot. The slant range is displayed on a meter called the Pilot's Deviation Indicator (PDI).

The ground-tracking unit is a Rawin AN/GMD-1 Weather Balloon Tracker (referred to as the GMD). A steerable parabolic-dish antenna (with rotating-dipole feed) tracks the aircraft beacon transmitter through the use of servomechanisms. The azimuth, elevation, and a sequence number (called the GMD time) are printed on adding-machine paper every 6 seconds. The position data (azimuth and elevation) are printed out to hundredths of a degree, but this information is precise only to tenths of a degree, with a stated accuracy of ±0.1 degree. We believe the equipment to be accurate at least ±0.3 degree for this application.

C. Receiving and Recording

The patterns of several antennas were measured simultaneously by feeding the RG-8 coaxial transmission lines from the antennas into antenna multicouplers. The input impedances at these terminals were held to within 1.5:1 VSWR (50-ohm reference) for the measurements at Lodi[2]

and within 1.2:1 VSWR for the measurements at Almanor and Ban Mun Chit.[3,4] The output signals of the antenna multicouplers were fed into R-390A/URR radio receivers, one for each antenna at each measurement frequency. The AGC voltages of these receivers were used to drive the pens on strip-chart recorders.

The system was calibrated before every orbit by injecting a calibration signal from an HP 606A signal generator into the multicouplers in place of the antenna signals, and then recording a 40-dB staircase in 10-dB steps on the strip-chart records. The dynamic range of the system was extended through the use of push-button attenuators that could be inserted manually between the multicoupler and receiver.

D. Data Processing

Two sets of data records were combined to determine one antenna pattern: the amplitude record on the strip-chart recordings and the printed azimuth and elevation records from the GMD. The data from the latter were simply key punched into IBM cards. The strip charts were read with a Gerber GOAT, (a semi-automatic analog-to-digital data scaling device) which converted the amplitude data (Xeledop pulse envelope) into digital values and punched these values into IBM cards. Similarly, the calibration records were punched into IBM cards.

These data cards were then used as the input to a series of computer programs. The first sequence of programs converted the AGC voltage amplitude readings to dB, corrected the azimuth and elevation data for parallax so that they were relative to the antenna position rather than the GMD position, corrected each amplitude for variations in slant range between the test antenna and the Xeledop by adding 20 $\log_{10}$ (R_{actual}/ $R_{nominal}$); and, if the measurement was performed with vertical polarization, each amplitude was corrected for the transmitting pattern of the Xeledop by adding 20 $\log_{10}$ cos (elevation angle).

The data were then normalized so that the maximum value recorded for an antenna, frequency, and polarization was established as 0 dB and all other values were referred to this maximum. The data were then contoured using a special contouring program* and plotted using a California Computer Products (Cal-Comp) incremental plotter.

E. Antenna Pattern Data Presentation

The measured antenna patterns are presented in the form of contours using an azimuthal equal-area projection of the measured signal strength (see appendices for examples). This display may appear at first glance to be unnecessarily complicated, but it has several advantages. The method of reading these maps is explained below, along with the advantages of using this type of display.

Each contour map shows all of the amplitude data taken at one site on one antenna for one polarization at one frequency. The plot can be visualized in several ways. For example, one may picture placing a large hemisphere over the antenna being measured, then drawing the field strength contours on its surface. For purposes of discussion the contour plots may be regarded as two-dimensional maps of this hemisphere as viewed from above (see Figure 7). Hence, the zenith angle is at the center of the plot, azimuth angles appear as radials, and elevation angles are equally spaced concentric circles.† The outer rim of the plot is

---

*This program is a proprietory item purchased from Computer Laboratories, Inc., Houston, Texas.

†The contour plot is not a stereographic mapping of the hemisphere as it has been referred to in Refs. 2 and 3. A stereographic projection of the hemisphere is a conformal (angle-preserving) mapping that would make the smaller elevation angles appear more closely spaced, whereas the azimuthal equal-area projection used here is not conformal but rather a mapping that allows equal solid angles to be projected as equal solid areas. An excellent discussion of both these projections is given by Hayden in Ref. 18.

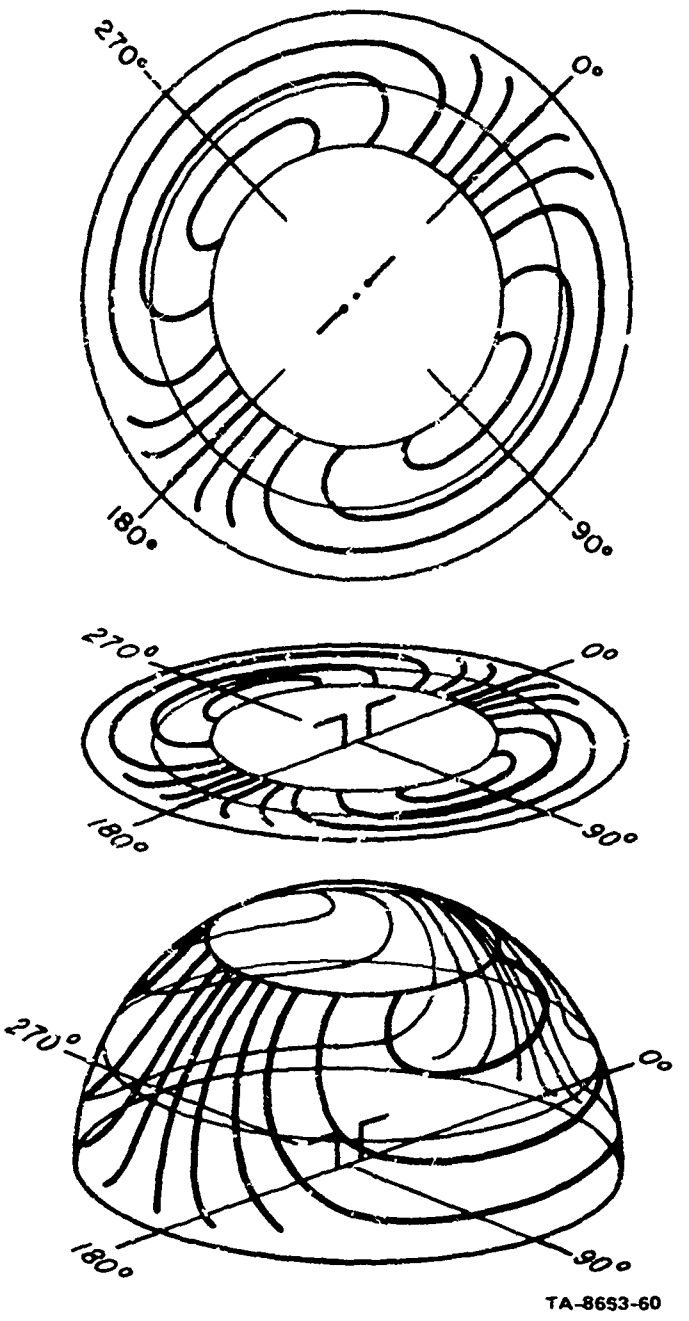

FIGURE 7 A CONTOUR PLOT AS A MAP OF A HEMISPHERE

the horizon (0° elevation). The azimuth angles numbered around the rim of the plot are in degrees relative to some principal axis of the antenna. A diagram of the antenna is drawn in the center of the contour plot to assist the reader in visualizing the relationship of the contour plot to the antenna.

The contour interval is 3 dB, with the highest amplitude recorded for each plot taken as 0 dB. The 0-dB point is not shown, because its exact position is misleading without detailed knowledge regarding the aircraft orbits, but its true location can be inferred from the other contours.

The contour plot has merits both intrinsically, as a data display, and extrinsically, through its adaptability to the Xeledop measurement technique. As a data display, it has the advantage of showing the complete characteristics of the antenna in one diagram much more clearly than a series of polar cuts. It also emphasizes the relative antenna response as a function of solid angle, a better measure of the usefulness of any antenna for communications than azimuthal beamwidth. Indeed, for HF tactical (low-gain) antennas, the concept of beamwidth is somewhat ambiguous and virtually useless. In addition to having these advantages as a display, the contour plots are very well adapted to the way in which the data were taken. Since the aircraft did not fly perfect orbits about each antenna, the elevation angles actually measured could vary considerably during any given orbit and from one set of antennas to another. Thus, it is neither accurate nor adequate simply to plot the measured amplitude as a function of azimuth on a polar chart. Some means of interpolating between the data taken at the various elevation angles is required, because the angles actually measured can change from one set of orbits to the next. The plot program does this by finding contours of equal response as indicated by the available amplitude data.

The accuracy of the pattern-measuring system is limited principally by the stability of the field equipment and that of the Xeledop (both of which appear to be very good), and the precision of the scaling of the strip charts. Evidence from overlaps, rereadings, and the general correlation of the data indicates that systematic and predictable errors have been effectively eliminated, leaving a random scattering of the data of about 1.5 dB, or one-half the contour interval. The best test for the significance of features in a pattern may be stated as follows: if the deviation is smaller than one-half the distance between the contour lines, it can be ignored; otherwise, it is significant. This is not strictly true for all plots since many data points on some plots were lost because of interfering signals which caused these plots to be distorted not by inaccurate readings but by missing data points. Most of the plots with possible inaccuracies due to this cause can be identified by observing that parts of the pattern above 5° to 10° are missing (e.g., see Figure A-15 or A-31).

The azimuth and elevation angles are measured and plotted to better than 1°; however, with the relatively coarse sampling used for contouring the data, a figure of ±3° would be a better estimate of accuracy.

An accurate scaling of the shape and depth of sharp nulls was not attempted, and the above discussion does not strictly apply to them. The angular position of a null was determined relatively accurately; however, the value shown on the contour plot is an upper bound for its signal strength. Hence, if -18 dB is shown, this means the null was as low as (or very likely lower than) -18 dB.

F. Power Patterns

A practical method for measuring the Poynting vector patterns (power patterns) over the entire hemisphere above an antenna was described

in detail in Ref. 3. This method relies on flying linear orthogonal passes over the antennas and then calculating the Poynting vector at the intersection points of the orthogonal passes. These data, combined with the Poynting vector data derived from the E_θ and E_ϕ measurements using orbits below approximately 50°, were used to produce power patterns for the antennas measured at Almanor and Ban Mun Chit.

These patterns are of particular interest because they provide an estimate of the effective directivity near the zenith--the direction of most interest for HF skywave applications on short ionospheric paths. It can be shown that although they are not strictly reciprocal, as are the individual polarization patterns, these power patterns do apply for antennas at both ends (i.e., transmitting and receiving terminals) of a communication system.

For the transmitting case, these plots show the relative power directivity, or the relative magnitude of the Poynting vector of the antenna. (The angle of the Poynting vector would be directed radially outward from the antenna in this case.)

For the receiving case, the power plots can be thought of as approximating the time-average response of the antenna to randomly polarized incident waves arriving at the receiving antenna after reflection from the ionosphere. Note, however, that the received signal level at any given instant depends upon the angle of arrival and resultant field strength of the incident wave(s), and the actual polarization of both the receiving antenna and the incident field. For near-vertical-incidence paths--the primary intended use of the field-expedient antennas under discussion in this report--the randomization is not quite complete in equatorial areas.[19-21]

When reviewing the power patterns presented in this report, the reader should recall that the power patterns for the antennas at Almanor

were produced with a contouring program using about twice as many grid points (data plotting points) as those produced from the Ban Mun Chit data. Consequently, the Ban Mun Chit power patterns will be slightly "smoother" than the power patterns from Almanor (for example see Figures A-30 and A-33). (This does not apply to the E_θ and E_ϕ contour plots which were produced with the same high-density grid for all three sites.)

IV DESCRIPTION OF ANTENNAS

The antennas whose patterns were measured under Contract DA 36-039 AMC-00040(E) are described in this section and the data available are summarized in Table 1. Pattern data for all of these antennas are not presented in the Appendices of this report but these data, as well as information regarding the exact locations of these antennas, can be found in the reports describing the individual measurements.[2-4]

These antennas, with the exception of the monopoles and the balanced dipoles over ground screens, were designed to conform as closely as possible to those commonly employed in tactical situations. This was easy in the case of the dipoles, since they are normally fed through a coaxial line. However, the slant wires and inverted L's are normally used with the radio set (and the operator) located at the feed point. This was not possible here, because the receivers and recorders were located at a distance from the antennas. For the inverted L's, the coaxial line was led in at right angles to the elevated horizontal element, and the shield was simply connected to a 2-ft grounding rod at the feed point. In all cases, the shields of the coaxial lines were continuous from the antenna feed point to the equipment van used for antenna pattern measurements. Contrary to tactical communication practice, grounding rods were used at various places to control currents on the coaxial lines--particularly to help define the limits of the coaxial-line counterpoise. It should be noted that these rods changed the current distributions in the ground systems to some extent, principally affecting the antenna impedances.[2-4,22]

Table 1

SUMMARY OF MEASURED HF ANTENNA PATTERN DATA
AVAILABLE IN REFS. 2, 3, AND 4

Antenna Type	f_o (MHz)	Data Available* f_m (MHz)	Lodi[2]	Almanor[3]	Ban Mun Chit[4]
Balanced Dipole with Ground Screen in Clearing-- 41-ft High	6.0	3.0			θ, ●, P
		4.0			θ, ●, P
		6.0			θ, ●, P
		8.0			θ ○, P
Balanced Dipole in Clearing-- 41-ft High	6.0	3.0			θ, ●, P
		4.0			θ, ●, P
		6.0			θ, ●, P
		8.0			θ, ○, P
Unbalanced Dipole in Clearing-- 41-ft High	6.0	3.0			θ, ●, P
		4.0			θ, ●, P
		6.0			θ, ○, P
		8.0			θ, ●, P
Balanced Dipole in Forest-- 41-ft High	6.0	6.0			., ●, P
Unbalanced Dipole in Forest-- 41-ft High	6.0	3.0			θ, ●, P
		4.0			θ, ●, P
		6.0			θ, ●, P
		8.0			θ, ○, P
Unbalanced Dipole in Forest-- 16-ft High	6.0	6.0			θ, ●, P
Unbalanced Dipole in Forest-- 8-ft High	6.0	6.0			θ, ●, P
2-ft-High Unbalanced Dipole--	6.0	2.0	θ	θ	
		4.0	θ	θ, ●, P	θ, ●, P
		6.0	θ, ●	θ, ●, P	θ, ●, P
		8.0			θ, ○, P
		10.0	θ, ○	θ, ●, P	
23-ft-High Unbalanced Dipole	8.0	2.67	θ, ●		
		5.0	θ, ●	θ, ● P	
		8.0	θ, ○	θ, ●, P	θ, ●, P
		15.0	θ, ●	θ, ●, P	
Balanced Dipole over Ground Screen-- 16.4 ft High	15.0	4.0	●	●	θ, ●, P
		5.0	●	●	
		6.0	●	●	θ, ●, P
		8.0	●	●	θ, ●, P
		10.0	●	●	
		12.0			θ, ●, P
		15.0	●	●	θ, ●, P

*Symbols for pattern data are as follows: θ is vertical polarization response, ● is horizontal polarization response, and P is power response.

Table 1 (continued)

Antenna Type	f_o (MHz)	Data Available* f_m (MHz)	Lodi[2]	Almanor[3]	Ban Mun Chit[4]
Sleeve Dipole	5.0	5.0		θ, ϕ, P	
		8.0		θ, ϕ, P	
Sleeve Dipole	6.0	6.0			θ, ϕ, P
J&B-Type 80-ft-High Balanced Dipole	6.0	6.0			θ, ϕ, P
J&B-Type 40-ft-High Balanced Dipole	6.0	6.0			θ, ϕ, P
J&B-Type 40-ft-High Balanced Dipole	12.0	12.0			ϕ
Monopole in Clearing	6.0	6.0			θ
Monopole on Edge of Clearing	6.0	4.0			θ
		6.0			θ
		8.0			θ
Monopole in Forest	6.0	4.0			θ
		6.0			θ
		8.0			θ
Monopole	15.0	2.0	θ	θ	
		2.67	θ		
		4.0	θ	θ	
		5.0	θ	θ	
		6.0	θ	θ	
		8.0	θ	θ	
		10.0		θ	
		15.0	θ	θ	
J&B-Type 80-ft-High Vertical	2.0	2.0			θ
J&B-Type 40-ft-High Vertical	6.0	6.0			θ
J&B-Type 20-ft-High Vertical	12.0	12.0			θ
2:1 Inverted L	6.0	3.0			θ, ϕ, P
		4.0			θ, ϕ, P
		6.0			θ, ϕ, P
		8.0			θ, ϕ, P
2:1 Inverted L	8.0	2.67	θ, ϕ	θ	
		5.0		θ, ϕ, P	
		8.0	θ, ϕ	θ, ϕ, P	θ, ϕ, P
5:1 Inverted L	6.0	4.0			θ, ϕ, P
		6.0			θ, ϕ, P
		8.0			θ, ϕ, P

*Symbols for pattern data are as follows: θ is vertical polarization response, ϕ is horizontal polarization response, and P is power response.

Table 1 (concluded)

Antenna Type	f_o (MHz)	Data Available* f_m (MHz)	Lodi[2]	Almanor[3]	Ban Mun Chit[4]
5:1 Inverted L	10.0	4.0		θ, ϕ, P	
		6.0		θ, ϕ, P	
		10.0	θ, ϕ	θ, ϕ, P	θ, ϕ, P
30° Slant Wire	4.0	2.0	θ	θ, ϕ, P	
		4.0	θ, ϕ	θ, ϕ, P	θ, ϕ, P
		6.0	θ, ϕ	θ, ϕ, P	
30° Slant Wire	6.0	3.0			θ, ϕ, P
		4.0			θ, ϕ, P
		6.0			θ, ϕ, P
		8.0			θ, ϕ, P
60° Slant Wire	5.0	5.0	θ, ϕ		
		15.0	θ, ϕ		
Loop in Clearing	6.0	6.0			θ, ϕ, P
Loop in Forest	6.0	6.0			θ, ϕ, P
Long Wire	5.0	3.0			θ, ϕ, P
		4.0			θ, ϕ, P
		6.0			θ, ϕ, P
		8.0			θ, ϕ, P

*Symbols for pattern data are as follows: θ is vertical polarization response, ϕ is horizontal polarization response, and P is power response.

The radiating elements of all antennas were made of No. 10 or 12 solid copper wire, unless otherwise noted.

A. Dipole Antennas

Various configurations of balanced and unbalanced dipole antennas were measured while they were located in and out of the forests to investigate the effects of the forests on the antenna radiation patterns.

1. 6-MHz Dipole Antennas

Eight 6-MHz dipole antenna configurations were measured at Ban Mun Chit to investigate the effect of the forest, antenna height, and matching circuits on the antenna radiation pattern. These included:

(1) A 41-ft-high balanced dipole with a ground screen, located in a clearing

(2) A 41-ft-high balanced dipole in a clearing

(3) A 41-ft-high unbalanced dipole in a clearing

(4) A 41-ft-high balanced dipole in the forest

(5) A 41-ft-high unbalanced dipole in the forest

(6) A 16-ft-high unbalanced dipole in the forest

(7) An 8-ft-high unbalanced dipole in the forest

(8) A 2-ft-high unbalanced dipole in the forest.

The first seven of these were measured only at Ban Mun Chit and the last one (the 2-ft-high unbalanced dipole) was measured at Lodi (cleared site), and in the forest at Almanor as well as at Ban Mun Chit.

A drawing of the 41-ft-high balanced dipole over a ground screen is shown in Figure 8. This antenna was supported above the ground screen by a dielectric rope and wooden poles. The ground screen consisted

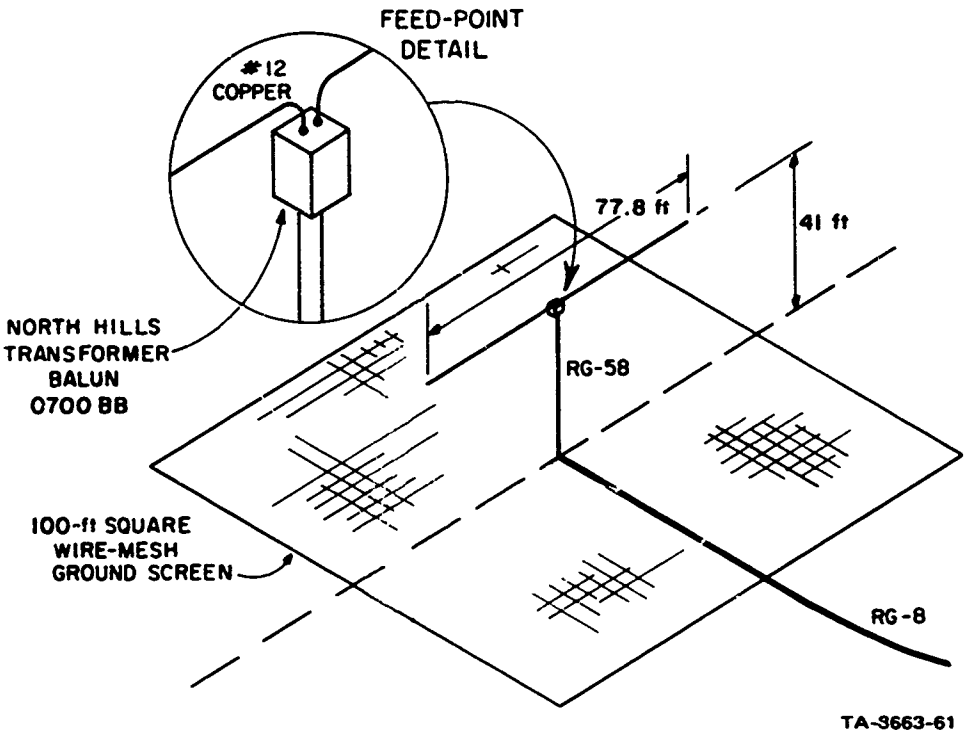

FIGURE 8 6-MHz BALANCED DIPOLE ANTENNA

of poultry netting laced together with No. 12 copper wire (with approximately 6 inches of overlap) to form a square ground plane 100 ft on each side. (This was the only 6-MHz dipole antenna with a ground screen.) A North Hills Model 0770-BB balun transformer was used with this antenna and the other 6-MHz balanced dipoles. This is a ferrite-core transformer, nominally matching 50 ohms (unbalanced) to 300 ohms (balanced). This high effective turns ratio was chosen to minimize the VSWR over the entire band of measurement frequencies, rather than match the resonant (6 MHz) impedance value to the 50-ohm receiver input at the instrumentation van. The feed line for this and the other 6-MHz dipole antennas--except the 2-ft-high unbalanced dipole--consisted of 100 ft of RG-58 coaxial cable from the feed point of the antenna which was then connected to the RG-8 coaxial transmission line that lead to the instrumentation van.

The other 6-MHz dipole antennas, except the 2-ft-high unbalanced dipole, were similar to the 41-ft-high balanced dipole over a ground screen except that no ground screen was used, the height was varied, and baluns were not always used.

The 2-ft-high unbalanced dipole antenna was supported along its length by four wooden stakes driven into the ground at approximately 20-ft intervals. The transmission line consisted of a 2-ft piece of RG-58 coaxial line with the braid connected to a copper grounding rod where it was adapted to RG-8 coaxial line leading to the instrumentation van (see Figure 9).

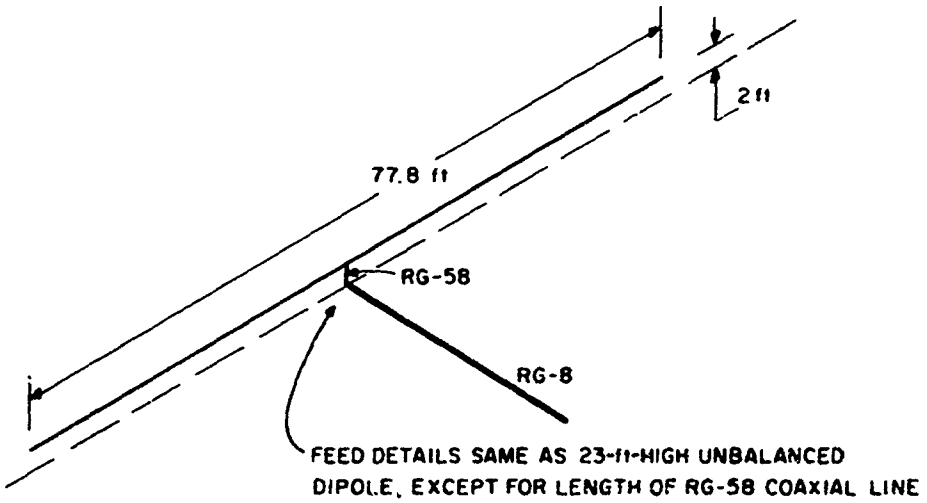

FIGURE 9 2-FOOT-HIGH UNBALANCED DIPOLE ANTENNA

2. 8-MHz, 23-ft-High Unbalanced Dipole Antenna

The 23-ft-high unbalanced dipole antenna was measured at Lodi, in the forest at Almanor, and in the forest at Ban Mun Chit. The elements of the dipole were 29.2 ft long as shown in Figure 10. The 23-ft-RG-58 coaxial line was perpendicular to the antenna and the ground with the braid connected to a copper rod. RG-8 coaxial line was used from the ground to the receiver van.

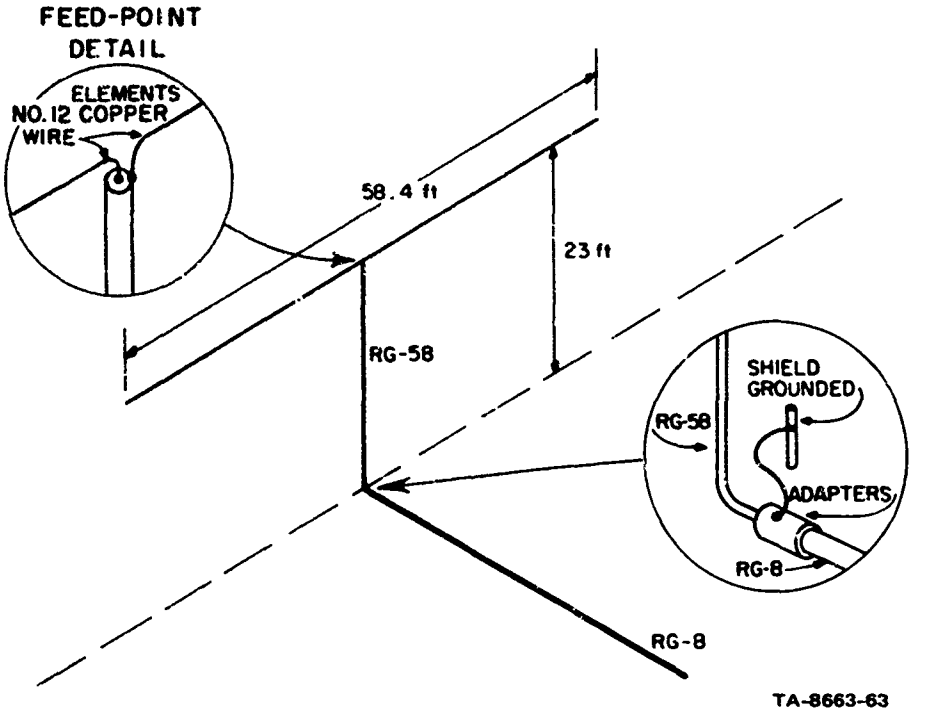

FIGURE 10 23-FOOT-HIGH UNBALANCED DIPOLE ANTENNA

3. 15-MHz Balanced Dipole Antenna

This antenna was measured at Lodi, in the forest at Almanor, and in a clearing at Ban Mun Chit. The antenna consisted of two 15.6-ft elements, 16.4 ft from the ground. The antenna was supported by dielectric rope from two wooden poles at the edge of the ground screen. The ground screen was constructed from poultry netting similar to that used with the 6-MHz balanced dipole in the clearing, described above; but in this case, the ground screen was only 50 ft on each side. A North Hills Model 0700-BB balun (300 ohm to 50 ohm) was used with the antenna. RG-58 coaxial line was used for the elevated portion of the feed line, while RG-8 coaxial line was used for the portion leading to the instrumentation van.

4. Sleeve-Dipole Antennas

Two horizontal sleeve-dipole antennas were measured--a 5-MHz sleeve dipole in the forest at Almanor and a 6-MHz sleeve dipole in the forest at Ban Mun Chit. The 5-MHz antenna consisted of 46.7 ft of tinned copper tubular braid over the insulation of RG-8 coaxial line and soldered to the shield of the coaxial line at the feed point. The center conductor of the coaxial line was soldered to 46.7 ft of No. 12 solid copper wire, as shown in Figure 11. The 6-MHz antenna was constructed similarly except that the braid and the solid copper wire were cut to 38.9 ft. Both antennas were laid in a straight line directly on the ground in the forests, but no direct connections were made to the ground through grounding rods.

5. Jansky-and-Bailey-Type Horizontal Balanced Dipole

Three Jansky-and-Bailey (J&B)-type horizontal balanced dipole configurations were measured at Ban Mun Chit. These antennas were constructed to duplicate, as closely as possible, the transmitting antennas used by J&B for tropical-forest path-loss measurements near Pak Chong, Thailand;[23] and they were erected and adjusted at Ban Mun Chit by J&B personnel.

A drawing of the J&B-type balanced dipole is shown in Figure 12. The antenna was supported by two telescoping aluminum towers. The tower sections were 5 ft long; the base section was 8 inches in diameter, and the uppermost section was 2 inches in diameter. The height of the dipole antenna was determined by the number of tower sections extended. The radiating elements consisted of two 19.5-ft elements with porcelain insulators at the ends. Another 19.5 ft of copper wire was connected to the insulators, as shown in Figure 12. When the antenna was measured as a 6-MHz dipole, jumpers were used to connect the two wires together to

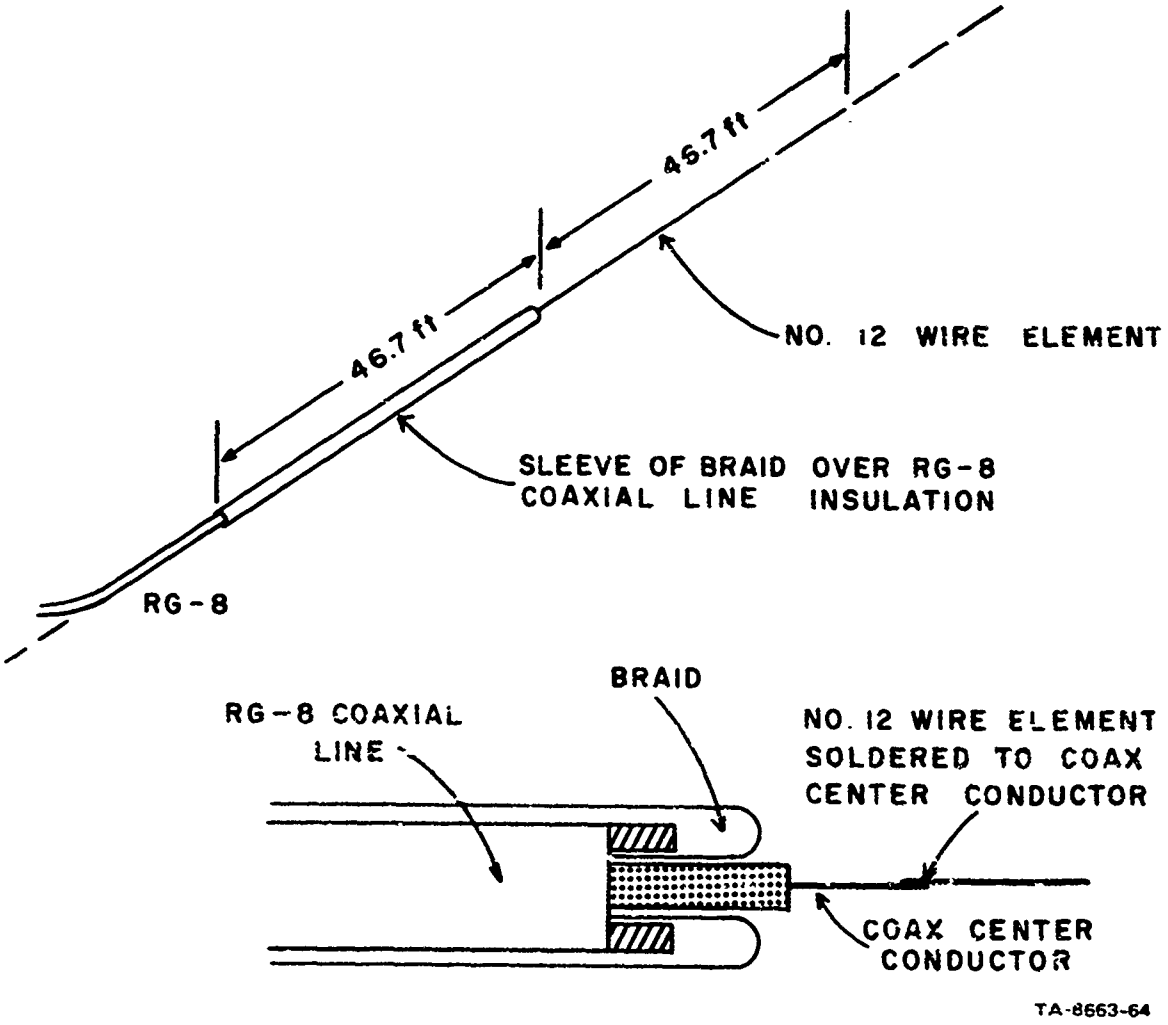

FIGURE 11 5-MHz SLEEVE-DIPOLE ANTENNA

form a 39-ft element; and when it was measured as a 12-MHz dipole, the jumpers were removed so that the elements were only 19.5-ft long. This procedure was similar to that used at the J&B site at Pak Chong, Thailand, except that at Pak Chong the towers were approximately 290 ft apart, so that they also could support a 2-MHz dipole.

The antenna feed line consisted of 72-ohm twin-lead transmission line from the antenna to a tunable balun on the ground and RG-8 coaxial transmission line from the balun to the instrumentation van. This antenna was measured when tuned for 6-MHz at heights of 40 and 80 ft, and when adjusted and tuned for 12 MHz at a height of 40 ft.

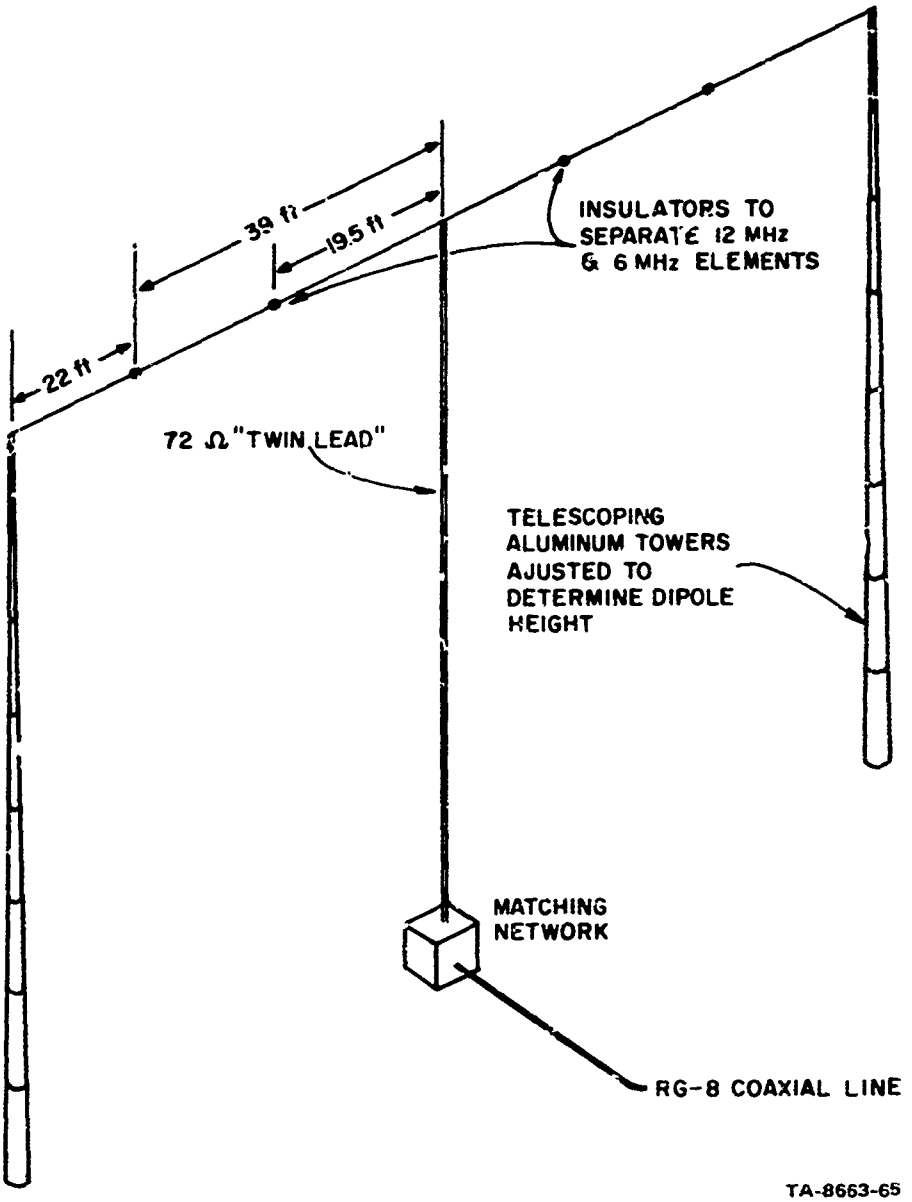

FIGURE 12 J&B-TYPE BALANCED DIPOLE ANTENNAS

B. Monopole Antennas

Several monopole antennas were measured. Quarter-wavelength monopoles were measured at Lodi and Almanor and tuned monopoles were measured at Ban Mun Chit.

1. 6-MHz Monopole Antennas

Three 6-MHz monopoles were measured at Ban Mun Chit in the following locations:

(1) In a clearing

(2) On the edge of the forest

(3) In the forest.

The radiating elements of the monopoles were constructed from one-inch-diameter copper tubing, 15.6 ft long and capped at both ends. The ground screens for these antennas were constructed from poultry netting, laced together with No. 12 copper wire with approximately 6 inches of overlap and then soldered at one-ft intervals. This screen was cut to form a 50-ft-diameter circle.

The antenna impedances were matched to the 50-ohm RG-8 coaxial cable at 6-MHz using a passive matching circuit consisting of a North Hills balun (300 ohm to 50 ohm) in parallel with the coaxial cable, and a slug-tuned inductor in series with the radiating element (see Figure 13).

2. 15-MHz Monopole Antenna

The 15-MHz monopole antenna was measured at Lodi and in the forest at Almanor. The antenna was constructed to the same dimensions as the 6-MHz monopole previously described. The ground screen was laced together but did not require soldering as with the 6-MHz monopole. This antenna was fed directly with the RG-8 coaxial line since the antenna was resonant at 15-MHz and no matching circuit was required.

DETAILS OF MATCHING NETWORK USED FOR 6-MHz MONOPOLE

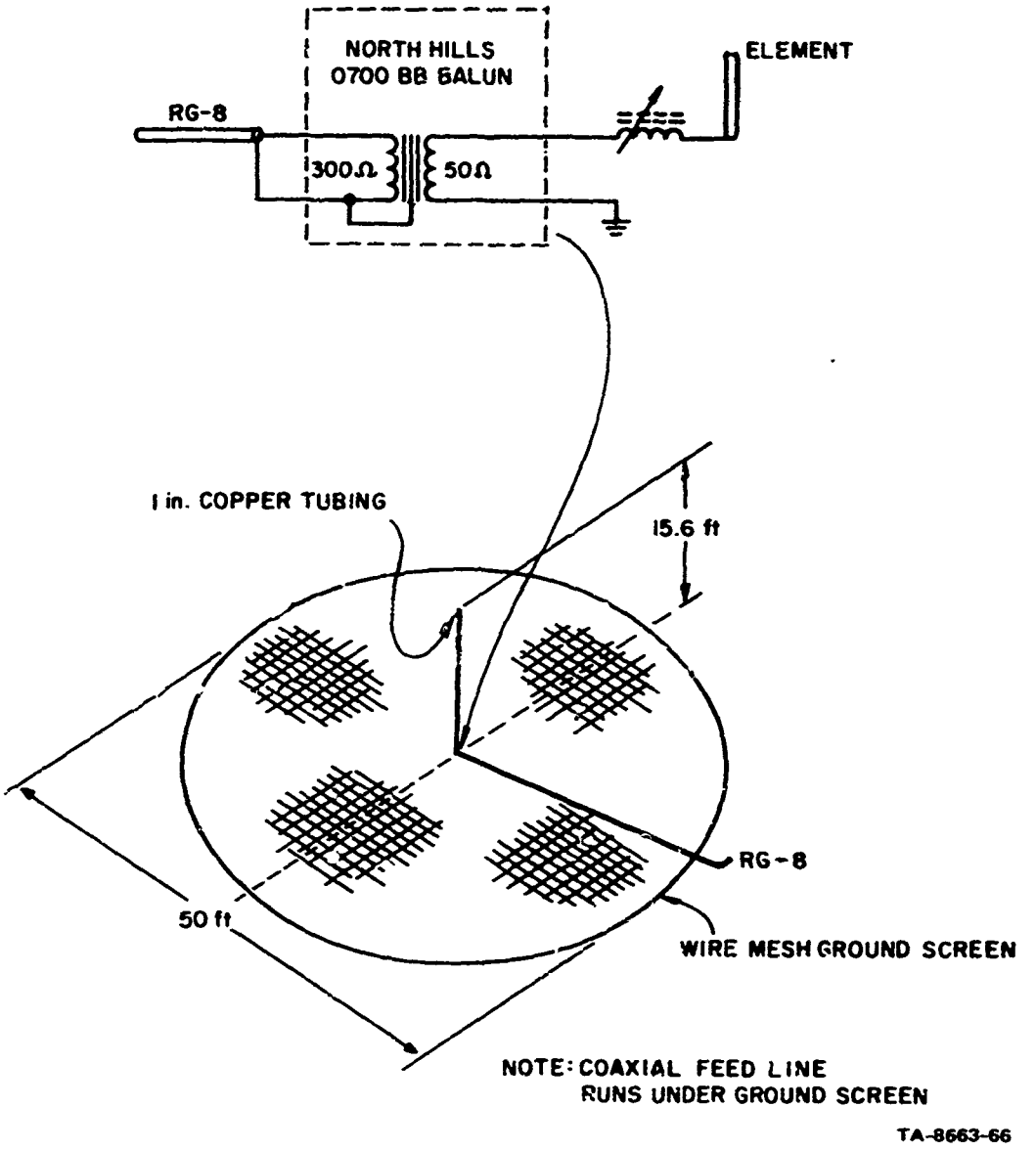

FIGURE 13 MONOPOLE ANTENNAS

3. Jansky-and-Bailey-Type Vertical Monopoles

The J&B-type vertical monopoles measured at Ban Mun Chit duplicated those used at Pak Chong, as was done with the J&B-type dipoles described previously.[23]

A drawing of the J&B-type vertical antenna is shown in Figure 14. The vertical element of this antenna was a telescoping aluminum

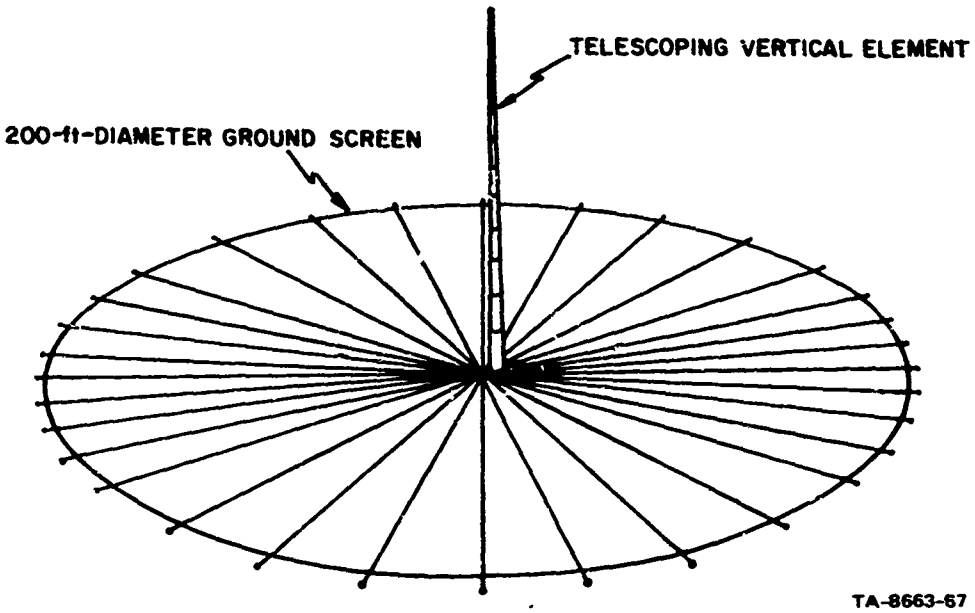

FIGURE 14 J&B-TYPE VERTICAL ANTENNAS

tower of the same construction as the towers used to support the dipole antennas. The element was isolated and elevated from the ground with a "Premax" insulator. The ground screen consisted of thirty-two 100-ft copper radials connected to a copper grounding rod at the center. Every fourth radial was No. 12 copper wire, and the remainder were No. 18 copper wire; the circumference of the circle was formed with No. 18 copper wire. Every other radial was terminated with 3-ft-long, 1/4-inch-diameter bronze welding rod, and the remaining radials were tied to wooden stakes. A tunable balun transformer was located at the feed point of the vertical element to match the impedance of the antenna to the 50-ohm RG-8 coaxial transmission line. The antenna was tuned for 2 and 6 MHz by adjusting the balun transformer for minimum VSWR (50 ohm reference) with 80- and 40-ft vertical elements, respectively. The length of the

vertical element was adjusted to approximately 20 ft to minimize the VSWR at 12 MHz without using the balun transformer.

C. 2:1 Inverted-L Antennas

Two 2:1 inverted-L antennas were measured. A 6-MHz 2:1 inverted L was measured in the forest at Ban Mun Chit and an 8-MHz 2:1 inverted L was measured at Lodi and in the forests at Almanor and Ban Mun Chit.

The total length of the elevated wire for these antennas was 95 percent of three-quarters of a wavelength. The ratio of the horizontal wire length to the vertical wire length was 2:1, as the name implies. The horizontal elements were suspended by wooden poles. The vertical elements of these antennas were suspended between their connection with the horizontal elements and their feed points on the ground, thus determining the height above ground of the horizontal elements. The antenna transmission lines were RG-8 coaxial lines, with the braid connected to copper grounding rods at the feed points. The dimensions of these antennas are given in Figure 15.

D. 5:1 Inverted-L Antennas

Two 5:1 inverted-L antennas were measured. A 6-MHz inverted L was measured in the forest at Ban Mun Chit and a 10-MHz 5:1 inverted L was measured at Lodi and in the forests at Almanor and Ban Mun Chit. The construction of these antennas was the same as that of the 2:1 inverted-L antennas, except that the ratio of the wire lengths was 5:1 in this case. The dimensions of these antennas also are given in Figure 15.

E. 30° Slant-Wire Antennas

The 30° slant-wire antennas were designed to resonate at 4 MHz and 6 MHz. The 4-MHz antenna was measured at Lodi and in the forests at

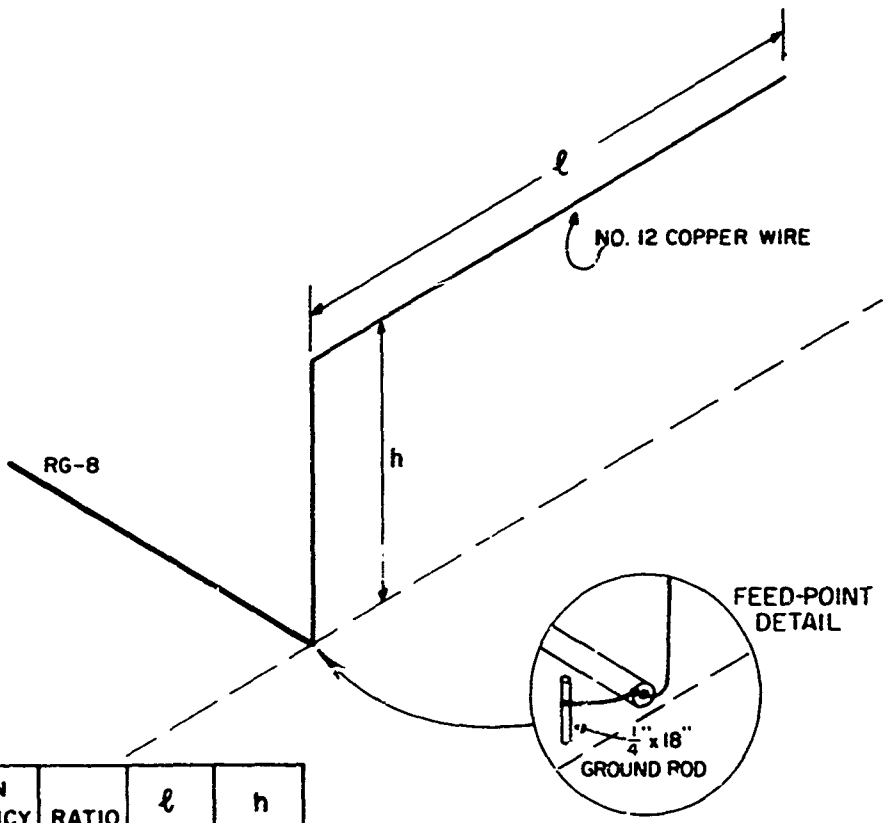

DESIGN FREQUENCY MHz	RATIO	ℓ (ft)	h (ft)
6	2:1	77.6	38.8
8	2:1	58.4	29.2
6	5:1	97.0	19.4
10	5:1	58.4	11.7

FIGURE 15 INVERTED-L ANTENNAS

Almanor and Ban Mun Chit. The 6-MHz antenna was measured only at Ban Mun Chit.

These antennas consisted of elevated radiators scaled for 95 percent of one-quarter wavelength. The counterpoises were located 135° in azimuth from the horizontal projection of the elevated radiators and were laid directly on the ground. The remote ends of the counterpoise wires were clamped to copper grounding rods. The transmission lines consisted of RG-8 coaxial cable, with the shield grounded at a distance equal to the

length of the counterpoise wire in order to define the other leg of the counterpoise as indicated in Figure 16.

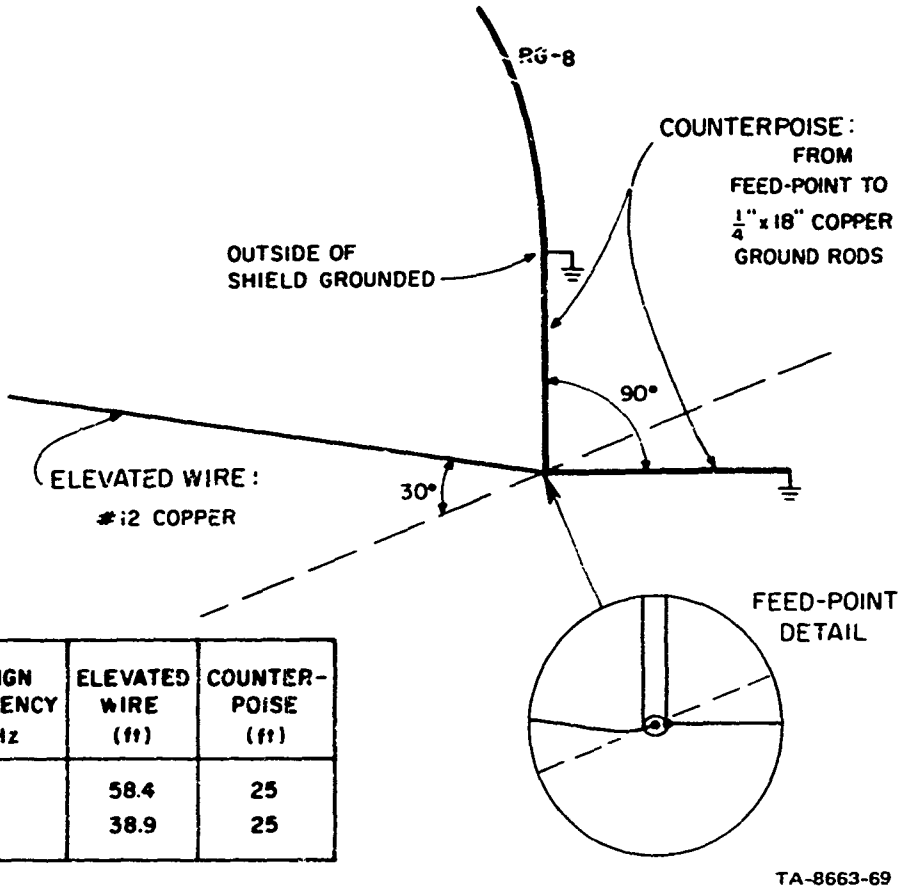

DESIGN FREQUENCY MHz	ELEVATED WIRE (ft)	COUNTER-POISE (ft)
4	58.4	25
6	38.9	25

FIGURE 16 30° SLANT-WIRE ANTENNAS

F. 60° Slant-Wire Antenna

The 60° slant-wire antenna was measured only at Lodi. This antenna was similar to the 30° slant wire antennas except that the elevated wire was 46.7 ft long (one quarter wavelength at 5 MHz) and elevated to an angle of 60° instead of 30°. The length of the counterpoise remained at 25 ft.

G. Loop Antennas

Two vertical-plane loop antennas were measured at Ban Mun Chit--one situated in the clearing and one in the forest. These square loops consisted of a single turn of No. 12 copper wire, 15 ft on a side, supported by wooden poles. The feed lines consisted of 50 ft of RG-58 coaxial cable connected to the loops through North Hills Model BB-1100 baluns (75 ohm to 75 ohm), as shown in Figure 17.

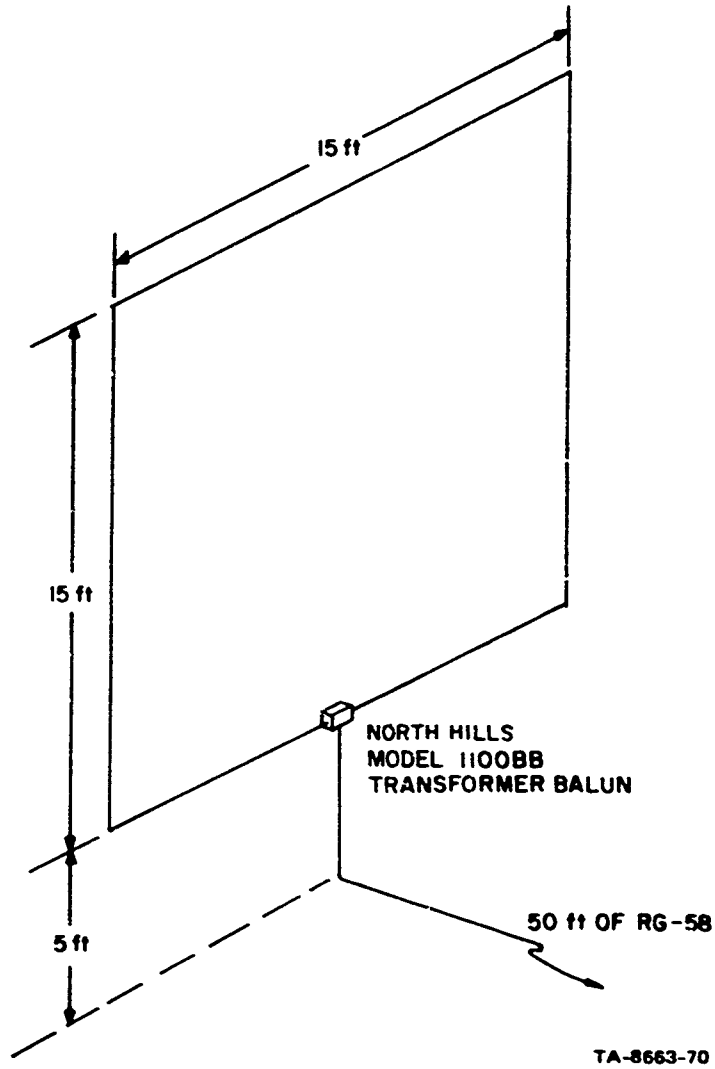

FIGURE 17 LOOP ANTENNAS

H. Long-Wire Antenna

The 6-MHz long-wire antenna measured in the forest at Ban Mun Chit consisted of 38.9 ft of No. 12 copper wire soldered to the center conductor of 75 ft of RG-174 coaxial cable, with the braid of the coaxial cable left open-circuited at this point. The center of the antenna was supported over a tree branch, as shown in Figure 18.

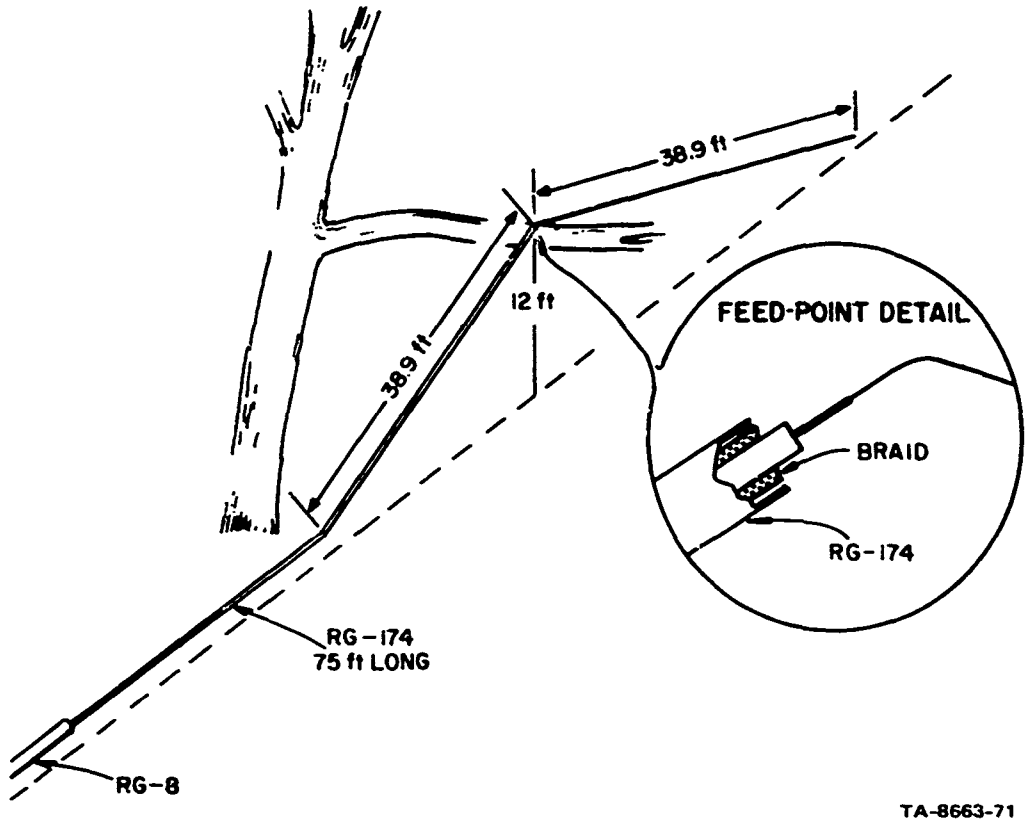

FIGURE 18 LONG-WIRE ANTENNAS

A. Dipole Antennas

Three dipole antennas were measured at the three sites considered in this section: the 6-MHz 2-ft-high unbalanced dipole, the 8-MHz 23-ft-high unbalanced dipole, and the 15-MHz balanced dipole. These antennas were described in Sec. IV-A.

Although one would expect the patterns from the measurements of the 2-ft-high unbalanced dipole to be more characteristic of a dipole antenna when the antenna was measured at Lodi, both the E_θ and E_ϕ patterns from this antenna were better (i.e., more symmetrical and having better formed lobes) when the antenna was measured at Ban Mun Chit (see Figures A-1 through A-8). The E_θ patterns were regular (as one would expect for a dipole) at all three sites, and exhibited only minor changes from site to site, whereas the E_ϕ patterns were regular only at Ban Mun Chit and exhibited significant changes at the other sites. Selecting the azimuth sector at each site with the better formed E_ϕ lobe, it can be observed from the patterns for Lodi (270° azimuth) and Ban Mun Chit (both 90° and 270° azimuth) that the decrease in relative directivity with decreasing elevation (roll-off or roll-under) was about the same, except at the small elevation angles where the roll-off was less for the forested site. At the Almanor forest site (lobe toward 90° azimuth) the roll-off was more rapid than at either Lodi or Ban Mun Chit for all elevation angles. The power patterns show that the antenna produced a pattern that was almost omnidirectional and most of the power was directed toward the zenith at both forested sites. By comparing the 3-dB and 6-dB contours for those two patterns, it can be seen that E_ϕ was the dominant polarization above 50° at Almanor, whereas E_θ was the dominant polarization at Ban Mun Chit. At the lower elevation angles, the power response of this antenna was slightly more omnidirectional at Ban Mun Chit than at Almanor, and the power directivity (relative to the antenna maximum) at low elevation angles (below about 20°) was less at Almanor.

V COMPARISON OF MEASURED ANTENNA PATTERNS OVER OPEN, FLAT TERRAIN, IN A U.S. PINE FOREST, AND IN A THAI TROPICAL FOREST

A summary of the antenna radiation pattern data available from the three measurement sites--Lodi (open, flat terrain),[2] Almanor (U.S. conifer forest),[3] and Ban Mun Chit (Thailand tropical forest)[4] was presented in Table I. Primarily, the data measured at the design frequency of the antennas are discussed in the following sections and the patterns are presented in Appendix A of this report. Measurement data for other frequencies can be found in the reports describing the measurements at the individual sites.

The pattern-measurement technique does not readily provide absolute gains and the radiated power from the Xeledop was not determined (the transmitters in the Xeledop were either replaced or retuned between sites). Consequently, the relative gains of these antennas cannot be compared among sites by using only the data from the pattern measurements. Therefore, only the effects of the forests on the directivity patterns of these antennas are discussed in this section (see Sec. X for data on relative antenna gains and estimates of absolute gains).

In the discussion that follows, the patterns for the two polarization components, E_θ (vertical polarization) and E_ϕ (horizontal polarization) are discussed first, followed by a discussion of the power patterns. The techniques for measuring the power patterns were not developed until after the measurements at Lodi were completed. Therefore, only the power patterns for the antennas at Almanor and Ban Mun Chit are available for comparison.

A. Dipole Antennas

Three dipole antennas were measured at the three sites considered in this section: the 6-MHz 2-ft-high unbalanced dipole, the 8-MHz 23-ft-high unbalanced dipole, and the 15-MHz balanced dipole. These antennas were described in Sec. IV-A.

Although one would expect the patterns from the measurements of the 2-ft-high unbalanced dipole to be more characteristic of a dipole antenna when the antenna was measured at Lodi, both the E_θ and E_ϕ patterns from this antenna were better (i.e., more symmetrical and having better formed lobes) when the antenna was measured at Ban Mun Chit (see Figures A-1 through A-8). The E_θ patterns were regular (as one would expect for a dipole) at all three sites, and exhibited only minor changes from site to site, whereas the E_ϕ patterns were regular only at Ban Mun Chit and exhibited significant changes at the other sites. Selecting the azimuth sector at each site with the better formed lobe, it can be observed from the patterns for Lodi (270° azimuth) and Ban Mun Chit (both 90° and 270° azimuth) that the decrease in relative directivity with decreasing elevation (roll-off or roll-under) was about the same, except at the small elevation angles where the roll-off was less for the forested site. At the Almanor forest site (lobe toward 90° azimuth) the roll-off was more rapid than at either Lodi or Ban Mun Chit for all elevation angles. The power patterns show that the antenna produced a pattern that was almost omnidirectional and most of the power was directed toward the zenith at both forested sites. By comparing the 3-dB and 6-dB contours for those two patterns, it can be seen that E_ϕ was the dominant polarization above 50° at Almanor, whereas E_θ was the dominant polarization at Ban Mun Chit. At the lower elevation angles, the power response of this antenna was slightly more omnidirectional at Ban Mun Chit than at Almanor, and the power directivity (relative to the antenna maximum) at low elevation angles (below about 20°) was less at Almanor.

Both the E_θ and E_ϕ response of the 8-MHz 23-ft-high unbalanced dipole indicate only slight changes (with the greater change in the E_ϕ patterns) when the antenna was moved from the open site at Lodi to the forested site at Almanor, but the data that are available from Ban Mun Chit indicated that the pattern was less well formed at this tropical forest site (see Figures A-9 through A-16). The pattern did not roll under as much as Lodi when the antenna was located at either of the forested sites. The power pattern data are limited for this antenna at Ban Mun Chit, but the available power patterns indicate that the response is similar at the two forested sites--the E_ϕ response dominates and the power is directed toward the zenith and broadside to the horizontal elements of the antenna.

Only the patterns of the E_ϕ response of the 15-MHz balanced dipole antenna are presented here since only this response was measured at all three sites (see Figures A-17 through A-19). Before comparing the patterns for the three sites, a few comments should be made regarding the placement of this antenna at each site--the exact location of this antenna can be observed on the site maps presented in the measurement reports.[2-4] At Lodi, the antenna was located in a freshly ploughed field--i.e., the optimum situation to simulate ideal conditions. At Almanor, the antenna was located in a clearing approximately 75 ft in diameter within the pine forest. There was a large clearing where the measurement equipment was located about 300 ft from the antenna in a direction of 270° from the axis of the antenna. At Ban Mun Chit, the forest was approximately 200 ft from the antenna at about 90° from the axis of the antenna. The pattern data show that the symmetry and smoothness of the lobes of the patterns degenerated as the antenna was moved from Lodi to Almanor and again from Almanor to Ban Mun Chit. The lobe is lower at Almanor in the direction toward the clearing and is again higher in the direction toward the forest at Ban Mun Chit. The pattern

at Ban Mun Chit shows some irregularity, such as splitting of the lobe, which possibly may be due to the tapioca growing in the cleared area beyond the antenna ground screen.

B. Monopole Antennas

The monopole antenna was basically a 15-MHz quarter-wavelength monopole as described in Sec. IV-B. The matching network used with this antenna when it was measured at Ban Mun Chit improved the efficiency at 6 MHz but should not have affected the directivity pattern of the antenna. Therefore, it is reasonable to compare the patterns of this antenna measured on 6 MHz at the three sites.

A comparison of the E_θ response of this antenna at 6 MHz at the three sites is shown in Figure A-20. The elevation angle of the maximum response of this antenna increased when the antenna was located in the forest at Almanor, but it remained relatively omnidirectional. The pattern broadened in elevation and became slightly less omnidirectional when measured in the tropical forest at Ban Mun Chit.

At 8 MHz, perturbations occurred in the pattern of this antenna when it was measured at Almanor (Figure A-23), whereas it remained relatively omnidirectional at Lodi (Figure A-21) and Ban Mun Chit (Figure A-25). The perturbations in the pattern of the antenna at Almanor occurred through 15 MHz (see Figure A-24) but it remained omnidirectional through 15 MHz when it was measured at Lodi (see Figure A-22). (No measurements were performed at 15 MHz at Ban Mun Chit.) The pattern break-up at Almanor at 8 MHz, but not at Ban Mun Chit, can possibly be explained by the fact that the tree trunks were about half as far apart at Ban Mun Chit. Although there were no measurements performed on the monopoles at Ban Mun Chit above 8 MHz, except VHF data[24] which exhibit fairly extreme break-up of the patterns, it appears reasonable to assume

the pattern would start to break up at approximately 16 MHz, assuming this criteria is dependent primarily upon the tree spacing.

C. Inverted-L Antennas

Two configurations of the inverted-L antenna were measured--an 8-MHz 2:1 inverted L and a 10-MHz 5:1 inverted L--at Lodi and in the forests at Almanor and Ban Mun Chit. The patterns from these two antennas are presented in Figures A-26 through A-39.

The patterns of the E_θ response of the 8-MHz 2:1 inverted L generally resembled those of a dipole antenna: the maximum response was off the ends of the horizontal elevated wire and at the higher elevation angles. The pattern resembled a dipole even more when it was located at the forested sites. The E_ϕ patterns of this antenna also resembled those of a dipole antenna, with the maximum response being broadside and upward from the elevated horizontal element. The roll-off of the E_ϕ response was significantly more rapid at the forested sites--with the least roll-off at the more densely forested site (Ban Mun Chit). The power patterns for this antenna are again essentially similar to those of a dipole antenna, with most of the power directed upward.

Although the patterns of the 10-MHz 5:1 inverted L were measured at Lodi, the data from these measurements have been omitted from this report because their validity is questionable. The E_θ patterns for the 10-MHz 5:1 inverted-L antenna indicate the antenna has a fairly strong vertically polarized component off the feed end (the end with the vertical element, that is often considered the back of the antenna). Some pattern perturbations can be observed in the E_θ patterns for the antenna at Almanor. At Ban Mun Chit, the E_θ pattern has a lobe above 40° elevation off the end of the L but this did not occur at Almanor. The E_ϕ response of this antenna resembles a dipole antenna and the power patterns for this

antenna indicate that the maximum radiation of this antenna is toward the zenith and toward the end with the vertical elements.

Generally, the inverted L should be used as a dipole antenna for skywave propagation--i.e., broadside. For ground-wave propagation, the antennas should be situated with the vertical element on the end toward the desired direction of propagation[25] (this siting criterion has more effect on the operation of the 5:1 inverted L than on the 2:1 inverted L).

D. 30° Slant-Wire Antennas

The 4-MHz 30° slant-wire antenna was measured at Lodi and in the forests at Almanor and Ban Mun Chit (see Figures A-40 through A-47). The E_θ response of this antenna was almost omnidirectional at Lodi, with the strongest directivity in the direction of the counterpoise--actually the lobe is slightly right of center (toward the counterpoise element formed by the braid of the coaxial transmission line). When measured in the two forested sites, the E_θ response was less omnidirectional and the lobe in the direction of the counterpoise became more distinct. The E_ϕ patterns for the antenna roughly resemble those of a dipole antenna but the power patterns show that the maximum response is between 30° and 60° elevation and in the direction of the counterpoise.

The measurements show that, contrary to popular belief, the 30° slant-wire antenna should be located so that the elevated element points away from the desired direction of propagation with the counterpoise pointing in the direction of desired propagation.[25]

VI EFFECT OF ROUGH TERRAIN ON ANTENNA RADIATION PATTERNS

During April 1967, exploratory measurements were performed under Contract DAHC07-67-C-0144 to investigate the effect of rough terrain on the radiation patterns of simple HF field-expedient antennas.[5] Several of these antennas were identical or quite similar to those measured under Contract DA 36-039 AMC-00040(E) and because of the common nature of the measurement programs and their relation to communications in tactical environments, selected examples of the data from those measurements are presented in Appendix B of this report.

The measurements were conducted in the hills near Livermore, California. These hills rise quite rapidly to an elevation of nearly 2,000 ft from a surrounding low, flat, bay plateau region with an elevation of approximately 600 ft. The terrain is rough and varied, providing several possible antenna sites such as hilltops, slopes, and deep gullies. The hills are covered with grass and scattered low trees, and there are occasional outcropping of rock. Figures 19 and 20 show some of the prominent terrain features of the area. The soil is what is commonly referred to as "adobe" and was quite moist at the time of the pattern measurements. Electrical ground constants were not measured at this site.

The measured antennas were located on the top of a ridge approximately 150 to 200 ft wide and on the side of a hill as shown in Figure 20.

The antenna measurement procedures were similar to those used for the tests performed under Contract DA 36-039 AMC-00040(E) except that the data were recorded digitally on magnetic tape (thus eliminating the necessity of hand-scaling the data). The data were presented in the

FIGURE 19 TERRAIN SURROUNDING LIVERMORE MEASUREMENT SITE WITH BAY FLATLANDS IN BACKGROUND

FIGURE 20 FIELD SITE FOR MEASUREMENTS IN ROUGH TERRAIN

form of contour plots, but the plotting techniques were slightly modified. The contouring program used a low-density grid (as was used for the power patterns in Ref. 4--see also Sec. III-E in this report). The plots were produced on a Control Data Corporation (CDC) 280 cathode ray tube (CRT) on-line display used with the CDC Model 3200 computer. The CRT was photographed with a 35-mm camera internal to the CDC 280 and the resulting contour plots were not of as high quality as those produced with the Cal Comp plotter. They are considerably less expensive, however, and still quite legible. Selected examples of these patterns are presented at the end of this report in Appendix B.

Two half-wave unbalanced dipoles were measured. Both antennas were similar to the 6-MHz unbalanced dipole antennas described in Sec. IV-A-1--the 6-MHz dipole was 40 ft above the ground and the 15-MHz dipole was 16.4 ft above the ground (no ground screen was used). The measured data from the 6-MHz dipole are shown in Figures B-1 through B-4. In Figures B-1 and B-2 it can be seen that although the dipole was parallel to the ridge, it was not located exactly in the center of the hilltop--i.e., the hill sloped downward more toward 90° than it did toward 270°. When the dipole was moved down the hill, the contour plots shown in Figures B-3 and B-4 were measured (the hill sloped down toward 90° azimuth and the antenna was maintained parallel to the hillside). Data for similar situations for the 15-MHz dipole are shown in Figures B-5 through B-8.

The patterns of the dipole antennas located on the hilltop were similar to those of the dipole antennas at Lodi (except for the dislocation of the lobes due to the antenna not being at the crest of the ridge). But when the antennas were moved down the slope, the relative directivity of the E_ϕ patterns increased at the lower elevation angles in the direction away from the hilltop and the lobes of the E_θ response rotated in azimuth away from the hilltop.

A 30-MHz monopole was constructed from one-inch-diameter aluminum tubing cut to 7.8 ft (95 percent of a quarter wavelength at 30 MHz). The ground system consisted of eight 50-ft radials elevated 18 inches above the ground. The E_θ patterns of this antenna measured on the hilltop and on the slope are shown in Figures B-9 and B-10. When the antenna was located on the slope, the element remained vertical (e.g., not perpendicular to the slope of the hill) and the hill sloped downward toward 270°. The pattern data show that the maximum directivity of the antennas occurs at lower elevation angles and is concentrated in the direction away from the hilltop when the antenna was on the hillside. The relative gain data presented in Reference 5 also showed the maximum observed signal was 3.2 dB higher when the antenna was located on the hillside than when it was on the hilltop.

The 4-MHz 30° slant-wire antenna measured at Livermore was identical to the one used at Lodi, Almanor, and Ban Mun Chit (described in Section IV-E). The E_θ (vertical polarization) response of this antenna was almost omnidirectional when it was located on the hilltop--with a slight increase in directivity in the direction of the counterpoise (see Figure B-11), as at Lodi, but the E_ϕ directivity was primarily toward 90° azimuth (see Figure B-12) because the antenna was located toward the right side of the ridge of the hill. When the antenna was moved down the hill the directivity patterns were quite irregular, but generally the strongest E_θ and E_ϕ responses were observed on the down-hill side of the antenna (270°) as can be seen in Figures B-13 and B-14.

These measurements in California hills, while clearly not exhaustive, give some indication of the pattern distortions to be expected in irregular terrain. From the patterns presented here, it appears that a preliminary conclusion can be extracted from this data. A dipole antenna should be used on a hillside instead of a slant wire (even though the slant wire is easier to erect) since the pattern of the dipole is more predictable under these circumstances.

VII COMPUTER MODELING OF ANTENNA RADIATION PATTERNS

The computer program developed under this contract to predict the expected radiation patterns of dipole antennas immersed in a forest[6] is described in this section. The model assumes that the forest is an idealized lossy dielectric slab and the antenna is a Hertzian dipole.

A. The Model of the Forest

The model approximates the forest as a multi-layer dielectric sandwich. The uppermost region is the space above the forest, characterized by ϵ_{ro} and μ_{ro}, the relative permittivity and permeability of free space. The i layers below this region are layers of forest (i = 1) and ground (i = 2) characterized by their complex refractive indecision where $n_i^2 = \epsilon_{ri}$, where the respective relative complex dielectric constants, ϵ_{ri}, are given:

$$\epsilon_{ri} = \epsilon'_{ri} - j\epsilon''_{ri} \quad .$$

Alternatively, the relative complex dielectric constant can be written

$$\epsilon_{ri} = \epsilon'_r - j60\,\sigma_i \lambda_o$$

or

$$\epsilon_{ri} = \epsilon'_{ri}\,(1 - j\delta_i) \quad ,$$

where the loss tangent, δ_i, is defined by

$$\delta_i = \frac{\epsilon''_{ri}}{\epsilon'_{ri}} = \frac{\sigma_i}{\omega\epsilon_o \epsilon'_{ri}} \quad ,$$

and σ_i is the conductivity (MKS units), λ_o is the free space wavelength at radian frequency ω, and ϵ_o is the permittivity of free space. Each region is assumed to be homogeneous and to possess the magnetic permeability of free space (μ_o).

The model originally was developed as a 3-layer model and later modified so that a total of 25 layers could be defined if required to approximate the profiles of complex dielectric constant of forest and ground. Because of limited measured data available from the open-wire transmission line measurements (we do not have profiles of ϵ' and δ for forest or ground), the forest and the ground were approximated as two individual layers, as shown in Figure 21, for the purposes of this report.

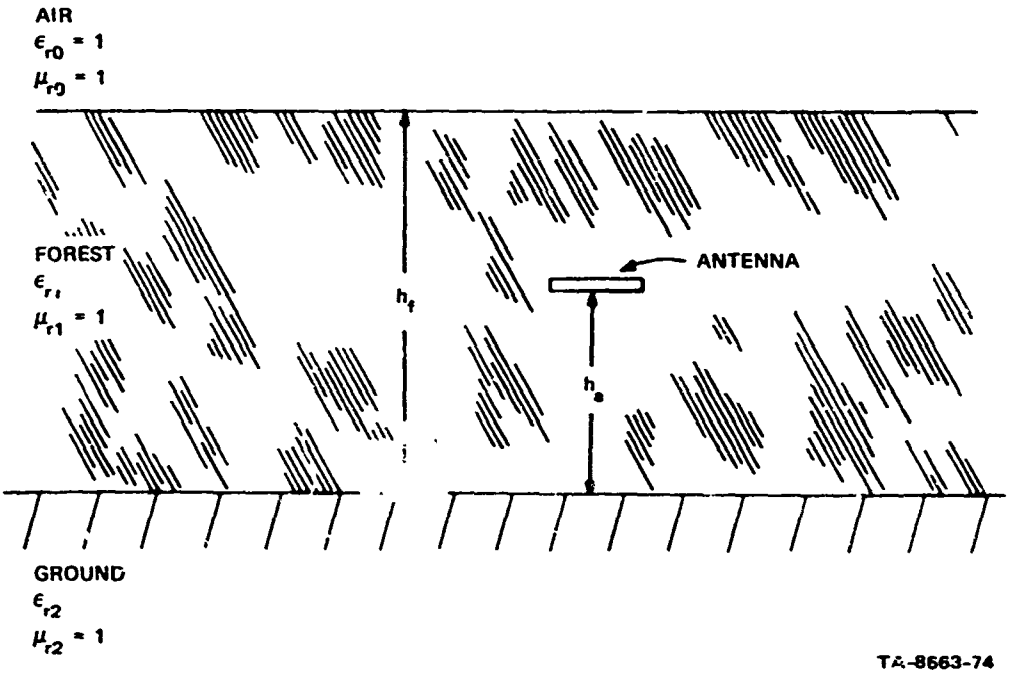

FIGURE 21 IDEALIZED LOSSY DIELECTRIC SLAB MODEL

It will be shown that this three-layer model, although simple, represents the forest quite well in the frequency range of 2 to 10 MHz, and its simplicity permits a reasonably rigorous analysis. The assumption of a flat surface on the top is justifiable when one considers that the surface roughness is small compared to the wavelength. The assumptions of homogeneity and isotropy in the vertical direction are harder to justify. It is probable that a multilayered slab or a layer with a tapered dielectric constant, lower at the top than at the bottom, would be a better approximation to the forest at Ban Mun Chit. Also, the effective conductivity for vertical polarization probably is greater than the effective conductivity for horizontal polarization.

B. Analysis

A thorough discussion of the model was presented in Reference 6 and is repeated here in part for the convenience of the reader. Consider a short electric dipole in the forest (see Figure 21) that is receiving a signal from a point source located in the air layer and far enough away to be in the far field* of the receiving antenna. For an electrically short dipole without end loading, the open circuit voltage at the antenna terminals is the product of one-half the antenna length and

---

*For far-zone approximations to be valid, the transmitting antenna must be far enough away from the receiving antenna so that the wavefront across the aperture is approximately plane. If, for example, it is assumed that the effective aperture is a region about four wavelengths in diameter (D_a) centered at the receiving antenna element, and if the usual far-zone criterion,

$$r \geq 2D_a^2/\lambda \quad ,$$

is used, then the transmitting antenna must be at least 4.8 km or approximately 3.0 miles away at a frequency of 2 MHz. Actually, pattern measurements in forests at several slant ranges have shown this distance to be more than sufficient at HF.

the component of electric field at the antenna which is in the direction of the antenna axis. But the open-circuit voltage of a receiving antenna is defined by the vector dot product

$$V_{oc} = \bar{h}(\theta, \phi) \cdot \bar{E}(\theta, \phi)$$

where $\bar{E}(\theta, \phi)$ is the electric field incident upon the air-forest interface, and $\bar{h}(\theta, \phi)$ is the vector effective length[26] of the slab-antenna combination. Hence, we can find $\bar{h}(\theta, \phi)$ from the field in the dielectric and the physical length and orientation of the antenna, and the problem of finding the antenna patterns applicable to the air-to-ground (or skywave) case has been reduced to that of finding the electric field within the dielectric layer representing the forest for various positions of the far-field point source. The computed radiation patterns given in this report are the ratio of $|\bar{h}|$ to the physical half-length of the dipole with no end loading.

Using the coordinates shown in Figure 22 we find that the pattern of a horizontal dipole in the plane perpendicular to the dipole is given by the electric field, E_{iz}, or E_ϕ* of a wave polarized normal to the plane of incidence. For a wave polarized in the plane of incidence, E_{ix} (or E_θ) is the pattern of a horizontal dipole in the plane of the dipole, and E_{iy} is the E_θ pattern of a vertical dipole in the plane of the dipole.

For both polarizations the propagation constants in Regions 1 (forest) and 2 (ground) are defined:

$$\gamma_1 = \alpha_1 + j\beta_1$$

---

*See Section VII-C for the relationship between the calculated patterns and the E_ϕ and E_θ measurement data.

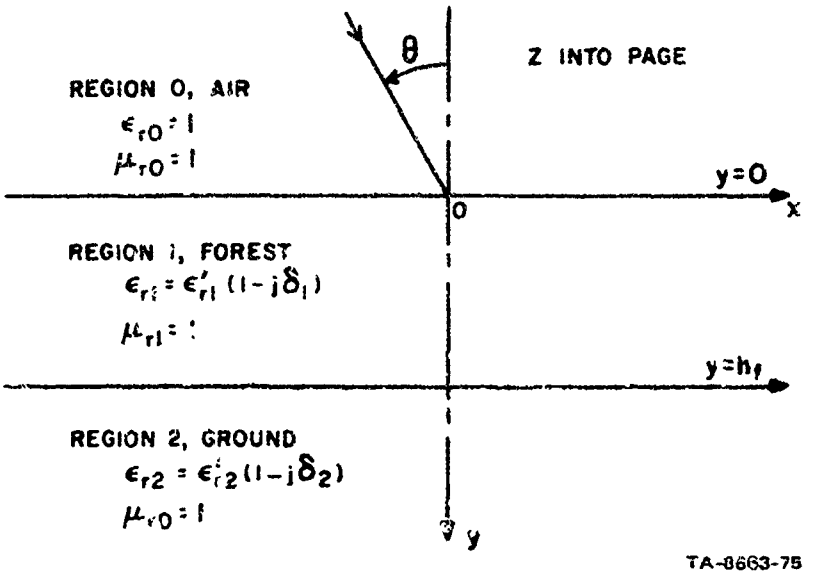

FIGURE 22 COORDINATES AND NOMENCLATURE FOR DIELECTRIC SLAB

and

$$\gamma_2 = \alpha_2 + j\beta_2 \quad ,$$

and they must satisfy the equations

$$\gamma_1^2 + \kappa_1^2 - k_0^2 \sin^2\theta = 0$$

and

$$\gamma_2^2 + k_2^2 - k_0^2 \sin^2\theta = 0$$

as a consequence of the fact that the vectors $\bar{E}$ and $\bar{H}$ are solutions of the wave equation,

$$\nabla^2\bar{E} + k^2\bar{E} = 0 \quad .$$

The real and imaginary parts of γ for Region 1 are given, then, by

$$\alpha_1^2 = 1/2 \left[(\sin^2\theta - \epsilon'_{r1}) + \sqrt{(\epsilon'_{r1} - \sin^2\theta)^2 + (\epsilon'_{r1}\delta_1)^2} \right]$$

$$\beta_1 = \begin{cases} \dfrac{\epsilon'_{r1}\delta_1}{2\alpha_1} & , \quad \text{for } \alpha_1 \neq 0 \\ \sqrt{\epsilon'_{r1} - \sin^2\theta} & , \quad \text{for } \alpha_1 = 0 \end{cases} .$$

In Region 2, α_2 and β_2 are obtained from the same equations, with ϵ'_{r1} and δ_1 replaced by ϵ'_{r2} and δ_2, respectively.

The resulting field patterns for short horizontal electric dipoles in Region 1 (forest) are of the form given below:[6]

(1) Horizontal dipole--in plane normal to dipole:

$$F_1(\theta) = |E_{1z}| \qquad \text{(for polarization normal to the plane of incidence)} .$$

Thus

$$F_1(\theta) = \frac{2\cos\theta \left| W_1 e^{\gamma_1 h_a} - W_2 e^{-\gamma_1 h_a} \right|}{\left| C_1 \left(W_1 e^{\gamma_1 h_f} + W_2 e^{-\gamma_1 h_f} \right) + j\cos\theta \left(W_1 e^{\gamma_1 h_f} - W_2 e^{-\gamma_1 h_f} \right) \right|} ,$$

where

$$W_1 = C_2 + C_1$$

$$W_2 = C_2 - C_1$$

$$C_1 = \gamma_1$$

and

$$C_2 = \gamma_2 .$$

(2) Horizontal dipole--in plane of dipole:

$$F_2(\theta) = |E_{1x}| \qquad \text{(for polarization in plane of incidence)} \quad .$$

Hence

$$F_2(\theta) = \frac{2\cos\theta \left| C_1\left(W_1 e^{\gamma_1 h_a} + W_2 e^{-\gamma_1 h_a}\right)\right|}{\left| C_1\left(W_1 e^{\gamma_1 h_f} + W_2 e^{-\gamma_1 h_f}\right) + j\cos\theta\left(W_1 e^{\gamma_1 h_f} - W_2 e^{-\gamma_1 h_f}\right)\right|} \quad .$$

where

$$W_1 = C_2 + C_1$$

$$W_2 = C_2 - C_1$$

$$C_1 = \frac{\gamma_1}{\epsilon_{r1}}$$

and

$$C_2 = \frac{\gamma_2}{\epsilon_{r2}} \quad .$$

C. Radiation Patterns

Once $F_1(\theta)$ and $F_2(\theta)$ are determined, the functions $E_\Phi(\theta, \Phi)$ and $E_\theta(\theta, \Phi)$ can be found by using the relationship:

$$E_\Phi(\theta, \Phi) \cong F_1(\theta, \Phi) = F_1(\theta) \sin\Phi^* \qquad 0° \leq \Phi \leq +50°$$

---

*Note that θ represents the zenith angle for the calculated patterns, but the measured data are displayed with θ representing the elevation angle. There is also a slight discrepancy between the measured and calculated elevation angle--this angle is referenced to the top of the forest slab for the calculated patterns (see Figure 22) but is referenced to the ground for the measured patterns--but this discrepancy is assumed to be relatively insignificant.

and

$$E_\theta(\theta, \Phi) \cong F_2(\theta, \Phi) = F_2(\theta) \cos\Phi^* \qquad -90° \leq \Phi \leq +90°$$

where

θ = Zenith angle (90° elevation angle)

Φ = Azimuth angle relative to the dipole axis.

$F_1(\theta)$ is the pattern of a horizontal dipole in the plane normal to the dipole, and $F_1(\theta, \Phi)$ would be the E_ϕ response at any desired azimuth and zenith angle. $F_2(\theta)$ is the pattern of a horizontal dipole in the plane of the dipole, and $F_2(\theta, \Phi)$ would be the E_θ response at any desired azimuth and zenith angle. In both cases the patterns are normalized so that F is the ratio of the effective length of the antenna to the physical half length.

A program was developed to provide contours of the calculated radiation patterns. This program determines at what zenith angle the -3, -6, -9, and -12 dB (relative to the maximum value of F) contours intersect a given elevation angle. The resulting contours of constant F can then be plotted to provide a contour map of computed relative signal strength similar to those produced from the measured data.

---

*See note on previous page.

VIII EFFECT OF FOREST AND GROUND ELECTRICAL CONSTANTS ON COMPUTED ANTENNA RADIATION PATTERNS

There are many factors that affect the radiation pattern of an elementary dipole antenna placed in a forest. Some of these factors cannot be accounted for in the present model (e.g., calculations of and corrections for the inhomogeneity and anisotropy of the layers), and among those factors that are input parameters of the model, it is not feasible to compute radiation patterns for all parameter combinations of interest. Therefore, the results shown here were obtained by choosing typical values of each model parameter and then varying them, one at a time, around this value. The parameters considered are:

(1) Antenna height (wavelengths)

(2) Relative dielectric constant of the forest (real part)

(3) Loss tangent of the forest

(4) Forest height (wavelengths)

(5) Relative dielectric constant of the earth (real part)

(6) Loss tangent of the earth.

A. Effect of Antenna Height

The most significant of the parameters considered here is the height of the antenna above ground. It affects both the effective length of the antenna and the input resistance, and, therefore, changes the gain function quite drastically. It is also one of the few factors that can be readily controlled in the field.

Figure 23 presents polar plots of $F_1(\theta)$ and $F_2(\theta)$ with antenna height in wavelengths as a parameter. Figure 23(a) is for the case of no forest; Figure 23(b) is for an antenna in a dense forest. To emphasize

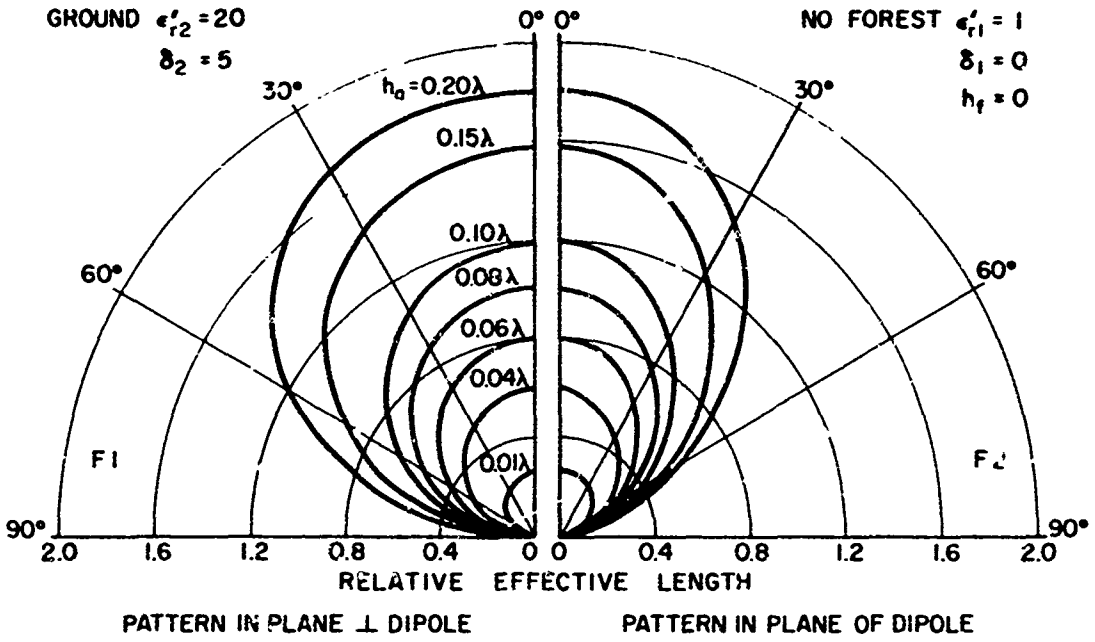

(a) EFFECTIVE ANTENNA LENGTH FOR VARIOUS HEIGHTS, h_a — NO FOREST

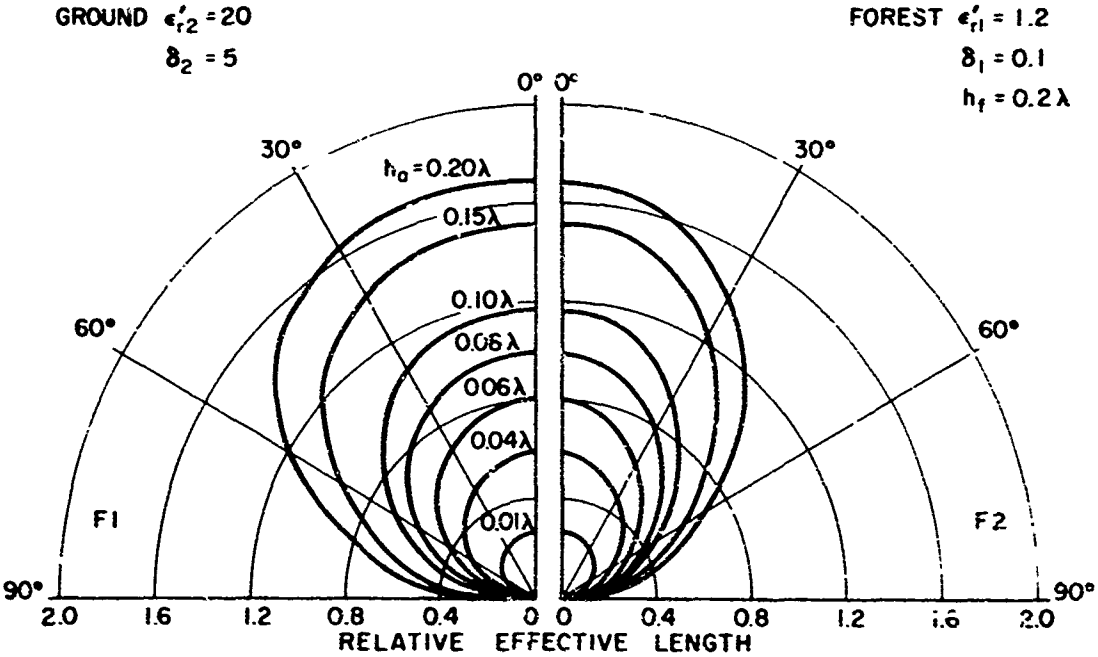

(b) EFFECTIVE ANTENNA LENGTH FOR VARIOUS HEIGHTS, h_a — FOREST

TA-8663-76

FIGURE 23 EFFECTIVE ANTENNA LENGTH FOR VARIOUS ANTENNA HEIGHTS IN CLEARING AND FOREST

the importance of raising the antenna above the ground, the same data are presented in a different way in Figures 24 and 25. Here F, the field-imaging function, is plotted as a function of antenna height for two specific angles, one at the zenith and one very near the horizon. Although it is not easy to see from these figures, the antenna height determines whether the stronger radiation is off the ends of the elements or broadside to the elements. Radiation off the ends predominates at very low antenna heights. It should be noted that the effects of antenna height upon antenna impedance are not included in Figures 23 through 25.

B. Effect of the Dielectric Constant of the Forest

Figure 26 shows the effect of the denseness of the vegetation on the radiation toward the zenith and horizon. The values of F_1 and F_2 are plotted as a function of the dielectric constant of the forest. Curves are plotted for two widely different values of ground constants. As would be expected, the radiation near the zenith is very little affected. The low-angle radiation is changed quite appreciably, however, with the vertically polarized wave nears the ends of the antenna being decreased as the dielectric constant increases and the horizontally polarized wave broadside to the dipole being greater than that with no forest.

Figures 27 and 28 show the effect of the dielectric constant on the radiation patterns for the sectors of the patterns broadside and off the ends of the elements of the dipole.

Figures 29 through 31 show the effect of the dielectric constant of the forest on the radiation toward the zenith and horizon for three different antenna heights. Again it can be seen that the dielectric constant of the forest has little effect on the radiation toward the zenith but has considerable effect on the radiation toward the horizon.

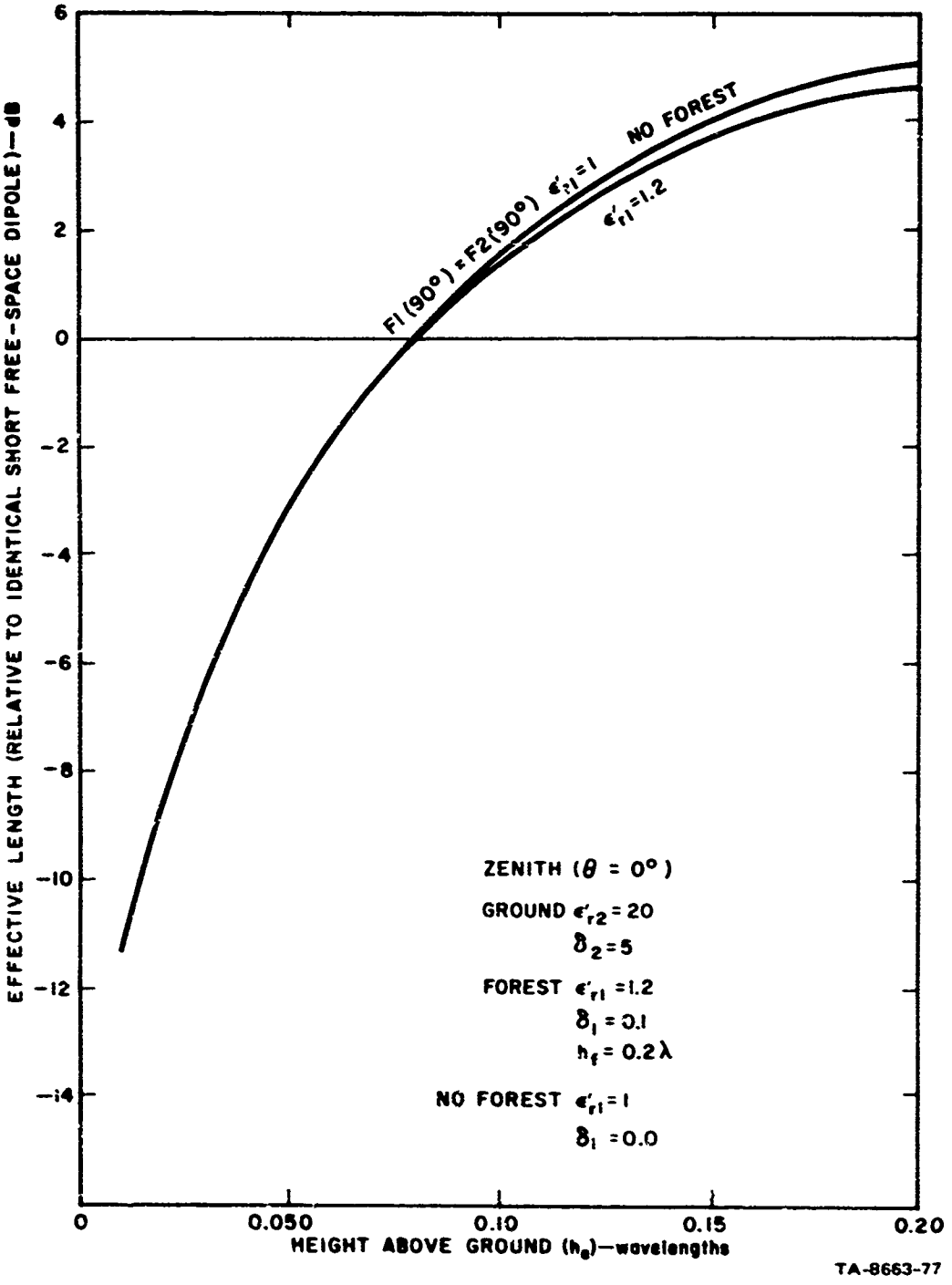

FIGURE 24 EFFECTIVE ANTENNA LENGTH AS A FUNCTION OF HEIGHT ABOVE GOOD GROUND—ZENITH

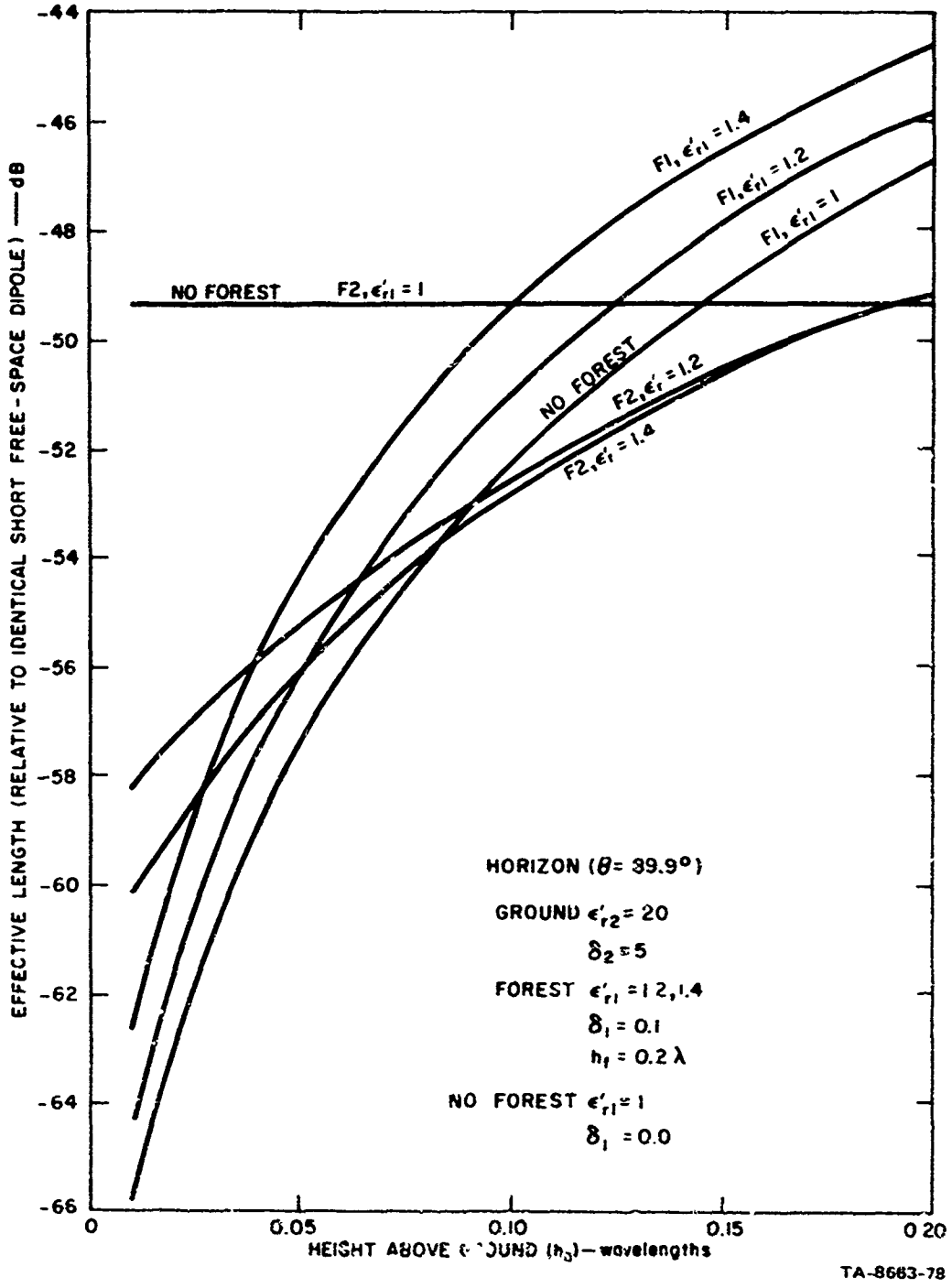

FIGURE 25 EFFECTIVE ANTENNA LENGTH AS A FUNCTION OF ANTENNA HEIGHT ABOVE GOOD GROUND—HORIZON

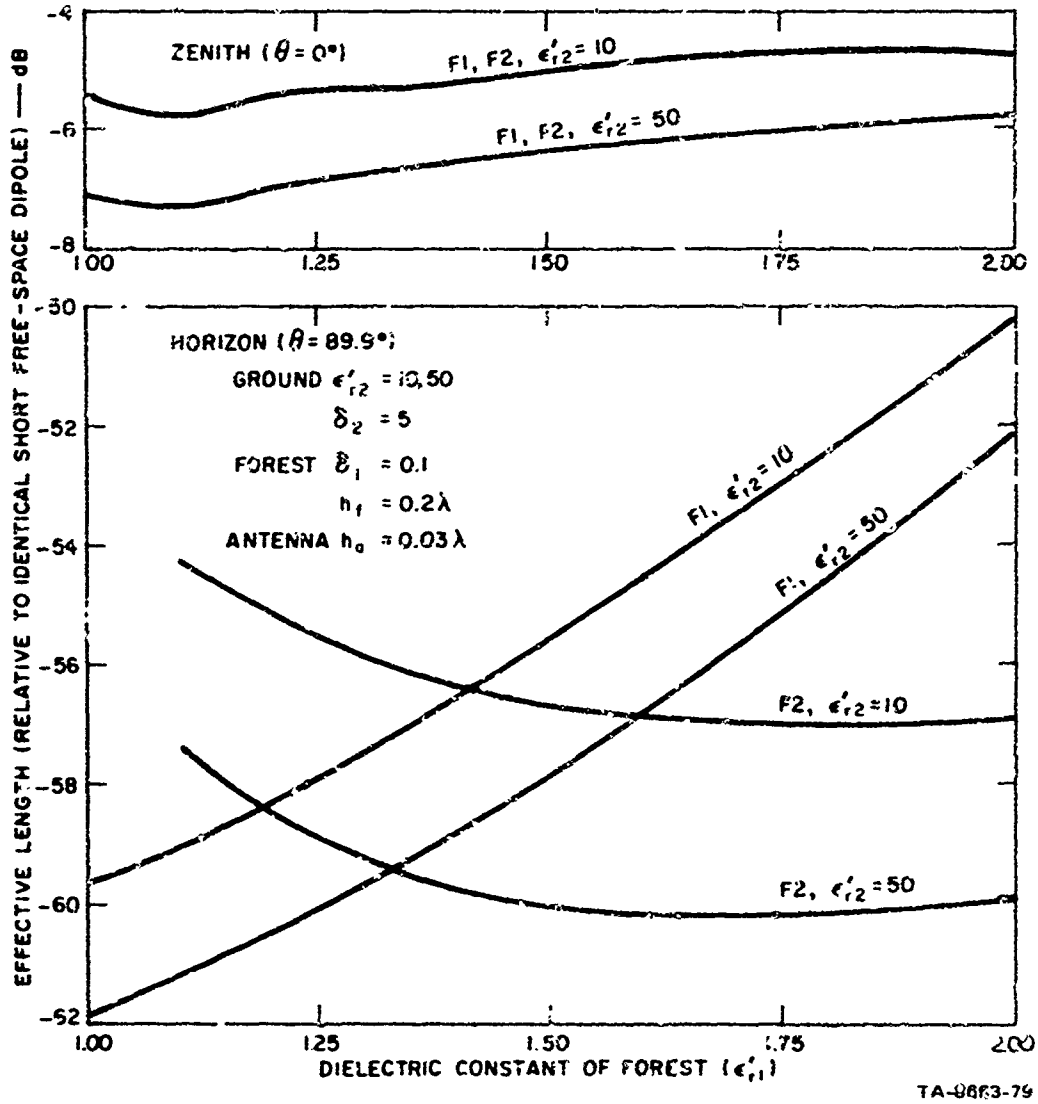

FIGURE 26 EFFECTIVE ANTENNA LENGTH AT ZENITH AND HORIZON AS A FUNCTION OF DIELECTRIC CONSTANT OF FOREST FOR TWO SETS OF GROUND CONSTANTS

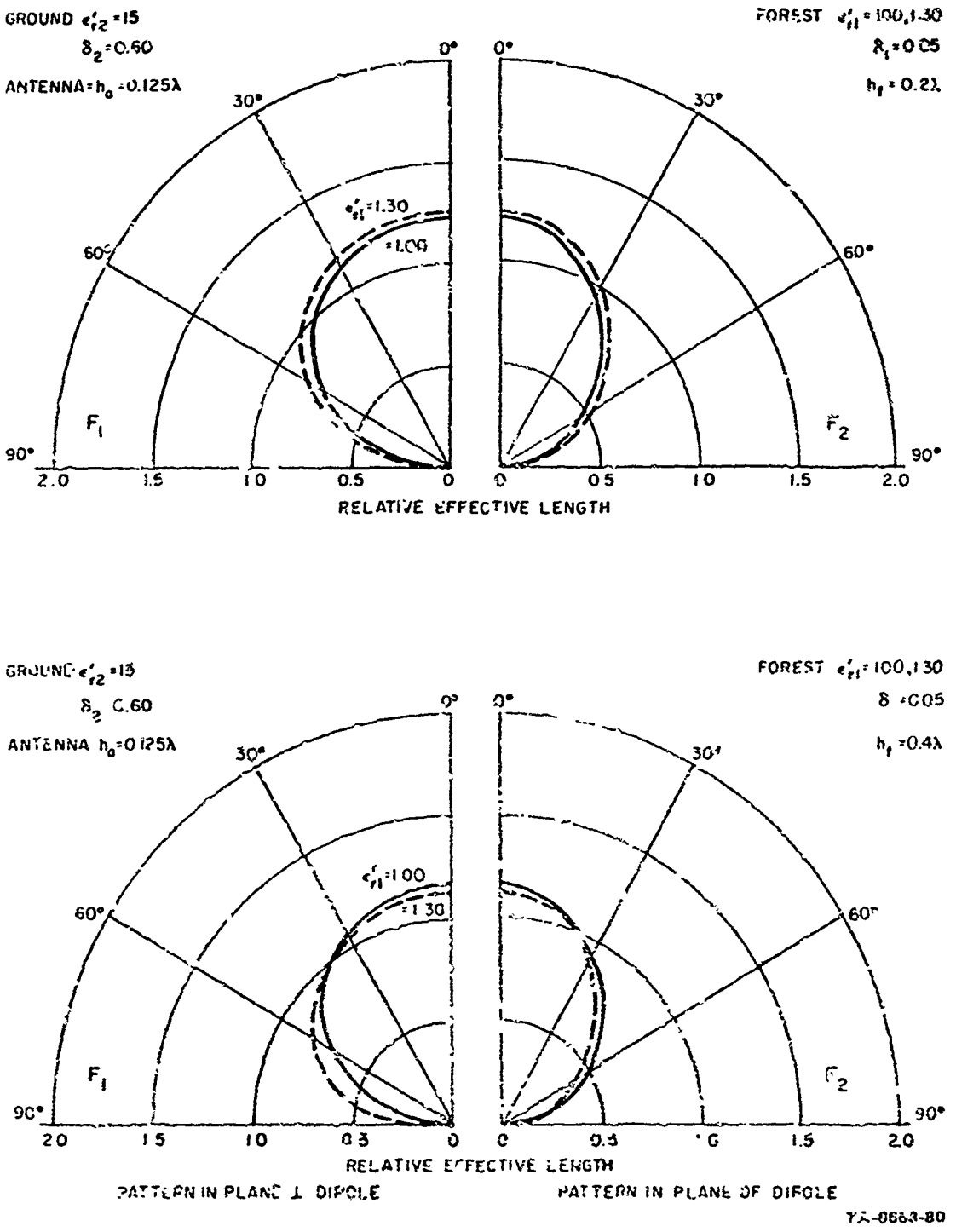

FIGURE 27 EFFECTIVE ANTENNA LENGTH VERSUS ELEVATION ANGLE FOR TWO FOREST DIELECTRIC CONSTANTS AND TWO FOREST HEIGHTS—h_a = 0.125 λ

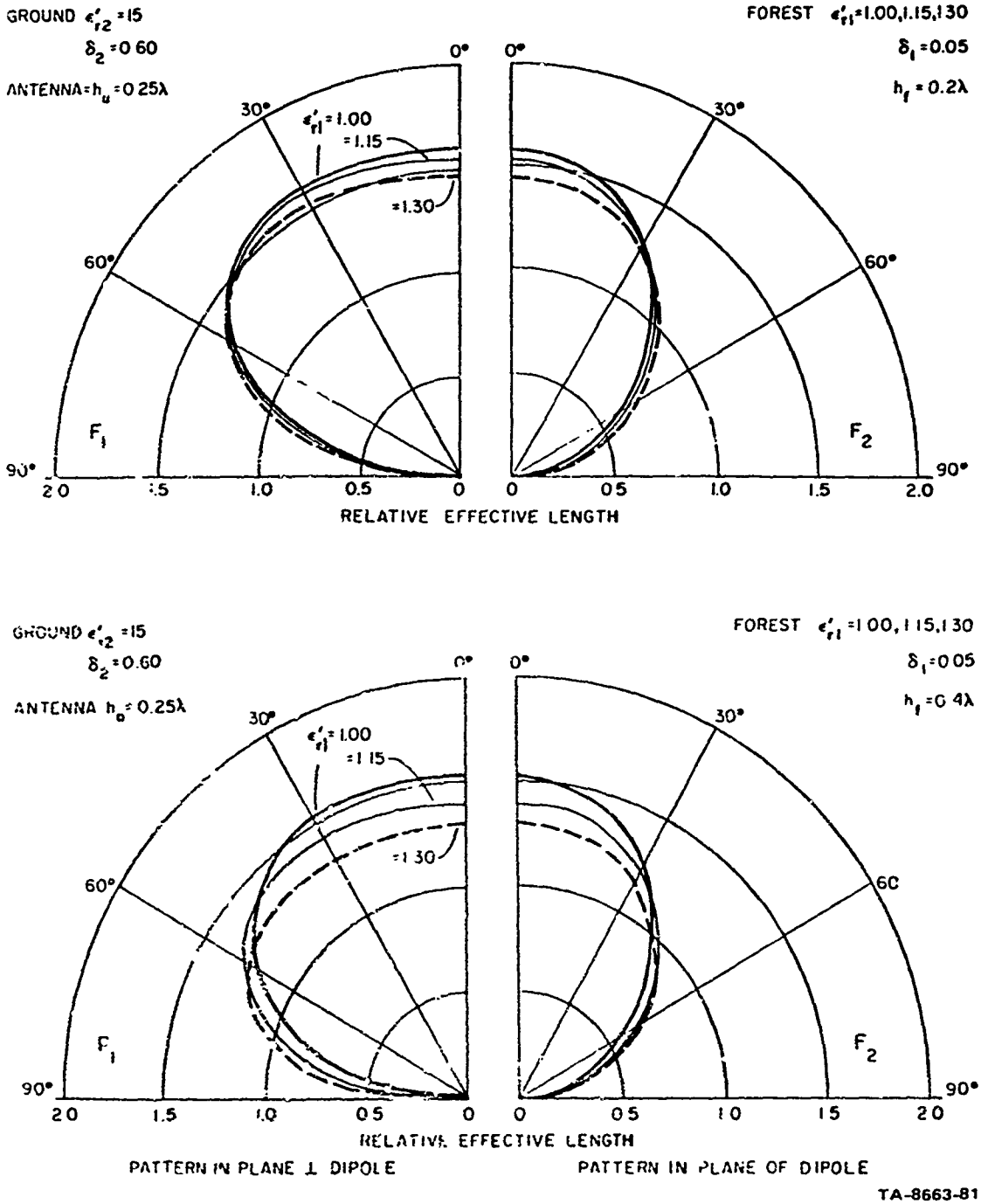

FIGURE 28 EFFECTIVE ANTENNA LENGTH VERSUS ELEVATION ANGLE FOR THREE FOREST DIELECTRIC CONSTANTS AND TWO FOREST HEIGHTS—h_a = 0.25 λ

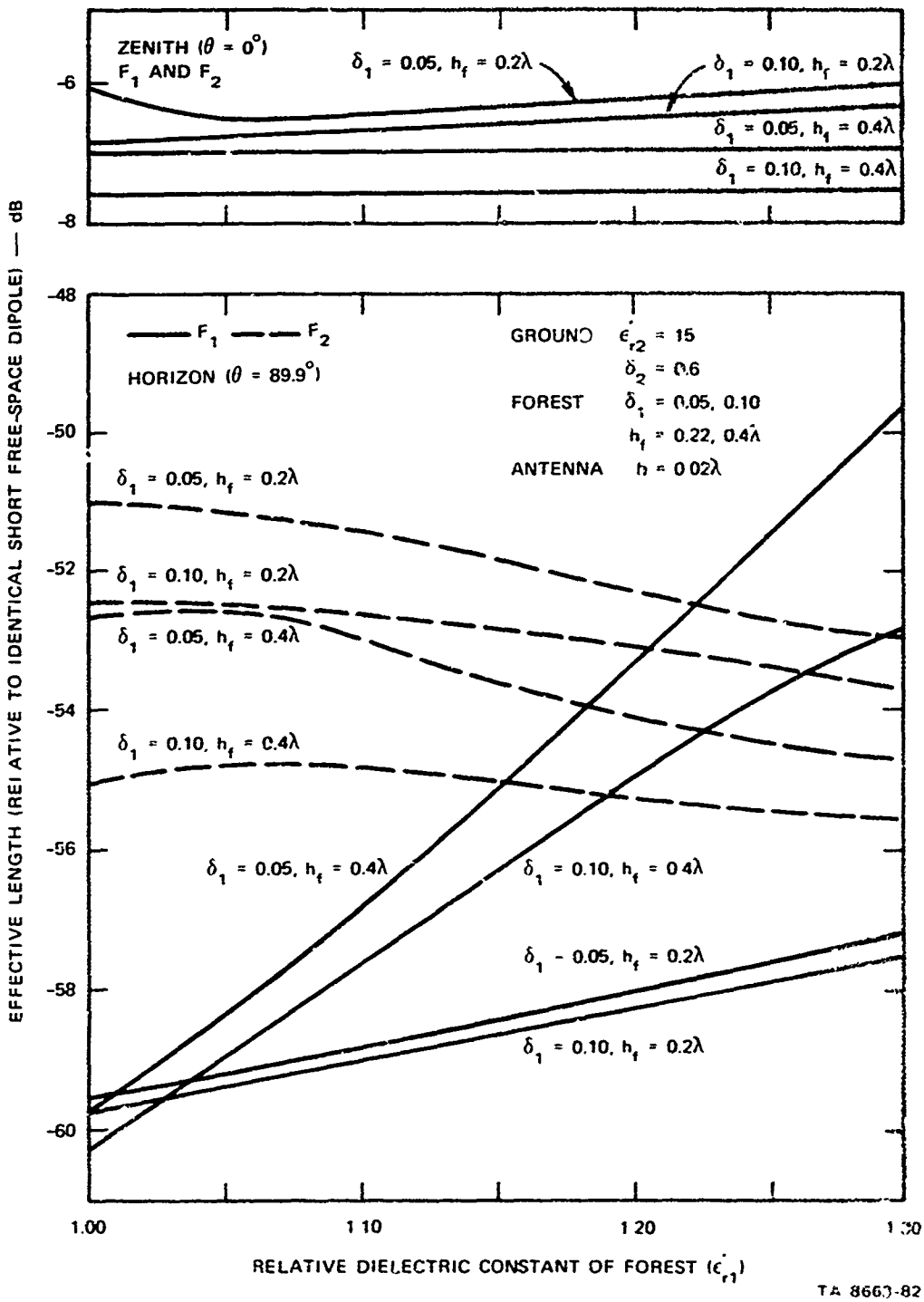

FIGURE 29 EFFECTIVE ANTENNA LENGTH AT ZENITH AND HORIZON AS A FUNCTION OF FOREST DIELECTRIC CONSTANT—h_a = 0.020 λ

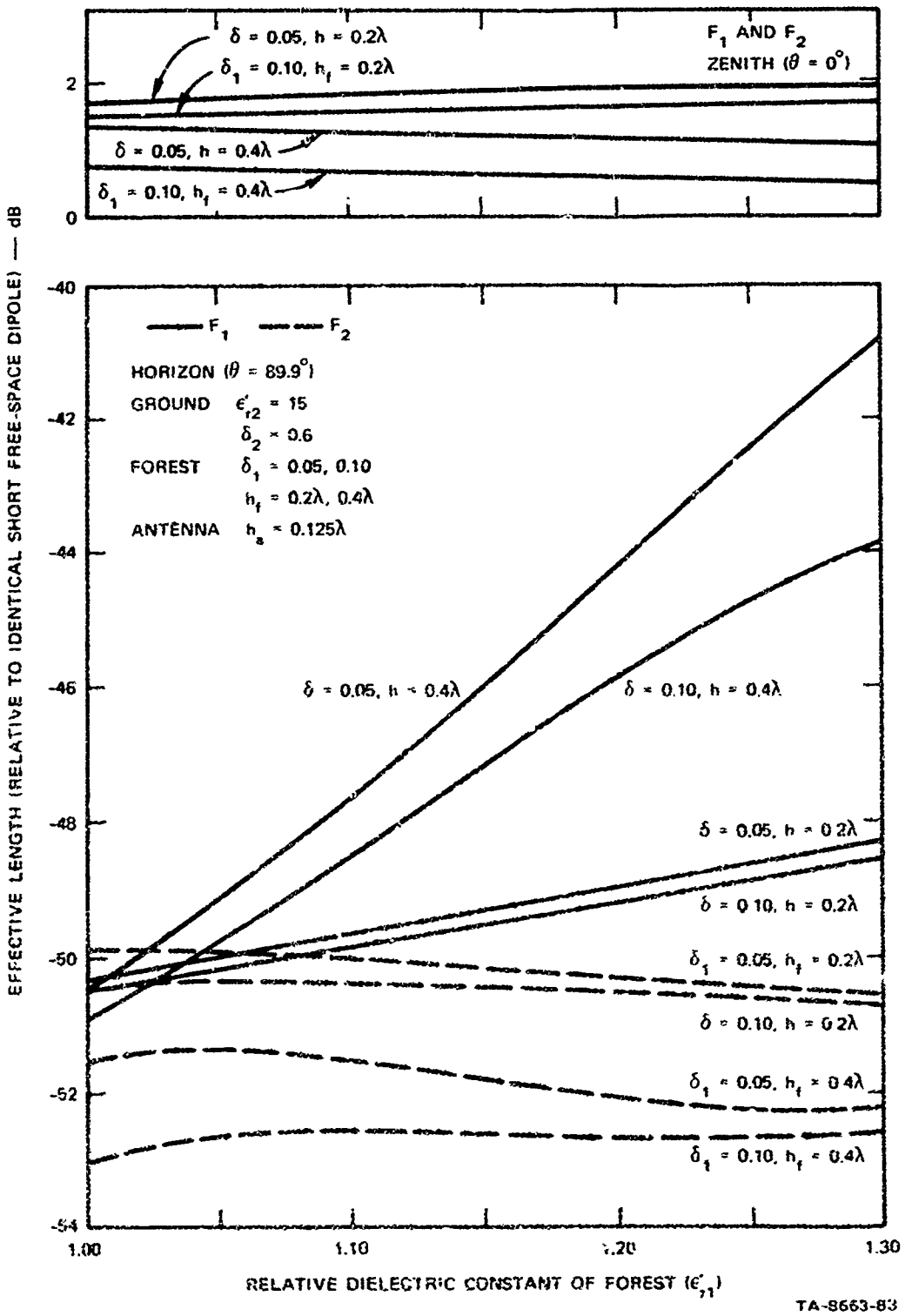

FIGURE 30 EFFECTIVE LENGTH AT ZENITH AND HORIZON AS A FUNCTION OF FOREST DIELECTRIC CONSTANT—h_a = 0.125 λ

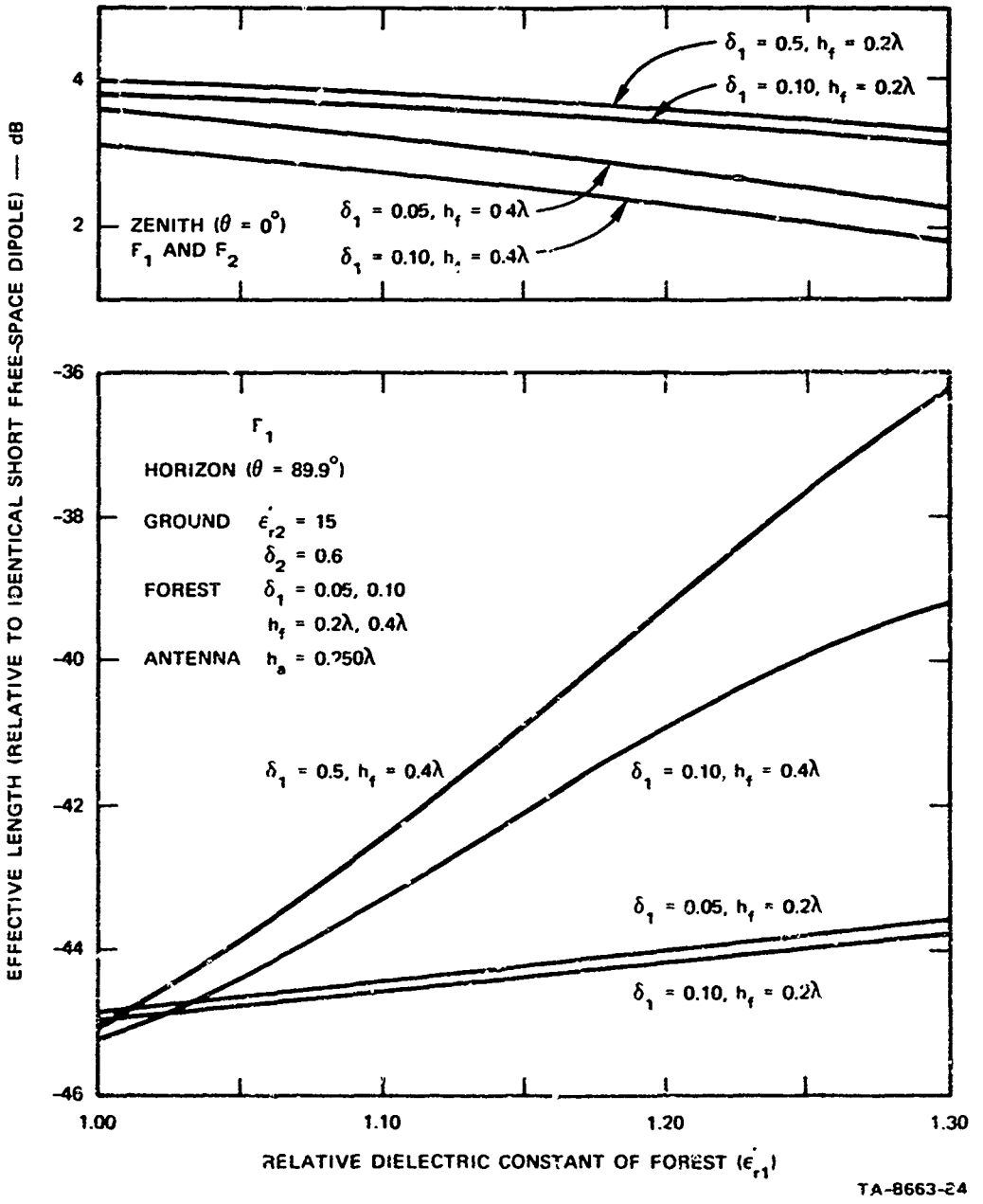

FIGURE 31 EFFECTIVE ANTENNA LENGTH AT ZENITH AND HORIZON AS A FUNCTION OF FOREST DIELECTRIC CONSTANT —h_a = 0.250 λ

C. Effect of the Loss Tangent of the Forest

In Figure 32 the variation of F_1 and F_2 for both high-angle and low-angle radiation is plotted as a function of the loss tangent of the forest. The effect of this parameter appears to be almost negligible.

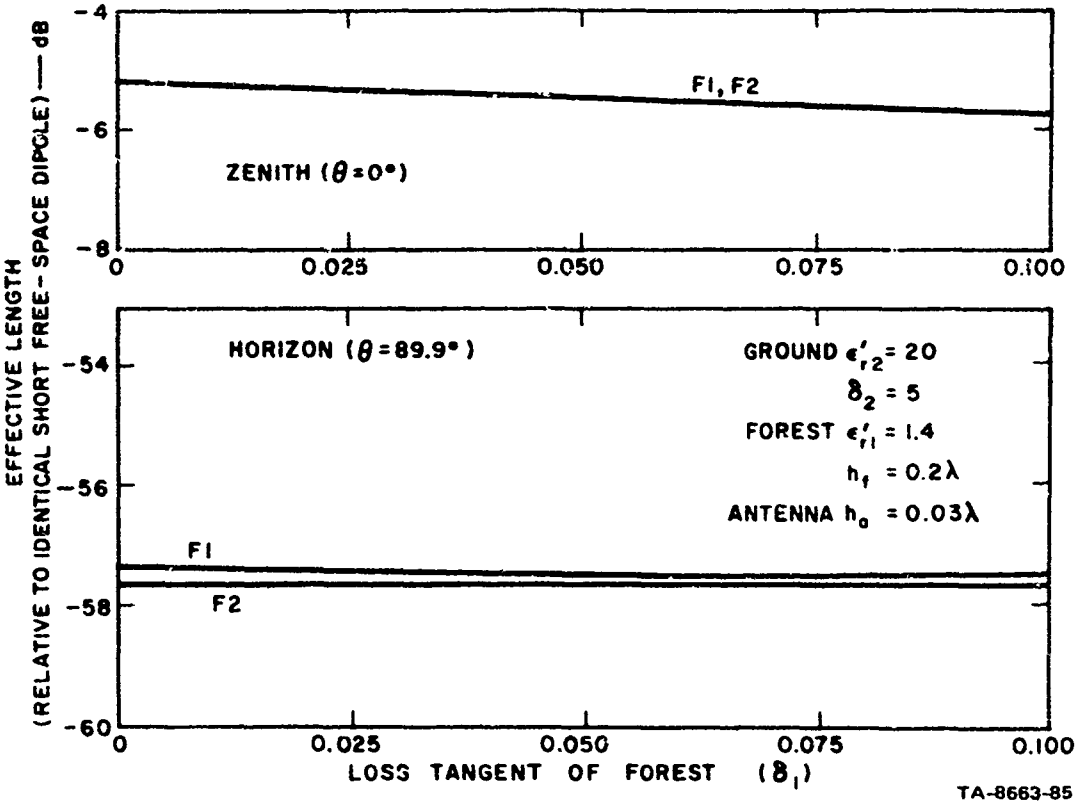

FIGURE 32 EFFECTIVE ANTENNA LENGTH AT ZENITH AND HORIZON AS A FUNCTION OF LOSS TANGENT OF FOREST

D. Effect of the Forest Height

Figure 33 shows the effect of forest height (in wavelengths) on the patterns. As in the case of the dielectric constant of the forest, the high-angle radiation is affected only slightly, while the low-angle radiation is affected rather markedly. The vertically polarized signal near the ends of the dipole decreases as forest height increases, while the horizontally polarized signal broadside to the antenna increases with forest height.

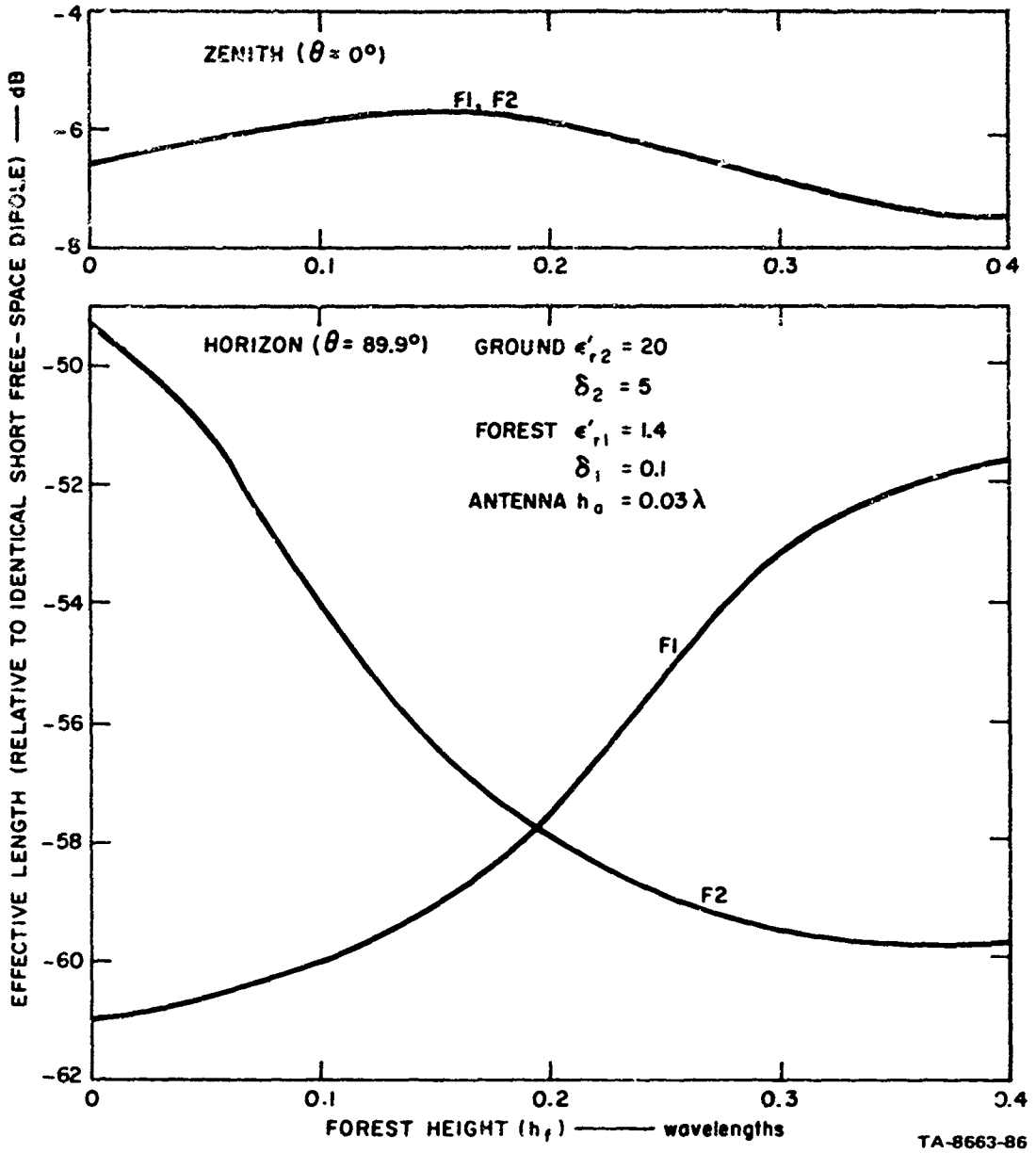

FIGURE 33 EFFECTIVE ANTENNA LENGTH AS A FUNCTION OF FOREST HEIGHT

E. Effect of Ground Constants

Figures 34 through 38 show the effect of ground constants on the patterns. Neither the effect of the dielectric constant nor that of the loss tangent is very marked and the affect lessened as the antenna height, h_a, increases. Note here that F_1 and F_2 vary with the same trend as the dielectric constant when it is changed, in contrast to the effect of the forest parameters.

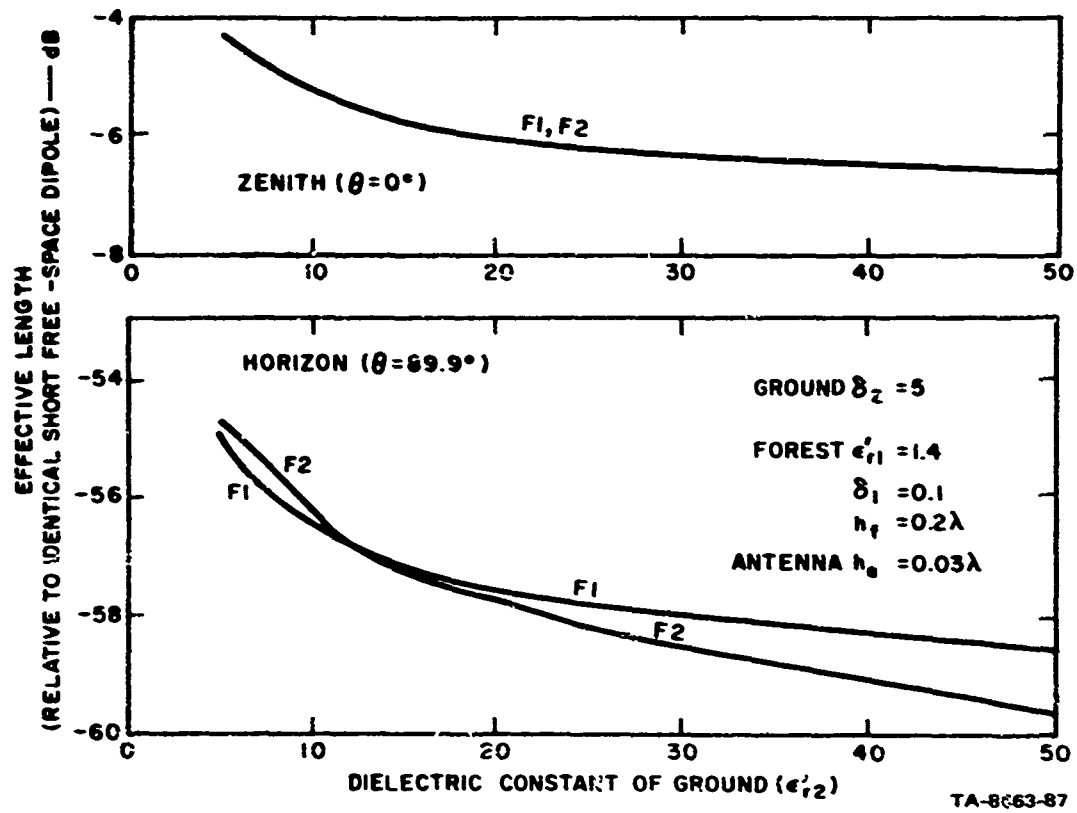

FIGURE 34 EFFECTIVE ANTENNA LENGTH AS A FUNCTION OF GROUND PERMITTIVITY

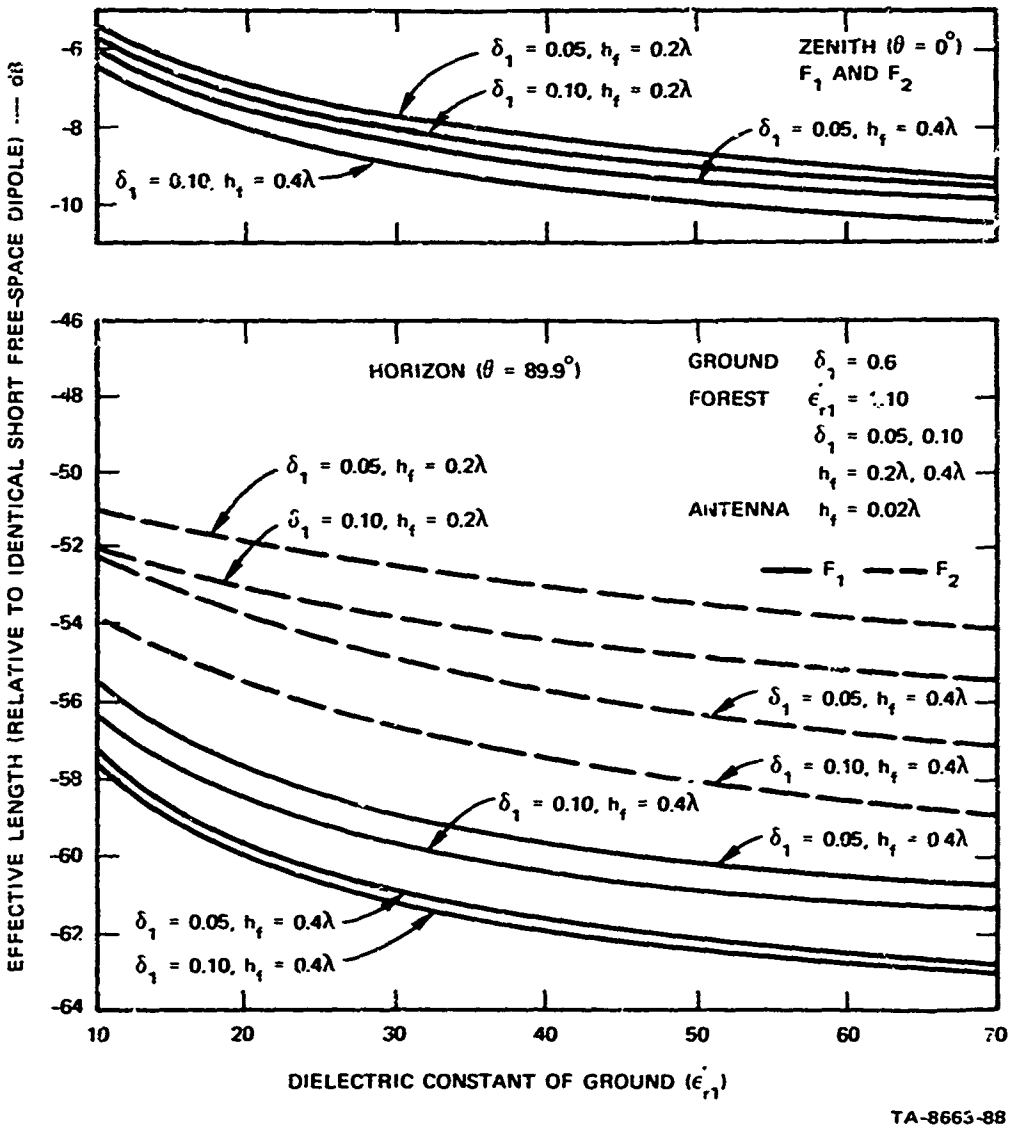

FIGURE 35 EFFECTIVE ANTENNA LENGTH AS A FUNCTION OF GROUND PERMITTIVITY—$h_a = 0.02\lambda$

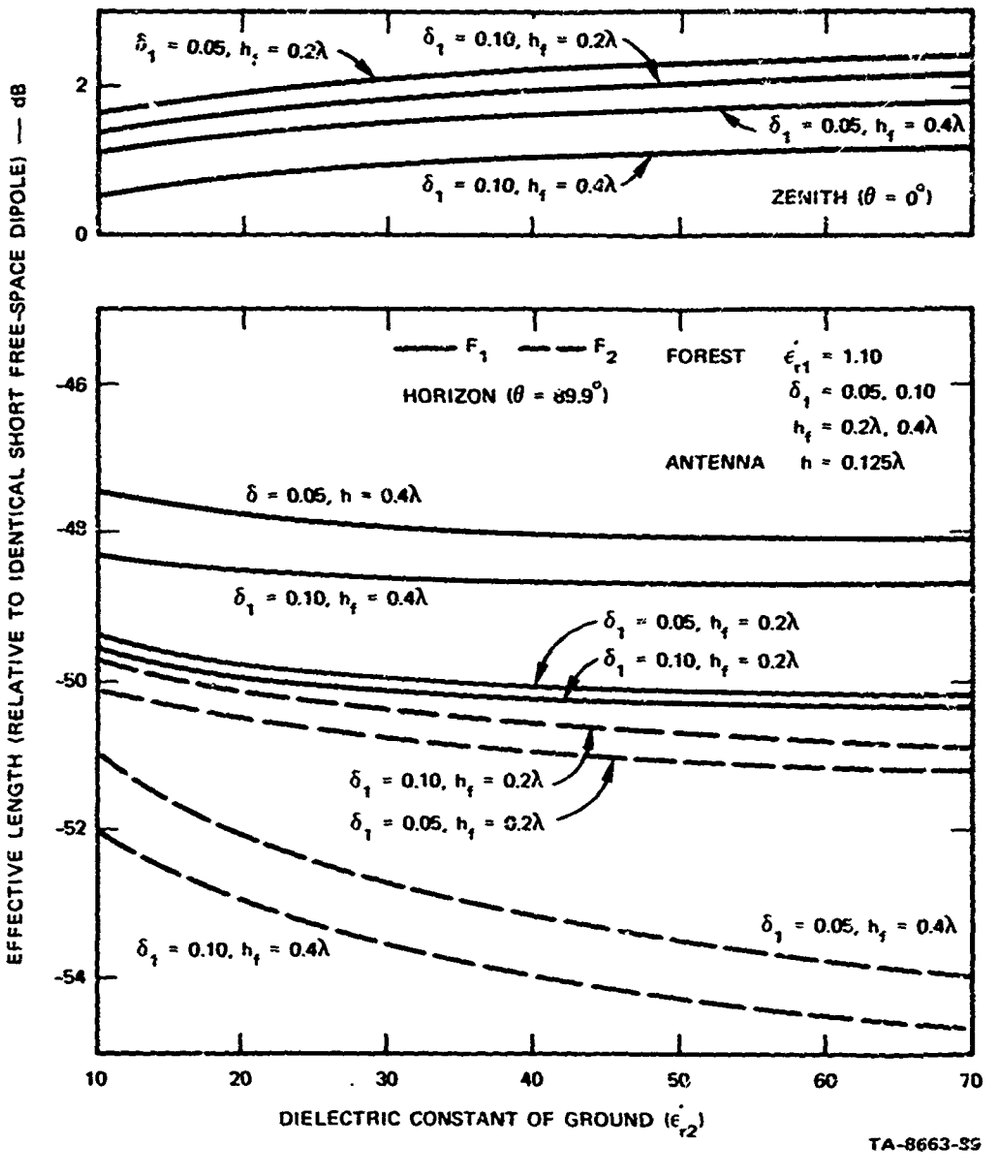

FIGURE 36 EFFECTIVE ANTENNA LENGTH AS A FUNCTION OF GROUND PERMITTIVITY—h_s 0.125 λ

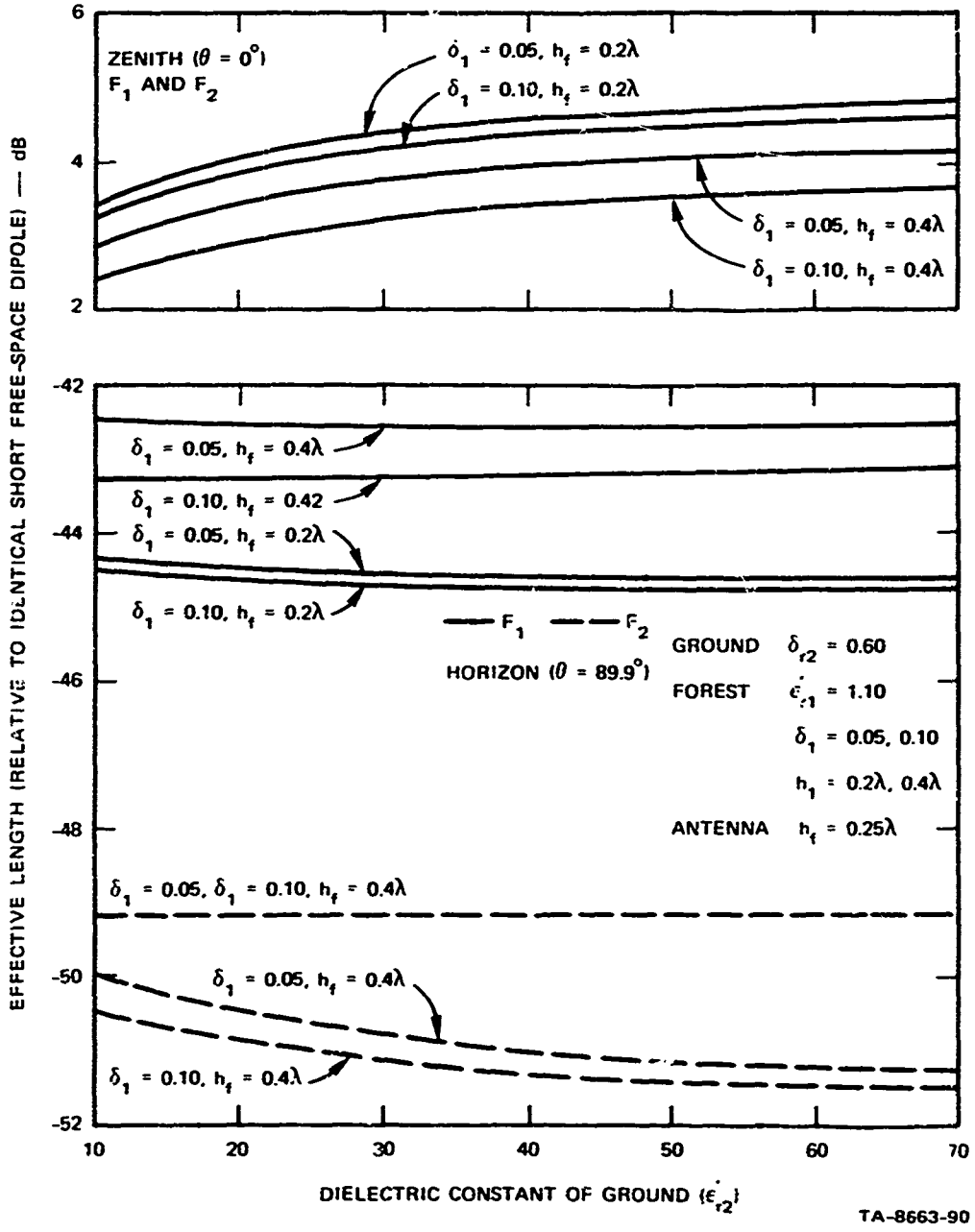

FIGURE 37 EFFECTIVE ANTENNA LENGTH AS A FUNCTION OF GROUND PERMITTIVITY—h_a = 0.25 λ

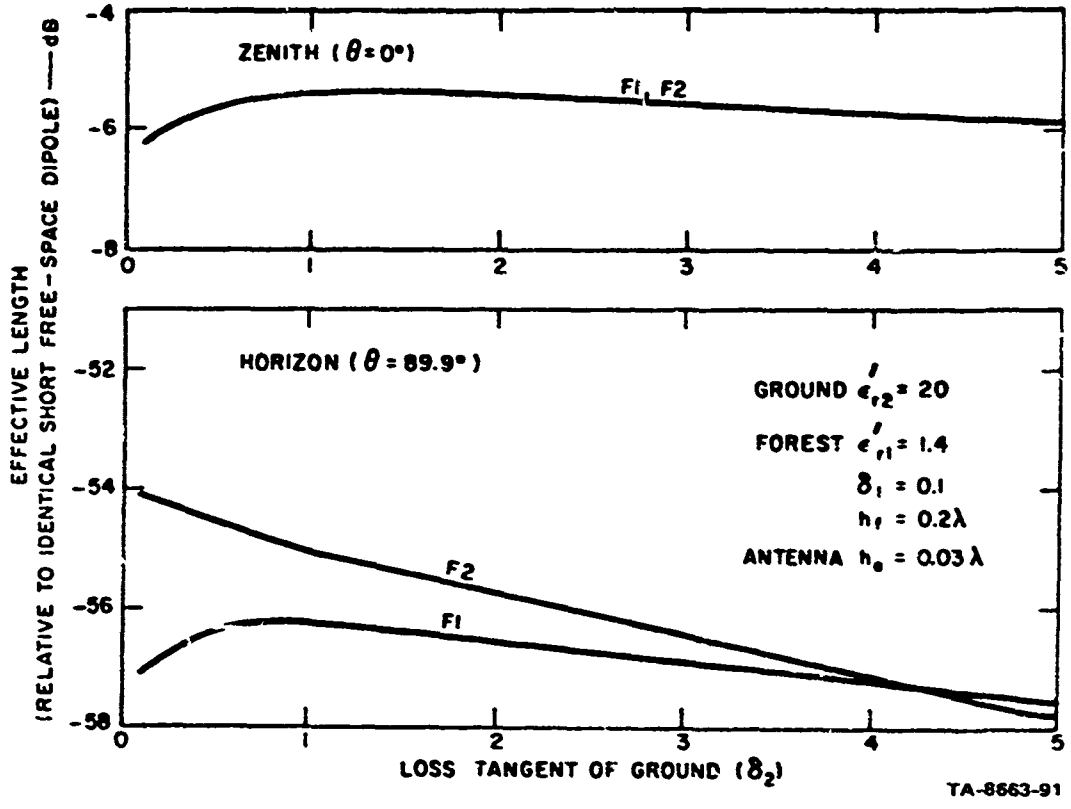

FIGURE 38 EFFECTIVE ANTENNA LENGTH AS A FUNCTION OF GROUND LOSS TANGENT

IX COMPARISON OF CALCULATED AND MEASURED PATTERNS

The computer program described in Section VII was used to calculate the expected radiation patterns of selected dipole antennas measured at Lodi, Almanor, and Ban Mun Chit. The ground and foliage electrical constants (σ and ϵ_r) were estimated for the computations of the Lodi and Almanor patterns and the values measured with the open-wire transmission line probe at Ban Mun Chit were used to predict the patterns at that site.

A. Comparison with Pattern Data from Lodi and Almanor

Example computations were performed previously and compared with the measured data at Lodi and Almanor to test the applicability of the model.[6,27]

Figures 39 and 40 show a comparison of the measured and computed radiation patterns of the 8-MHz horizontal dipole 23 ft above ground. The measured values were taken from measurements performed at Lodi and Almanor. Figure 39(a) is for the antenna at Lodi and Figure 39(b) is for the antenna in the forest at Almanor. The foliage electrical constants used for the application of the model of the antenna at Almanor were estimated from experimental measurements made in a similar conifer forest in the state of Washington.[7] Figure 40 is a composite of Figures 39(a) and 39(b). Of particular significance are the crossover of the (directivity) functions F_1 from the open field (solid curve in Figure 40) to the forest (dashed curve) case and the similar behavior of the measured values. Note also that at low elevation angles, the directivity

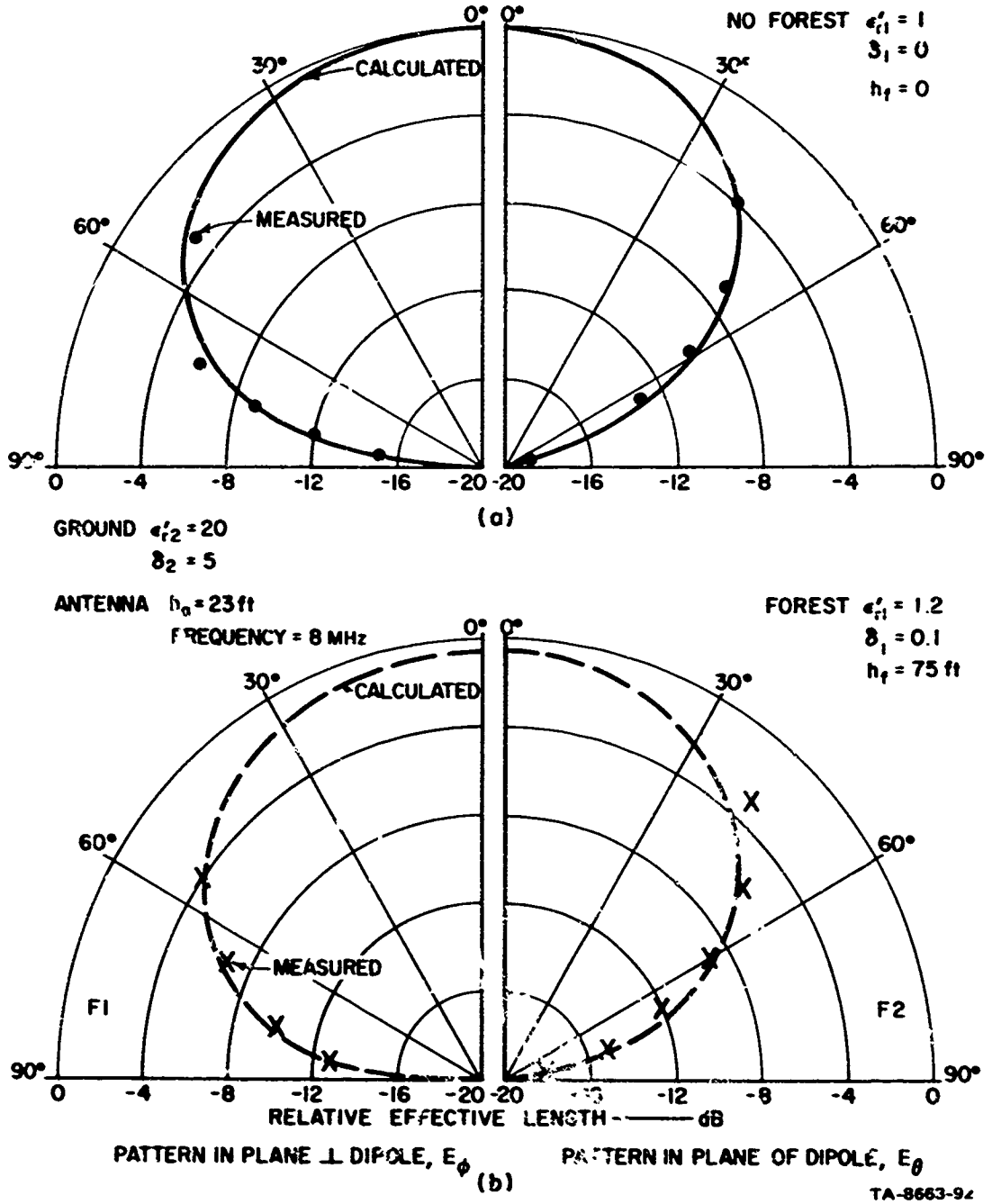

FIGURE 39 EFFECTIVE ANTENNA LENGTH, MEASURED AND CALCULATED, FOR DIPOLE ANTENNA

pattern in both planes was enhanced* when the antenna was immersed in the forest, as predicted by the model.

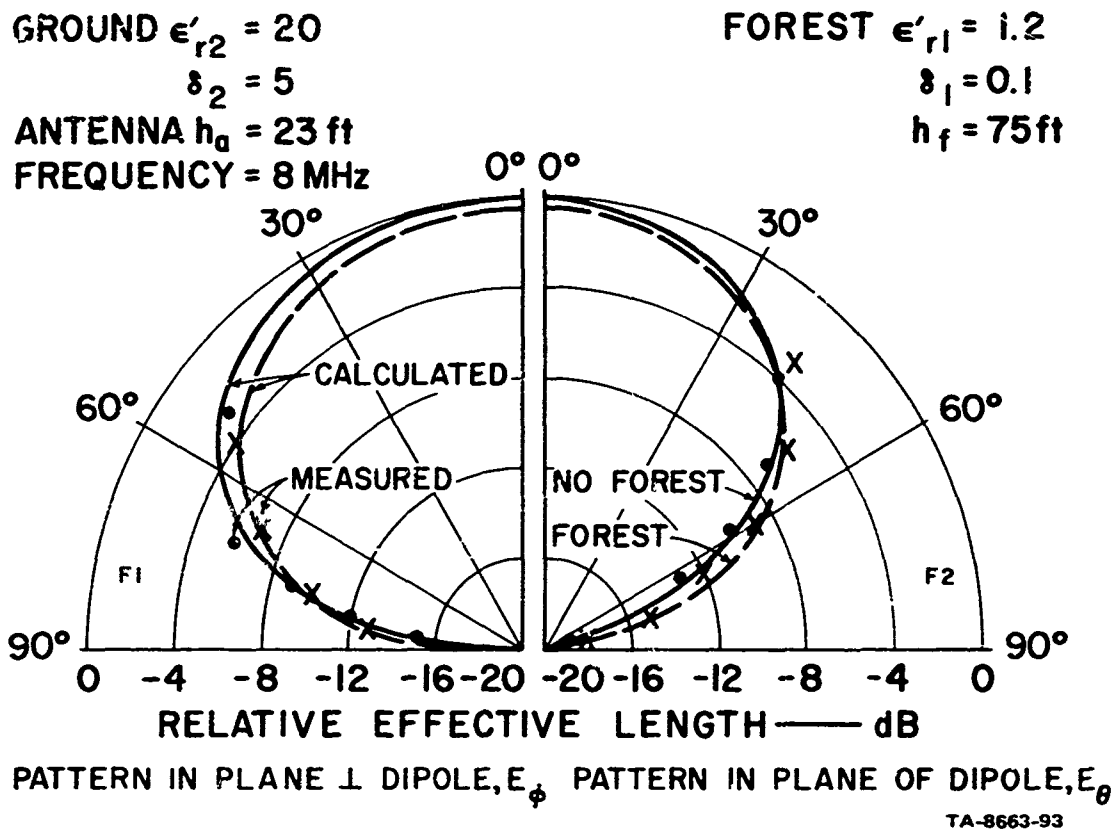

FIGURE 40 COMPARISON OF MEASURED AND CALCULATED EFFECTIVE ANTENNA LENGTHS FOR DIPOLE IN FOREST AND IN OPEN

*Relative to the open-field conditions.

B. Comparison with Pattern Data at Ban Mun Chit

The model was used to predict the expected radiation patterns of the dipole antennas measured at Ban Mun Chit and provide sufficient data points so that contours of computed signal strength could be drawn on the contour plots of the measured data.

In order to facilitate comparison of the calculated E_θ and E_ϕ patterns, the computed pattern data were normalized to the measured pattern data. The computed data were normalized by adding (or substracting) a constant value from the calculated values so that the lower-elevation portion of the calculated 3-dB contour would align itself to the estimated mean elevation angle of the lower portion of the 3-dB contour from the measured data (this was estimated by visual inspection of the contour plot of the measured data in each case). Physically, this procedure is similar to adding a constant gain to the antenna through the use of an amplifier or a loss of gain because of a matching circuit or impedance mismatch. On the plots comparing the measured and calculated data in Appendix C, the measured data are shown as solid curves and the computed data are shown as dashed curves. The contours for the computed data were calculated for 3-dB intervals from -3 dB to -15 dB but in some cases all contours are not shown on the contour plots.

The ground and foliage electrical constants used in the model were based on the measured data presented in Figures 5 and 6. These constants were $\epsilon_r = 15.0$, $\delta = 0.60$ for the ground, and $\epsilon_r = 1.12$, $\delta = 0.09$ for the forest. These parameters have been defined in Section VII-A. For modeling purposes the forest height (h_f) at Ban Mun Chit was assumed to be 65 ft. Only 2 percent of the trees at this site exceeded this height.

The calculated and measured patterns of the 6-MHz balanced dipole in the clearing, over a ground screen, compare reasonably well at the

design frequency of the antenna although the E_θ pattern data compare slightly better than the E_ϕ pattern data as can be seen in Figures C-1 and C-2.

The measured pattern data for the 6-MHz balanced dipole and the 6-MHz unbalanced dipole antenna in the clearing should be quite similar since these patterns resulted from the same antenna (except for the balun) measured in the same location. The measured data for the two cases compare favorably at resonance but the pattern of the unbalanced dipole becomes distorted at frequencies below resonance--possibly because of the impedance mismatch between the antenna and the 50-Ω coaxial transmission line causing the transmission line to become an active part of the antenna. At 3 MHz the computed and measured data compare more favorably for the balanced dipole than for the unbalanced dipole. The patterns for the complete hemisphere above the antenna were calculated for the balanced dipole at 3 MHz (instead of one-half of the pattern as was done in most cases). At 4 MHz, the computed and measured patterns become more similar for the respective antennas, and the measured patterns for the balanced and unbalanced dipole antennas also become more similar. Two estimates of the mean value of the elevation angle for the 3-dB contour for both the E_ϕ pattern at 4 MHz and the E_θ pattern at 6 MHz for balanced dipole were used with the model and the results of these calculations are shown in Figures C-6 and C-7. These plots show the effect that a small change in the estimated elevation angle of the 3-dB contour (2°) can cause in the elevation angle of the lower contours. The calculated and measured patterns for the balanced and unbalanced dipole are similar at 6 MHz. From the results of these two antennas, it appears that the computer model predicts the patterns of the antennas reasonably well at the resonant frequency and the correlation between the calculated and measured results decreases as the frequency is decreased below the design frequency of the antenna.

The measured patterns of the 6-MHz balanced dipole antenna 41 ft above the ground in the forest and the 6-MHz unbalanced dipole antenna 41 ft above the ground in the forest resulted from two antenna configurations (i.e., with and without balun) in the same location, as was the case with the balanced and unbalanced dipoles in the clearing. Ideally, the measured patterns from these two antennas should be similar. Calculated and measured data are available only for the unbalanced dipole at 3 MHz, and the measured pattern is quite distorted; thus there is little similarity between the measured and predicted patterns for this antenna at 3 MHz as can be seen in Figures C-17 and C-18. At 6 MHz, the measured patterns for the two antennas are similar for the E_ϕ response but the E_θ response of the unbalanced dipole is distorted. The measured and computed patterns for the E_ϕ response of these antennas are similar for elevation angles above 10° and in the areas in the pattern maxima. The least similarity between the calculated and measured patterns occurs for the unbalanced dipole for both polarizations.

As the height of the 6-MHz unbalanced dipole was decreased to 16, 8, and 2 ft, the discrepancy between the calculated and measured patterns became worse, but not extreme, as can be seen in Figures C-21 through C-28. The discrepancies usually occur at elevation angles below 20° elevation, where there is a 3-dB difference between the calculated and measured results. The worst discrepancy appears on the pattern of the dipole when it is 2 ft high, but the measured pattern data indicate that the coaxial feed line was apparently acting as part of the active antenna circuit and thus forming three lobes at 4 MHz (Figure C-25 in particular) and this probably also distorts the pattern somewhat at 6 MHz (Figures C-27 and C-28).

The measured and calculated patterns for the E_ϕ response of the 8-MHz, 23-ft-high unbalanced dipole in the forest are reasonably similar,

whereas the measured $E_{\hat{\theta}}$ pattern is distorted and does not agree with the calculated contours. But from the measured patterns of the monopole at Ban Mun Chit (Figure A-25) it can be seen that the E_{θ} polarization becomes somewhat scattered at 8 MHz whereas the model approximates the forest as an isotropic slab.

X ANTENNA GAINS

Relative gains for the measured antennas were presented in the reports describing the antenna pattern measurements.[2,3,4] This section summarizes these relative gain data and outlines a method for estimating the absolute gains of these antennas. The relative gains and the estimated absolute gains of the measured antennas are presented at the end of Section B of this section (Table 8), but before using this table it is recommended that the following two sections of this chapter be reviewed in order to fully understand the data presented in the table.

A. Measured Relative Gains

The term "relative" gain is used in this section to distinguish it from "absolute" gain, which is usually derived theoretically and expressed in decibels above a standard reference level--e.g., an isotropic radiator. The relative gains of the antennas provided in this report are derived from the maximum observed voltage across the 50-ohm inputs of the receivers used for the pattern measurements--e.g., 0-dB on the contour plots. The relative gains of the antennas into the 50-ohm receiver inputs can be calculated by subtracting the attenuations of the coaxial antenna feed lines from the maximum observed signals. Such relative gain values for the antennas were presented in Refs. 2, 3, and 4 and are repeated in Tables 2 through 4 of this report for the convenience of the reader. Knowing the relative gains of the antennas into 50-ohm loads and knowing the feedpoint impedance of the antennas at the pattern measurement frequency, one can easily calculate the loss due to the mismatch of antennas to the 50-ohm receiver input and thus derive

Table 2

RELATIVE VOLTAGE GAINS ACROSS 50-OHM LOADS AT PATTERN MAXIMA--LODI

Antenna and Design Frequency, f_o	Measurement		Relative Voltage (dB)	E_θ/E_ϕ (dB)
	Frequency (MHz)	Polarization		
30° Slant wire	2.0	θ	-50.1	+5.7
(4 MHz)		φ	-55.8	
	4.0	θ	-28.9	+6.6
		φ	-35.5	
	6.0	θ	-30.5	+4.8
		φ	-35.3	
2:1 Inverted L	2.6	θ	-66.4	
(8 MHz)	5.0	θ	-44.8	+3.4
		φ	-48.2	
	8.0	θ	-32.6	-5.1
		φ	-27.5	
5:1 Inverted L	4.0	θ	-29.6	+5.4
(10 MHz)		φ	-35.0	
	6.0	θ	-30.3	+4.7
		φ	-35.0	
	10.0	θ	-26.6	+0.6
		φ	-27.2	
Unbalanced dipole	5 0	θ	-50.2	+6.0
23 ft high		φ	-56.2	
(8 MHz)	8.0	θ	-22.1	-0.5
		φ	-21.6	
	15.0	θ	-20.3	-2.5
		φ	-17.8	
Unbalanced dipole	2.0	θ	-54.9	
2 ft high	4.0	θ	-45.1	+0.6
(6 MHz)		φ	-45.7	
	6.0	θ	-31.8	-6.0
		φ	-25.8	
	10.0	θ	-40.0	-4.9
		φ	-35.1	
Sleeve dipole	5.0	θ	-44.8	+4.7
(5 MHz)		φ	-49.5	
	8.0	θ	-45.4	+2.8
		φ	-48.2	
Monopole	2.0	θ	-72.5	--
(15 MHz)	4.0	θ	-49.8	--
	5.0	θ	-61.8	--
	6.0	θ	-48.1	--
	8.0	θ	-39.3	--
	10.0	θ	-27.1	--
	15.0	θ	-10.8	--
Balanced dipole	4.0	φ	-53.8	--
(15 MHz)	5.0	φ	-63.0	--
	6.0	φ	-47.8	--
	8.0	φ	-37.9	--
	10.0	φ	-28.0	--
	15.0	φ	- 9.8	--

NOTE: These relative gains should not be compared between sites or between different frequencies at the same site.

Table 3

RELATIVE VOLTAGE GAINS ACROSS 50-OHM LOADS AT PATTERN MAXIMA--ALMANOR

Antenna and Design Frequency	Measurement		Relative Voltage (dB)	E_θ/E_ϕ (dB)
	Frequency (MHz)	Polarization		
30° Slant wire	2	θ	-39.7	--
(4 MHz)	4	θ	-21.3	+9.8
		φ	-31.1	
	6	θ	-23.1	+2.7
		φ	-25.8	
60° Slant wire	5	θ	-25.3	+10.8
(5 MHz)		φ	-36.1	
	15	θ	-13.9	+6.1
		φ	-20.0	
2:1 Inverted L	2.67	θ	-23.7	+10.1
(8 MHz)		φ	-33.8	
	8	θ	-11.3	-2.3
		φ	-9.0	
5:1 Inverted L	10	θ	-17.8	-5.1
(10 MHz)		φ	-12.7	
Unbalanced	2.67	θ	-47.2	+11.9
dipole		φ	-58.3	
23 ft high	5	θ	-36.7	+8.9
(8 MHz)		φ	-45.6	
	8	θ	-6.9	-0.5
		φ	-6.4	
	15	θ	-14.6	0.0
		φ	-14.6	
Unbalanced	2	θ	-61.4	--
dipole	4	θ	-40.9	--
2 ft high	6	θ	-20.7	+5.6
(6 MHz)		φ	-26.3	
	10	θ	-23.8	+10.5
		φ	-34.3	
Monopole	2	θ	-56.8	
(15 MHz)	2.67	θ	-56.6	
	4	θ	-42.4	
	5	θ	-46.8	
	6	θ	-36.4	
	8	θ	-26.0	
	10	θ	-21.0	
	15	θ	-12.9	
Balanced	2	φ	--	
dipole	2.67	φ	-62.0	
(15 MHz)	4	φ	-53.7	
	5	φ	-52.0	
	6	φ	-40.6	
	8	φ	-27.8	
	10	φ	-24.0	
	15	φ	-12.4	

Table 4

RELATIVE VOLTAGE GAINS ACROSS 50-OHM LOADS AT PATTERN MAXIMA--BAN MUN CHIT

Antenna and Design Frequency	Measurement		Relative Voltage (dB)	E_θ/E_ϕ (dB)
	Frequency (MHz)	Polarization		
Balanced dipole over ground screen in clearing (6 MHz)	3.0	θ	-44.2	+6.5
		φ	-50.7	
	4.0	θ	-39.9	-0.6
		φ	-39.3	
	6.0	θ	-26.3	-2.9
		φ	-23.4	
	8.0	θ	-25.5	-5.3
		φ	-20.2	
Balanced dipole in clearing (6 MHz)	3.0	θ	-53.5	-2.4
		φ	-51.1	
	4.0	θ	-41.4	+0.2
		φ	-41.6	
	6.0	θ	-26.9	-2.8
		φ	-24.1	
	8.0	θ	-26.5	-5.8
		φ	-20.7	
Unbalanced dipole in clearing (6 MHz)	3.0	θ	-49.2	+9.2
		φ	-58.4	
	4.0	θ	-47.5	+2.6
		φ	-50.1	
	6.0	θ	-26.2	-5.4
		φ	-20.8	
	8.0	θ	-33.5	-5.1
		φ	-28.4	
Balanced dipole in foliage (6 MHz)	6.0	θ	-57.5	-3.0
		φ	-54.5	
Unbalanced dipole in foliage (6 MHz)	3.0	θ	-56.1	>5.5
		φ	-[illegible].6	
	4.0	θ	-[illegible].1	+2.8
		φ	-49.9	
	6.0	θ	-20.3	+3.5
		φ	-23.8	
	8.0	θ	-34.6	-6.3
		φ	-28.3	
Unbalanced dipole in foliage 16 ft high (6 MHz)	6.0	θ	-26.7	-3.6
		φ	-23.1	
Unbalanced dipole in foliage 8 ft high (6 MHz)	6.0	θ	-26.5	+1.0
		φ	-27.5	
Unbalanced dipole 2 ft high (6 MHz)	4.0	θ	-55.1	0.0
		φ	-55.1	
	6.0	θ	-34.4	+2.8
		φ	-37.2	
	8.0	θ	-39.6	+1.4
		φ	-41.0	

Table 4 (continued)

Antenna and Design Frequency	Measurement		Relative Voltage (dB)	E_θ / E_ϕ (dB)
	Frequency (MHz)	Polarization		
Unbalanced dipole 23 ft high (8 MHz)	8.0	θ	-22.8	-2.9
		φ	-19.9	
Balanced dipole over ground screen in clearing (15 MHz)	4.0	θ	-63.0	-0.7
		φ	-62.3	
	6.0	θ	-50.3	-1.8
		φ	-48.5	
	8.0	θ	-41.3	-2.6
		φ	-38.7	
	12.0	θ	-29.0	-4.2
		φ	-24.8	
	15.0	θ	-20.4	-4.0
		φ	-16.4	
Sleeve dipole (6 MHz)	6.0	θ	-41.9	+2.7
		φ	-44.6	
Monopole in clearing (6 MHz)	6.0	θ	-27.5	--
Monopole on edge of clearing (6 MHz)	4.0	θ	-63.9	--
	6.0	θ	-29.6	--
	8.0	θ	-47.2	--
Monopole in foliage (6 MHz)	4.0	θ	-61.0	--
	6.0	θ	-37.0	--
	8.0	θ	-43.8	--
2:1 Inverted L (6 MHz)	3.0	θ	-46.5	+0.7
		φ	-47.2	
	4.0	θ	-44.7	-0.1
		φ	-44.6	
	6.0	θ	-29.2	-3.0
		φ	-26.2	
	8.0	θ	-34.1	-1.5
		φ	-32.6	
2:1 Inverted L (8 MHz)	8.0	θ	-34.3	-1.0
		φ	-33.3	
5:1 Inverted L (6 MHz)	4.0	θ	-43.2	+1.3
		φ	-44.5	
	6.0	θ	-32.4	-4.3
		φ	-28.1	
	8.0	θ	-31.0	+2.8
		φ	-33.8	
5:1 Inverted L (10 MHz)	10.0	θ	-32.4	-3.5
		φ	-28.9	
30° Slant wire (4 MHz)	4.0	θ	-38.6	+4.6
		φ	-43.2	
30° Slant wire (6 MHz)	3.0	θ	-57.8	+9.2
		φ	-67.0	
	4.0	θ	-51.4	+7.3
		φ	-58.7	
	6.0	θ	-39.4	+5.8
		φ	-45.2	
	8.0	θ	-35.5	+5.4
		φ	-40.9	

Table 4 (concluded)

Antenna Design Frequency	Measurement Frequency (MHz)	Measurement Polarization	Relative Voltage (dB)	E_θ/E_ϕ (dB)
Loop in clearing (6 MHz)	6.0	θ	-51.0	+1.4
		φ	-52.4	
Loop in foliage (6 MHz)	6.0	θ	-52.9	+0.7
		φ	-53.6	
Longwire (6 MHz)	3.0	θ	-62.5	+2.5
		φ	-65.0	
	4.0	θ	-55.8	-1.3
		φ	-54.5	
	6.0	θ	-42.3	+3.0
		φ	-45.3	
	8.0	θ	-42.1	+1.5
		φ	-43.6	
Balanced dipole, J&B type, 40 ft high (6 MHz)	6.0	θ	-21.1	-4.5
		φ	-16.6	
Balanced dipole, J&B type, 80 ft high (6 MHz)	6.0	θ	-24.6	-3.5
		φ	-21.1	
Balanced dipole, J&B type, 40 ft high (12 MHz)	12.0	φ	-16.1	--
J&B type 40-ft vertical (6 MHz)	6.0	θ	-28.9	--
J&B type 80-ft vertical (2 MHz)	2.0	θ	-42.3	--
J&B type 20-ft vertical (12 MHz)	12.0	θ	-17.5	--

the relative gains of the antennas into matched loads (see Tables 5 through 7). It can be assumed that the data in Tables 5 through 7 are accurate to ±3 dB.* The cases where the sum of the errors, including the impedance and voltage-gain errors, is potentially in excess of 3 dB have been designated by an asterisk. Potential errors of the unmarked values are less than 3 dB. Again, it should be remembered that the values presented in Tables 5 through 7 are not the maximum obtainable signal but the maximum observed signal. For example, the maximum for a short monopole is usually observed within the 5° to 60° elevation range of the measurements (typically the maximum occurs at about 40°), whereas the maximum of a half-wavelength dipole situated a quarter-wavelength above the ground is at the zenith and was not observed while the Xeledop was being towed in circular orbits.

Tables 2 through 4 and 5 through 7 can be used for comparison of the relative gains of different antennas into 50-ohm and matched loads, respectively, as long as this is done at the same frequency and at the same site or for comparing the relative maximum response of the same antennas to the two polarizations, E_θ and E_ϕ; but when comparisons are to be made between sites or between frequencies, one is then considering comparisons of absolute gain, which is discussed in the next section. In order to obtain a conservative comparison of relative gain between antenna types, however, the data of Tables 2 through 4 (relative observed maximum voltage across 50-ohm receiver inputs) have been used for the following discussion.

---

*In most cases these relative gains are accurate to better than ±2 dB (as indicated in References 2, 3, and 4), and ±3 dB can be regarded as a conservative estimate of the accuracy of these relative-gain data.

Table 5

RELATIVE POWER GAINS INTO MATCHED LOADS
AT PATTERN MAXIMA--LODI

Measurement Frequency (MHz)	Antenna Type	Antenna Design Frequency (MHz)	Potential Error*	Gain† E_θ (dB)	Gain† E_ϕ (dB)
2.67	2:1 Inverted L	8		0.0	-10.1
	Balanced dipole	15	x	--	-33.4
4	30° Slant wire	4		0.0	-9.8
	Unbalanced dipole 2 ft high	6	x	-15.2	--
	Balanced dipole	15		--	-29.1
5	60° Slant wire	5		0.0	-10.8
	Unbalanced dipole 23 ft high	8	x	-7.8	-16.7
	Balanced Dipole	15		--	-26.1
6	30° Slant wire	4	x	0.0	-2.7
	Unbalanced dipole 2 ft high	6		-3.0	-8.6
	Balanced dipole	15		--	-19.2
8	Unbalanced dipole 23 ft high	8		-0.5	0.0
	2:1 Inverted L	8		-4.9	-2.6
	Balanced dipole	15		--	-18.5
10	5:1 Inverted L	10		-5.1	0.0
	Monopole	15	x	-1.7	--
	Balanced dipole	15		--	-8.6
15	Unbalanced dipole 23 ft high	8	x	0.0	0.0
	60° Slant wire	5		-1.2	-7.3
	Monopole	15		-3.5	--
	Balanced dipole	15		--	-1.9

*Potential amplitude errors greater than ±3 dB due to VSWR measurement errors.

†All gains on one frequency normalized to set highest equal to 0.0 dB.

Table 6

RELATIVE POWER GAINS INTO MATCHED LOADS
AT PATTERN MAXIMA--ALMANOR

Measurement Frequency (MHz)	Antenna		Potential Error*	Gain†	
	Type	Design Frequency, f_o (MHz)		E_θ (dB)	E_ϕ (dB)
4.0	30° Slant wire	4		0.0	-6.6
	5:1 Inverted L	10	x	-0.2	-5.6
	Unbalanced dipole 2 ft high	8	x	-13.5	-14.1
	Balanced dipole	15	x		-20.1
5.0	2:1 Inverted L	8	x	0.0	-3.4
	Sleeve dipole	5	x	-0.2	-4.9
	Unbalanced dipole 23 ft high	8	x	-5.2	-11.2
6.0	5:1 Inverted L	10	x	0.0	-4.7
	Unbalanced dipole 2 ft high	8		-8.2	-2.2
	30° Slant wire	4		-3.2	-8.0
	Balanced dipole	15	x		-17.6
	Monopole	15	x	-17.9	
8.0	Unbalanced dipole 23 ft high	8		-0.5	0.0
	2:1 Inverted L	8	x	-7.8	-2.7
	Sleeve dipole	5	x	-17.9	-20.7
15.0	Balanced dipole	15			0.0
	Monopole	15		-0.8	
	Unbalanced dipole 23 ft high	8	x	-4.0	-1.5

*Potential amplitude errors greater than ±3 dB due to VSWR measurement errors.

†All gains on one frequency normalized to set highest equal to 0.0 dB.

Table 7

RELATIVE POWER GAINS INTO MATCHED LOADS
AT PATTERN MAXIMA--BAN MUN CHIT

Measurement Frequency (MHz)	Antenna	Potential Error*	Gain† E_θ (dB)	Gain† E_ϕ (dB)
3.0	Balanced dipole over ground screen in clearing (6 MHz)	x	0.0	-6.5
	2:1 Inverted L (6 MHz)		-4.1	-4.8
	Unbalanced dipole in clearing (6 MHz)		-5.8	-15.0
	Balanced dipole in clearing (6 MHz)	x	-10.5	-8.1
	Long wire (6 MHz)	x	-11.6	-14.1
	Unbalanced dipole in foliage (6 MHz)		-14.7	-20.2
	30° Slant wire (6 MHz)	x	-15.8	-25.0
4.0	Balanced dipole over ground screen in clearing (6 MHz)		-0.6	0.0
	5:1 Inverted L (6 MHz)		-2.3	-4.1
	30° Slant wire (4 MHz)		-2.9	-7.5
	Balanced dipole in clearing (6 MHz)		-3.9	-4.1
	Unbalanced dipole in foliage (6 MHz)	x	-5.5	-8.3
	2:1 Inverted L (6 MHz)	x	-5.9	-5.8
	Unbalanced dipole in clearing (6 MHz)	x	-7.6	-10.2
	Long wire (6 MHz)	x	-9.4	-8.1
	30° Slant wire (6 MHz)	x	-12.8	-20.1
	Dipole, 2 ft high (6 MHz)	x	-16.4	-16.4
	Balanced dipole (15 MHz)	x	-22.6	-21.9

*Potential amplitude errors greater than ±3 dB because of VSWR measurement errors.

†All gains on one frequency normalized to set highest equal to 0.0 dB.

Table 7 (continued)

Measurement Frequency (MHz)	Antenna	Potential Error*	Gain†	
			E_θ (dB)	E_ϕ (dB)
4.0 (continued)	Monopole on edge of clearing (6 MHz)	x	-23.5	--
	Monopole in foliage (6 MHz)	x	-24.8	--
6.0	Balanced dipole, J&B type, 40 ft high (6 MHz)		-4.5	0.0
	Unbalanced dipole in foliage (6 MHz)		-3.6	-7.1
	Unbalanced dipole in clearing (6 MHz)		-9.7	-4.3
	Balanced dipole, J&B type, 80 ft high (6 MHz)		-8.4	-4.9
	Balanced dipole over ground screen in clearing (6 MHz)		-8.6	-5.7
	Balanced dipole in foliage (6 MHz)		-9.5	-6.5
	Unbalanced dipole in foliage 16 ft high (6 MHz)		-10.4	-6.8
	Balanced dipole in clearing (6 MHz)		-10.2	-7.4
	2:1 Inverted L (6 MHz)		-11.5	-8.5
	J&B type 40-ft vertical (6 MHz)	x	-8.8	--
	5:1 Inverted L (6 MHz)		-13.4	-9.1
	Unbalanced dipole in foliage 8 ft high (6 MHz)		-10.2	-11.2
	Monopole in clearing (6 MHz)		-11.3	--
	Monopole on edge of clearing (6 MHz)		-13.1	--
	Long wire (6 MHz)	x	-14.9	-17.9
	Sleeve dipole (6 MHz)	x	-15.5	-18.2

*Potential amplitude errors greater than ±3 dB because of VSWR measurement errors.

†All gains on one frequency normalized to set highest equal to 0.0 dB.

Table 7 (continued)

Measurement Frequency (MHz)	Antenna	Potential Error*	Gain† E_θ (dB)	Gain† E_ϕ (dB)
6.0 (continued)	30° Slant wire (6 MHz)		-20.5	-26.3
	Loop in clearing (6 MHz)	x	-23.6	-25.0
	Loop in foliage (6 MHz)	x	-25.6	-26.3
	Balanced dipole over ground screen in clearing (15 MHz)	x	-28.3	-26.5
8.0	Balanced dipole over ground screen in clearing (6 MHz)	x	-5.3	0.0
	Balanced dipole in clearing (8 MHz)		-11.9	-6.1
	Dipole, 23 ft high (8 MHz)		-8.7	-3.8
	Unbalanced dipole in foliage (6 MHz)	x	-16.6	-10.3
	Unbalanced dipole in clearing (6 MHz)		-18.1	-13.0
	5:1 Inverted L (6 MHz)	x	-13.3	-16.1
	Long wire (6 MHz)	x	-17.8	-19.3
	2:1 Inverted L (8 MHz)		-19.2	-18.2
	30° Slant wire (6 MHz)	x	-19.0	-24.4
	2:1 Inverted L (6 MHz)		-20.8	-19.3
	Balanced dipole over ground screen in clearing (15 MHz)	x	-23.7	-21.1
	Unbalanced dipole, 2 ft high (6 MHz)		-24.8	-26.2

*Potential amplitude errors greater than ±3 dB because of VSWR measurement errors.

†All gains on one frequency normalized to set highest equal to 0.0 dB.

Table 7 (concluded)

Measurement Frequency (MHz)	Antenna	Potential Error*	Gain†	
			E_θ (dB)	E_ϕ (dB)
8.0 (continued)	Monopole on edge of clearing (6 MHz)	x	-26.6	--
	Monopole in foliage (6 MHz)		-29.4	--
12.0	Balanced dipole, J&B type, 40 ft high (12 MHz)		-29.4	--
	J&B type 40-ft vertical (12 MHz)		-0.8	--
	Balanced dipole over ground screen in clearing (15 MHz)	x	-8.6	-4.4

*Potential amplitude errors greater than ±3 dB because of VSWR measurement errors.

†All gains on one frequency normalized to set highest equal to 0.0 dB.

One of the most meaningful relative-gain comparisons is between different antenna types designed for and measured on the same frequency at the same site. Unfortunately such comparisons are limited for the Lodi and Almanor sites because different design frequencies were used for most of the different antenna types, but at Ban Mun Chit all of the major antenna types were measured on 6 MHz. It was possible to compare the 15-MHz results for the monopole and balanced dipole at Lodi and Almanor, however, and at both sites the E_θ response of the monopole was within 1 dB of the maximum observed E_ϕ response for the dipole. Another such comparison is possible at 8 MHz between the 2:1 inverted L and the 23-ft dipole at all three sites. The maximum observed response of the 23-ft dipole exceeded that of the 2:1 inverted L by 2.6 dB, 5.9 dB, and 13.4 dB at Lodi, Almanor, and Ban Mun Chit respectively. An analogous comparison can be made at 6 MHz for the 41-ft unbalanced dipole and the 2:1 inverted L in the foliage at Ban Mun Chit where the dipole exhibited a gain of 5.9 dB over the inverted L. This result is in good agreement with the 8-MHz result for Almanor but not for Ban Mun Chit. The maximum observed response for the same 6-MHz dipole at Ban Mun Chit exceeded that of the 5:1 inverted L by 7.8 dB. This result is in reasonable agreement with the results from the sounder studies of relative gain at the zenith[13,25,28] after allowance for the different elevation angle (the power patterns indicate that the relative gain of the dipole over the 5:1 inverted L at about 50° elevation angle should be about the same as the relative gain at the zenith). Tests with the tuned monopole indicated that the maximum observed relative response dropped about 2 dB when the antenna was moved from the clearing to the edge of the forest and about another 9 dB when the antenna was moved into the forest. The monopole in the forest was down 16.7 dB from the unbalanced dipole in the forest. The relative response of the 30° slant wire in the forest at Ban Mun Chit was comparable to (actually 2.4 dB less than) the response

of the tuned monopole in the forest. The long wire was down about 22 dB from the dipole in the forest and the loop (in clearing and forest) was down more than 30 dB below the dipole.

Of the various relative gain results the most accurate is the ratio of the maximum observed response for E_θ to the maximum observed response for E_ϕ for the same antenna at the same site measured on the same frequency with the same receiver. When considering antennas measured on their design frequencies we observe that to within about ±3 dB the slant wires exhibited an E_θ/E_ϕ of about +7.7 dB, whereas the dipoles (excluding those at very low heights) and inverted Ls exhibited an E_θ/E_ϕ of about -3.0 dB. When the slant-wire antennas were measured on frequencies above or below their design frequency the maximum E_θ response still exceeded the maximum E_ϕ response, whereas for the dipoles and inverted Ls the E_θ/E_ϕ ratio was typically positive when the measurement frequency was lower than the design frequency, and negative when the measurement frequency exceeded the design frequency. The above comments apply for all three sites and for antennas both in and out of the forest.

B. Estimated Absolute Gains

As indicated previously, in order to compare the gains of antennas between two frequencies or between two different measurement sites, one must consider the absolute gains of the antennas. Since the effective radiated power of the Xeledop is not known, absolute gains cannot be derived directly from the measurement data.

The next best method for estimating the absolute gains of the antennas would be to erect a half-wave dipole antenna as a reference antenna for each frequency of the Xeledop transmitter and then calculate the absolute gains of these reference dipole antennas. Once the absolute gain of the reference dipole is determined, the absolute gains of all

other antennas on this frequency could be established by relating the gains through the relative-gain data.

The absolute gain of a half-wave dipole can be calculated using the relationship,[6]

$$G_{iso} = G_{fs} + 20 \log_{10} F(\theta, \phi) - 10 \log_{10} (R_a/R_d)$$

where

G_{fs} = Gain of a half-wave dipole in free space relative to isotropic

$F(\theta, \phi)$ = The field imaging factor

R_a = Measured antenna feed-point resistance

R_d = Antenna feed-point resistance in free space (73 ohms for a half-wave dipole).

The maximum gain of a half-wave dipole in free space is 1.64 (2.15 dB). The field imaging factor would be 2.0 for a horizontal dipole at $\lambda/4$ above perfect ground. For imperfect ground and radiation toward the zenith from a horizontal dipole, the imaging factor is given approximately as.[29]

$$F \cong \left[1 + A^2 - 2A \cos (\varphi + 4\pi h_a/\lambda)\right]^{1/2}$$

where $A < \phi$ is the reflection coefficient of the ground for horizontal polarization,* and h_a/λ is the antenna height above ground in wavelengths.

---

*It should be noted that Terman defines ϕ as the phase shift over actual ground relative to the phase shift caused by a perfect conductor (which, for horizontal polarization is 180°).

The term (R_a/R_d) includes both the effect of the change in the ease or difficulty of driving the antenna in the location near ground relative to that for driving it in free space, and the effect of losses in the ground and the antenna wire. R_a can be defined to equal the sum of an effective radiation resistance (R_r) and an effective loss resistance (R_ℓ). Then

$$10 \log_{10}(R_a/R_d) = 10 \log_{10}\left[\frac{R_r + R_\ell}{R_r}\right] + 10 \log_{10}(R_r/R_d)$$

where the first term can be recognized as the antenna efficiency, and the second term pertains to the relative ease or difficulty of maintaining the free-space input current to an equivalent lossless radiating element. This logarithm may be termed the ground proximity loss (or gain for the case when $R_a < 73$ ohms).

Combining terms for the dipole gain in free space, imaging factor, and ground proximity loss, the absolute gains of the dipole antennas can be estimated.[6]

Using this procedure, the absolute gain of the dipole antennas measured at Lodi, Almanor, and Ban Mun Chit were calculated. In some cases, it was necessary to calculate the gain at a frequency other than the design frequency of the dipole since a reference antenna was not erected for each measurement frequency. In these cases, the gain of the antenna in free space was assumed to be 2.15 dB. This assumption should not cause an error of more than 0.41 dB since the gain of a short (Hertzian) dipole in free space is 1.74 dB.

No measurements of the electrical ground constants were obtained at Lodi or Almanor; thus it was necessary to use values provided in the literature. The values used for Lodi were $\epsilon_r = 10$ and $\sigma = 2$ mmho/m, and the values for Almanor were $\epsilon_r = 13$ and $\sigma = 5$ mmho/m. For Ban Mun

Chit, the values of the electrical ground constants were measured with open-wire-transmission-line probes (see Figure 5).

After the absolute gain of a dipole antenna was estimated for a given frequency it was possible to determine a constant value to be added to the relative gain values of all the antennas measured at the same site on that frequency to obtain the absolute gain of these antennas. In some cases the absolute gains of several dipoles were calculated on the same frequency and it was possible to determine the best constant to be added to the relative gain data and also estimate the accuracy of the absolute gain information. The accuracy of the absolute gain data presented in Table 8 is estimated at ±3 dB unless it is marked with a dagger (†), which indicates that the possible inaccuracy is greater than ±3 dB. The asterisk (*) is used to indicate potential errors in the relative gain data and also indicates a potential error in the estimated absolute gain. Those absolute gains marked with both an asterisk and a dagger have a potential error of 6 dB or more. The values of absolute gain presented in Table 8 are the absolute gains of the antennas at the measured pattern maximum (zero dB on the contour plot).

Inter-site comparisons using the estimates of absolute gain are possible for four of the antennas: the 4-MHz 30° slant wire, the 8-MHz 2:1 inverted L, the 8-MHz 23-ft dipole, and the 15-MHz balanced dipole over a ground screen. The results for the 4-MHz 30° slant wire seem reasonable and consistent. This antenna exhibited nearly an isotropic absolute gain when measured in the cleared site, and the gain dropped 3 to 4 dB when the antenna was measured at the two forested sites. The 8-MHz 2:1 inverted L showed a reasonable gain at the cleared site (+3.3 dB) and a reasonable drop of -1.6 dB when placed in the forest at Almanor, but the gain value of -9.6 dB at Ban Mun Chit seems excessively low. (Note that this value has a dagger indicating significant uncertainty.)

Table 8

SUMMARY OF ESTIMATED ABSOLUTE GAINS (NORMALIZATION CONSTANTS)
FOR MEASURED ANTENNA PATTERNS IN REFERENCES 2 THROUGH 4

Antenna Type	f_o (MHz)	f_m (MHz)	Estimated Absolute Gains (dB)					
			Lodi		Almanor		Ban Mun Chit	
			E_θ	E_ϕ	E_θ	E_ϕ	E_θ	E_ϕ
Balanced dipole with ground screen in clearing--41 ft high	6.0	3.0					-0.4*	-6.9*
		4.0					-0.9*	-0.3*
		6.0					-1.0	+1.9
		8.0					+3.3*	+8.6*
Balanced dipole in clearing--41 ft high	6.0	3.0					-10.9	-8.2
		4.0					-4.2	-3.6
		6.0					-2.6	+0.0
		8.0					-3.3	+3.2
Unbalanced dipole in clearing--41 ft high	6.0	3.0					-6.2*†	-15.4*†
		4.0					-7.9*	-10.5*
		6.0					-2.1	+4.3
		8.0					-9.5*	-4.4*
Balanced dipole in forest--41 ft high	6.0	6.0					-1.9	+1.1
Unbalanced dipole in forest--41 ft high	6.0	3.0					-15.1†	-20.6†
		4.0					-5.8	-8.6
		6.0					+4.0	+0.5
		8.0					-8.0*	-1.7*
Unbalanced dipole in forest--16 ft high	6.0	6.0					-2.8	+0.8
Unbalanced dipole in forest--8 ft high	6.0	6.0					-2.6	-3.6
Unbalanced dipole 2 ft high	6.0	2.0	n/a		n/a			
		4.0	-15.6		-17.9*	-18.5*	-16.7*	-16.7*
		6.0	-5.1	-10.7	-15.7	-9.7	-10.1	-12.9
		8.0					-16.0	-18.2
		10.0	+4.0*	-6.5*	-7.1*	-4.2*		
Unbalanced dipole 23 ft high	8.0	2.67	n/a	n/a				
		5.0	-16.8*	-22.7*	-3.9*	-9.9*		
		8.0	+4.1	+4.6	+4.0	+4.5	-0.1	+2.8
		15.0	+7.9*	+7.9*	+0.6	+3.1		
Balanced dipole over ground screen 16.4 ft high	15.0	4.0		-29.5*		-24.6*	-22.9*	-24.2*
		5.0		-24.9*		-13.7*		
		6.0		-21.0*		-31.7*	-20.7*	-18.9*
		8.0		-12.6*		0.0*	-15.1*	-12.5*
		10.0		-0.6*		+3.4*†		
		12.0					+0.5	+4.7
		15.0		+5.7		+4.6	+2.6	+6.6
Sleeve dipole	5.0	5.0			+1.1*†	-3.6*†		
		8.0			-13.4*	-16.2*		
Sleeve dipole	6.0	6.0					-7.9*†	-10.6*†
Balanced dipole, J&B type--80 ft high	6.0	6.0					+0.8	+2.7
Balanced dipole, J&B type--40 ft high	6.0	6.0					+3.1†	+7.6†

*Potential relative gain error greater than ±3 dB due to VSWR measurement errors.

†Error of estimated absolute gain potentially greater than ±3 dB.

Table 8 (concluded)

Antenna Type	f_n (MHz)	f_o (MHz)	Estimated Absolute Gains (dB)					
			Lodi		Almanor		Ban Mun Chit	
			E_θ	E_ϕ	E_θ	E_ϕ	E_θ	E_ϕ
Balanced dipole, J&B type--40 ft high	12.0	12.0						+7.7†
Monopole in clearing	6.0	6.0					-3.7	
Monopole on edge of clearing	6.0	4.0					-23.8*	
		6.0					-5.8	
		8.0					-18.0*	
Monopole in forest	6.0	4.0					-25.1*	
		6.0					-12.0	
		8.0					-20.8*	
Monopole	15.0	2.0	n/a		n/a			
		2.67	n/a					
		4.0	-13.7*		-16.8*			
		5.0	-15.9*		-12.5*			
		6.0	-22.4*		-32.0*†			
		8.0	-6.1*		-4.2*			
		10.0			+3.1*†			
		15.0	+4.1		+3.8			
J&B type 80-ft vertical	2.0	2.0					n/a	
J&B type 40-ft vertical	6.0	6.0					-1.2	
J&B type 20-ft vertical	12.0	12.0					-8.7*	
2:1 Inverted L	6.0	3.0					-5.5	-5.2
		4.0					-6.2*	-6.1*
		6.0					-3.9	-0.9
		8.0					-22.2*	-19.7*
2:1 Inverted L	8.0	2.67	-3.5	-1.6	n/a			
		5.0			+1.3*	-2.1*		
		8.0	+1.0	+3.3	-3.4*	+1.7*	-10.6†	-9.6†
5:1 Inverted L	6.0	4.0					-3.1*	-4.4*
		6.0					-5.8	-1.5
		8.0					-4.7*	-7.5*
5:1 Inverted L	10.0	4.0			-4.6*	-10.0*		
		6.0			-14.2*†	-18.9*†		
		10.0	-4.0	-9.1	-3.1*†	-3.0*†	n/a	n/a
30° Slant wire	4.0	2.0	n/a		n/a	n/a		
		4.0	+0.4	-10.2	-4.4	-11.0	-3.2	-7.7
		6.0	-3.1*	-4.8*	-14.4	-18.2		
30° Slant wire	6.0	3.0					-16.2*	-25.4*
		4.0					-13.1*	-20.4*
		6.0					-12.9†	-18.7†
		8.0					-10.5*	-22.8*
60° Slant wire	5.0	5.0	+1.0*	-8.8*				
		15.0	+6.4*	+0.3*				
Loop in clearing	6.0	6.0					-16.0*	-17.4*
Loop in forest	6.0	6.0					-18.0*	-18.7*
Long wire	6.0	3.0					-12.0*	-14.4*
		4.0					-9.7*	-8.4*
		6.0					-7.3*	-10.3*
		8.0					-9.2*	-10.7*

*Potential relative gain error greater than ±3 dB due to VSWR measurement errors.

†Error of estimated absolute gain potentially greater than ±3 dB.

The gain of the 6-MHz 2:1 inverted L was -0.9 dB, and this casts further doubt on the result at 8 MHz. The absolute gain values for the 8-MHz 23-ft dipole of +4.6, +4.5, and +2.8 dB for Lodi, Almanor, and Ban Mun Chit seem quite reasonable, as do the corresponding values of +5.7, +4.6, and +6.6 dB for the 15-MHz balanced dipole with ground screen. At Lodi and Ban Mun Chit this latter antenna was placed in a cleared area, whereas at Almanor there were trees around the edge of the ground screen (possibly accounting for the slightly lower gain at Almanor).

At Ban Mun Chit the sleeve dipole laid upon the ground and the long-wire antenna both had the surprisingly high gain of about -7.9 dB, whereas the 6-MHz 30° slant wire and tuned monopole in the forest both exhibited an absolute gain of only about -12.5 dB. This latter result seems low since it is quite likely that the pattern maxima for both the slant wire and monopole actually were observed. On the other hand, it is worthy of comment that the Jansky-and-Bailey-type antennas all seemed quite efficient.

C. Gain of Dipole Antennas at the Zenith

From the 6-MHz unbalanced dipoles measured in the forest at Ban Mun Chit, there are sufficient data available to provide an indication of the variation of the absolute and relative gain at the zenith of a dipole antenna as a function of the antenna height. The calculated and measured data are presented in Figure 41. The calculated data were obtained by adding 2.15 dB (the gain of a half-wavelength dipole in free space) and the impedance correction factor [- 10 log (R_a/R_d) as described previously] to the F values derived from the model described in Section VII.* The measured values were derived from the absolute

*Note that impedance data for the calculated absolute gain were available only at 2, 8, 16, and 41 ft. The fact that the maximum gain occurs below $\lambda/4$ is a conclusion that is discussed in Ref. 31.

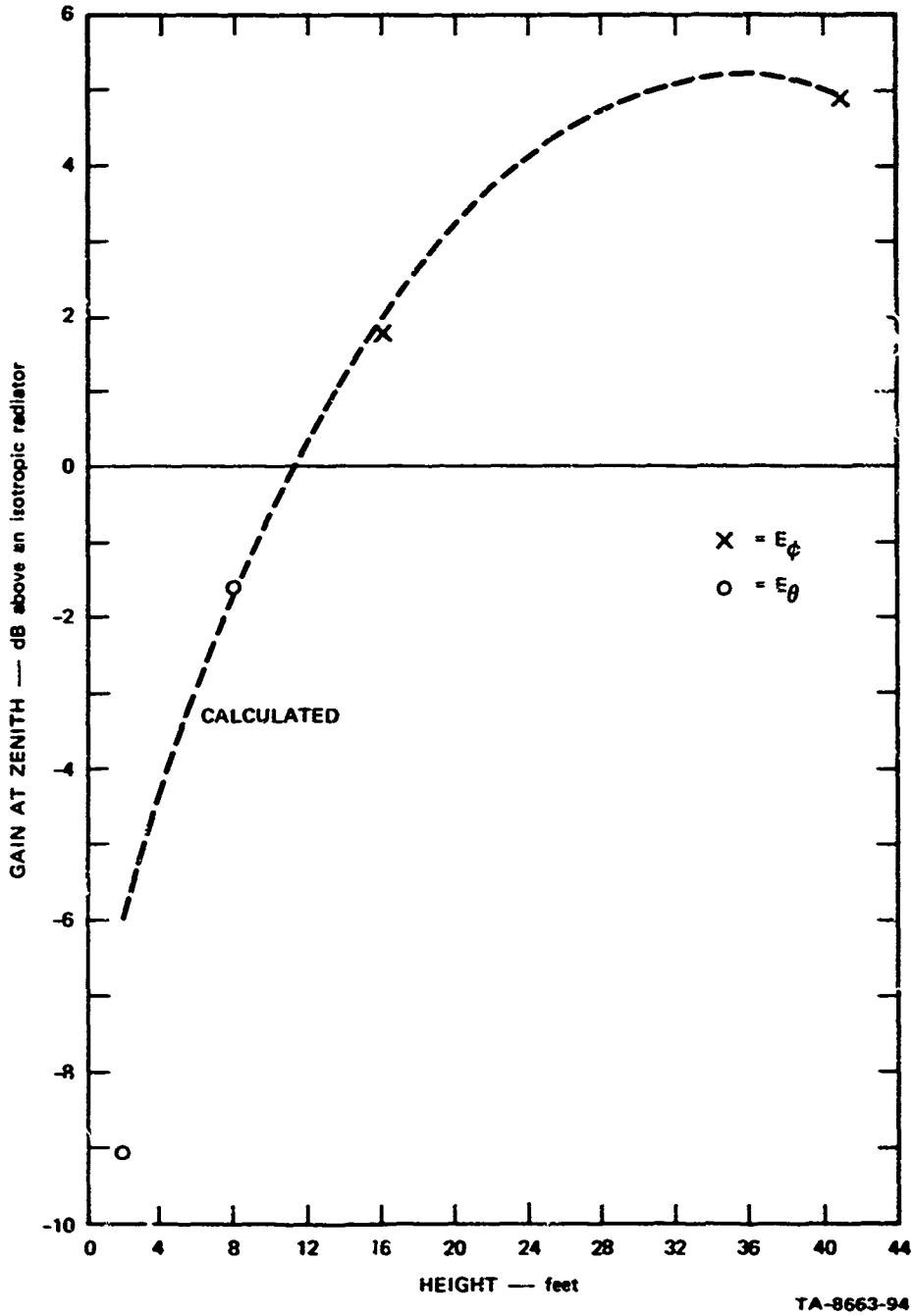

FIGURE 41 MEASURED AND CALCULATED GAIN VERSUS ANTENNA HEIGHT FOR 6-MHz UNBALANCED HORIZONTAL DIPOLE IN FOREST

gain normalizing constant by adding 1 dB to account for the increase in signal strength caused by the pattern factor as the elevation angle increases from the location of the E_ϕ or E_θ maximum (typically the largest elevation angle measured) to the zenith. More information on dipole gain at the zenith as a function of antenna height can be found in Ref. 25.

XI SUMMARY

Although the vertically incident skywave is the predominant mode in the lower part of the HF band over forested terrain at ranges greater than a few miles, it has been indicated that the complete radiation pattern of the antenna should be determined in order to know what effect unwanted noise and interference (including jamming signals) will have on the receiving system, and to know the susceptibility of the system to interception. The radiation patterns of selected HF field-expedient antennas were measured using the Xeledop technique when the antennas were erected over an open, flat field near Lodi, California, in a pine forest near Almanor, California, in a tropical forest near Ban Mun Chit, Thailand, and (under a different contract) over hilly terrain near Livermore, California. In order to better understand the effect of the forest and ground on the radiation patterns of these simple antennas, a multilayer-slab computer model was developed to predict the expected radiation patterns of Hertzian dipole antennas immersed in a forest.

The measured dipole directivity patterns show that generally the E_θ (vertical polarization) patterns tend to be affected more by the scattering from the surrounding vegetation than do the E_ϕ (horizontal polarization) patterns. But for either polarization, the relative response of the antennas tends to be enhanced at low elevation angles when the antennas were measured at the two forested sites. When considering the dipole antenna (and other simple antennas) one should not rely on only the primary polarization but should consider both polarization components and their effect on the total radiated power. It has been shown that the dipole antenna exhibits an almost omnidirectional power pattern near the zenith (see Figure A-13), and, in some cases (especially

for the lower antenna heights and for measurement frequencies below resonance), the E_θ response of the antenna is the stronger component. The E_ϕ component typically exceeded the E_θ component by about 3 dB for resonant dipoles, however, and the E_ϕ component also tended to dominate the power patterns for measurement frequencies above resonance. The absolute gain of the dipoles when placed at heights greater than $\lambda/8$ exceeded the isotropic level.

The measured patterns for the monopole antennas indicate that the location of the maximum response of these antennas tended to occur at higher elevation angles when the antennas were situated in the forests. Although the pattern was slightly disturbed at Ban Mun Chit, the most pronounced case of pattern perturbation was evident at 8 MHz and above when the antenna was measured at Almanor (note that this effect did not occur for the horizontal dipoles measured at Almanor). The E_θ response of the monopoles greatly exceeded the E_ϕ response--indeed, it proved difficult to measure the E_ϕ response.

Two configurations of the inverted-L antenna were measured: a 2:1 inverted L and a 5:1 inverted L. The E_ϕ patterns of these antennas resemble those of dipole antennas, whereas the E_θ patterns deviate from those of a dipole in that a fairly strong lobe was formed in one direction. The maximum E_θ (and power) response of these antenna is slightly down from the zenith, in the direction toward the vertical element of the antennas. The absolute gain of this antenna is slightly below that of a half-wave resonant horizontal dipole; but, like a dipole, the E_ϕ response usually exceeds the E_θ response by about 3 dB. Off resonance, the polarization trends were similar to those already discussed for the dipoles.

The measured E_ϕ pattern of the 30° slant-wire antenna resembles a dipole antenna although the gain of this antenna is considerably lower than that of a dipole antenna. The E_θ and power patterns of this antenna

show that the maximum response of the antenna is slightly down from the zenith and--contrary to what is often commonly assumed--the direction of maximum gain is in the direction of the counterpoise which is an active part of this antenna. The E_θ response of this antenna typically exceeded the E_ϕ response by about 7.7 dB.

The results of the measurements at Livermore show that the antennas installed on the top of rounded hills performed about as they did when installed over flat terrain at Lodi. No significant pattern distortion or alteration was observed when the hilltop data were compared with the results obtained at Lodi, although measurable differences were detected. The E_ϕ component appears to be somewhat larger than the E_θ component, rather than nearly equal as in the Lodi measurements. When the dipole antennas were installed on mild slopes, considerable distortion of their radiation patterns was observed. Both the E_ϕ and E_θ components were perturbed, compared to results obtained on the hilltop and at Lodi, and when a dipole was installed with its axis along the terrain contour lines the E_ϕ component toward the hilltop was attenuated. The E_ϕ component away from the hillside was considerably lowered in elevation angle, resulting in stronger signals at low elevation angles in the direction away from the hill. The E_θ response was complex. The deep E_θ null, normal to the dipole axis, was not evident toward the hill. The E_θ lobes along the axis of the dipole were shifted so that they appear to be aligned with the terrain contour lines, instead of occurring on the dipole axis. It may be concluded that irregular terrain features (such as hills) can cause gross pattern perturbations (such as a shift of a lobe away from the hillside) in excess of those caused by a forest where the average tree spacing is less than $\lambda/16$ at the radio wavelength of interest.

The three-layer slab model consisting of air, forest, and ground presented in Ref. 6 was reviewed and it was recalled that the most significant variable affecting gain toward the zenith was antenna height.

The model was run for the case of the forest at Ban Mun Chit, and, when measured feed-point impedance data were employed to determine ground proximity loss, predicted reasonably well the height-gain function of the 6-MHz unbalanced dipole measured with the Xeledop. Notice that this is a model for a Hertzian dipole being used to predict the field-imaging factor of a half-wave dipole.

The radiation patterns calculated with the multilayer slab model were compared with the measured radiation pattern data. This comparison shows that the measured and modeled data compared quite favorably for the resonant frequencies of the antennas, but the comparison deteriorated for frequencies below resonance. The measured and calculated results should be quite similar for frequencies below resonance since the model assumes an electrically short dipole antenna. Part of the dissimilarity between the measured and calculated patterns can possibly be explained by the presence of the antenna feed line, which becomes an active part of the antenna when the antenna is used off resonance, obviously the computer model does not take this into consideration. The patterns of the balanced dipole were predicted more accurately than those of the unbalanced dipoles--again a possible indication of the feedline distorting the pattern.

The relative gains for all of the measured antennas were tabulated. When the antennas were located in the forest the horizontal dipoles placed $\lambda/8$ or more above ground exhibited the greatest relative gain. The dipoles typically were followed by the 2:1 inverted L, 5:1 inverted L, 30° slant wires, monopoles, and loops in that order. This is essentially the same result as obtained with the ionospheric sounders when used to measure the relative gain at the zenith.[25] The relative gain data obtained for measurement frequencies a few MHz off the design frequency indicate the rather extreme penalty to be paid for not employing an antenna of the proper design. It should be noted that the Jansky-Bailey-type antennas measured at Ban Mun Chit were observed to be relatively efficient.

The absolute gains for many of the antennas were estimated. Several assumptions were necessary to calculate absolute gains, but if they are used cautiously, considerable information can be withdrawn from the values (e.g., inter-site gain comparisons, etc.). Such comparisons indicated that the vegetation typically caused a decrease in gain of about 3 dB (±3 dB) for most of the antennas.

Appendix A

CONTOUR PLOTS OF RADIATION PATTERNS OF ANTENNAS MEASURED OVER OPEN, FLAT TERRAIN, IN A U.S. PINE FOREST, AND IN A TROPICAL FOREST IN THAILAND

Appendix A

CONTOUR PLOTS OF RADIATION PATTERNS OF ANTENNAS MEASURED OVER OPEN, FLAT TERRAIN, IN A U.S. PINE FOREST, AND IN A TROPICAL FOREST IN THAILAND

Contour plots of the radiation patterns of identical antennas that were measured over open, flat terrain (Lodi, California), in a U.S. pine forest (Almanor, California), and in a tropical forest (Ban Mun Chit, Thailand) under Contract DA 36-039 AMC-00040(E) are presented in this appendix. The patterns are presented in order of antenna type as they were discussed in Sec. IV (e.g., dipoles, monopoles, inverted L's, and slant wires). For each type, patterns are presented for the three sites with Lodi first, followed by data from Almanor and Ban Mun Chit. The data for the sites are then presented in order of increasing frequency, if data for more than one frequency is presented, and for each frequency the E_θ (vertical polarization), E_ϕ (horizontal polarization), and power patterns (where available) are presented. A description of the contour plots has been presented previously in Sec. III of this report.

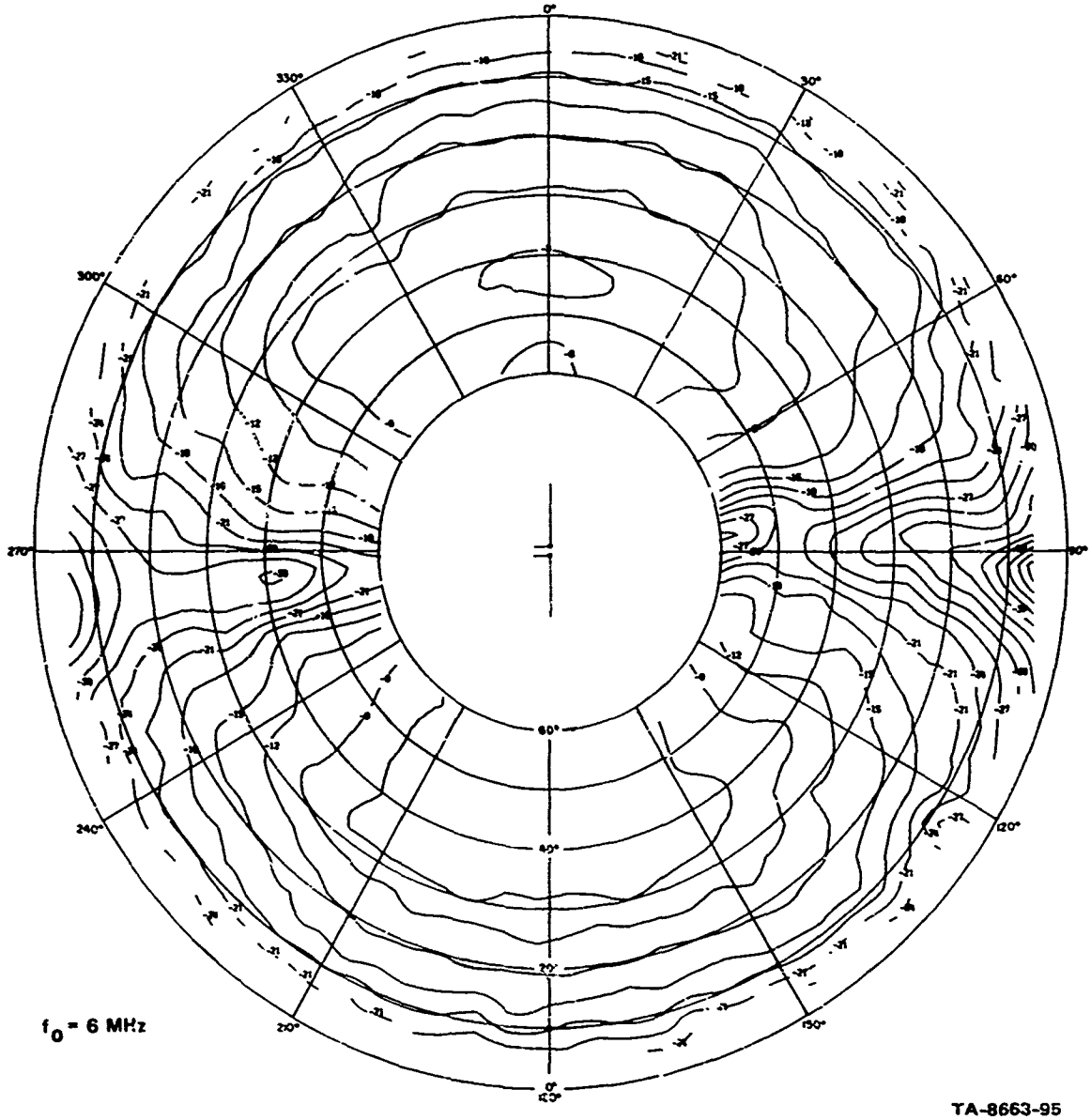

FIGURE A-1 MEASURED PATTERN OF 2-FOOT-HIGH UNBALANCED DIPOLE AT LODI, E_θ AT 6 MHz

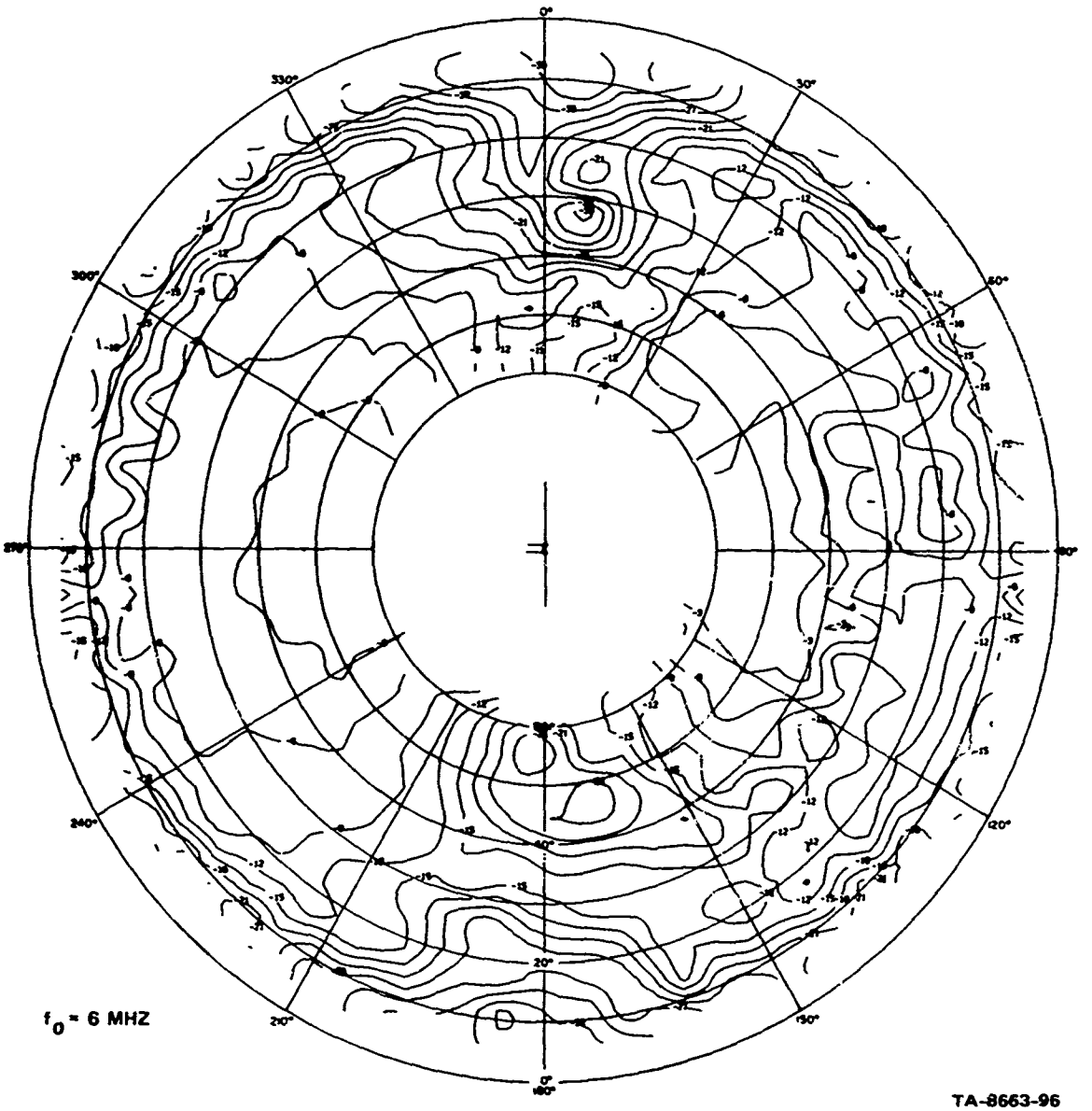

FIGURE A-2 MEASURED PATTERN OF 2-FOOT-HIGH UNBALANCED DIPOLE AT LODI, E_ϕ AT 6 MHz

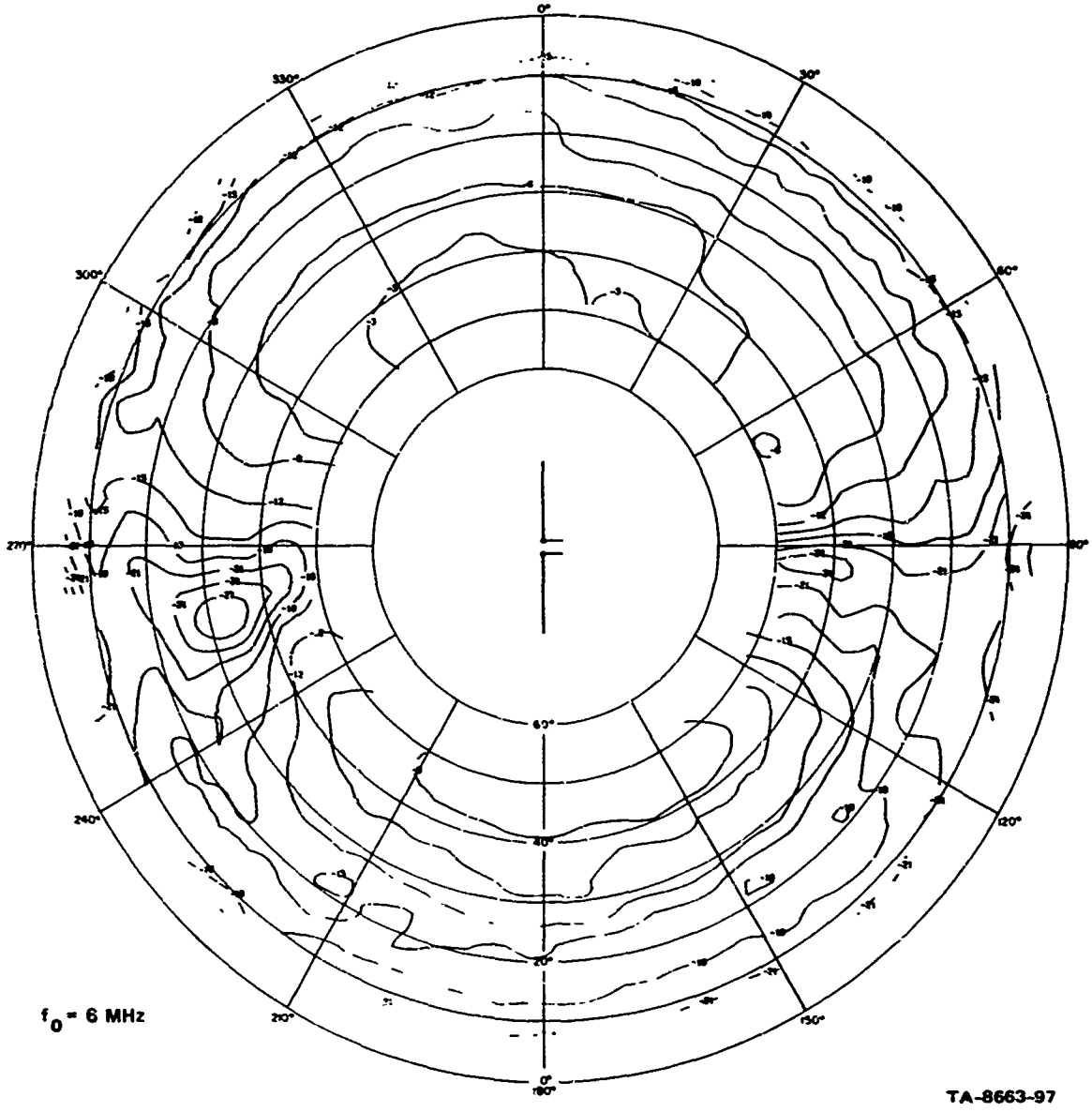

FIGURE A-3 MEASURED PATTERN OF 2-FOOT-HIGH UNBALANCED DIPOLE IN FOREST AT ALMANOR, E_θ AT 6 MHz

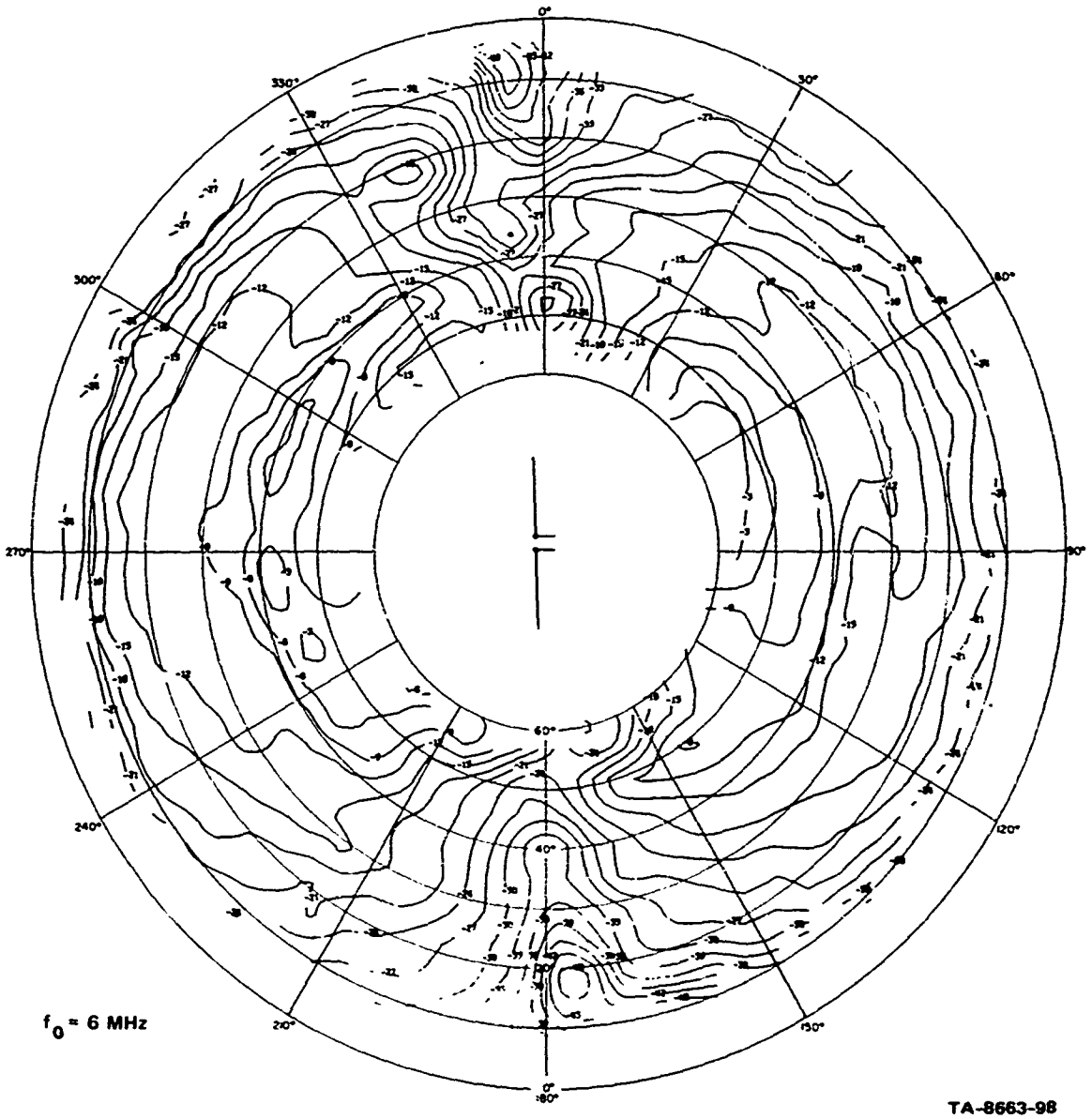

FIGURE A-4 MEASURED PATTERN OF 2-FOOT-HIGH UNBALANCED DIPOLE IN FOREST AT ALMANOR, E_ϕ AT 6 MHz

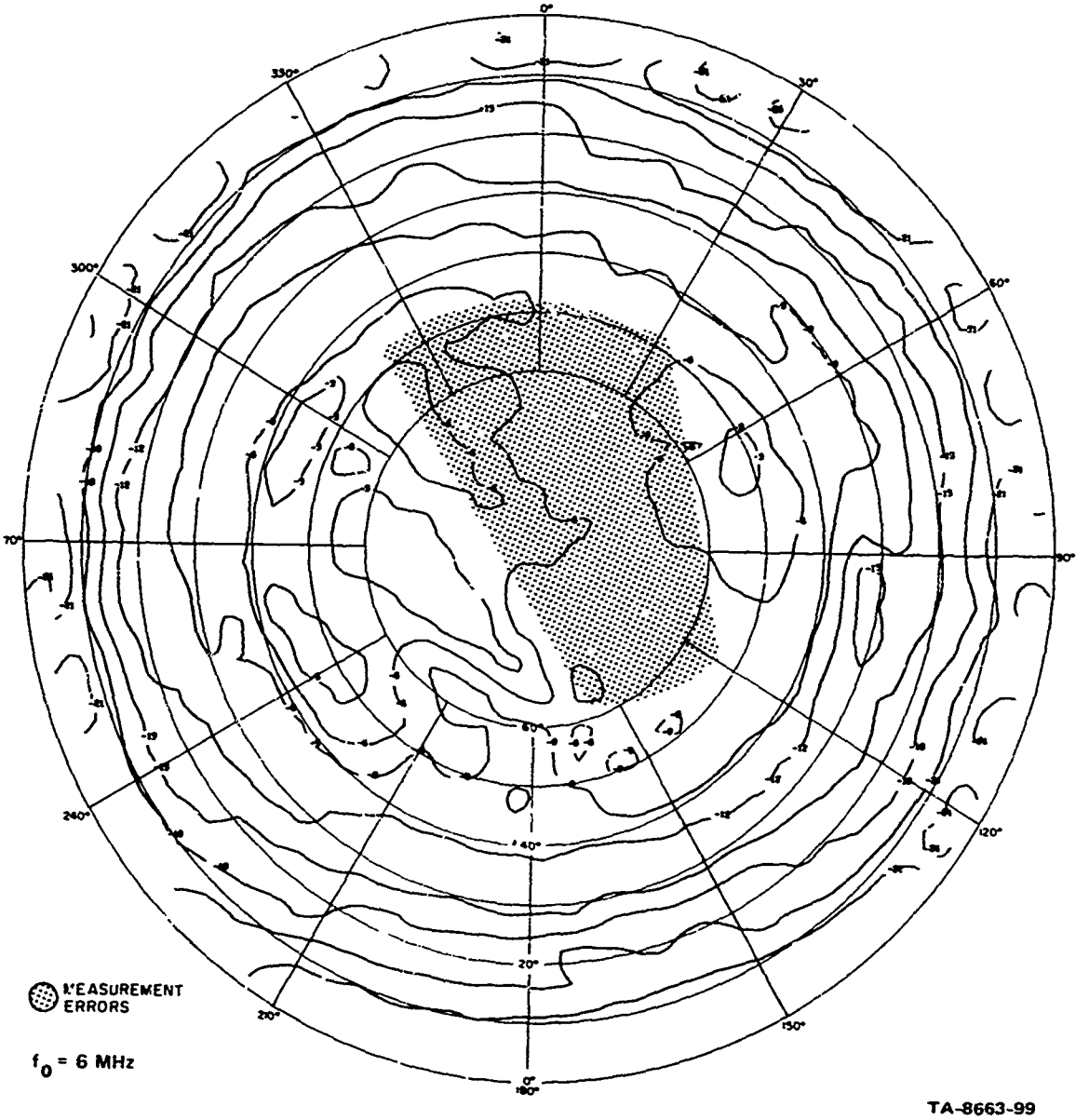

FIGURE A-5 MEASURED PATTERN OF 2-FOOT-HIGH UNBALANCED DIPOLE IN FOREST AT ALMANOR, POWER AT 6 MHz

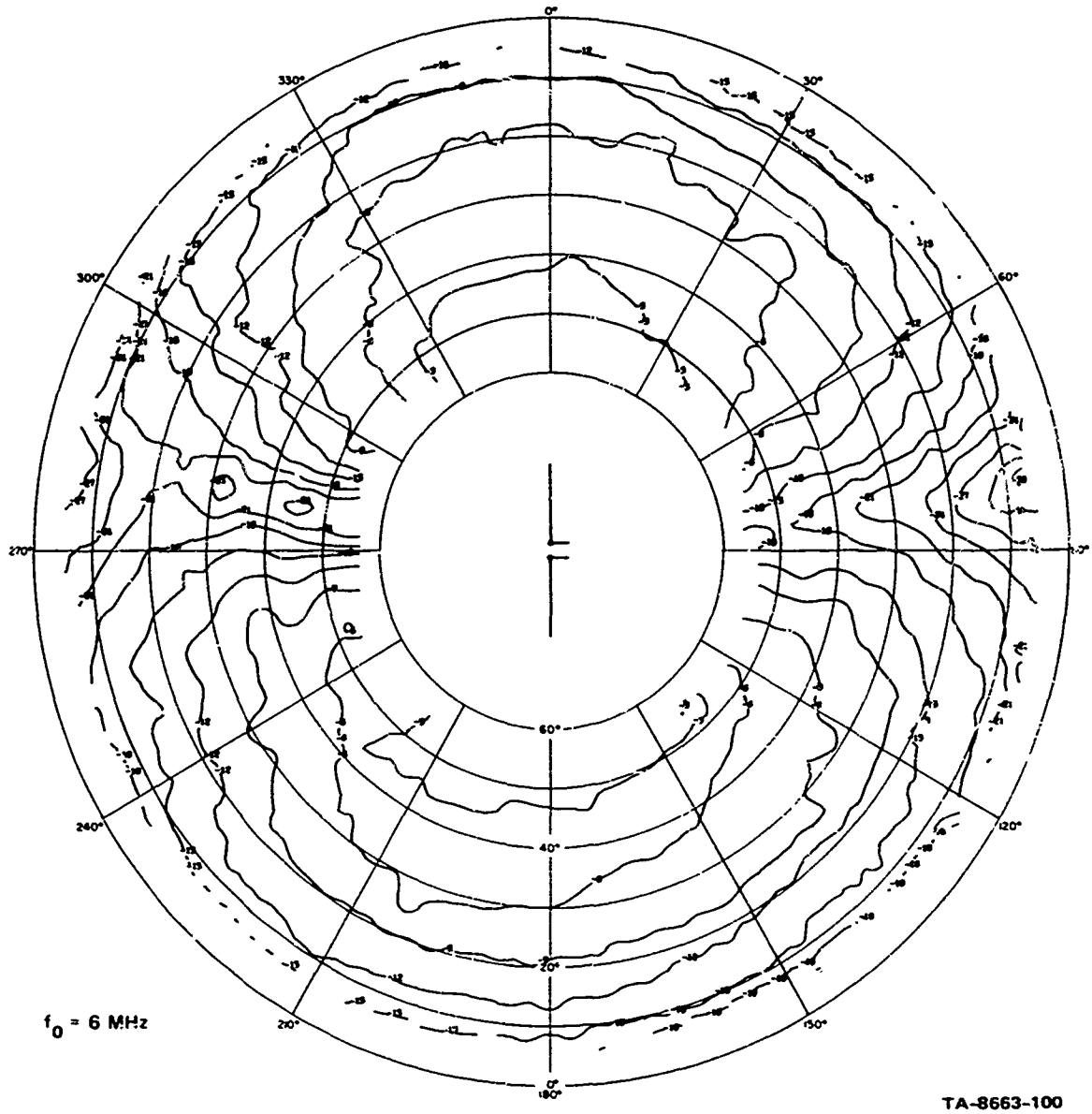

FIGURE A-6 MEASURED PATTERN OF 2-FOOT-HIGH UNBALANCED DIPOLE IN FOREST AT BAN MUN CHIT, E_θ AT 6 MHz

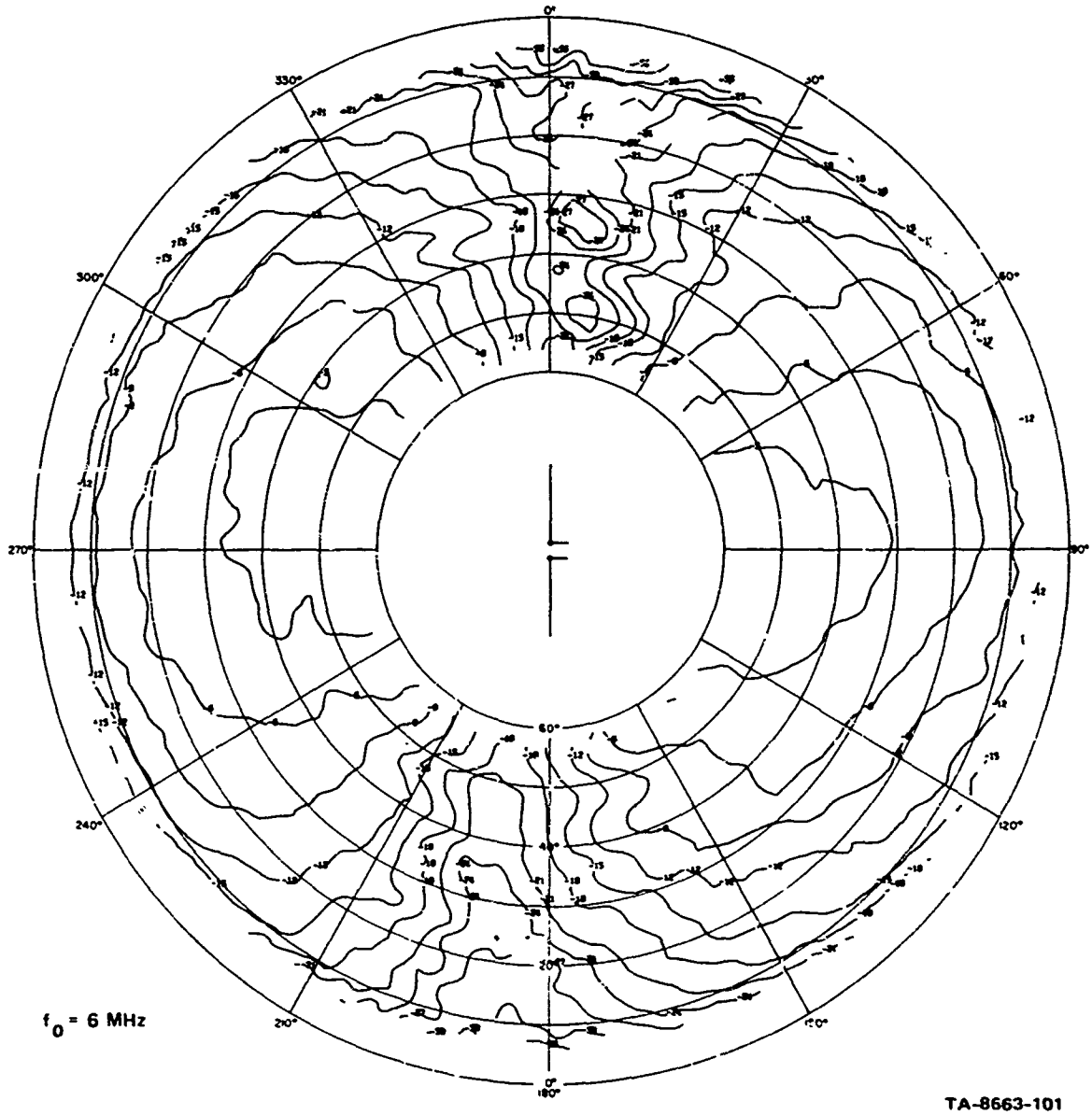

FIGURE A-7 MEASURED PATTERN OF 2-FOOT-HIGH UNBALANCED DIPOLE IN FOREST AT BAN MUN CHIT, E_ϕ AT 6 MHz

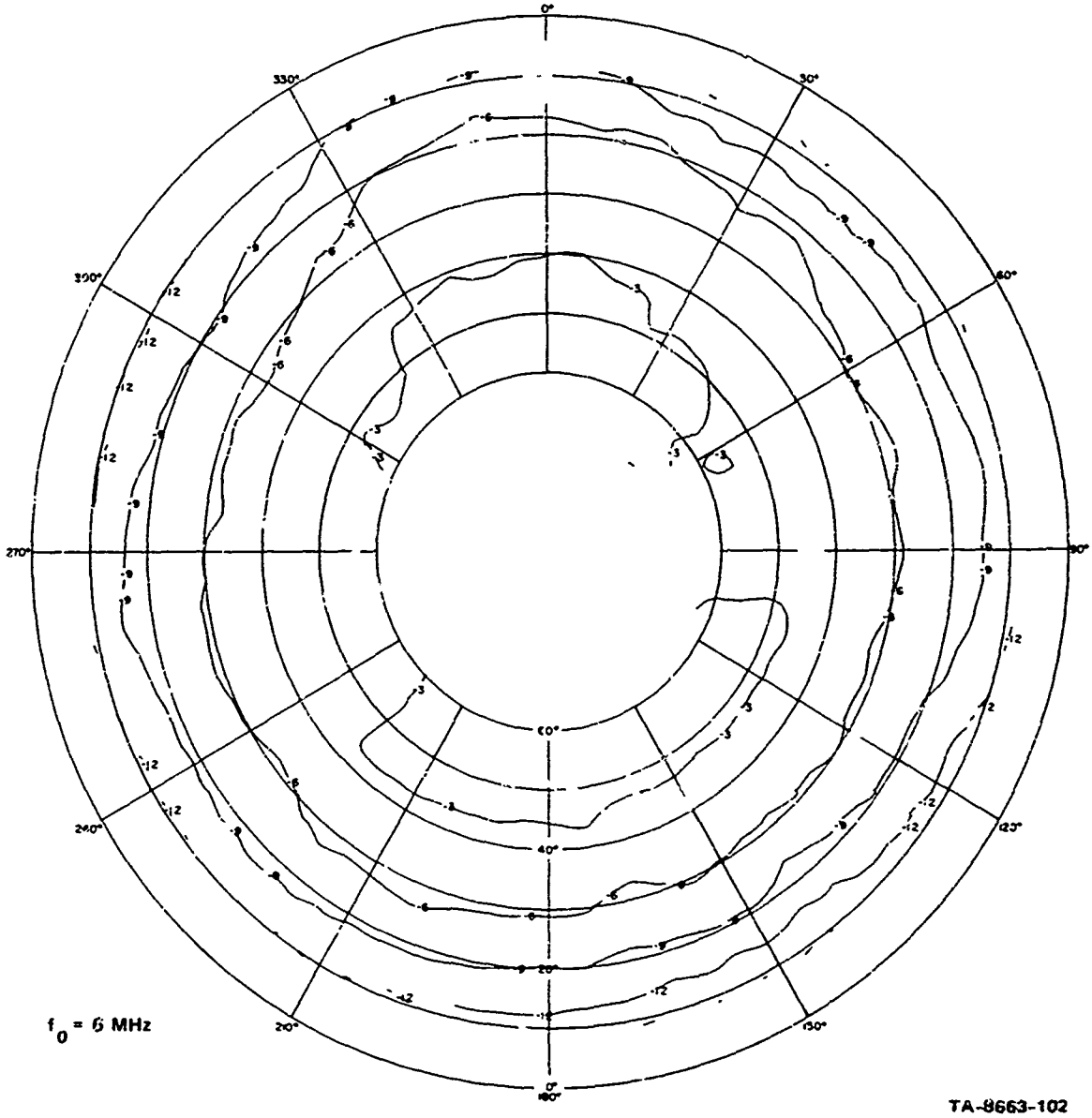

FIGURE A-8 MEASURED PATTERN OF 2-FOOT-HIGH UNBALANCED DIPOLE IN FOREST AT BAN MUN CHIT, POWER AT 6 MHz

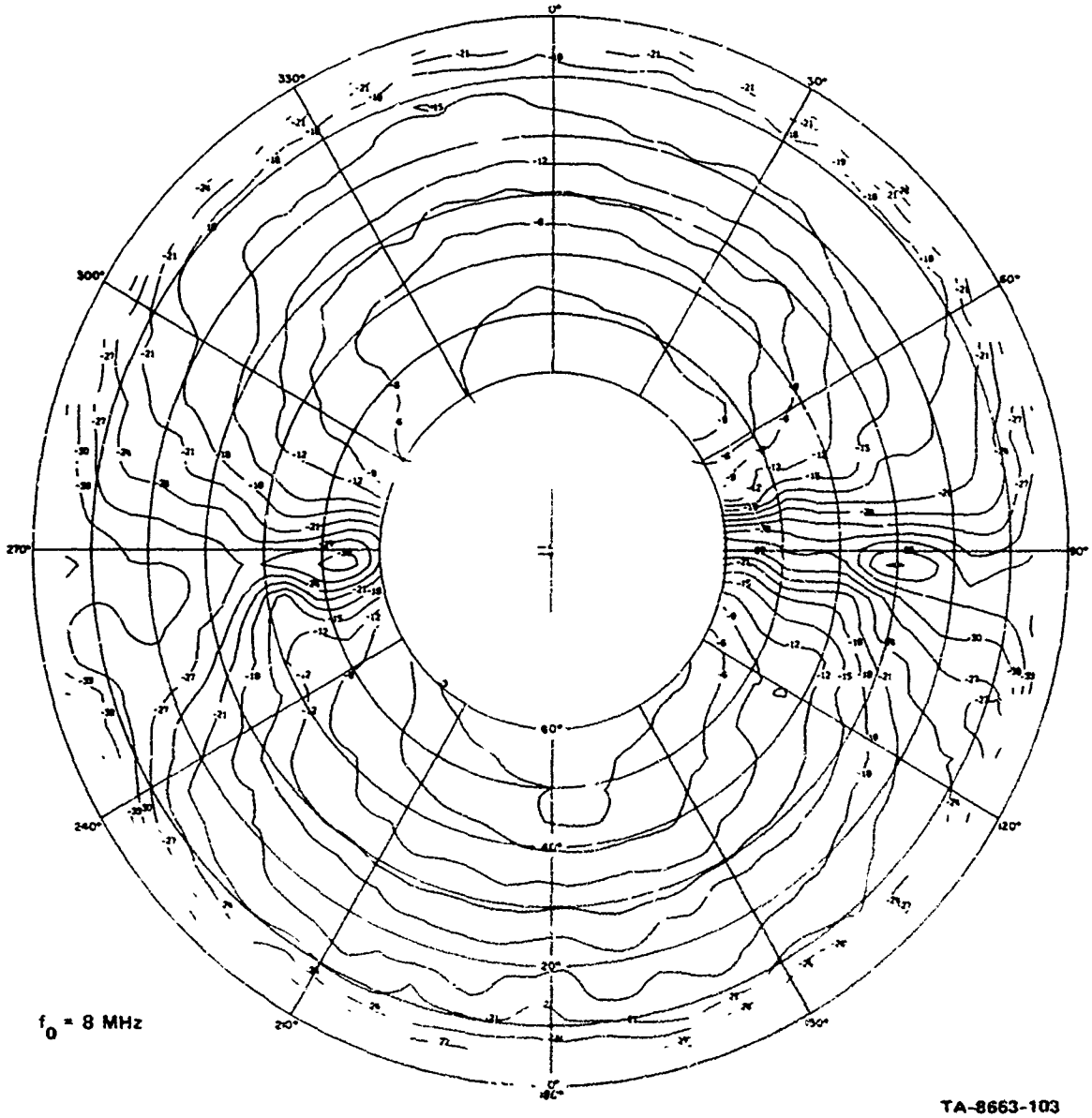

FIGURE A-9 MEASURED PATTERN OF 23-FOOT-HIGH UNBALANCED DIPOLE AT LODI, E_θ AT 8 MHz

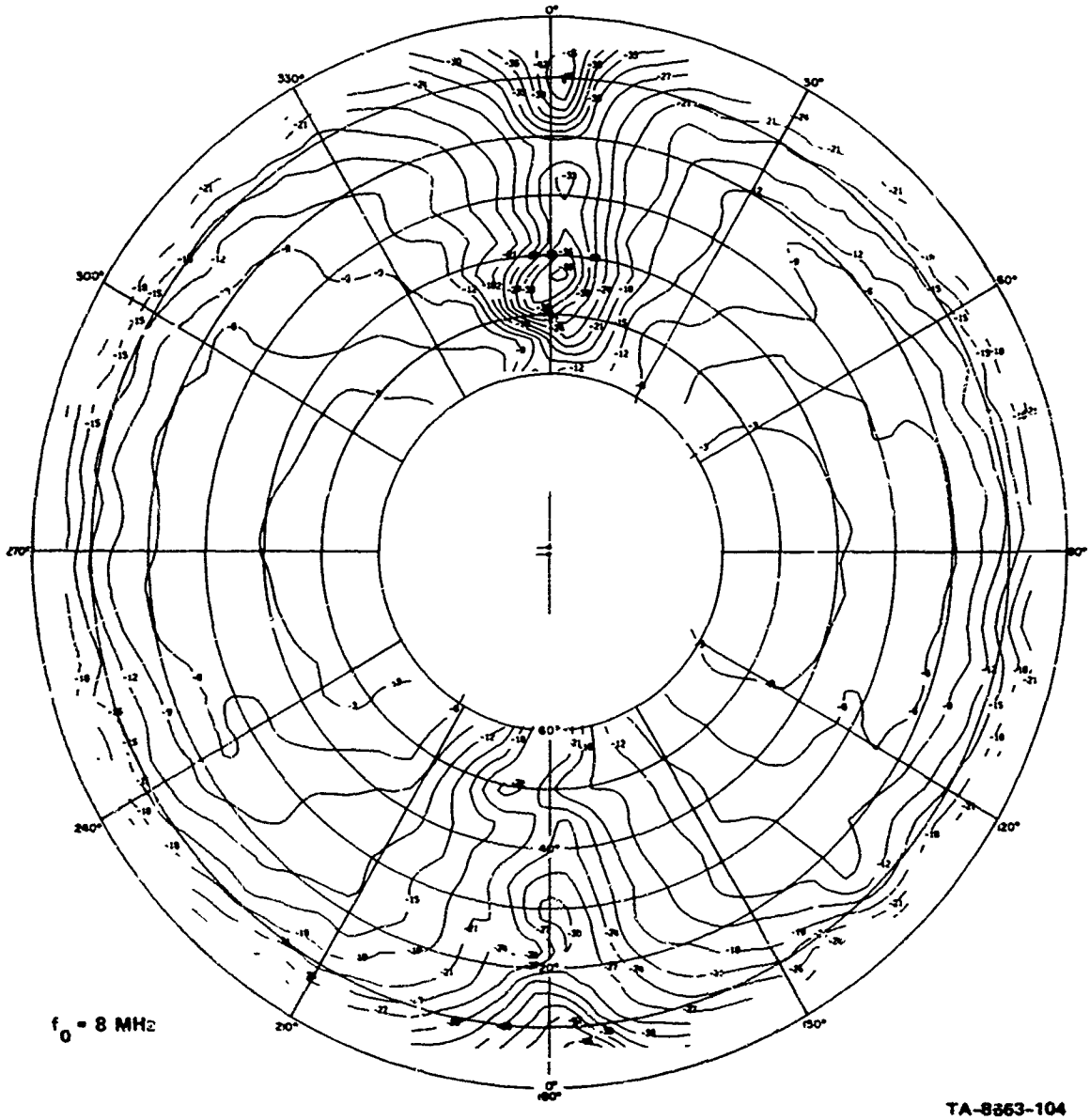

FIGURE A-10 MEASURED PATTERN OF 23-FOOT-HIGH UNBALANCED DIPOLE AT LODI, E_ϕ AT 8 MHz

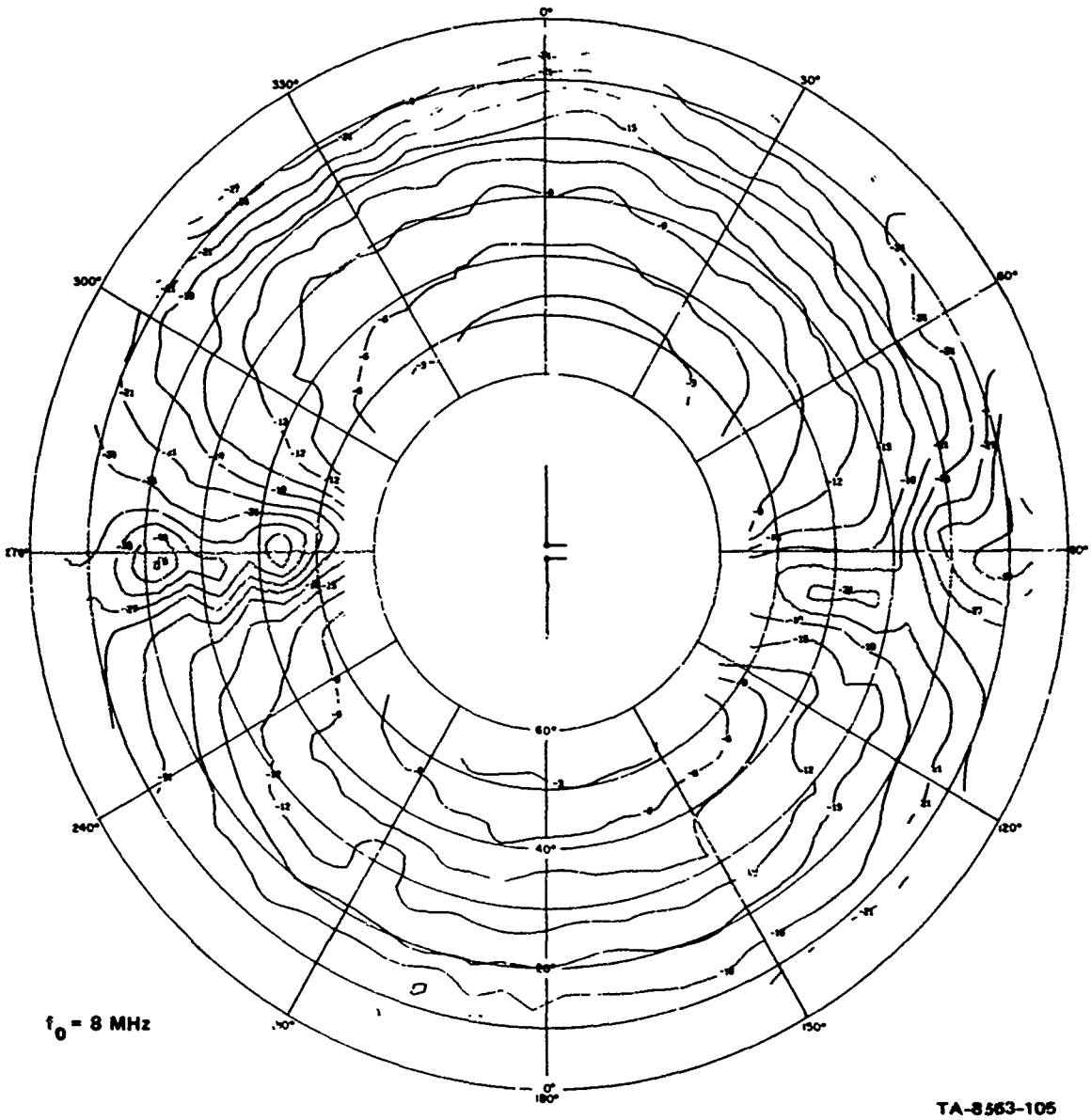

FIGURE A-11 MEASURED PATTERN OF 23-FOOT-HIGH UNBALANCED DIPOLE IN FOREST AT ALMANOR, E_θ AT 8 MHz

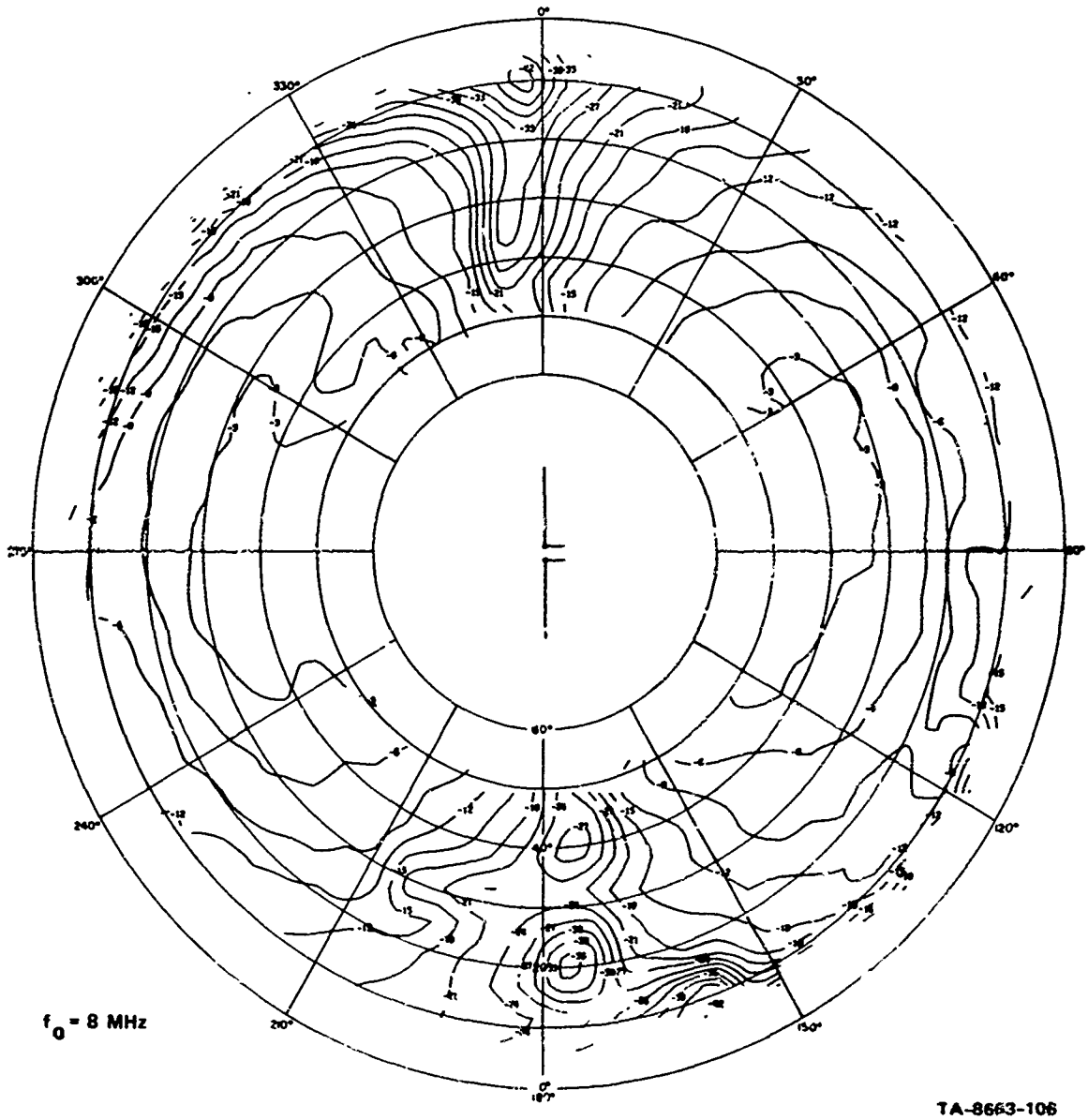

FIGURE A-12 MEASURED PATTERN OF 23-FOOT-HIGH UNBALANCED DIPOLE IN FOREST AT ALMANOR, E_ϕ AT 8 MHz

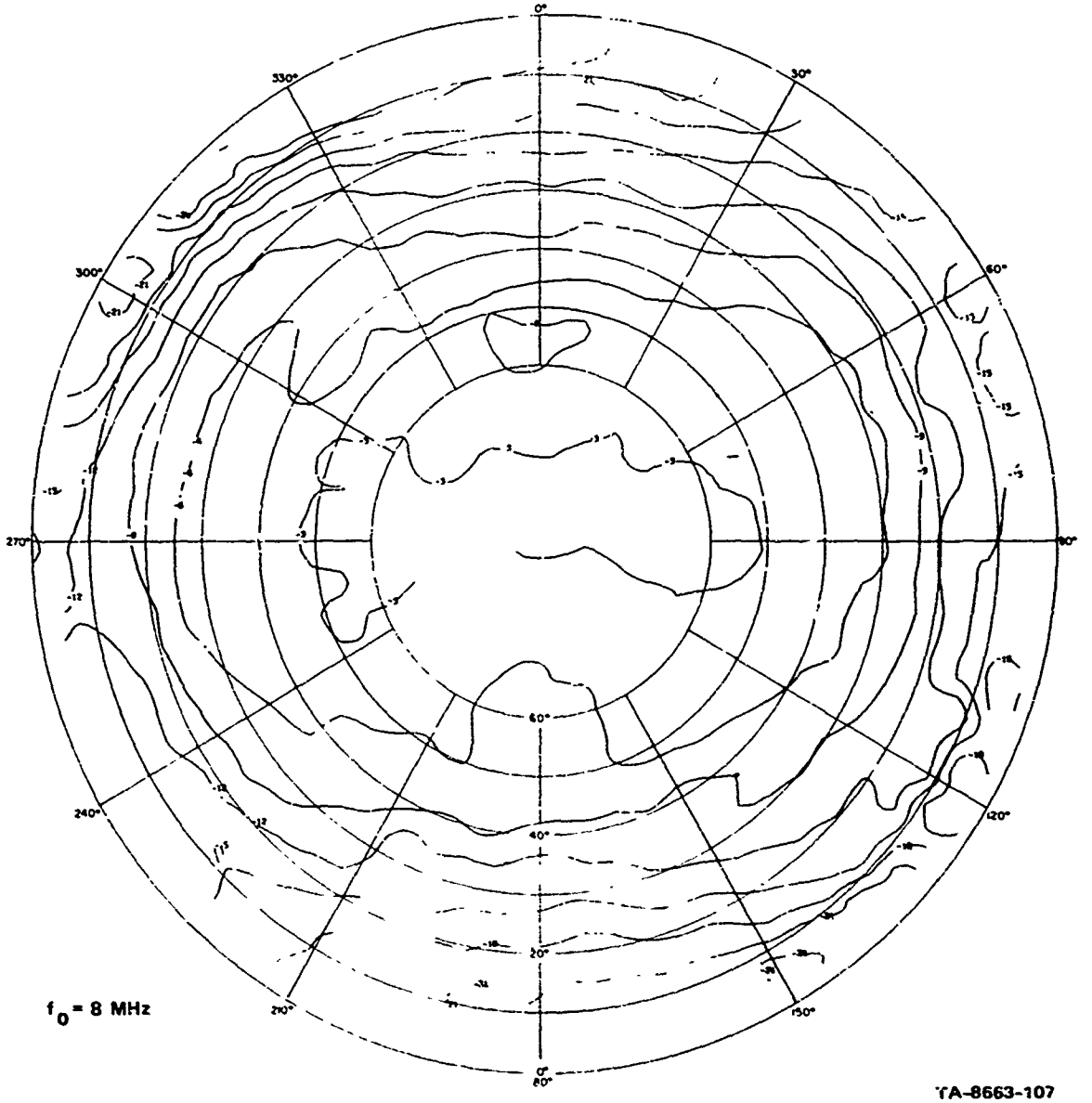

FIGURE A-13 MEASURED PATTERN OF 23-FOOT-HIGH UNBALANCED DIPOLE IN FOREST AT ALMANOR, POWER AT 8 MHz

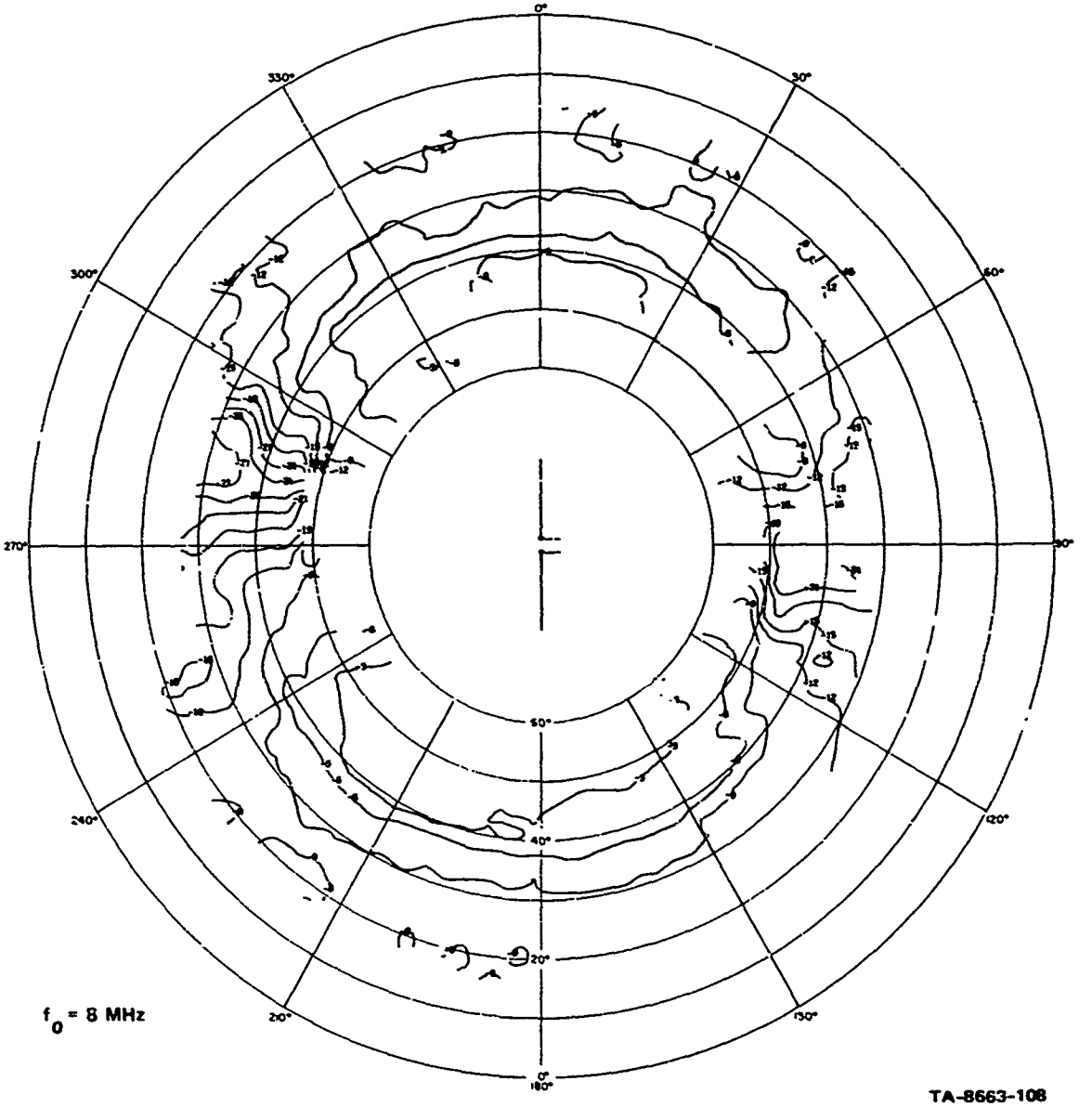

FIGURE A-14 MEASURED PATTERN OF 23-FOOT-HIGH UNBALANCED DIPOLE IN FOREST AT BAN MUN CHIT, E_θ AT 8 MHz

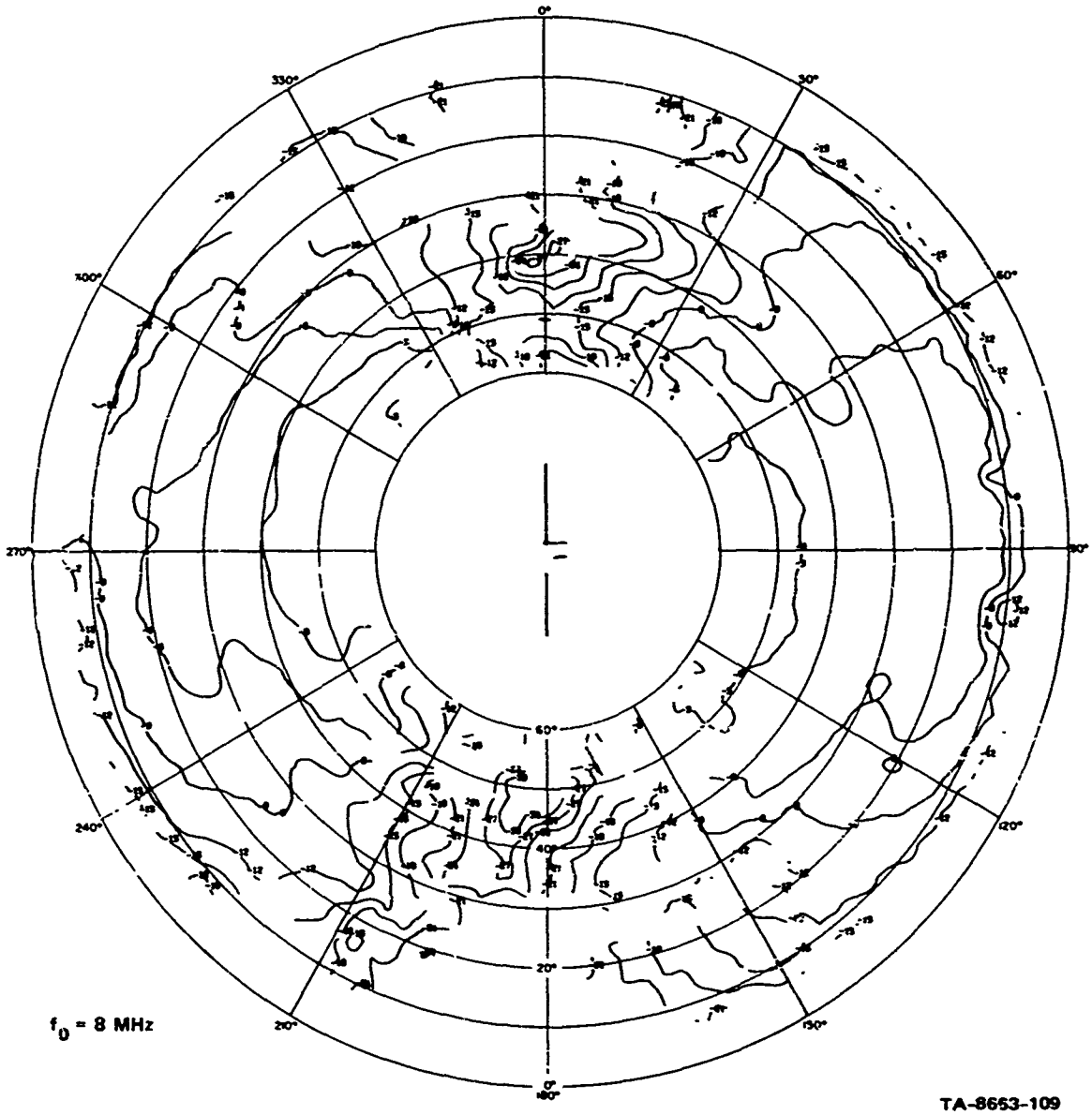

FIGURE A-15 MEASURED PATTERN OF 23-FOOT-HIGH UNBALANCED DIPOLE IN FOREST AT BAN MUN CHIT, E_ϕ AT 8 MHz

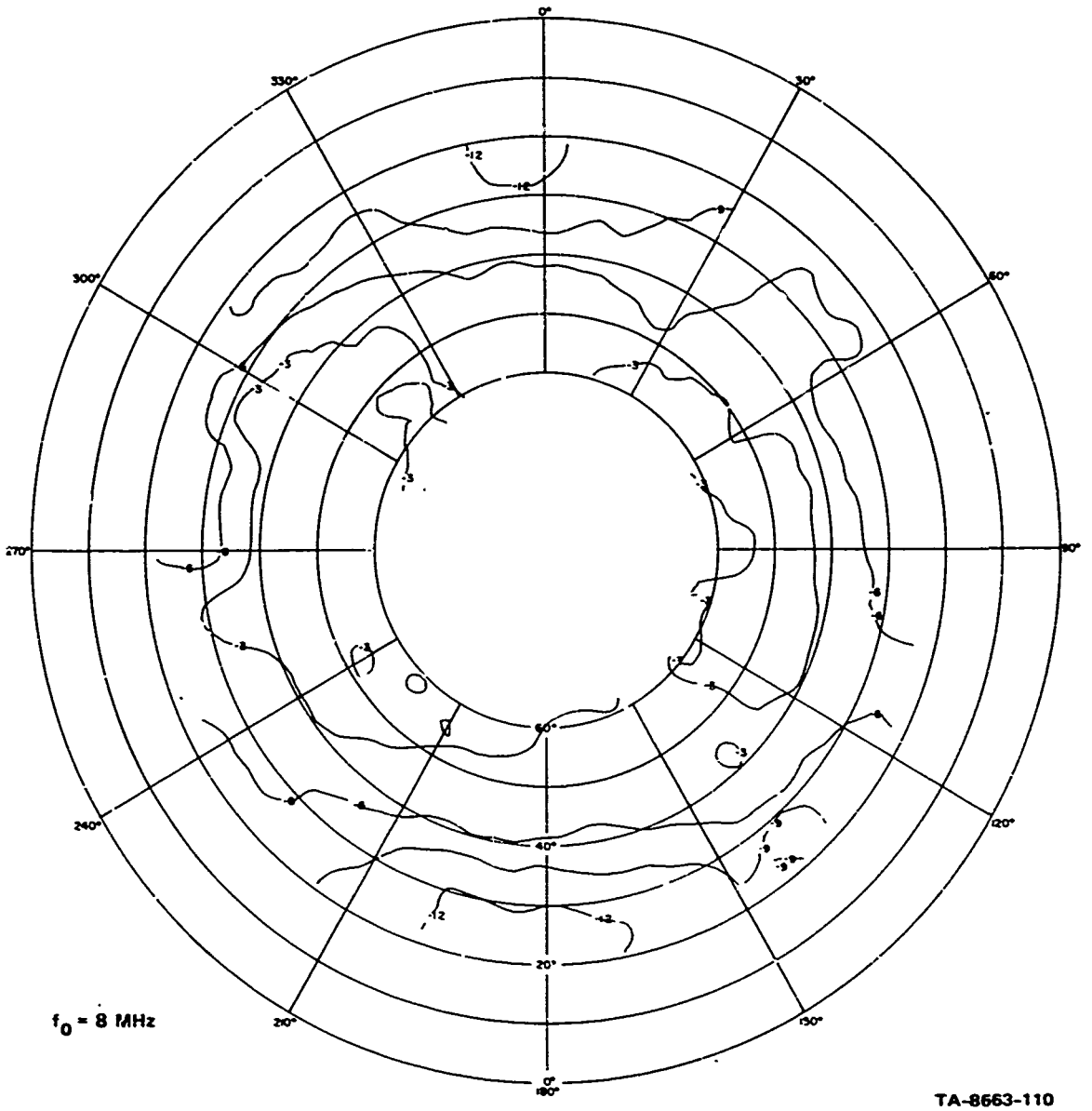

FIGURE A-16 MEASURED PATTERN OF 23-FOOT-HIGH UNBALANCED DIPOLE IN FOREST AT BAN MUN CHIT, POWER AT 8 MHz

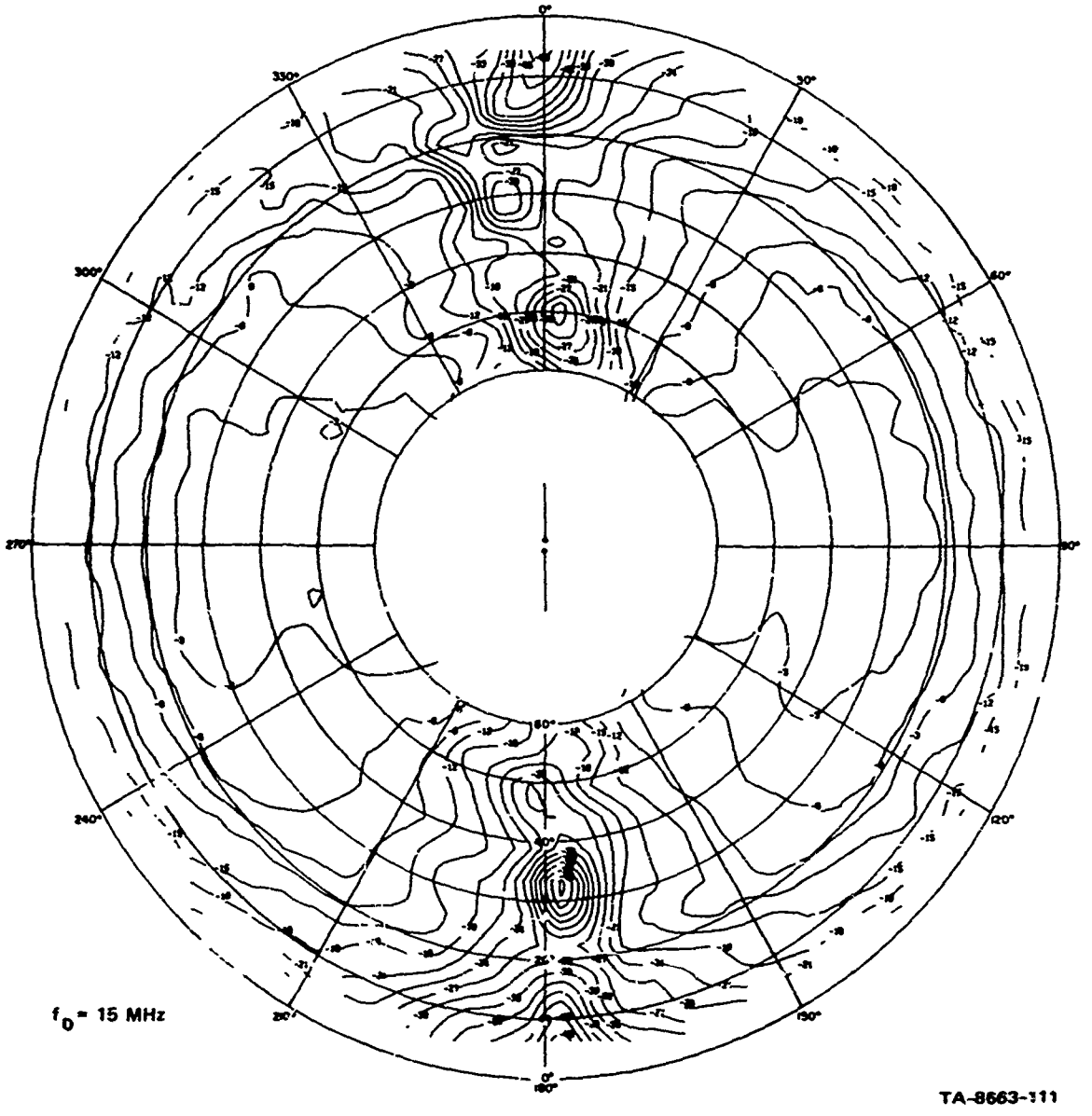

FIGURE A-17 MEASURED PATTERN OF 15-MHz BALANCED DIPOLE AT LODI, E_ϕ AT 15 MHz

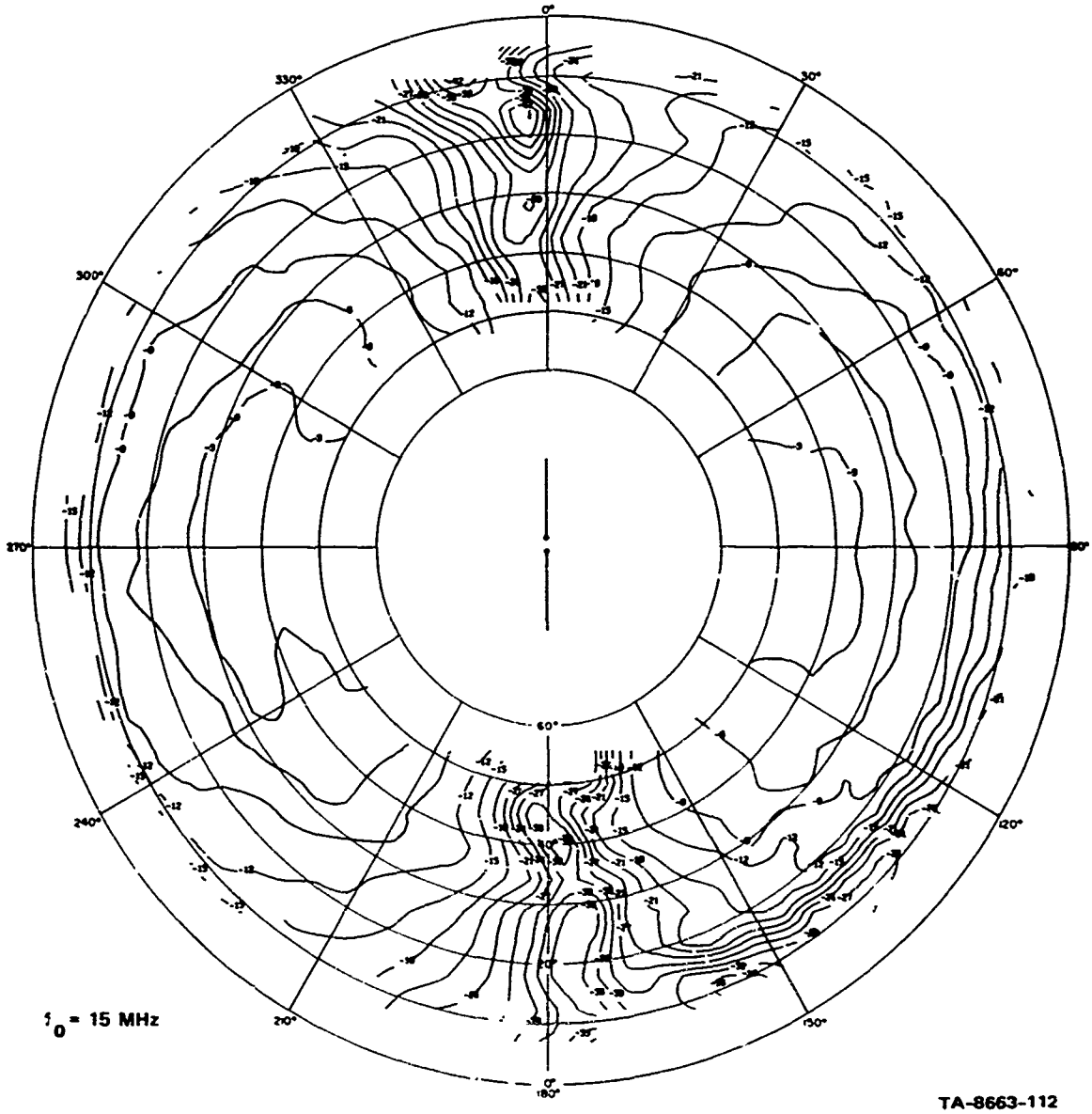

FIGURE A-18 MEASURED PATTERN OF 15-MHz BALANCED DIPOLE IN CLEARING AT ALMANOR, E_ϕ AT 15 MHz

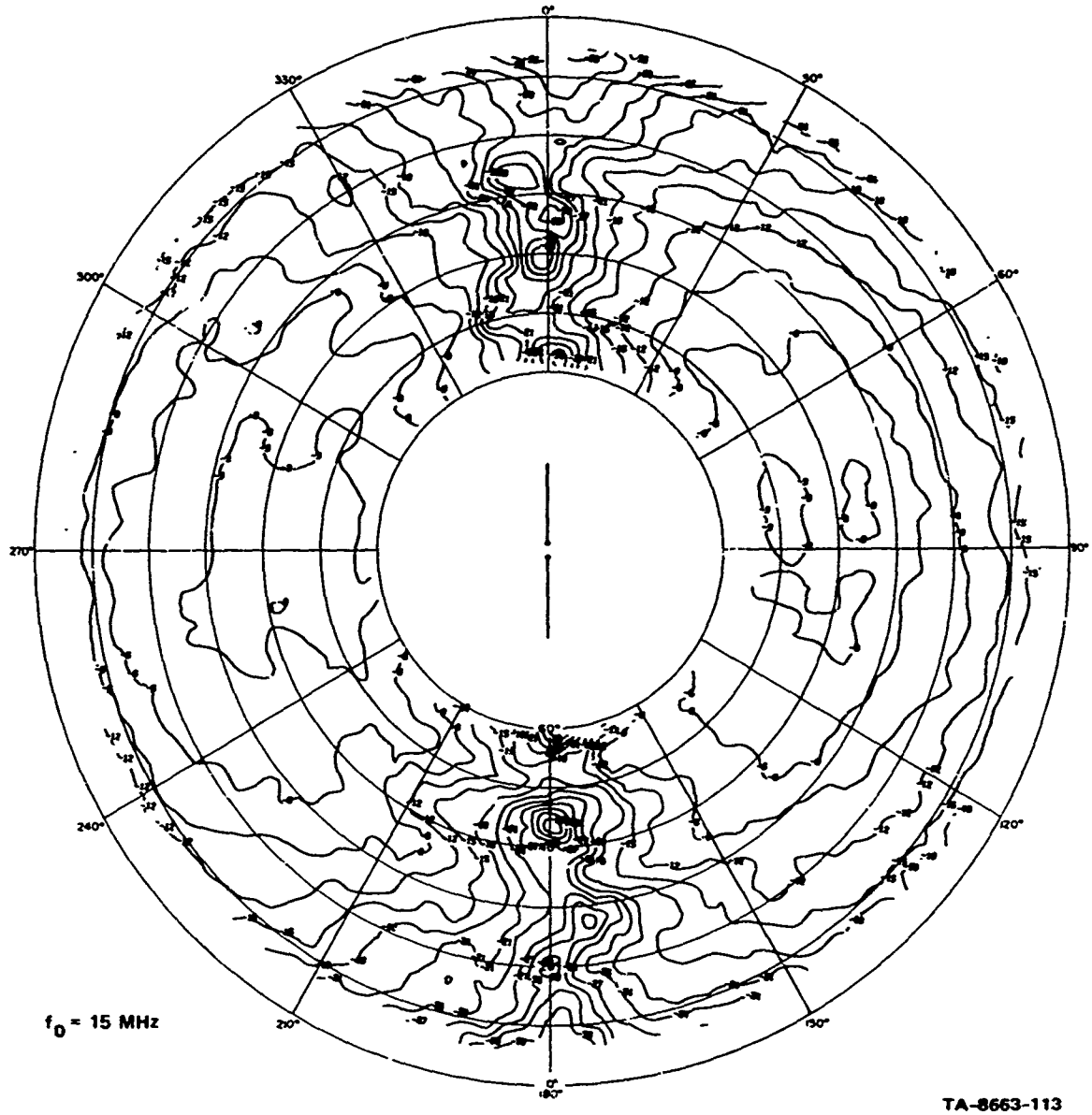

FIGURE A-19 MEASURED PATTERN OF 15-MHz BALANCED DIPOLE IN CLEARING AT BAN MUN CHIT, E_ϕ AT 15 MHz

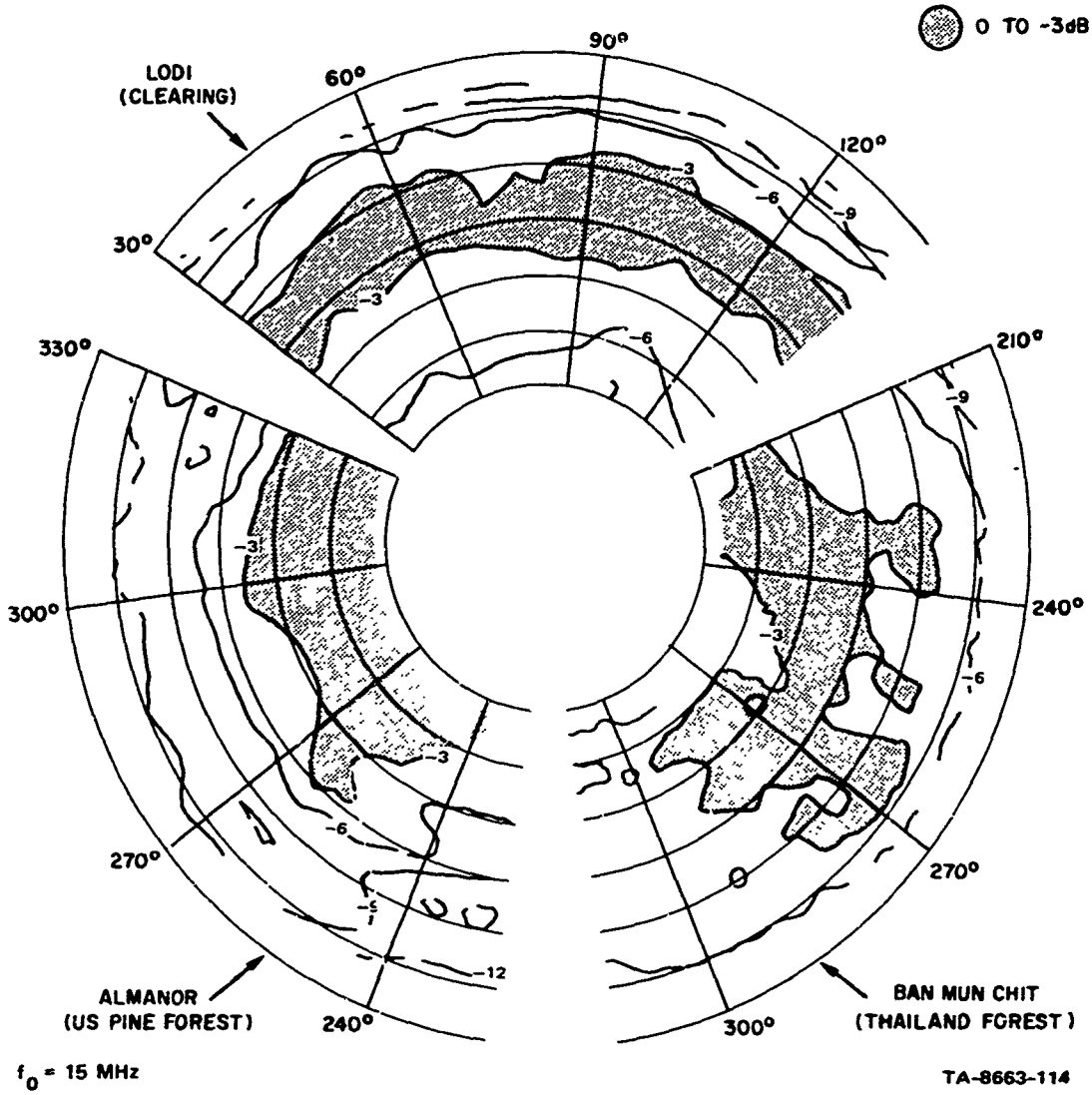

FIGURE A-20 COMPARISON OF MEASURED PATTERNS OF MONOPOLE ANTENNAS AT LODI AND IN FORESTS IN ALMANOR AND BAN MUN CHIT, E_θ AT 6 MHz

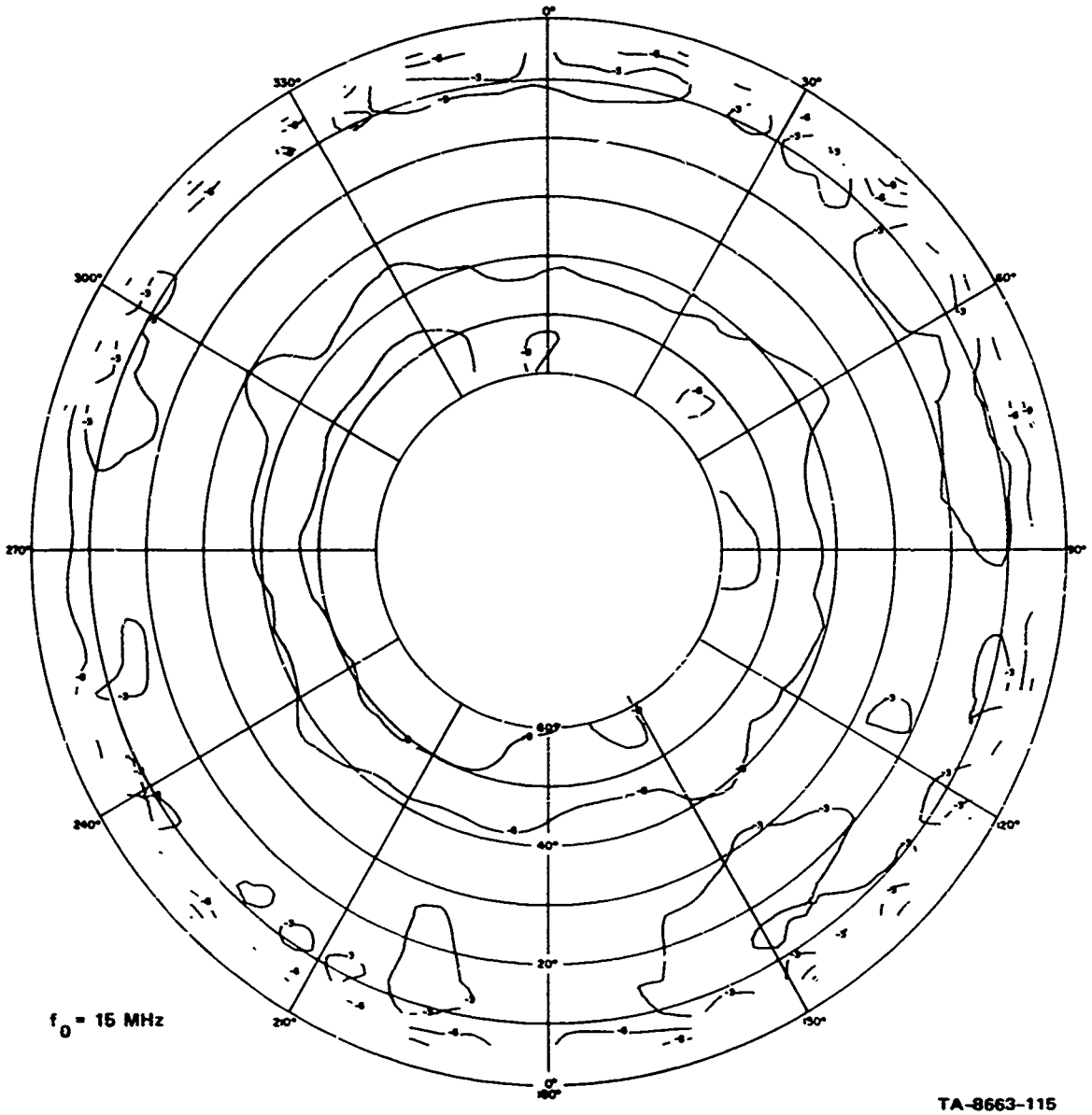

FIGURE A-21 MEASURED PATTERN OF MONOPOLE ANTENNA AT LODI, E_θ AT 8 MHz

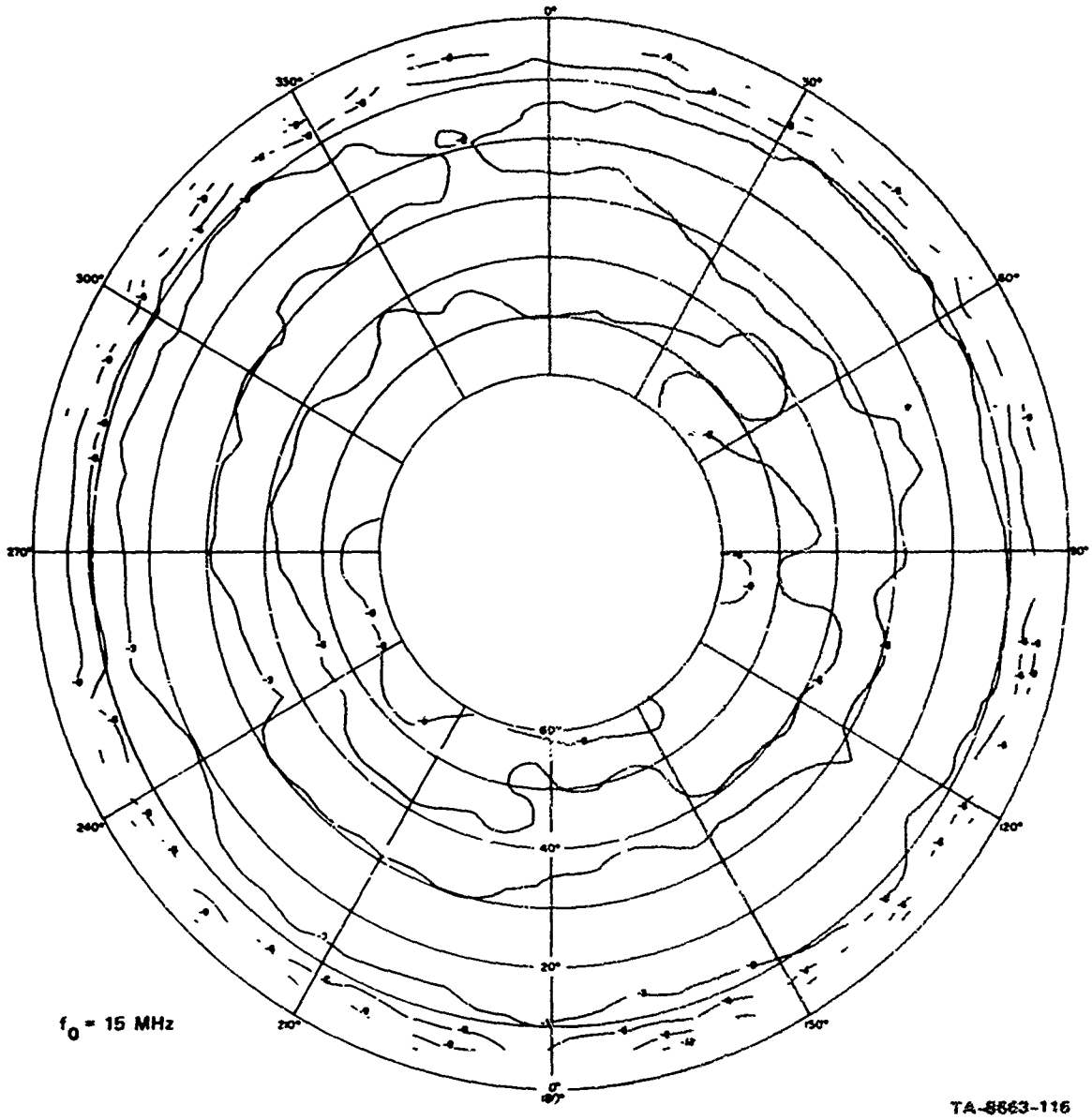

FIGURE A-22 MEASURED PATTERN OF MONOPOLE ANTENNA AT LODI, E_θ AT 15 MHz

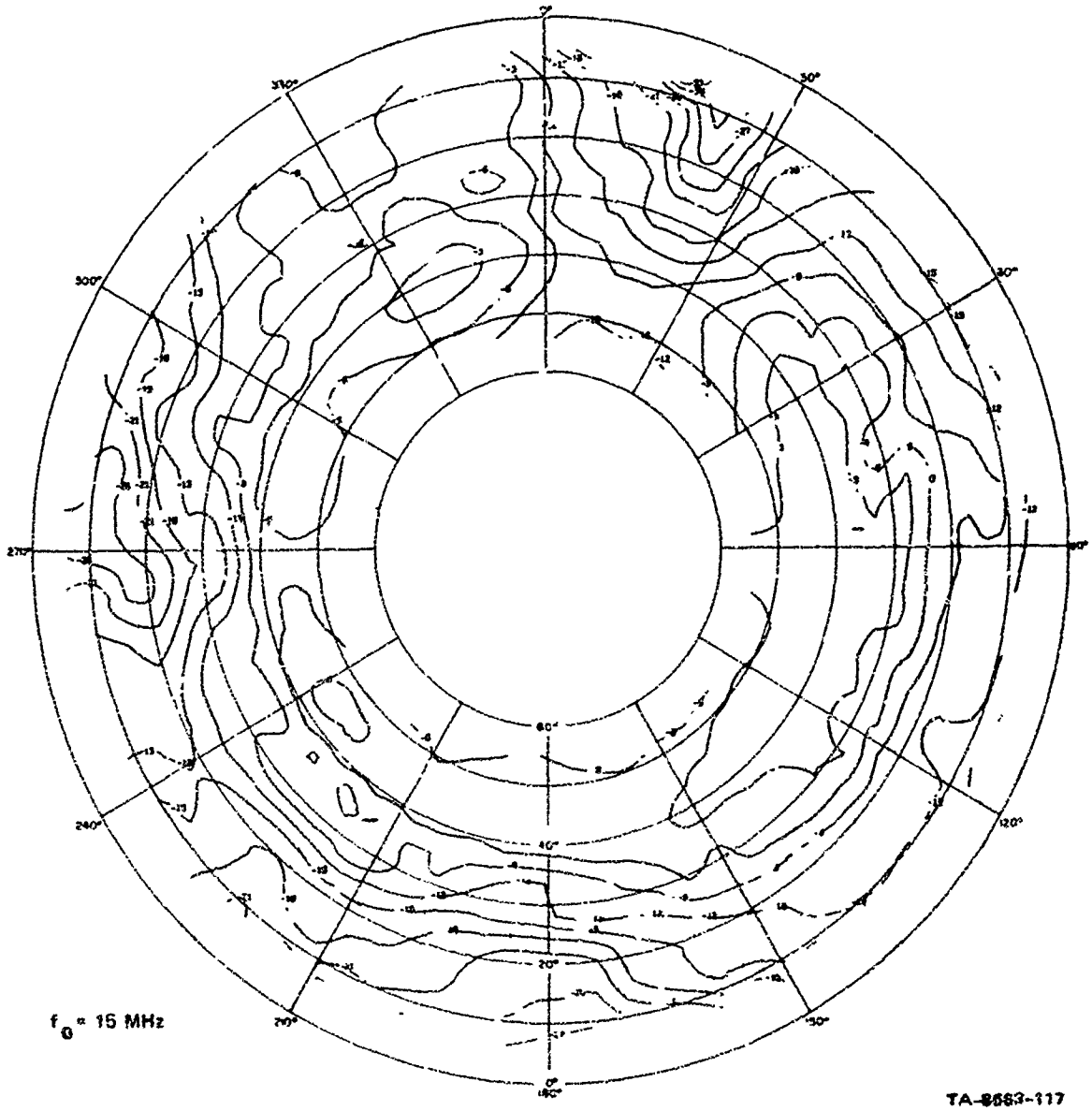

FIGURE A-23 MEASURED PATTERN OF MONOPOLE ANTENNA IN FOREST AT ALMANOR, E_θ AT 8 MHz

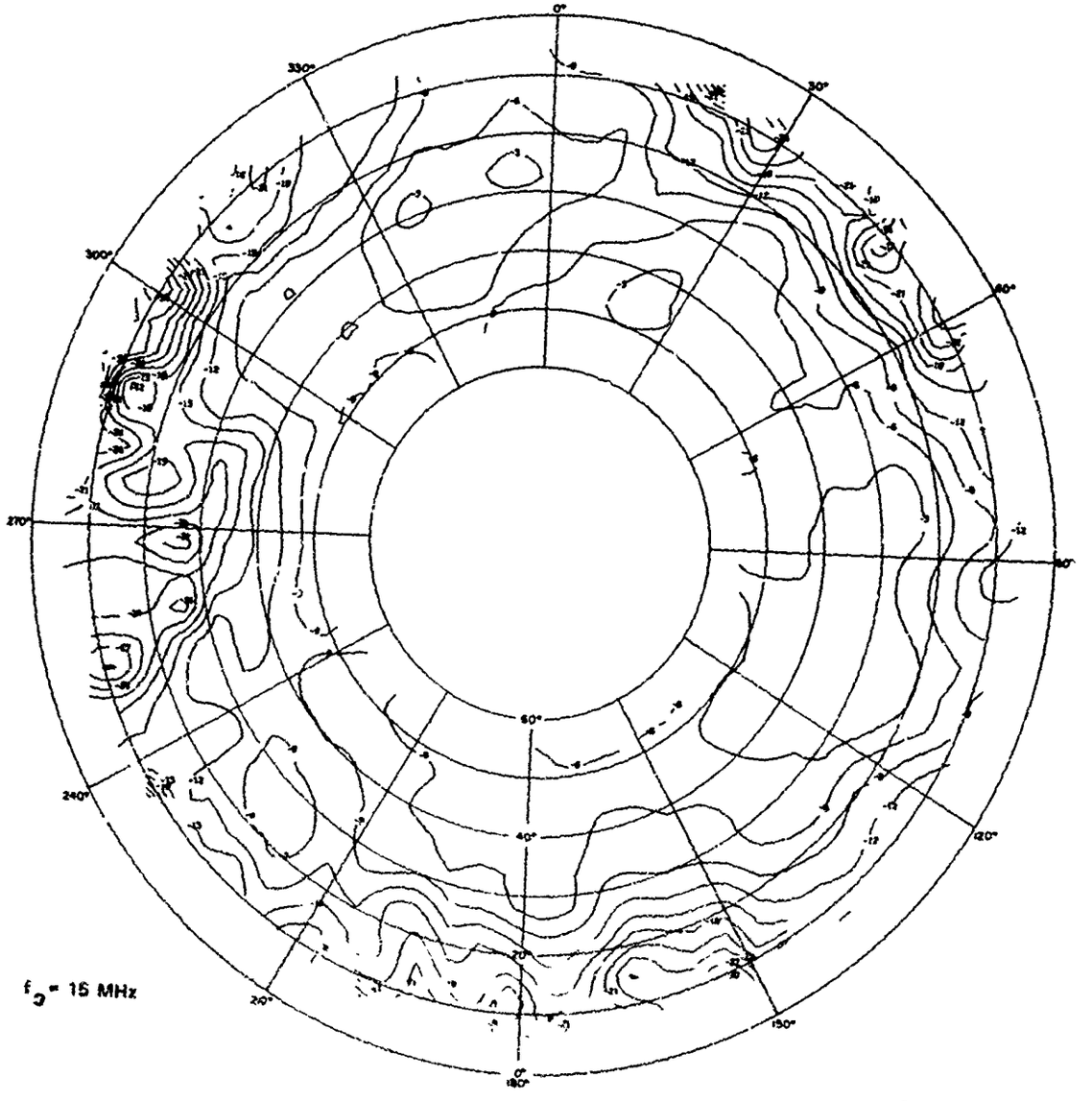

TA-8663-118

FIGURE A-24 MEASURED PATTERN OF MONOPOLE ANTENNA IN FOREST AT ALMANOR, E_θ AT 15 MHz

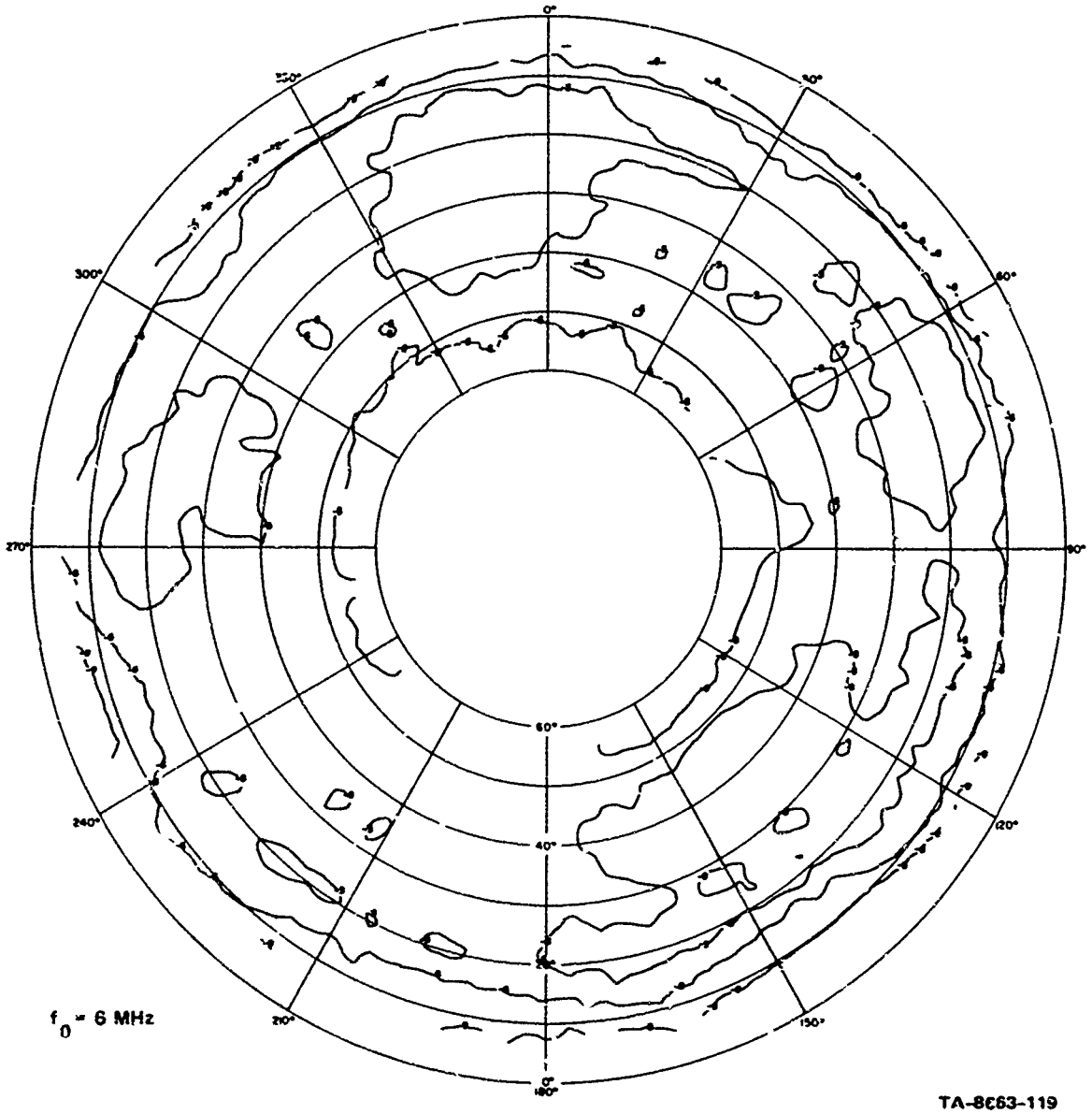

FIGURE A-25 MEASURED PATTERN OF MONOPOLE IN FOREST AT BAN MUN CHIT, E_θ AT 8 MHz

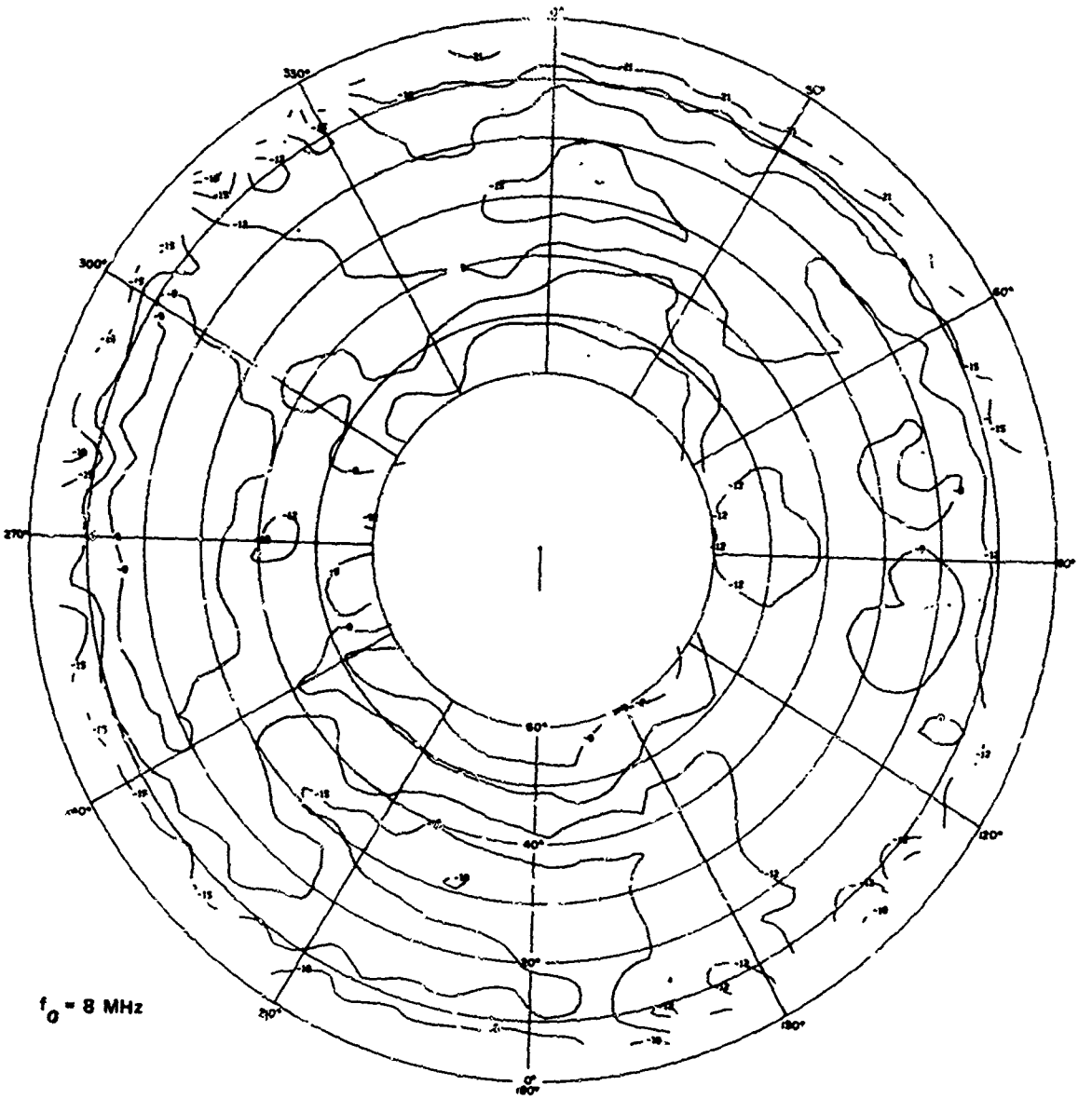

FIGURE A-26 MEASURED PATTERN OF 2:1 INVERTED-L ANTENNA AT LODI, E_θ AT 8 MHz

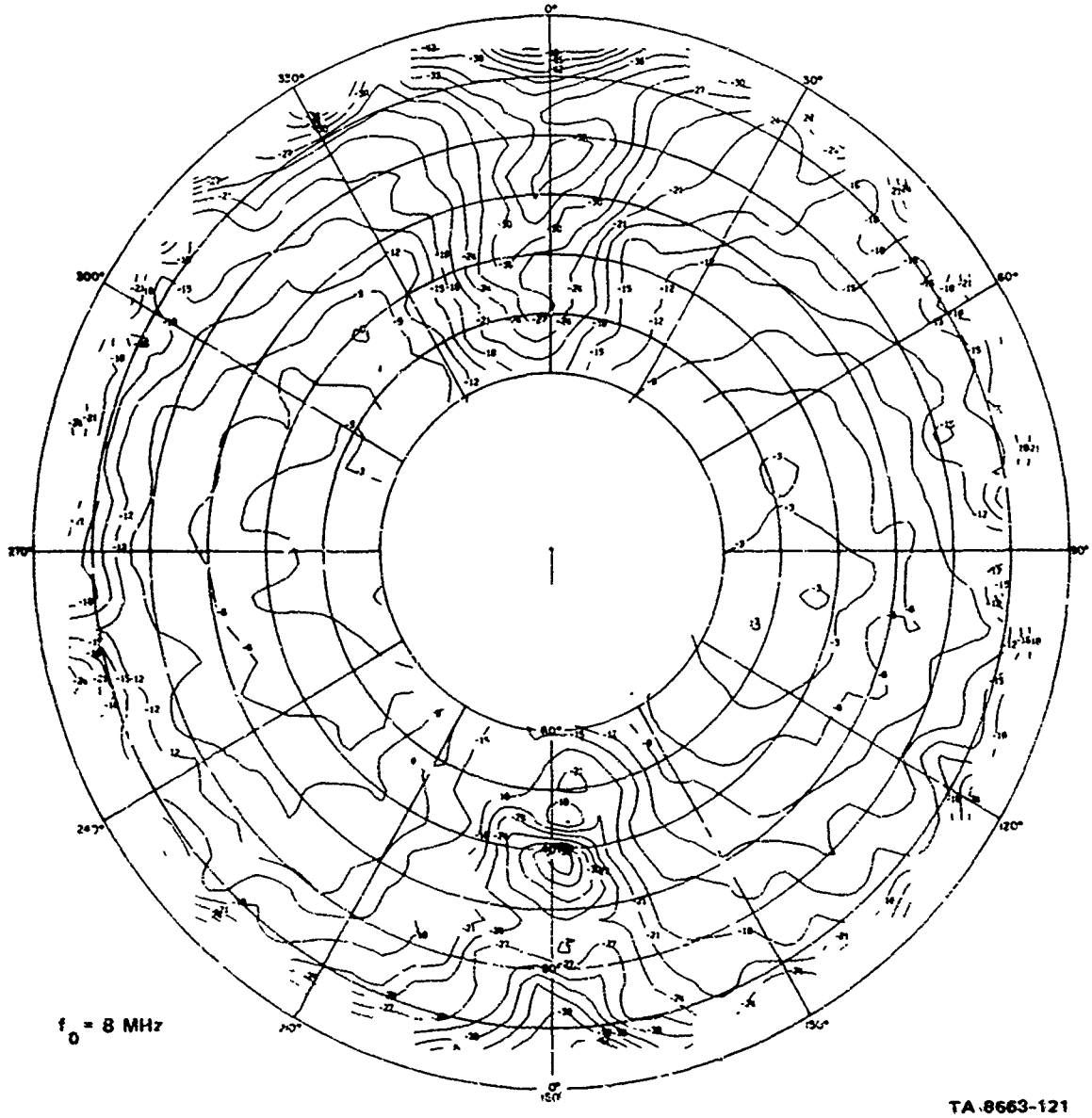

FIGURE A-27 MEASURED PATTERN OF 2:1 INVERTED-L ANTENNA AT LODI, E_ϕ AT 8 MHz

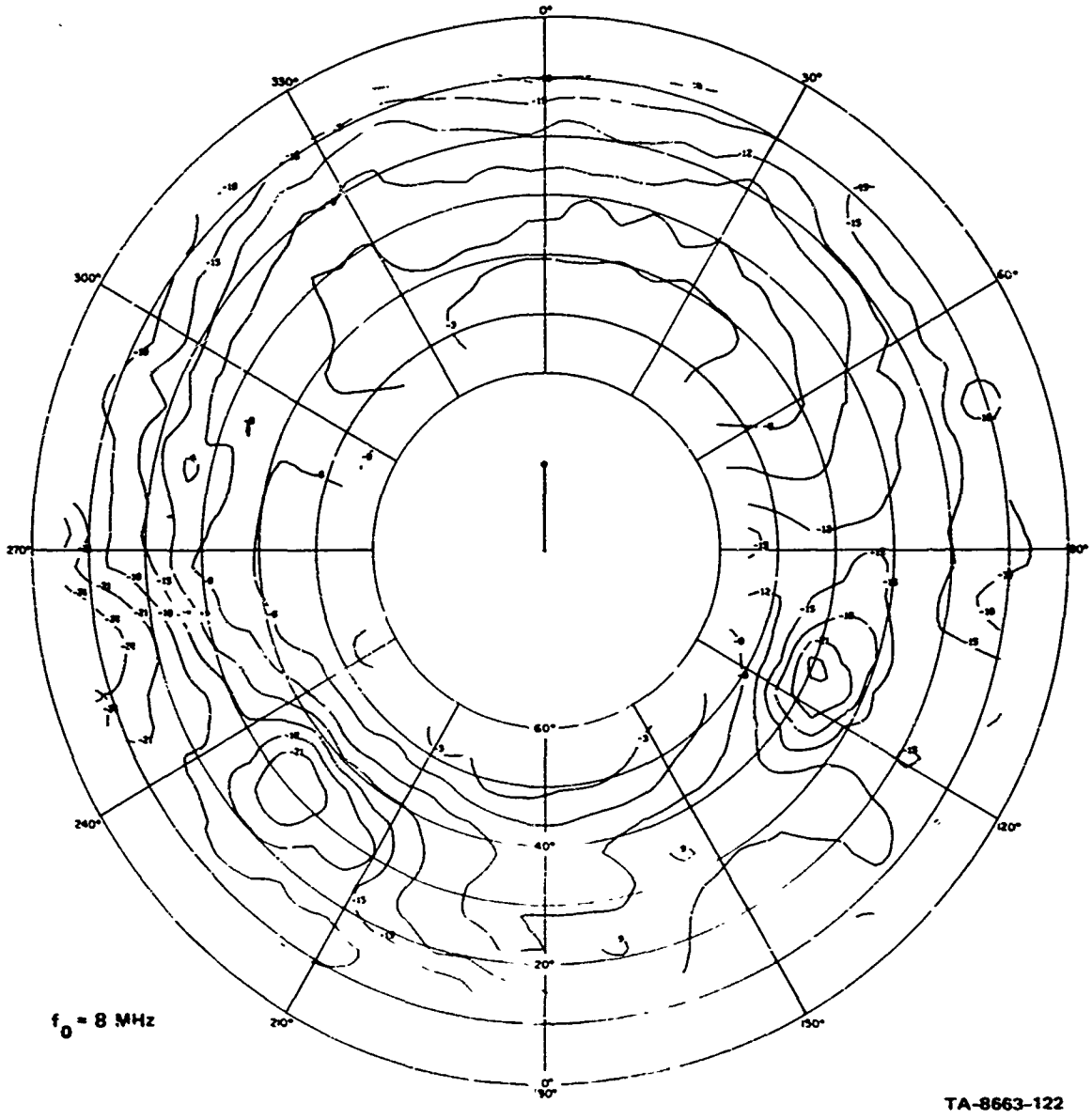

FIGURE A-28 MEASURED PATTERN OF 2:1 INVERTED-L ANTENNA IN FOREST AT ALMANOR, E_ζ AT 8 MHz

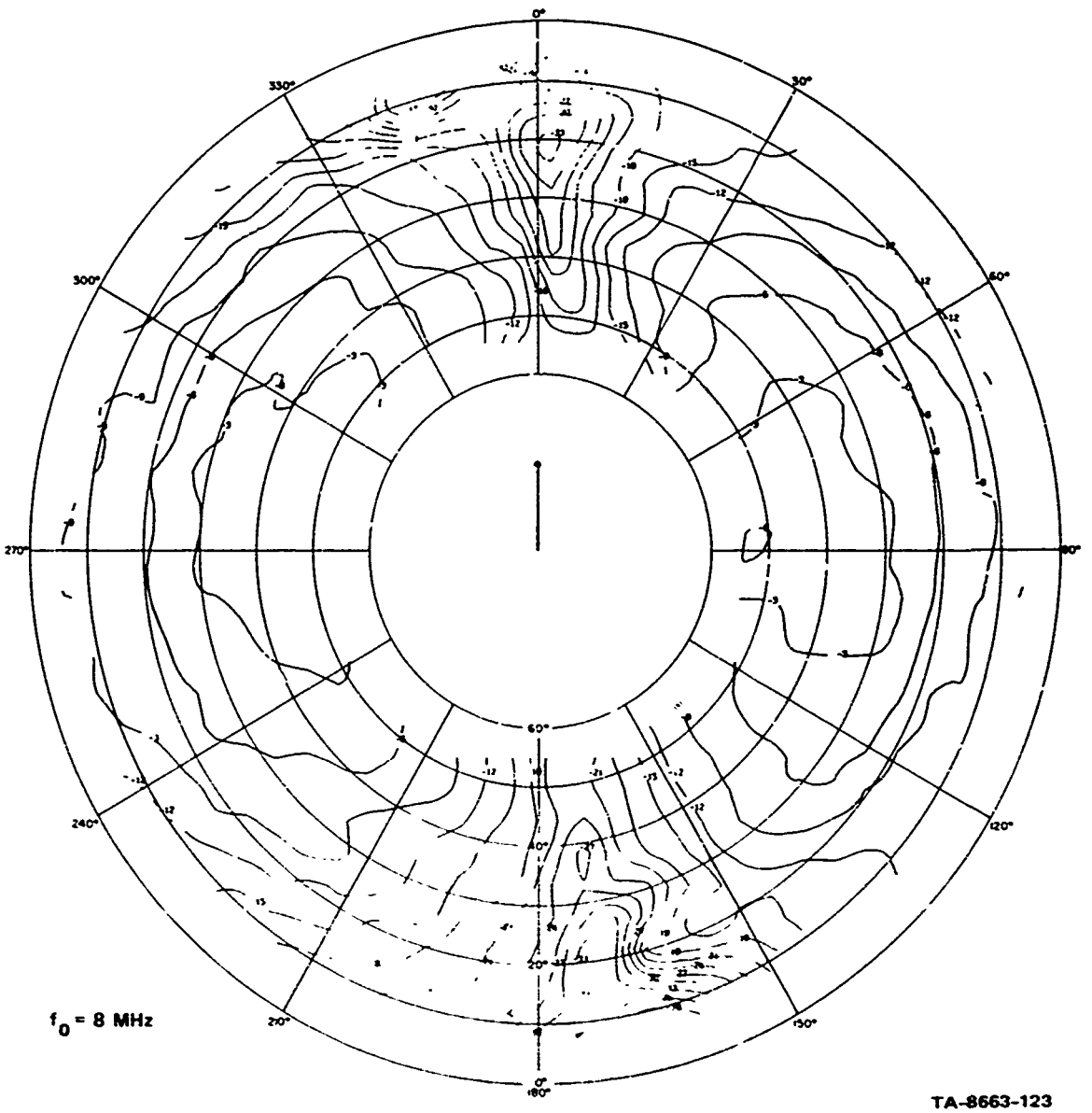

FIGURE A-29 MEASURED PATTERN OF 2:1 INVERTED-L ANTENNA IN FOREST AT ALMANOR, E_ϕ AT 8 MHz

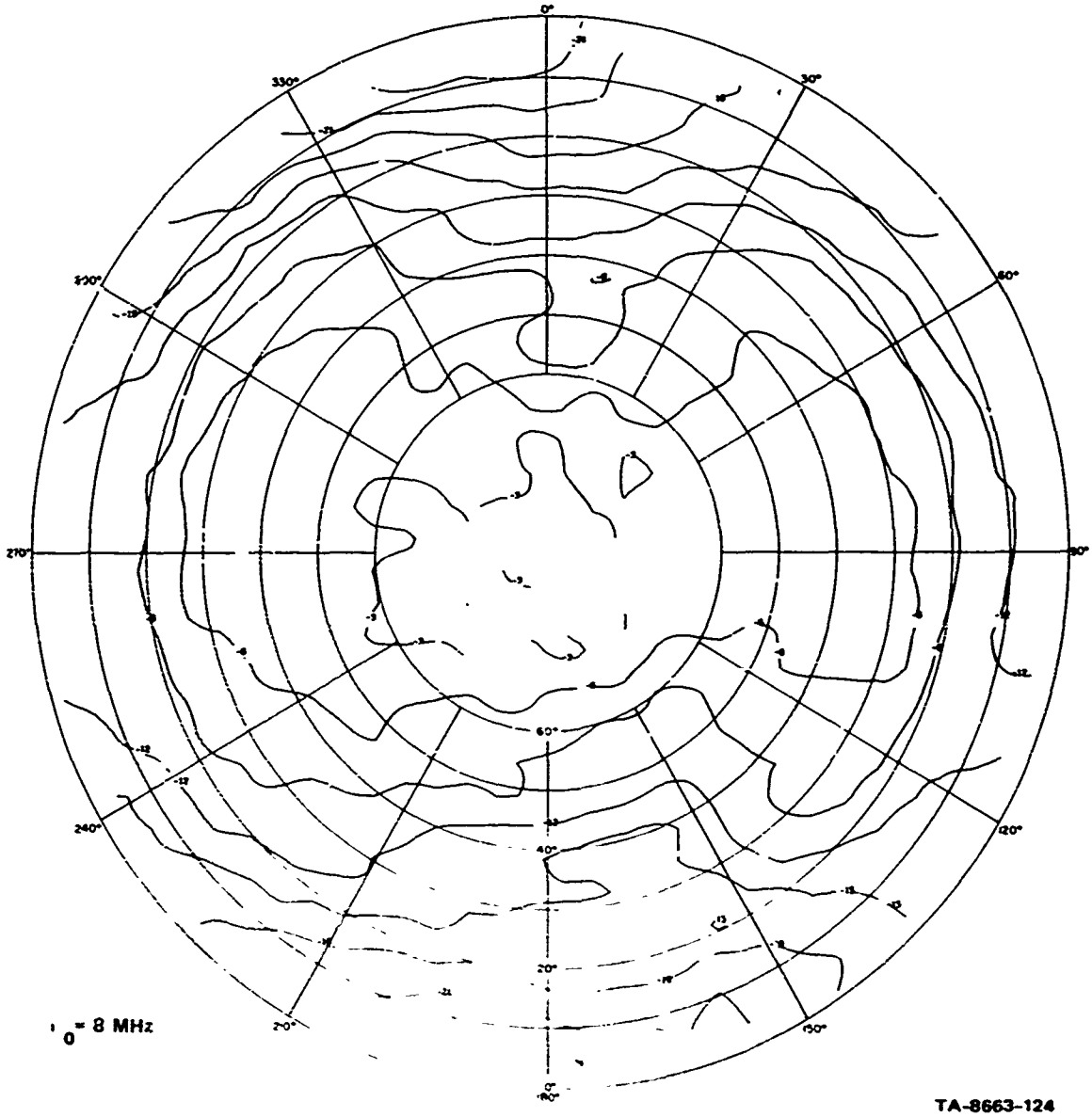

FIGURE A-30 MEASURED PATTERN OF 2:1 INVERTED-L ANTENNA IN FOREST AT ALMANOR, POWER AT 8 MHz

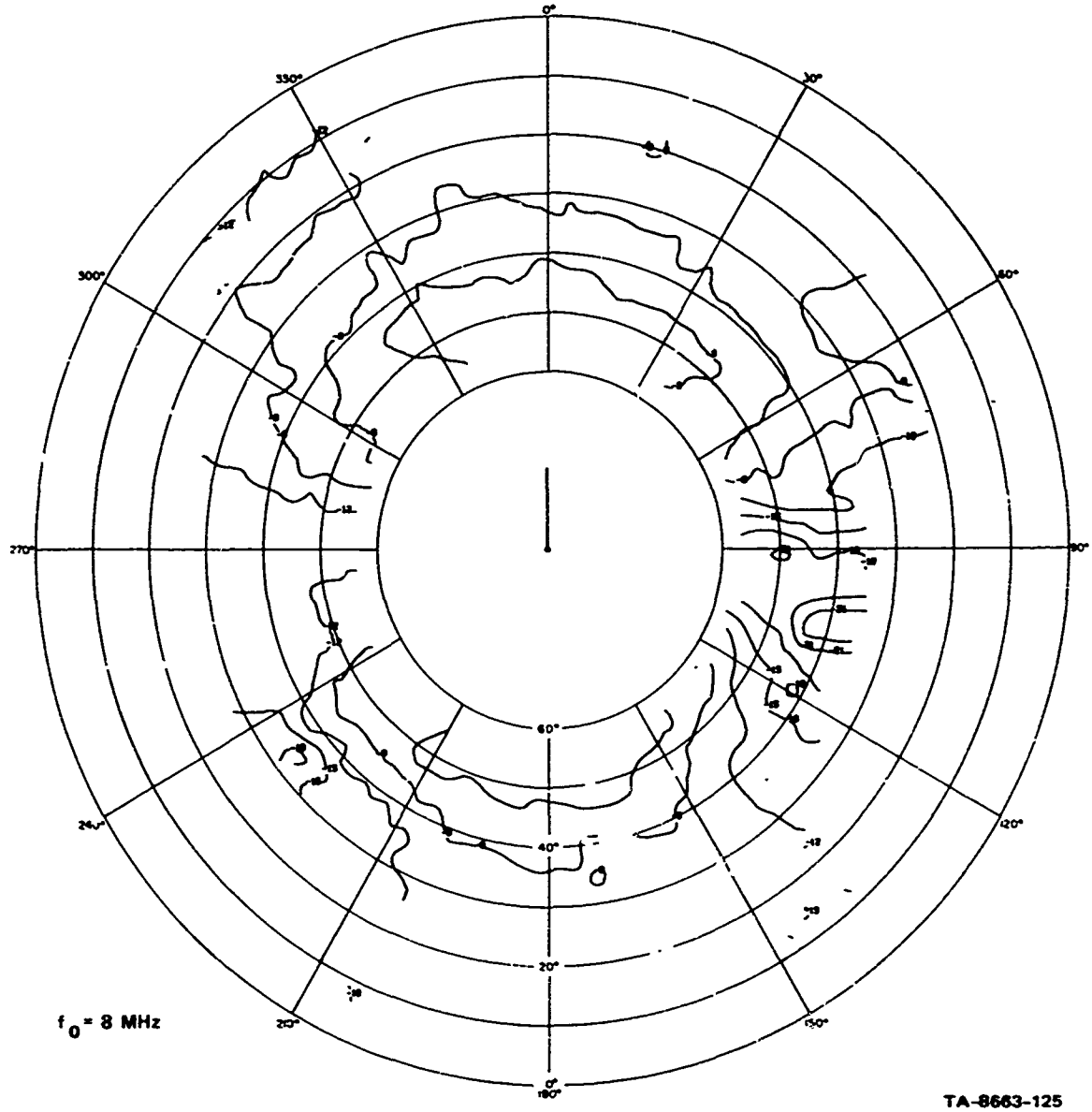

FIGURE A-31 MEASURED PATTERN OF 2:1 INVERTED-L ANTENNA IN FOREST AT BAN MUN CHIT, E_θ AT 8 MHz

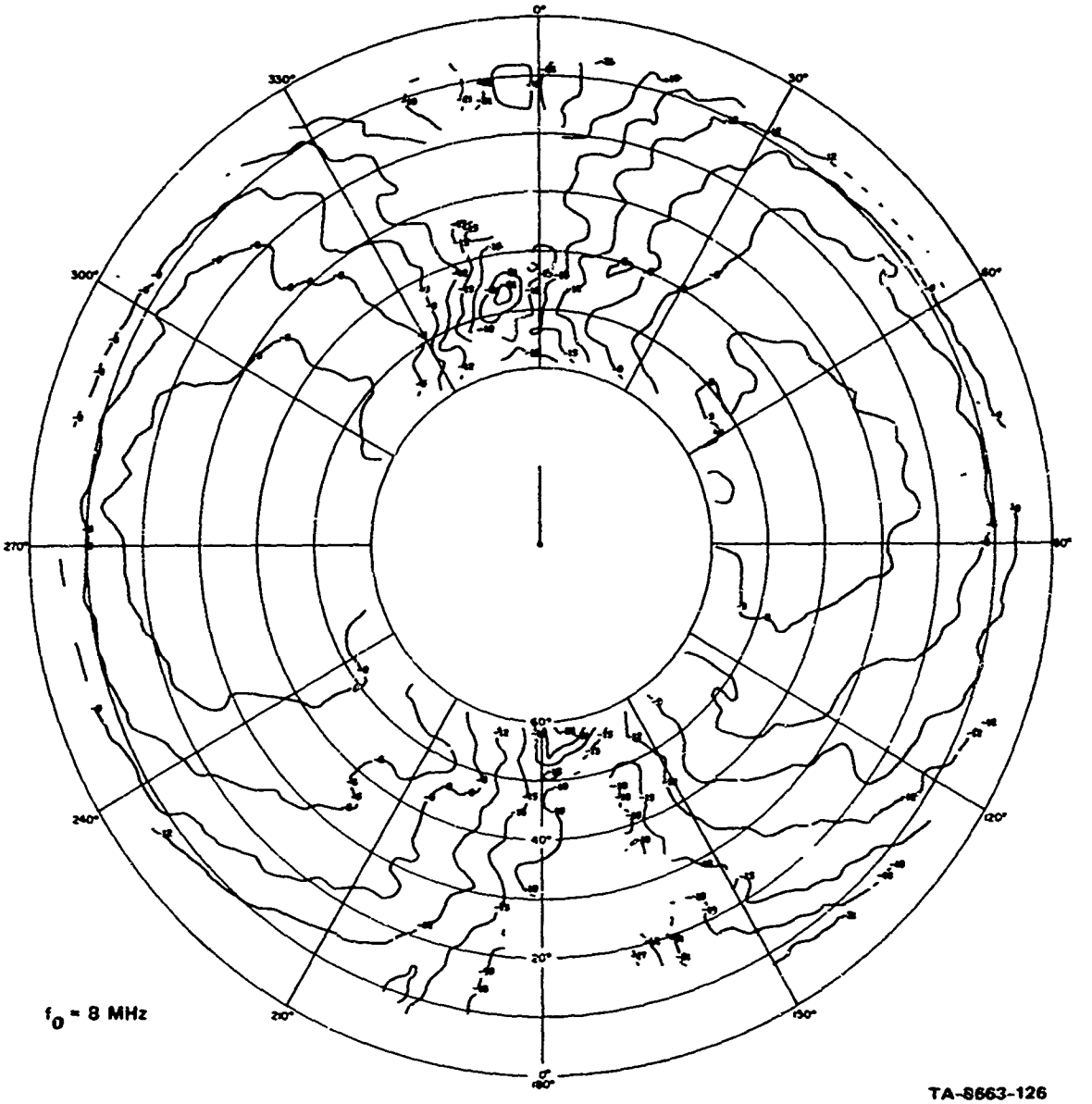

FIGURE A-32 MEASURED PATTERN OF 2:1 INVERTED-L ANTENNA IN FOREST AT BAN MUN CHIT, E_ϕ AT 8 MHz

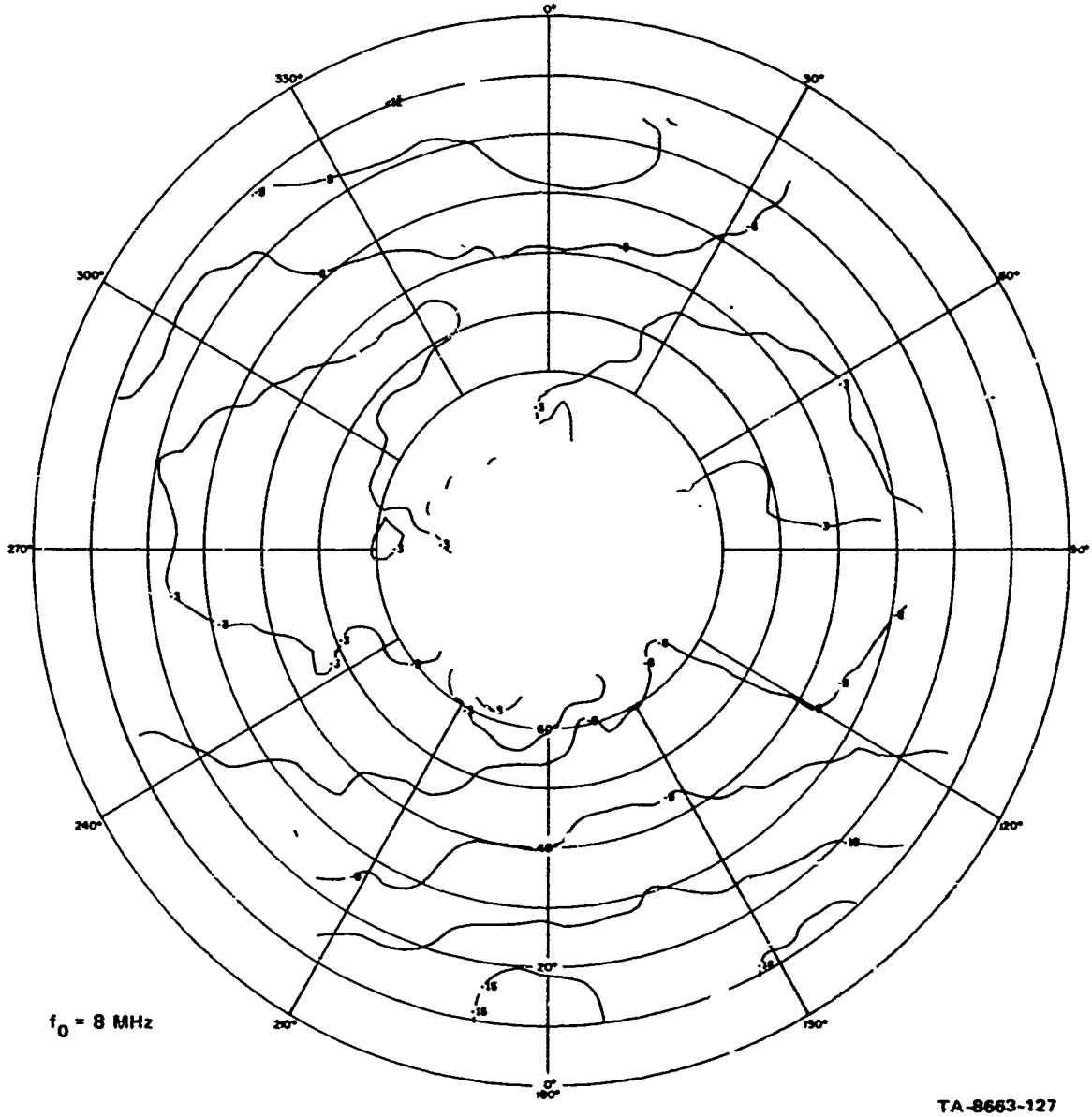

FIGURE A-33 MEASURED PATTERN OF 2:1 INVERTED-L ANTENNA IN FOREST AT BAN MUN CHIT, POWER AT 8 MHz

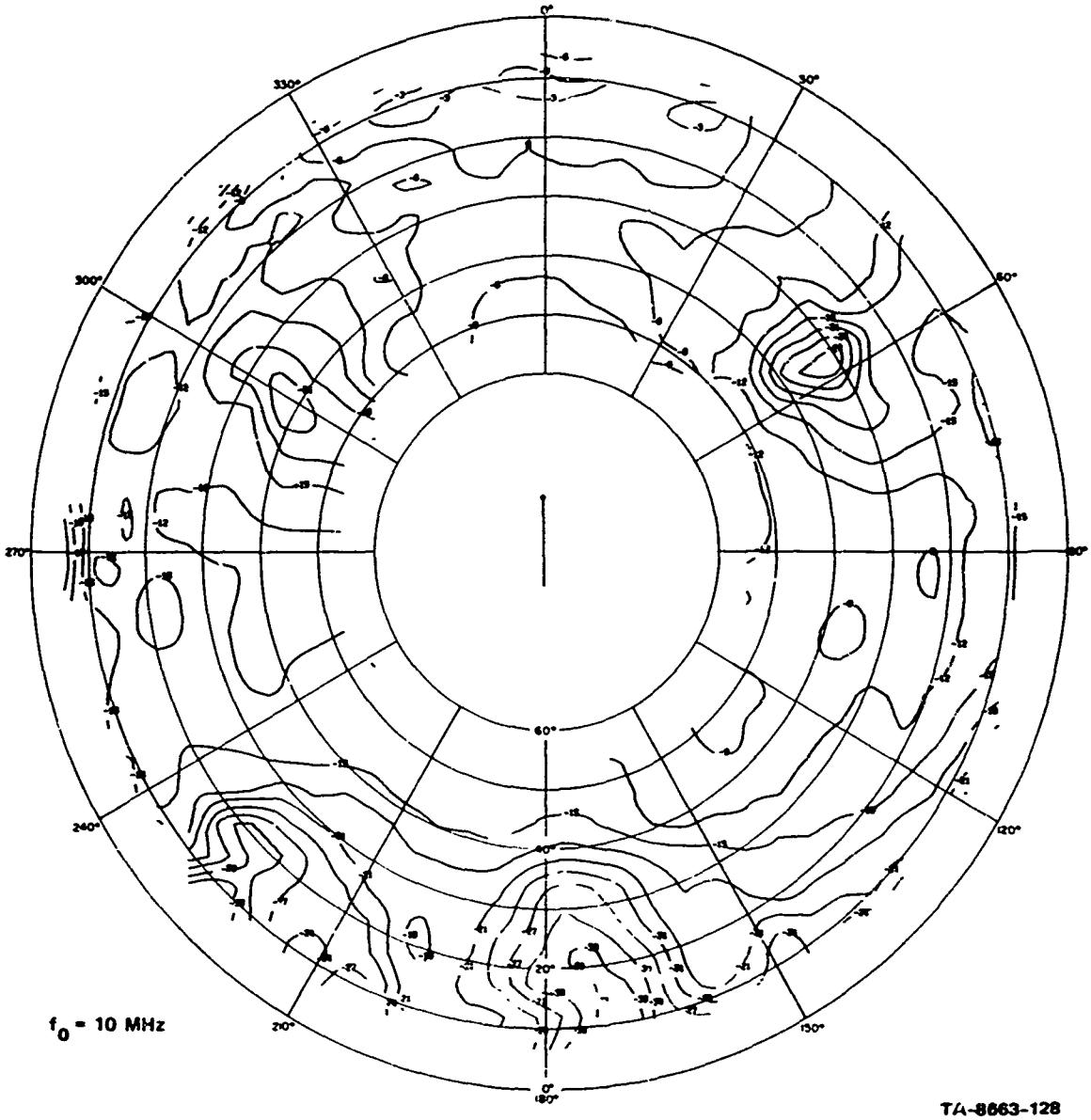

FIGURE A-34 MEASURED PATTERN OF 5:1 INVERTED-L ANTENNA IN FOREST AT ALMANOR, E_θ AT 10 MHz

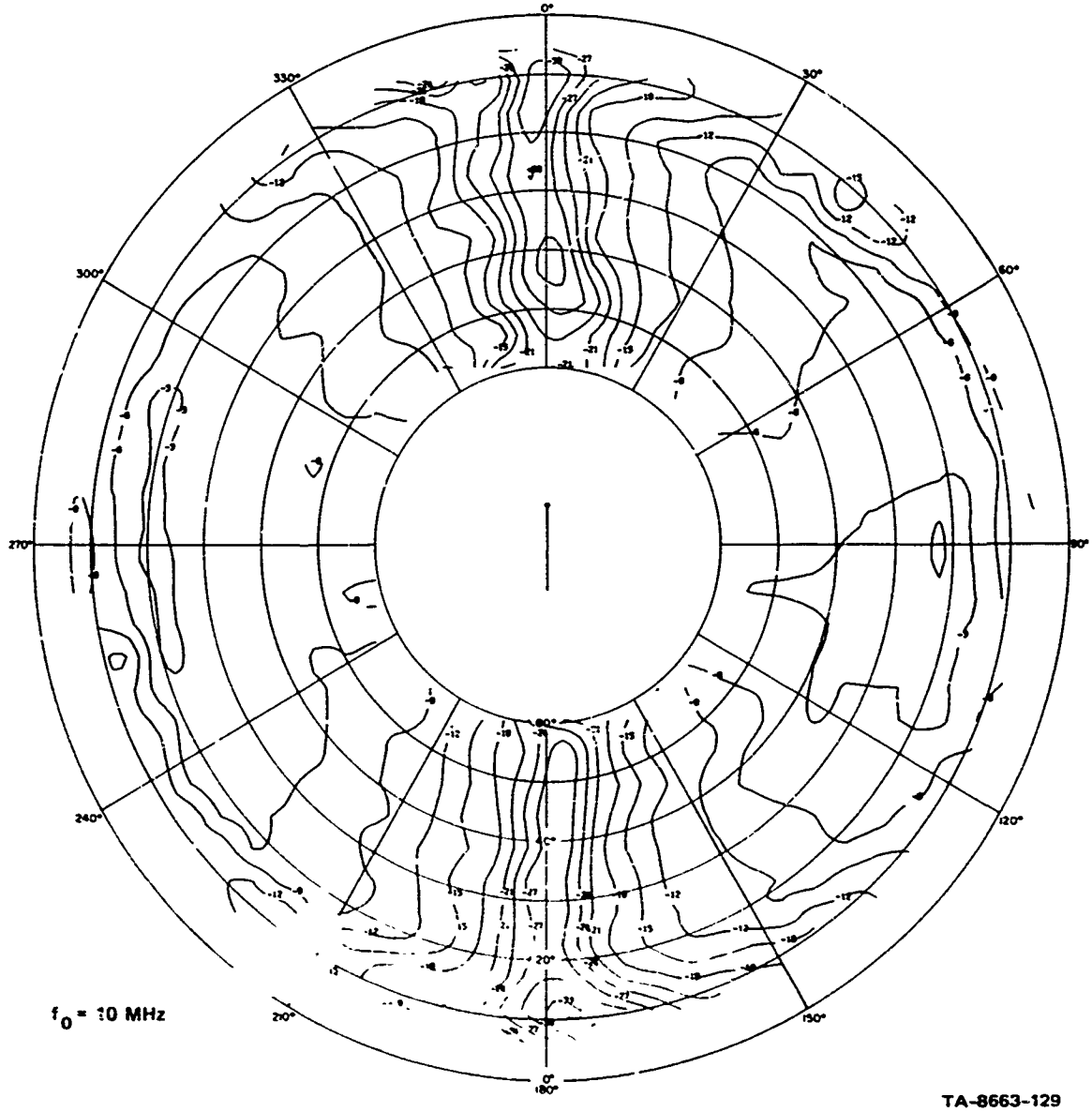

FIGURE A-35 MEASURED PATTERN OF 5:1 INVERTED-L ANTENNA IN FOREST AT ALMANOR, E_ϕ AT 10 MHz

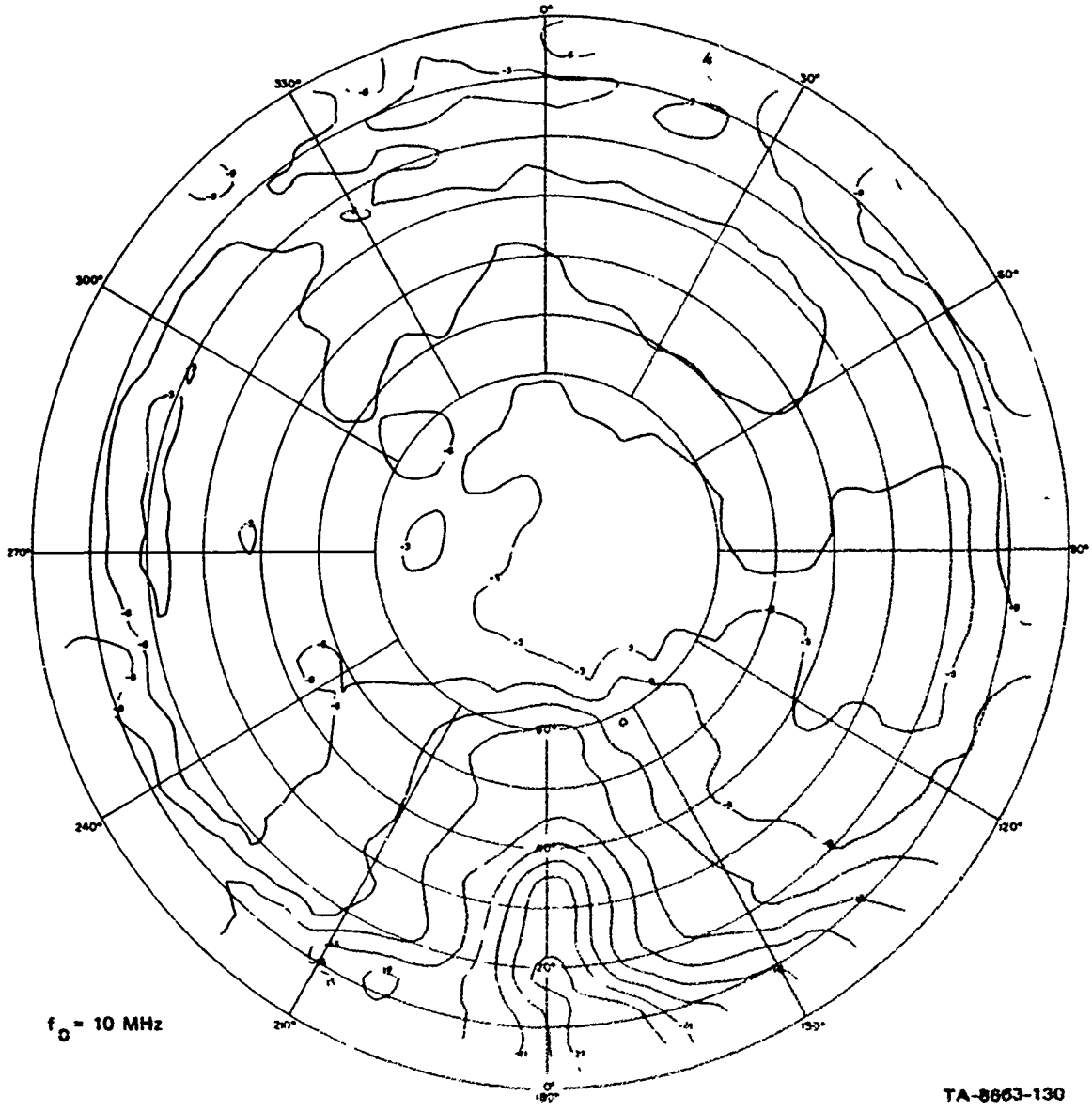

FIGURE A-36 MEASURED PATTERN OF 5:1 INVERTED-L ANTENNA IN FOREST AT ALMANOR, POWER AT 10 MHz

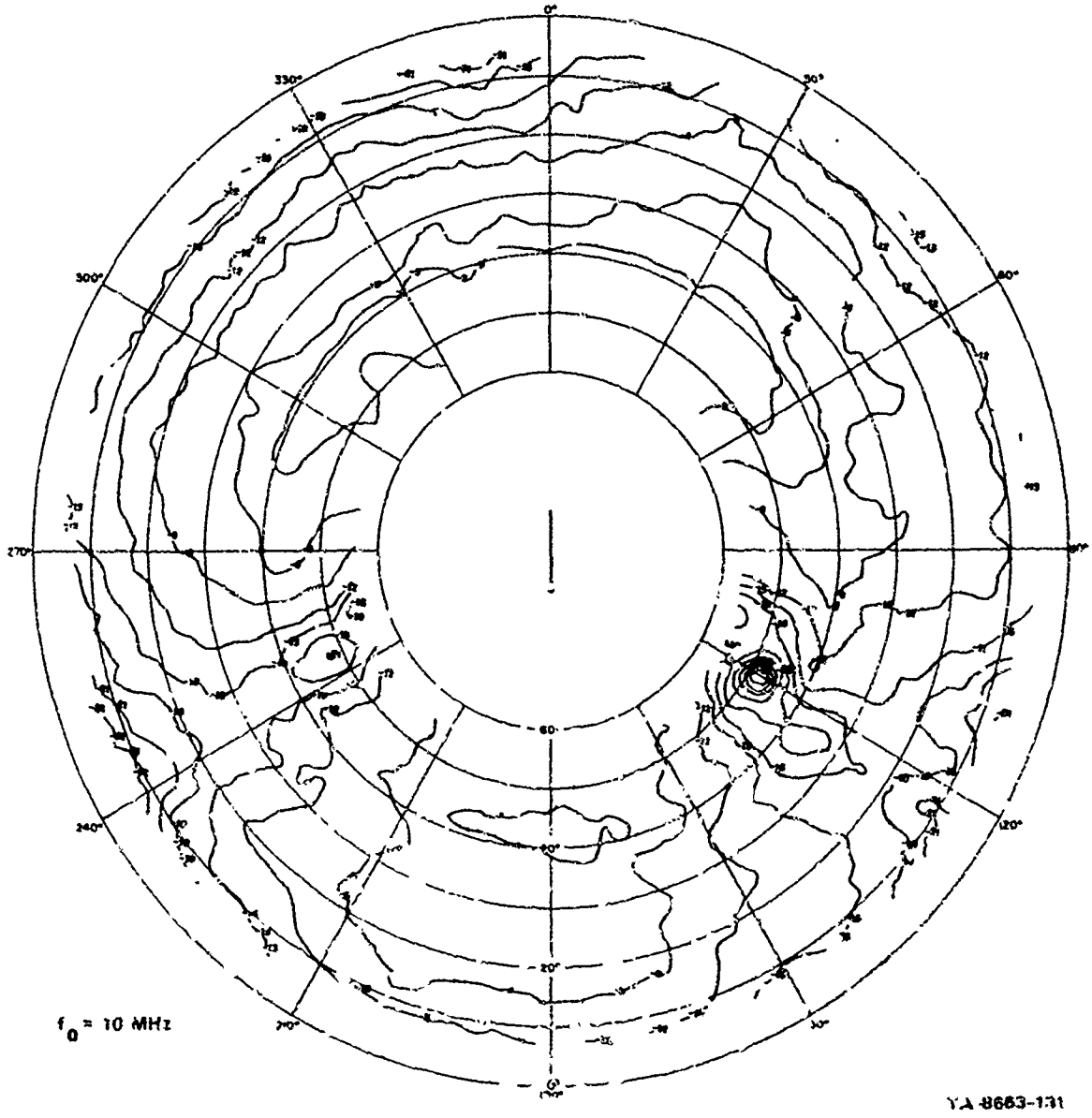

FIGURE A-37 MEASURED PATTERN OF 5.1 INVERTED-L ANTENNA IN FOREST AT BAN MUN CHIT, E_θ AT 10 MHz

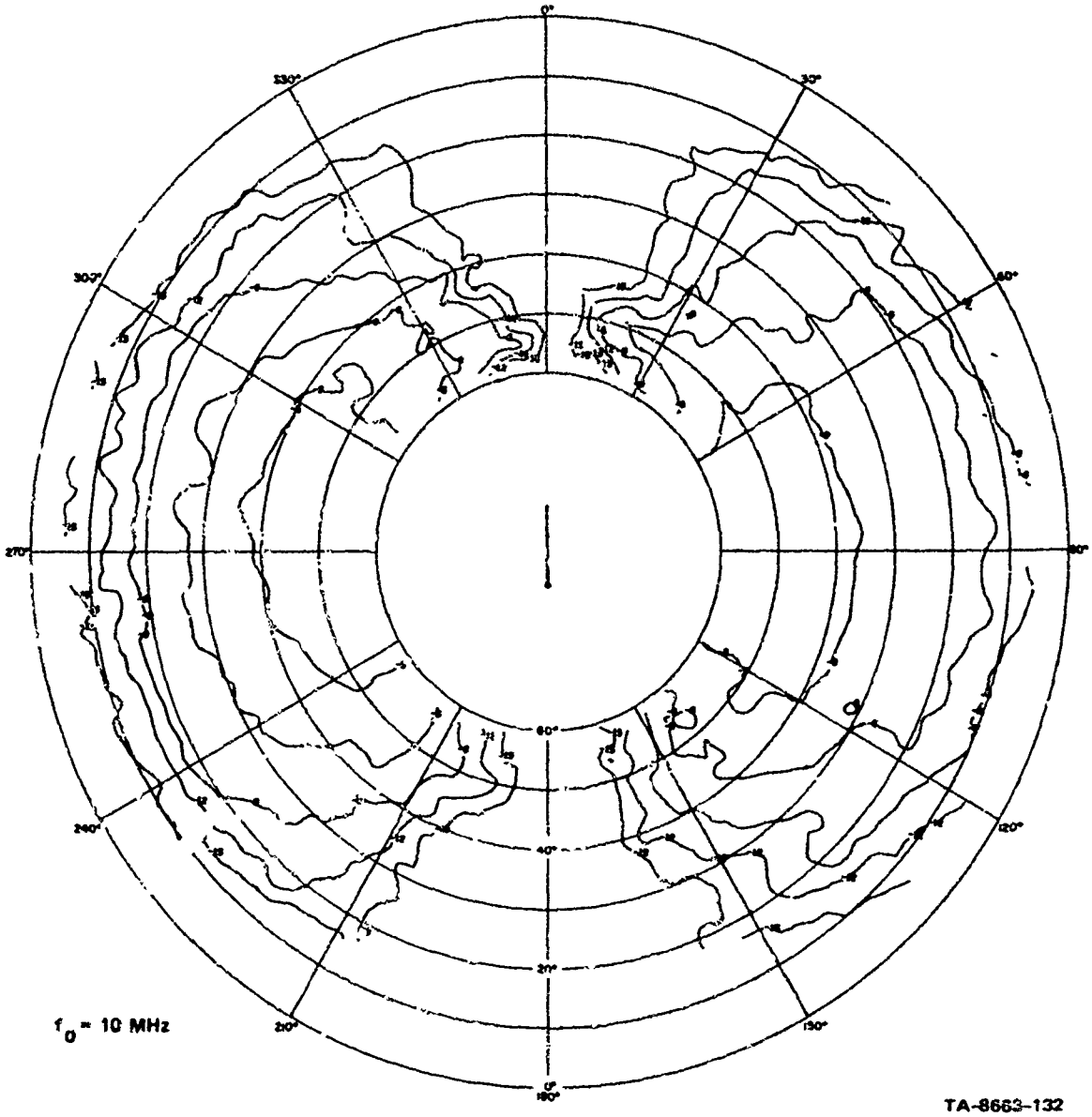

FIGURE A-38 MEASURED PATTERN OF 5:1 INVERTED-L ANTENNA IN FOREST AT BAN MUN CHIT, E_φ AT 10 MHz

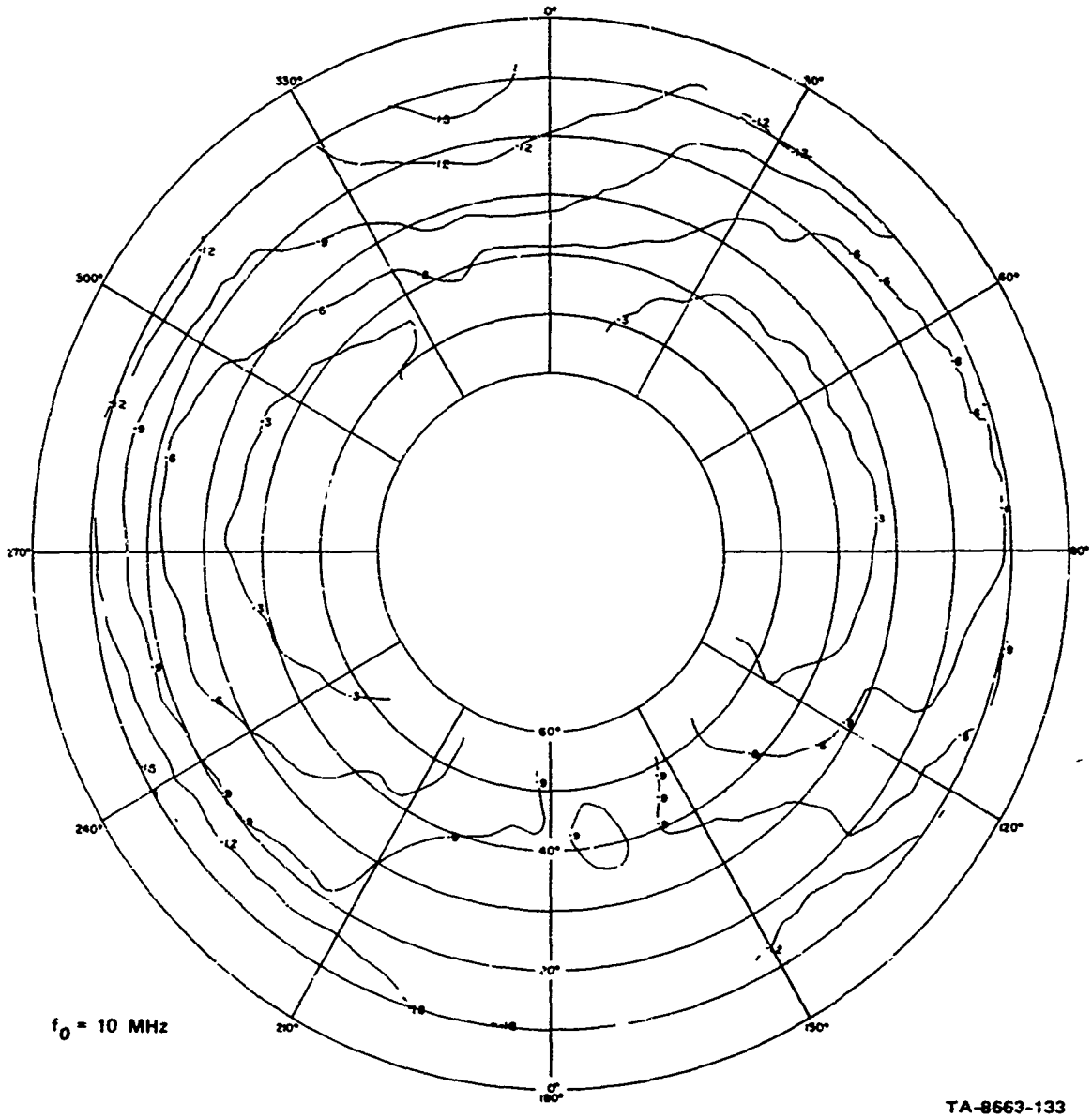

FIGURE A-39 MEASURED PATTERN OF 5:1 INVERTED-L ANTENNA IN FOREST AT BAN MUN CHIT, POWER AT 10 MHz

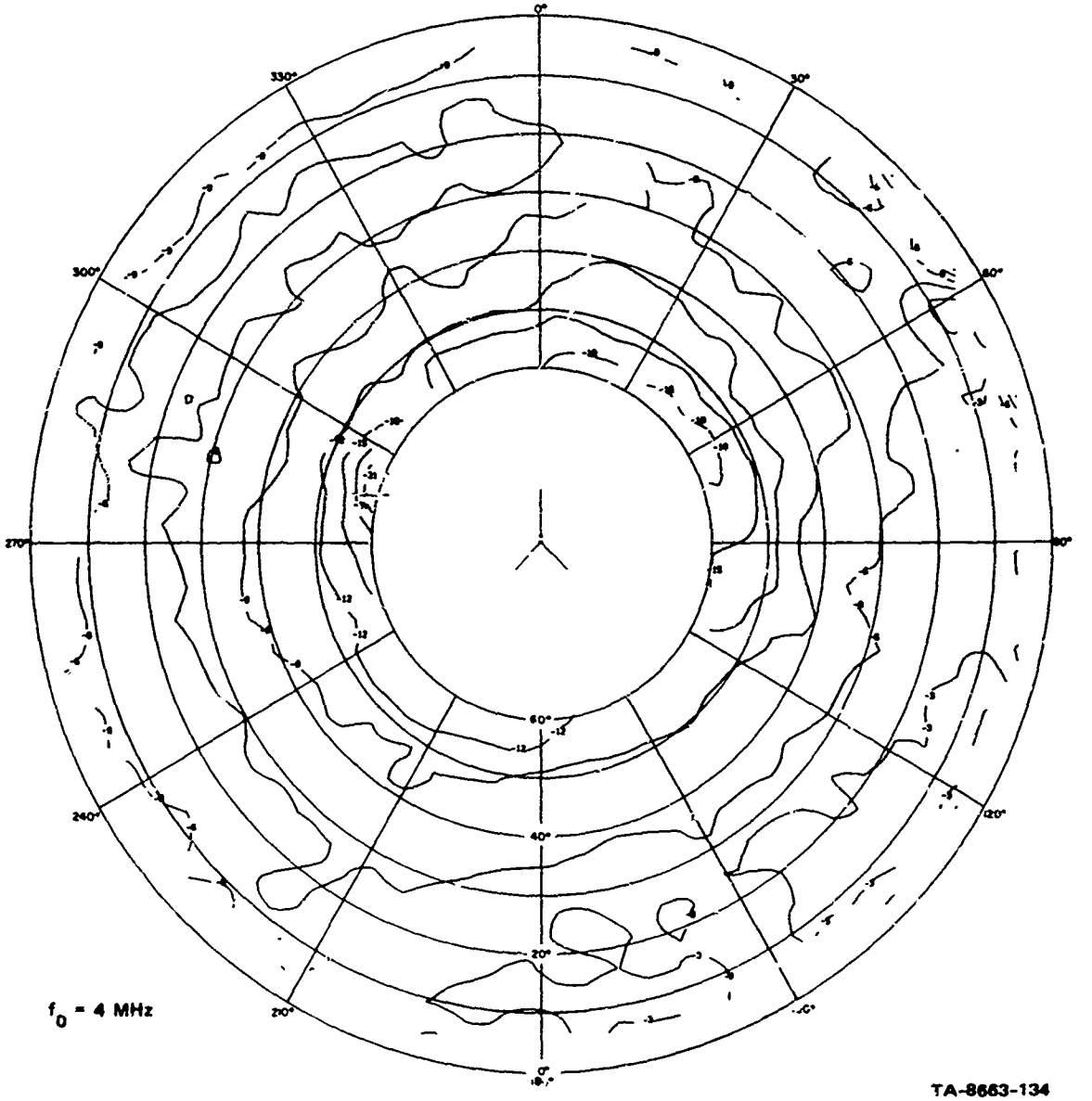

FIGURE A-40 MEASURED PATTERN OF 30° SLANT-WIRE ANTENNA AT LODI. E_θ AT 4 MHz

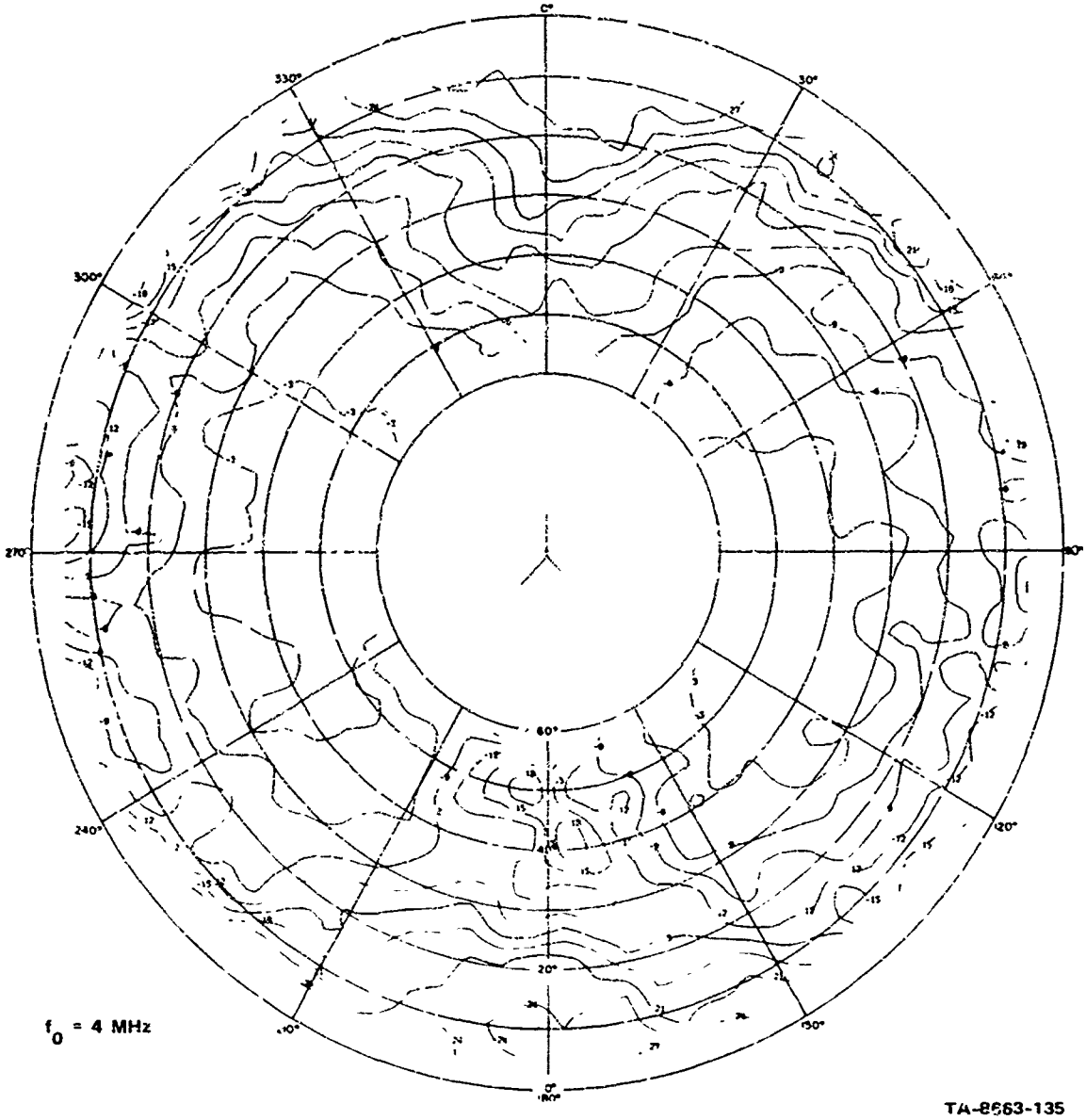

FIGURE A-41 MEASURED PATTERN OF 30° SLANT-WIRE ANTENNA AT LODI, E_ϕ AT 4 MHz

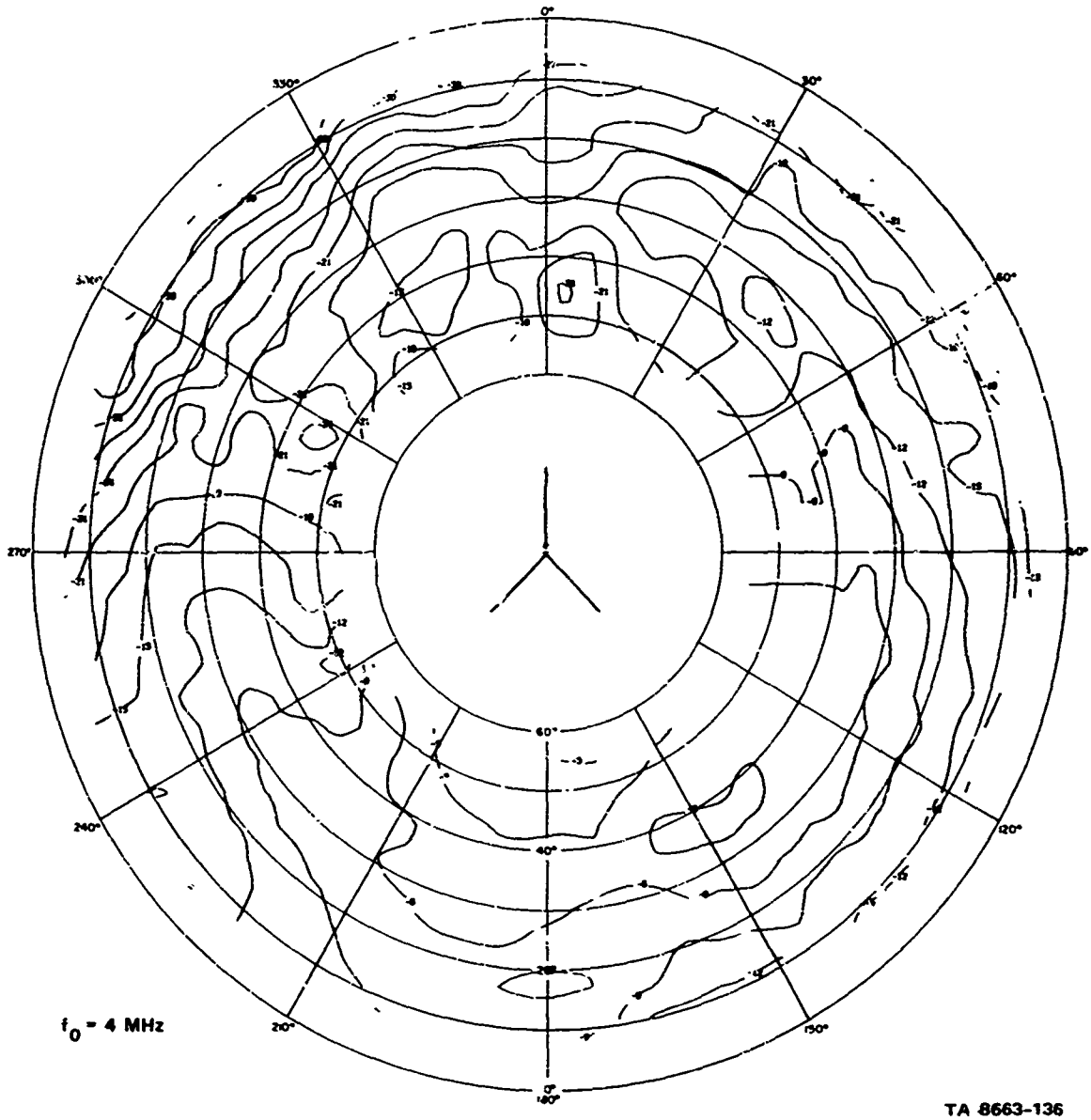

FIGURE A-42 MEASURED PATTERN OF 30° SLANT-WIRE ANTENNA IN FOREST AT ALMANOR, E_θ AT 4 MHz

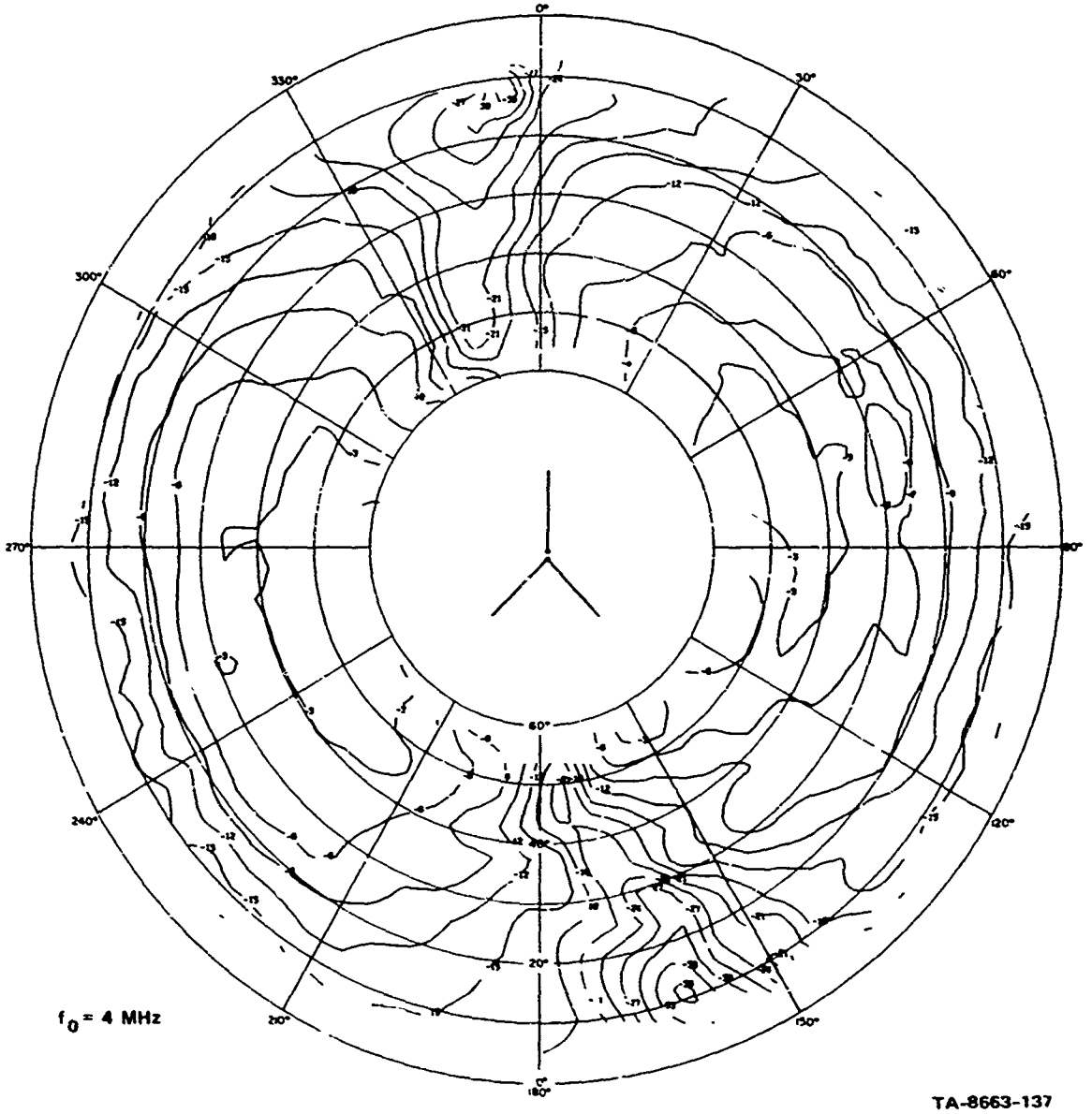

FIGURE A-43 MEASURED PATTERN OF 30° SLANT-WIRE ANTENNA IN FOREST AT ALMANOR, E_ϕ AT 4 MHz

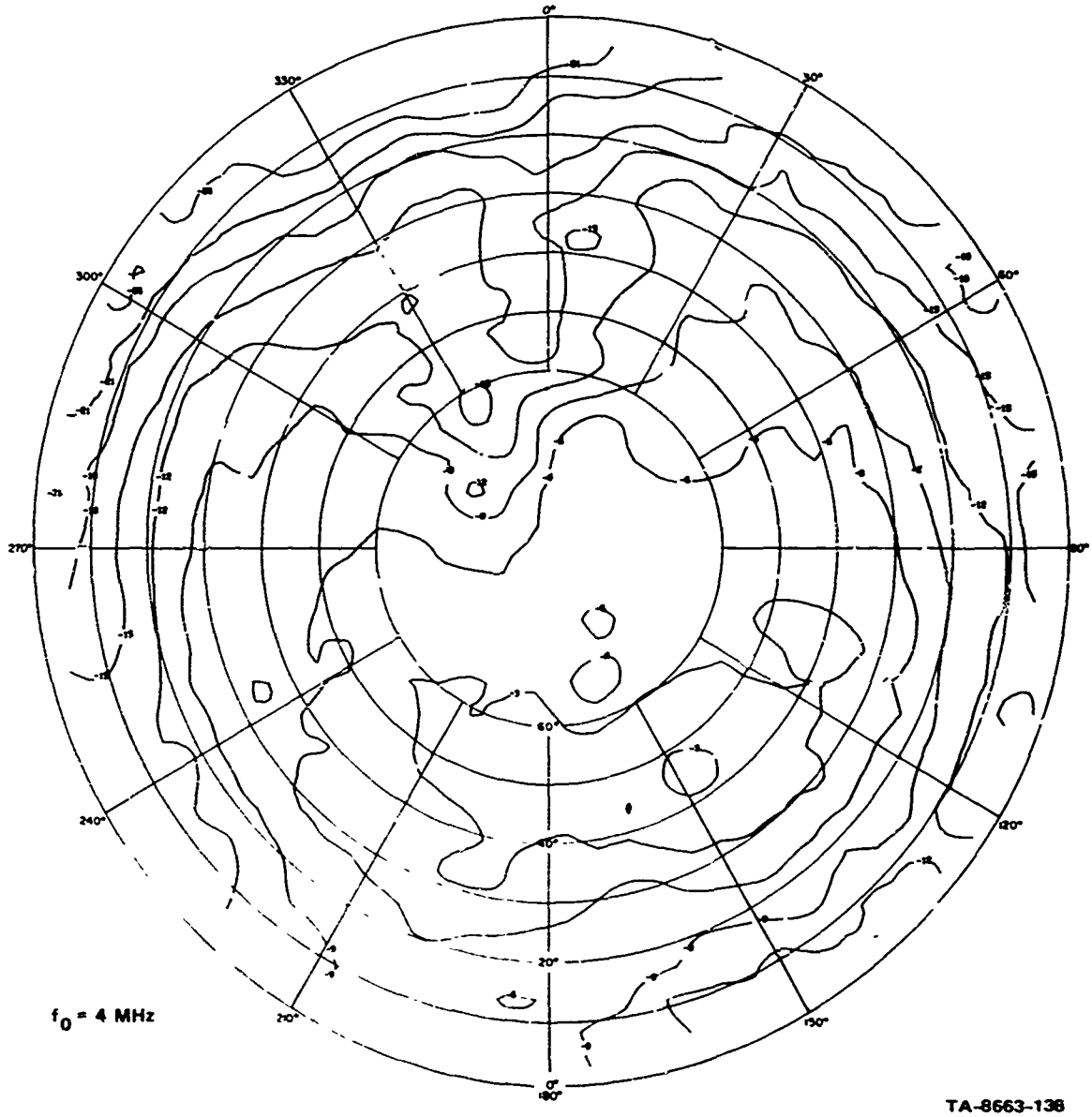

FIGURE A-44 MEASURED PATTERN OF 30° SLANT-WIRE ANTENNA IN FOREST AT ALMANOR, POWER AT 4 MHz

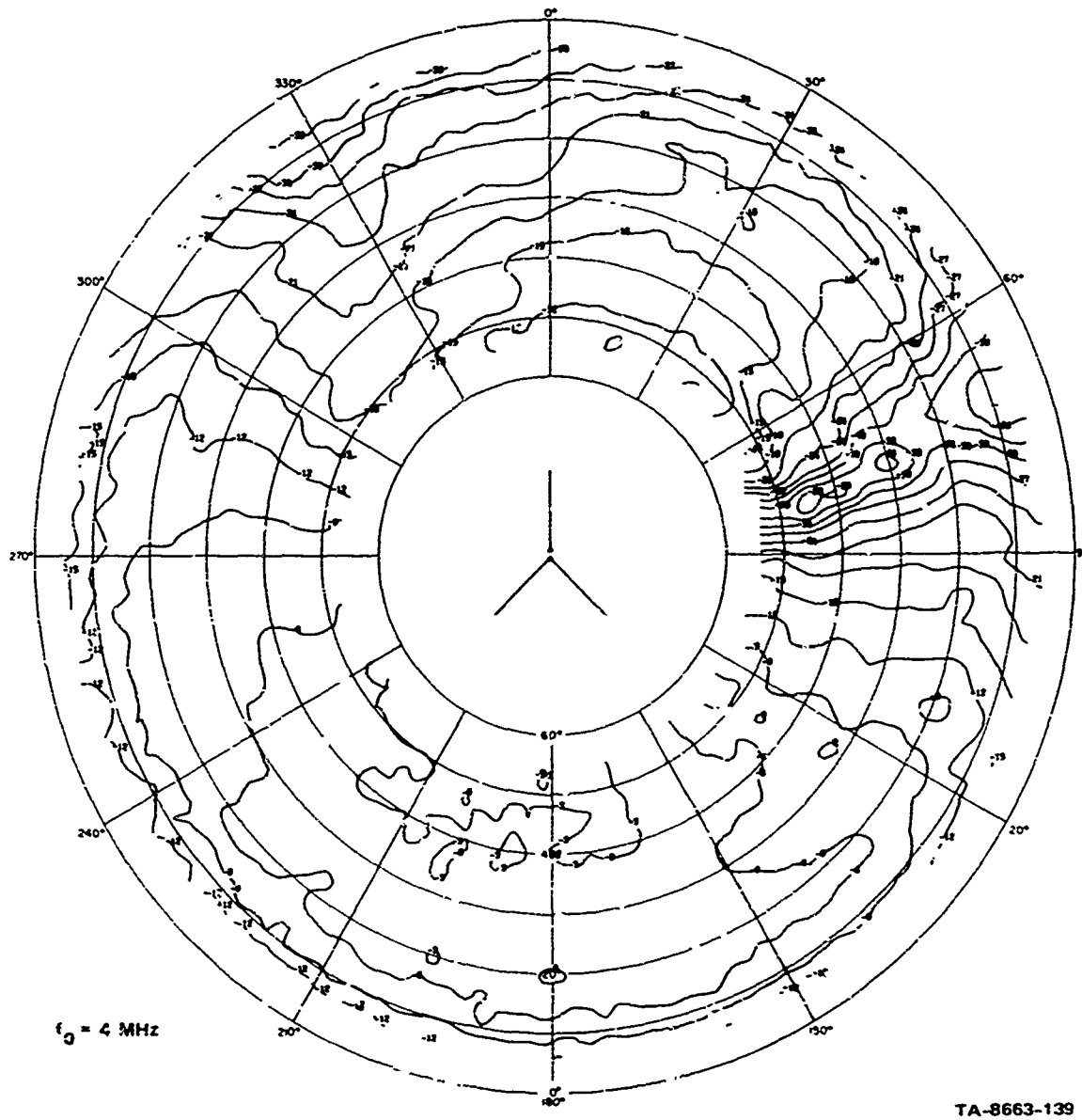

FIGURE A-45 MEASURED PATTERN OF 30° SLANT-WIRE ANTENNA IN FOREST AT BAN MUN CHIT, E_θ AT 4 MHz

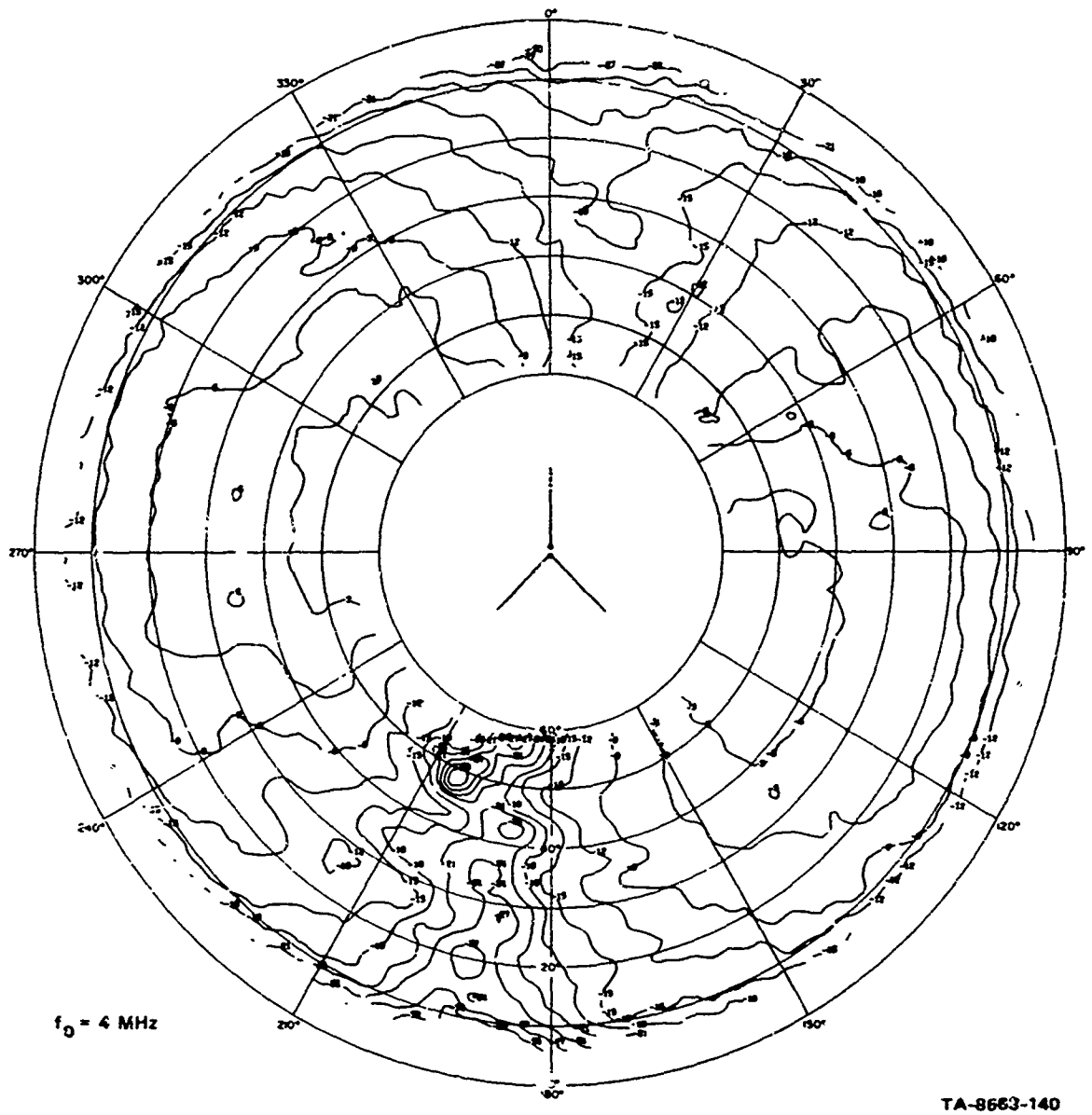

FIGURE A-46 MEASURED PATTERN OF 30° SLANT-WIRE ANTENNA IN FOREST AT BAN MUN CHIT, E_ϕ AT 4 MHz

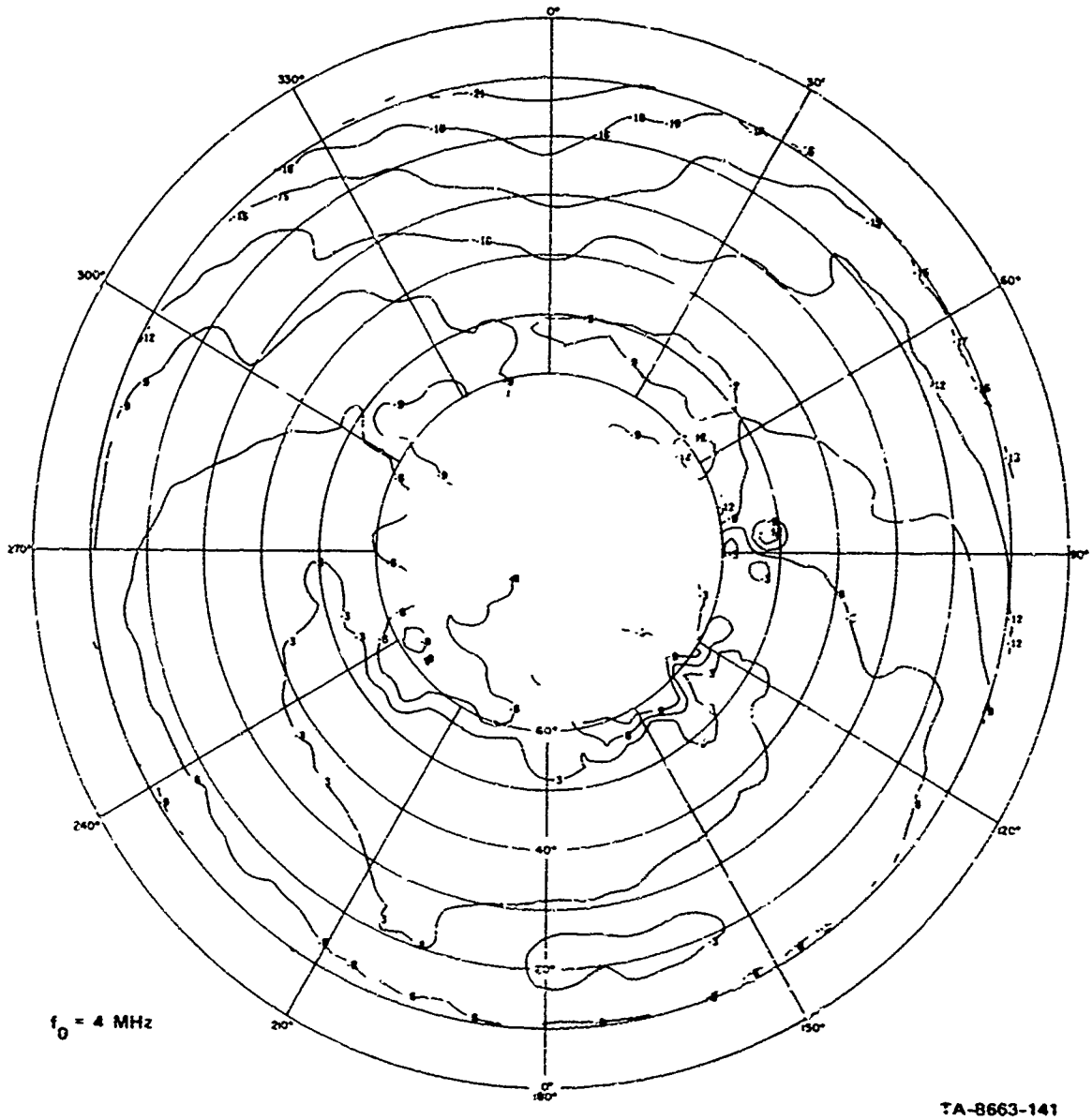

FIGURE A-47 MEASURED PATTERN OF 30° SLANT-WIRE ANTENNA IN FOREST AT BAN MUN CHIT, POWER AT 4 MHz

Appendix B

CONTOUR PLOTS OF THE RADIATION PATTERNS OF ANTENNAS MEASURED OVER HILLY TERRAIN

Appendix B

CONTOUR PLOTS OF THE RADIATION PATTERNS OF ANTENNAS MEASURED OVER HILLY TERRAIN

This appendix contains selected examples of the radiation patterns of antennas measured over hilly terrain near Livermore, California (under Contract DAHC07-67-C-0144) as discussed in Sec. VI of this report. The patterns are grouped by antenna type (e.g., dipoles, monopoles, and slant wire, in that order) with those located on the hilltop presented first and those on the hillside presented second. The E_θ (vertical polarization) response data are presented first, followed by the E_ϕ (horizontal polarization) response data for each antenna. A description of the contour plot was provided in Sec. III of this report.

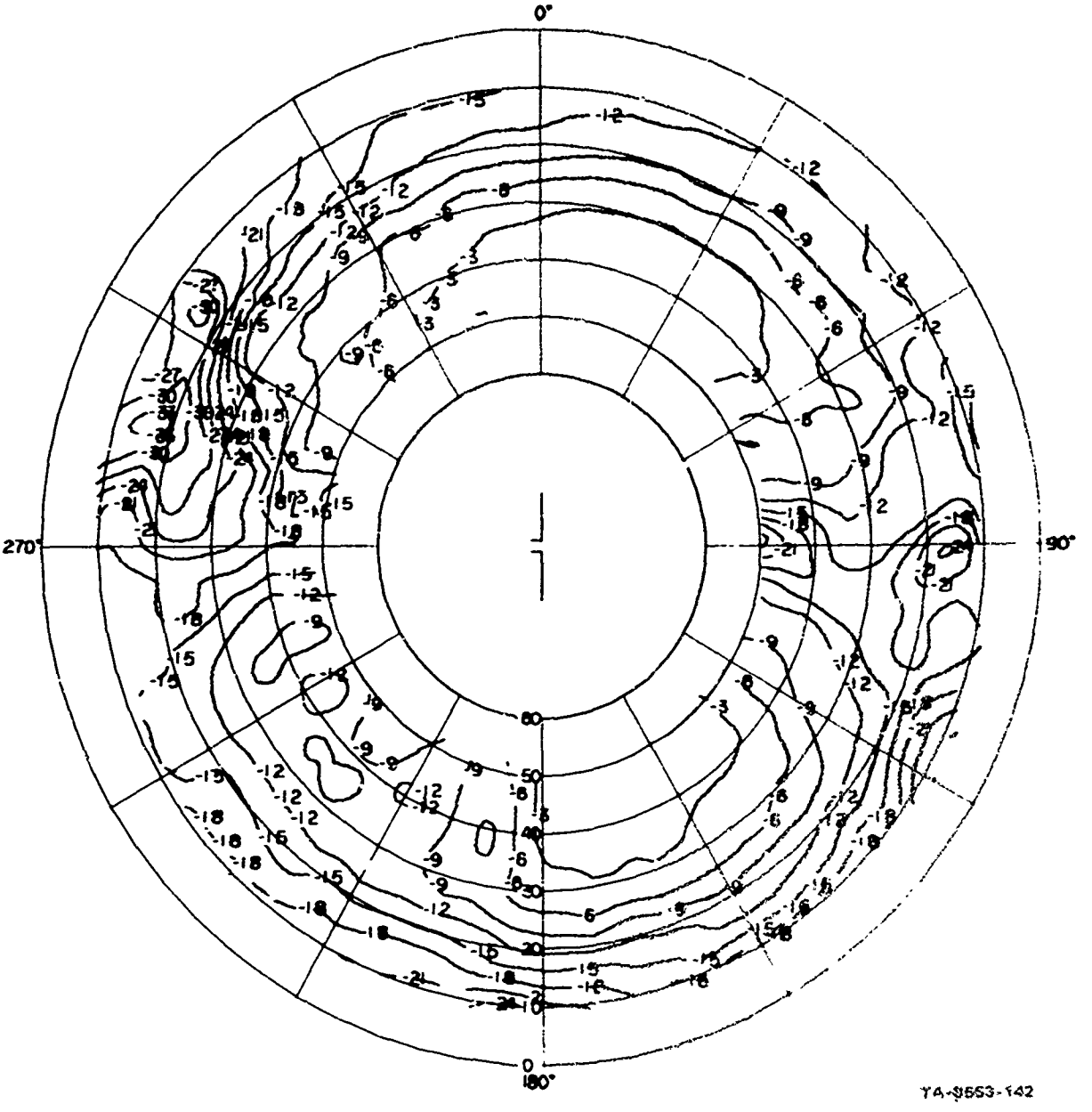

FIGURE B-1 MEASURED PATTERN OF 6-MHz UNBALANCED DIPOLE ON HILLTOP. E_θ AT 6 MHz

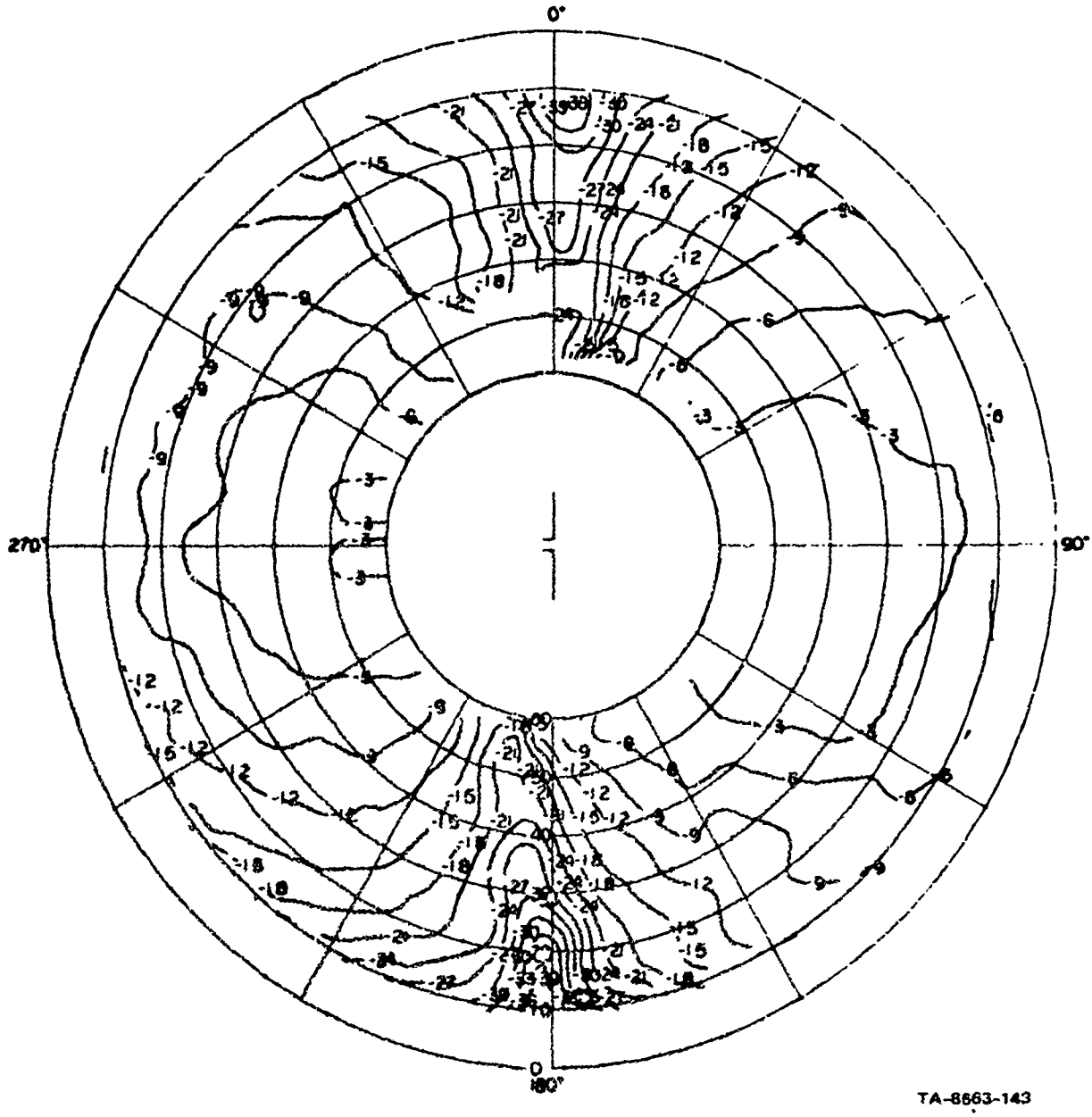

FIGURE 8-2 MEASURED PATTERN OF 6-MHz UNBALANCED DIPOLE ON HILLTOP, E_ϕ AT 6 MHz

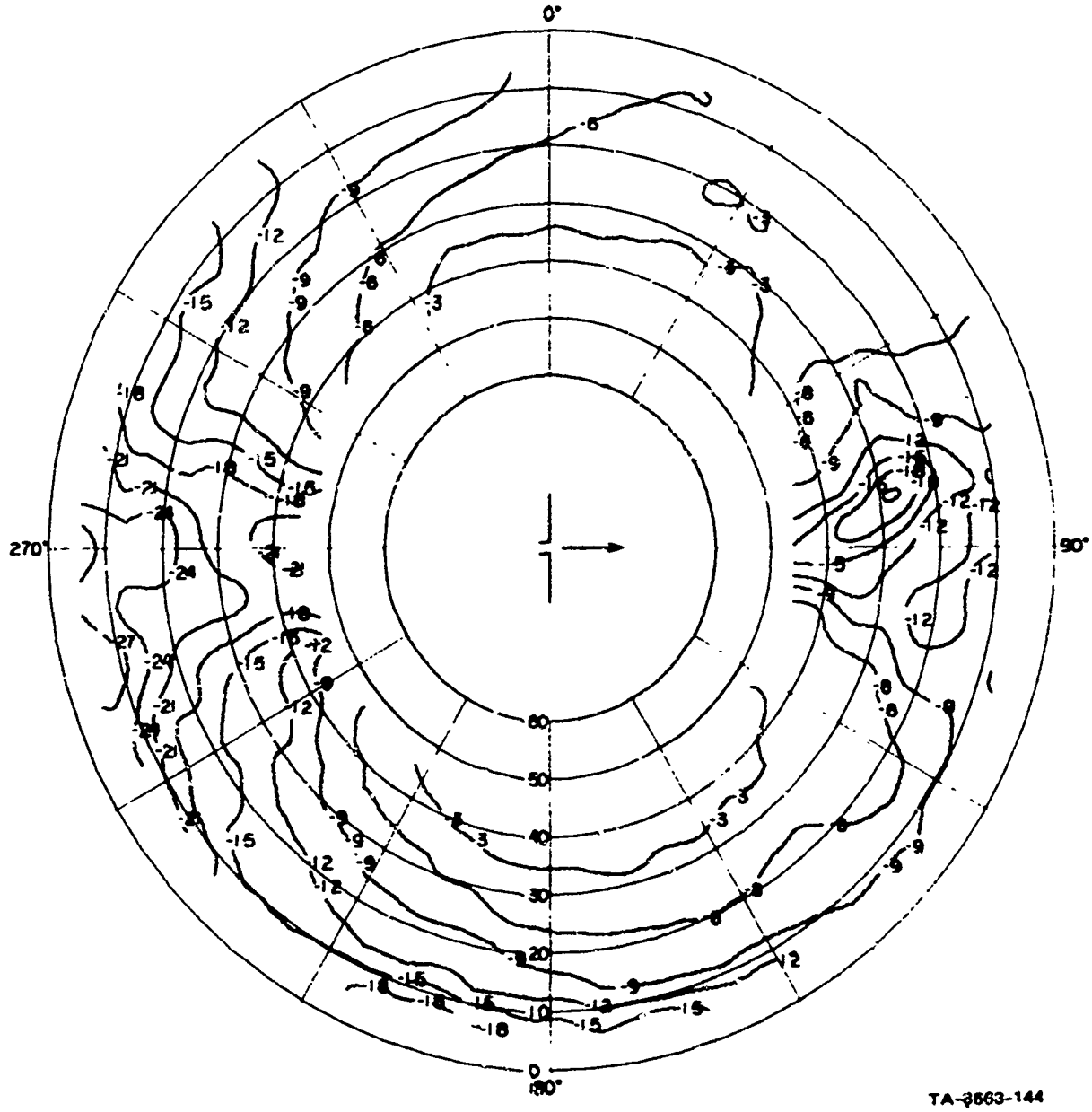

FIGURE 8-3 MEASURED PATTERN OF 6-MHz UNBALANCED DIPOLE ON HILLSIDE, E_θ AT 6 MHz

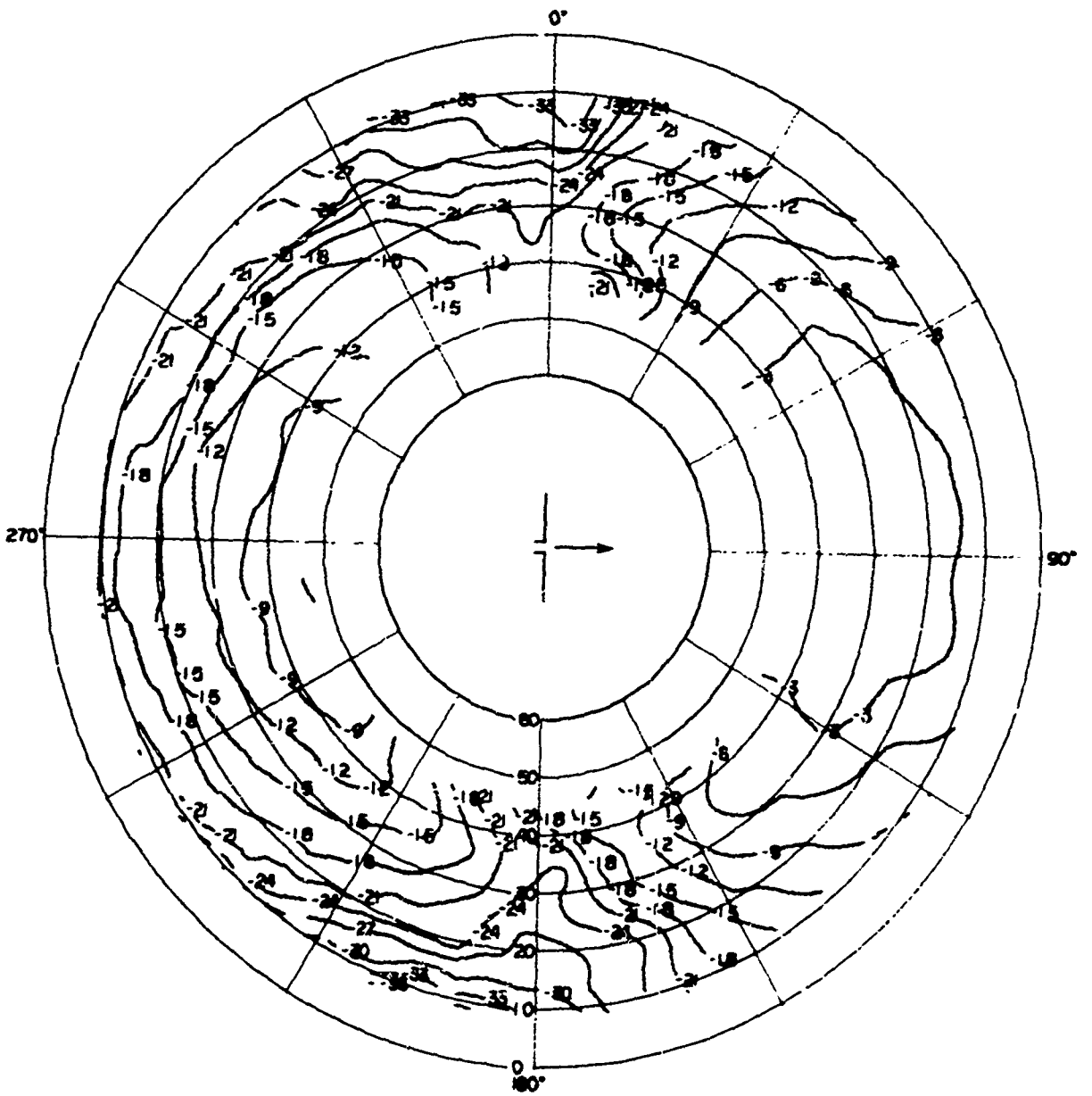

FIGURE B-4 MEASURED PATTERN OF 6-MHz UNBALANCED DIPOLE ON HILLSIDE, E_ϕ AT 6 MHz

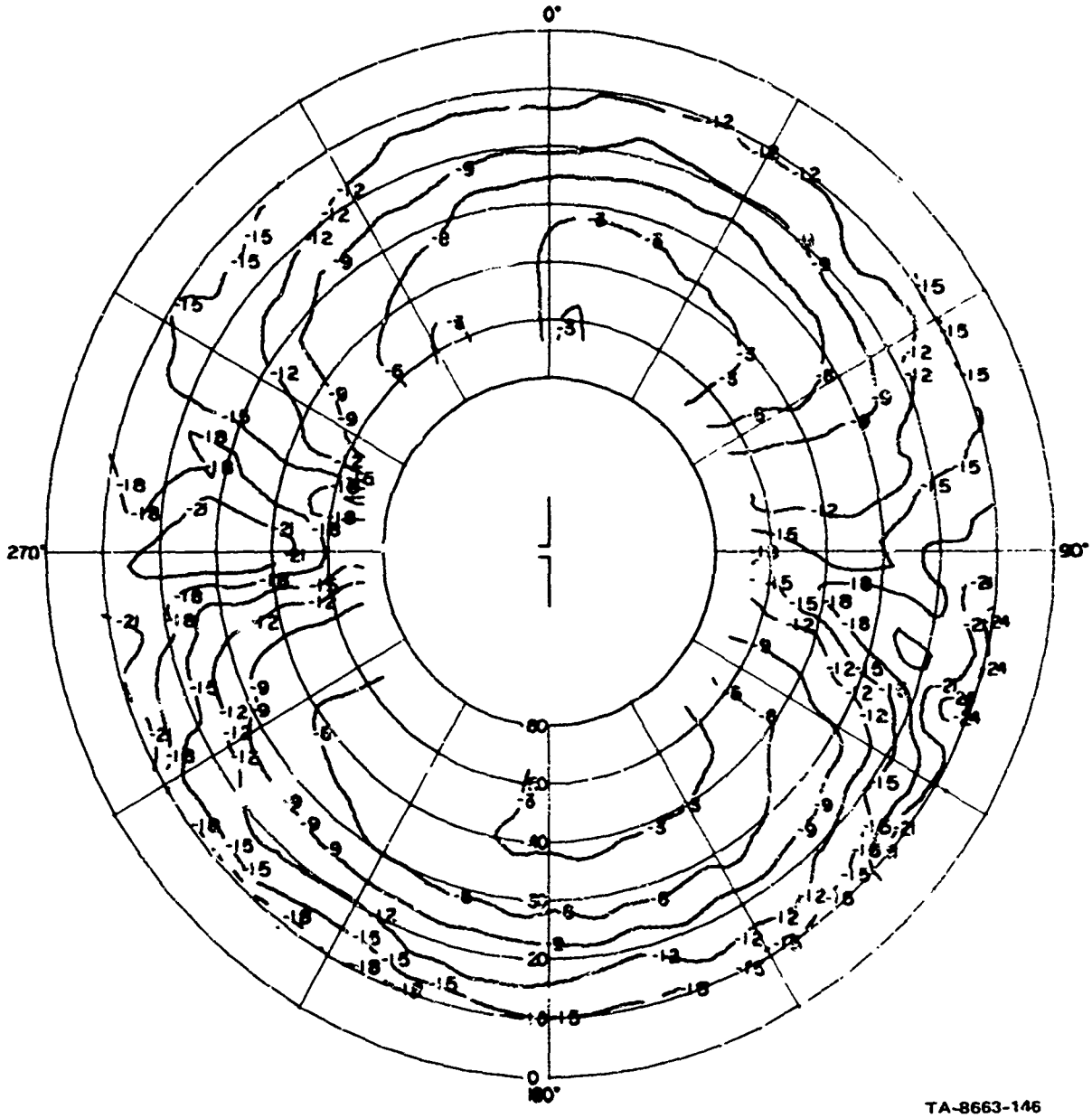

FIGURE B-5 MEASURED PATTERN OF 15-MHz UNBALANCED DIPOLE ON HILLTOP, E_θ AT 15 MHz

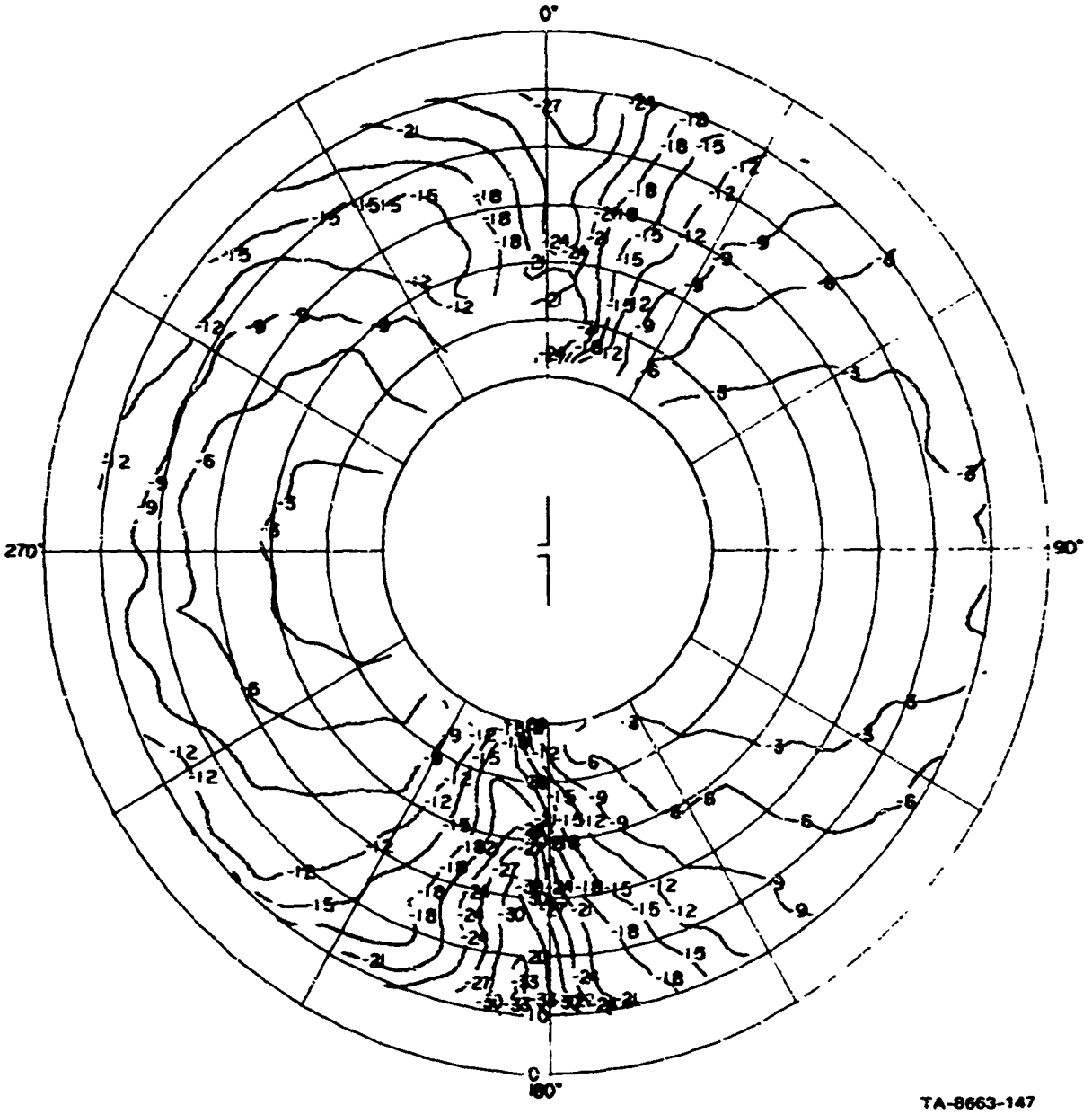

FIGURE B-6 MEASURED PATTERN OF 15-MHz UNBALANCED DIPOLE ON HILLTOP, E_ϕ AT 15 MHz

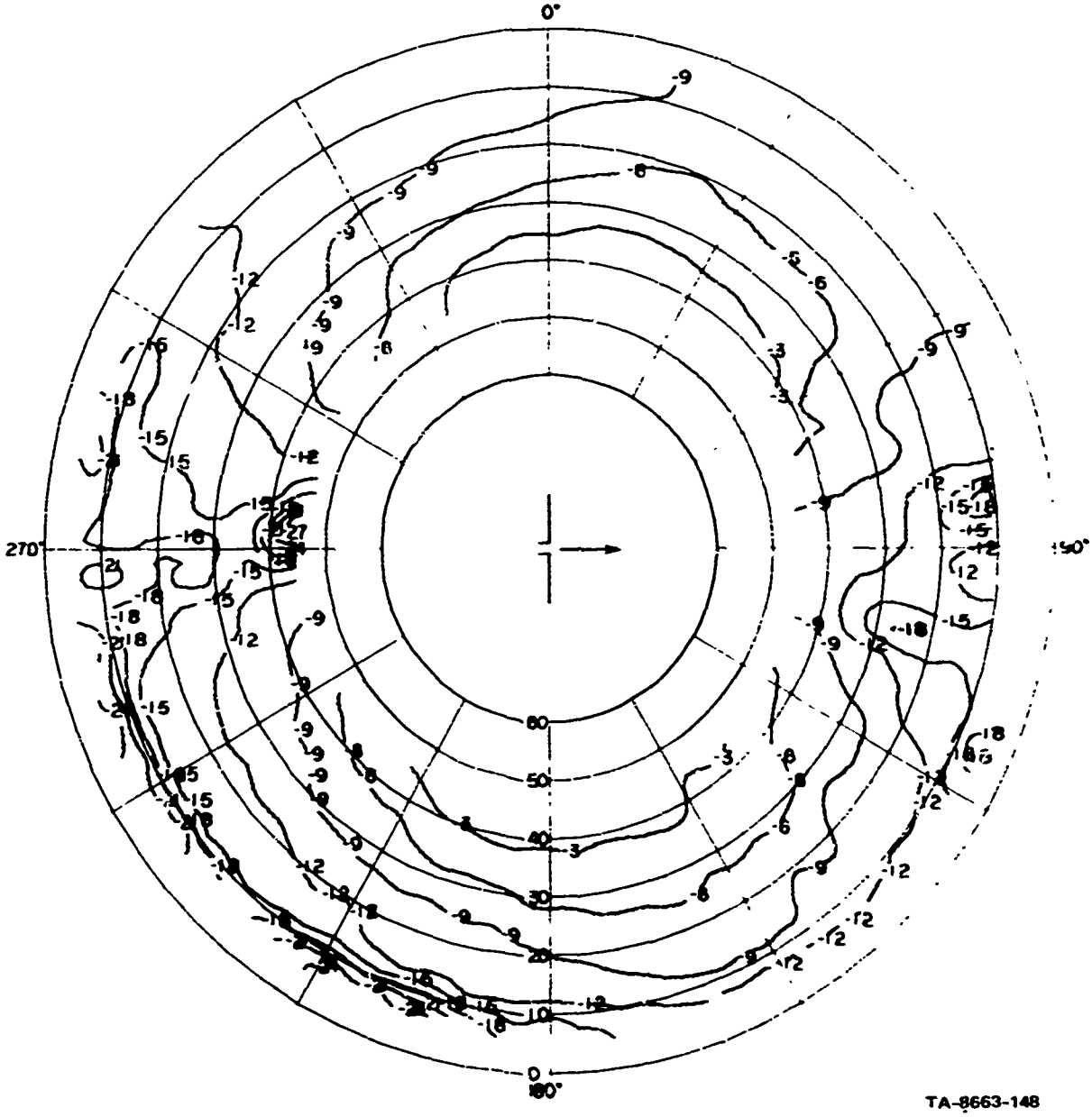

FIGURE B-7 MEASURED PATTERN OF 15-MHz UNBALANCED DIPOLE ON HILLSIDE, E_θ AT 15 MHz

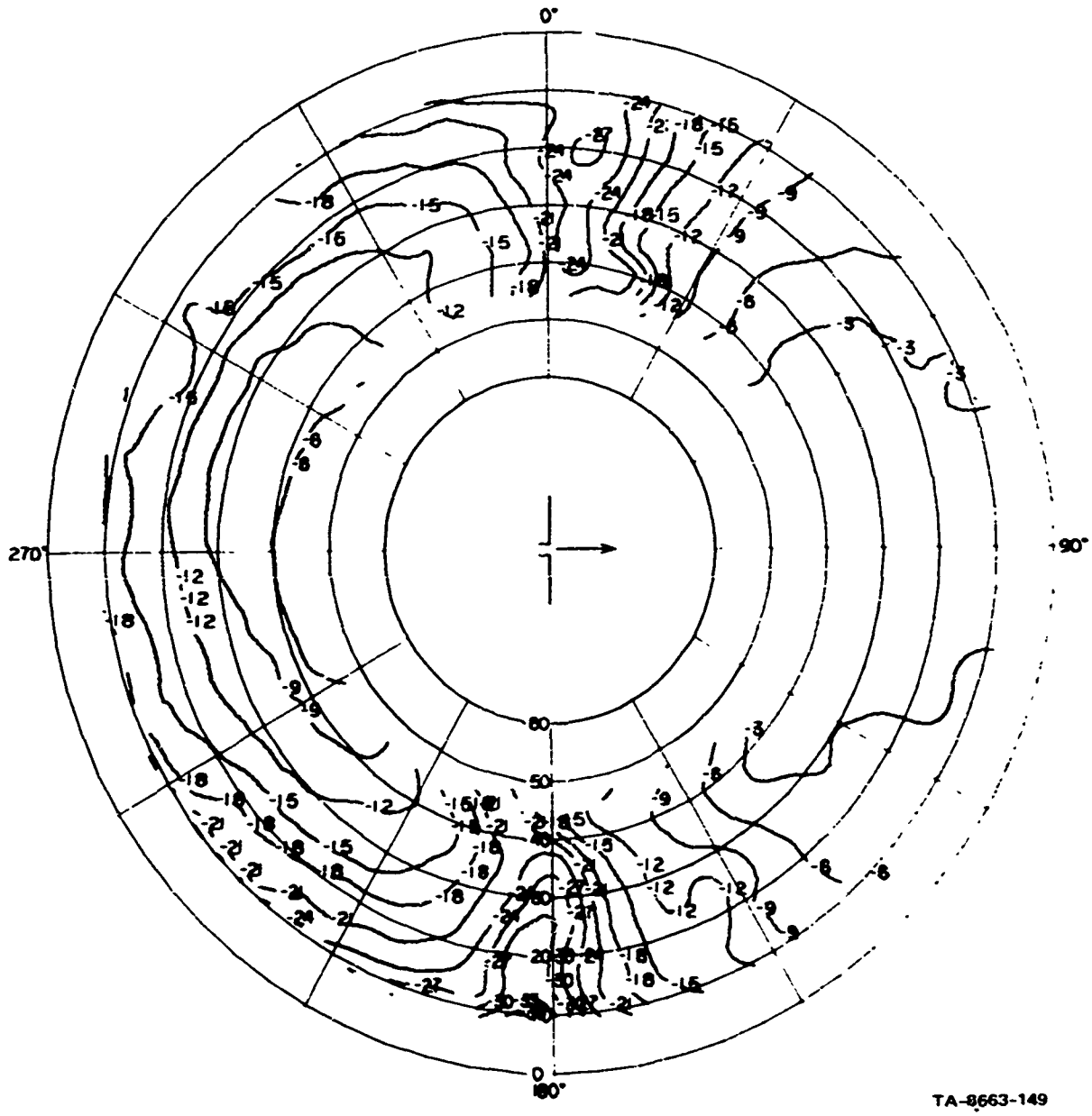

FIGURE B-8 MEASURED PATTERN OF 15-MHz UNBALANCED DIPOLE ON HILLSIDE, E_ϕ AT 15 MHz

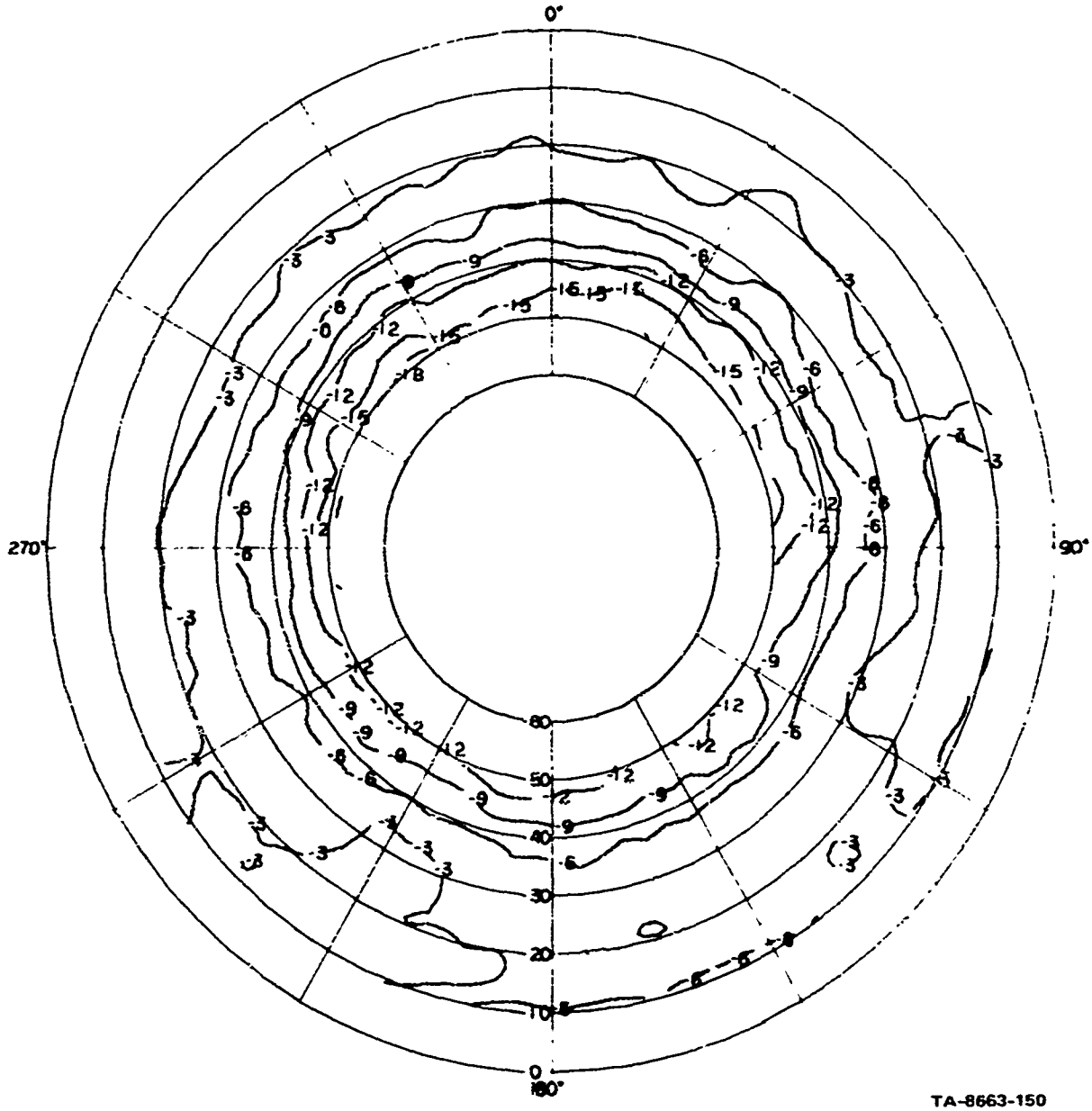

FIGURE 8-9 MEASURED PATTERN OF 30-MHz MONOPOLE ON HILLTOP, E_θ AT 30 MHz

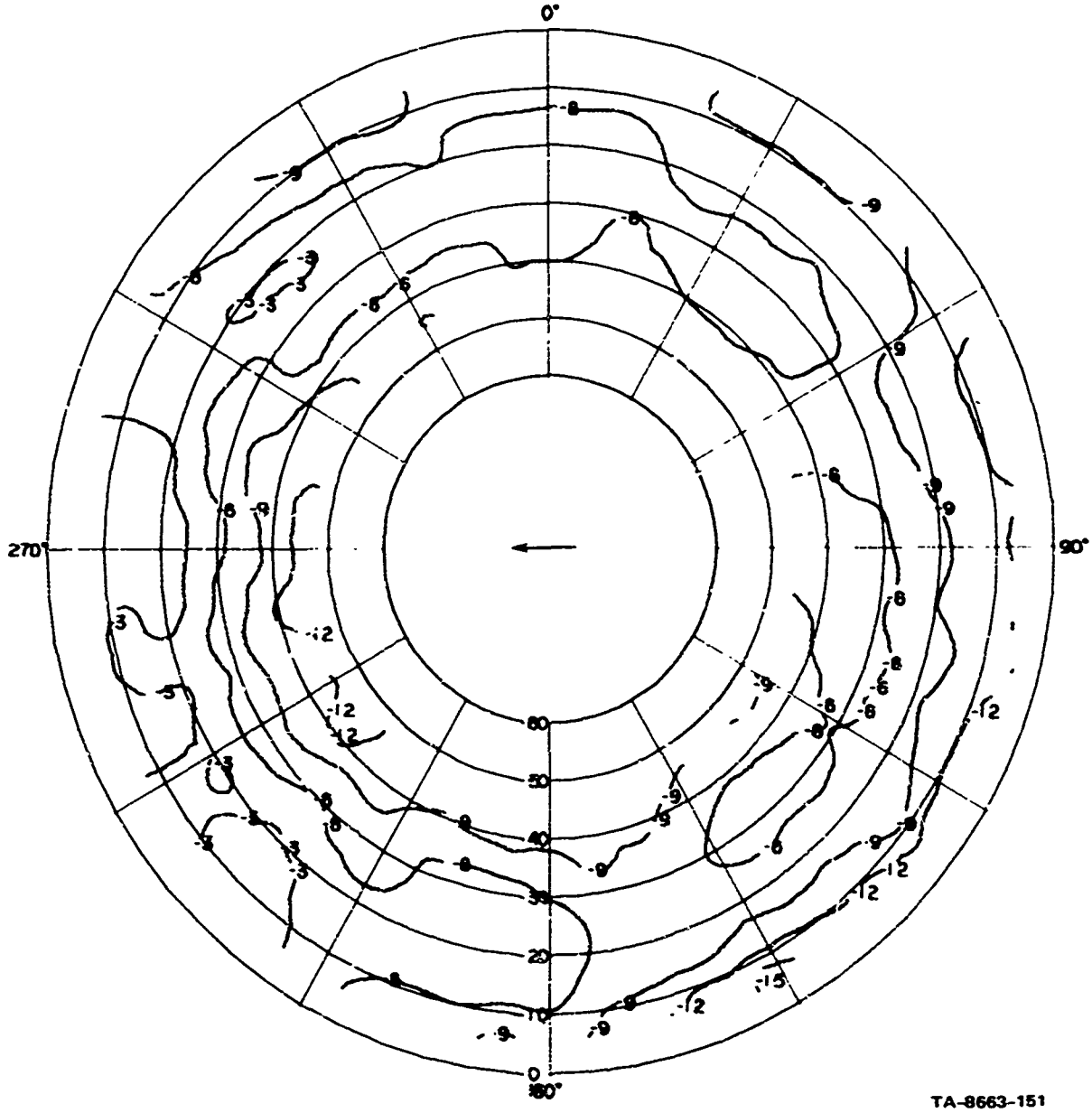

FIGURE 8-10 MEASURED PATTERN OF 30-MHz MONOPOLE ON HILLSIDE, E_θ AT 30 MHz

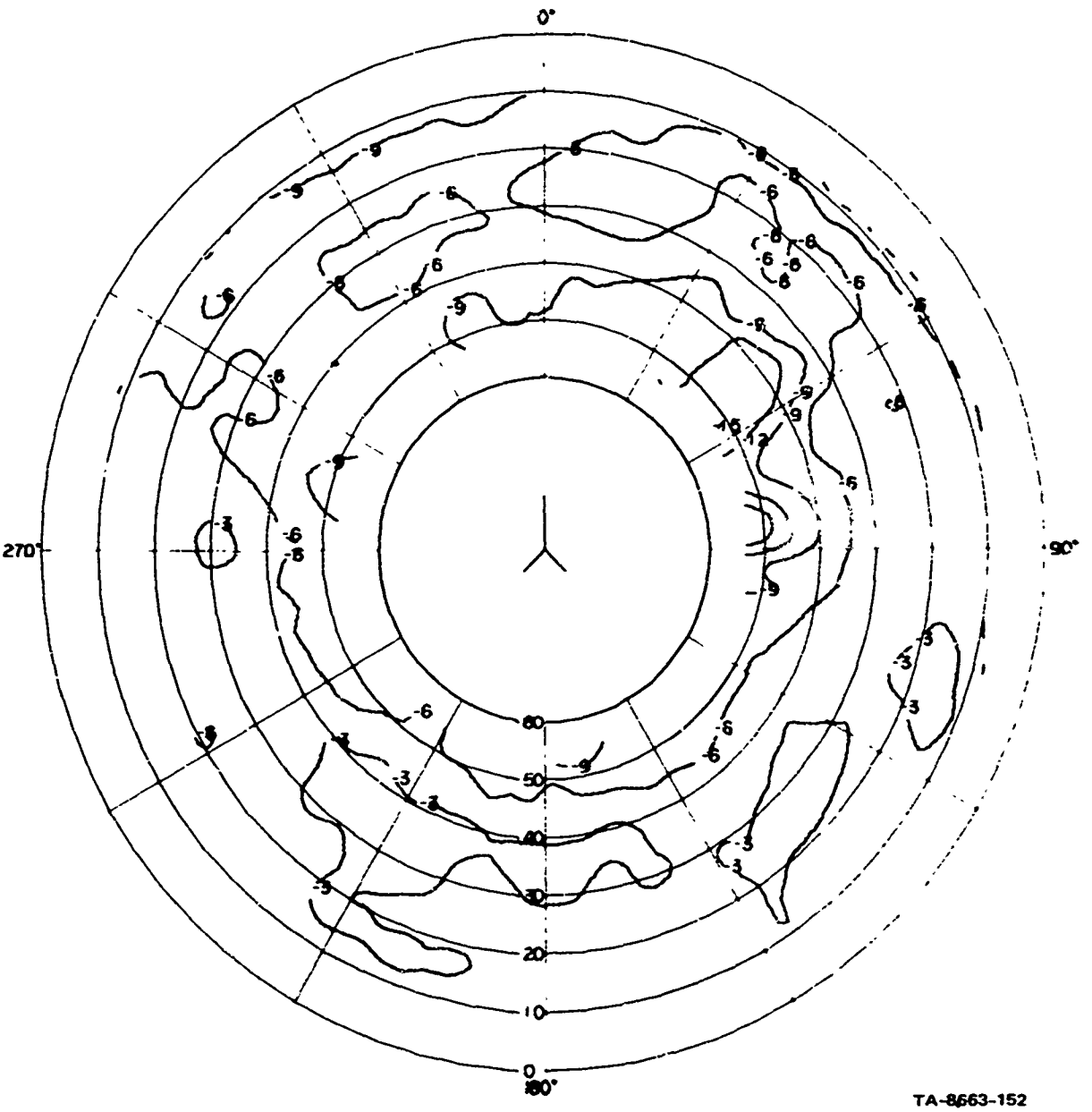

FIGURE B-11 MEASURED PATTERN OF 30° SLANT-WIRE ANTENNA ON HILLTOP, E_θ AT 4 MHz

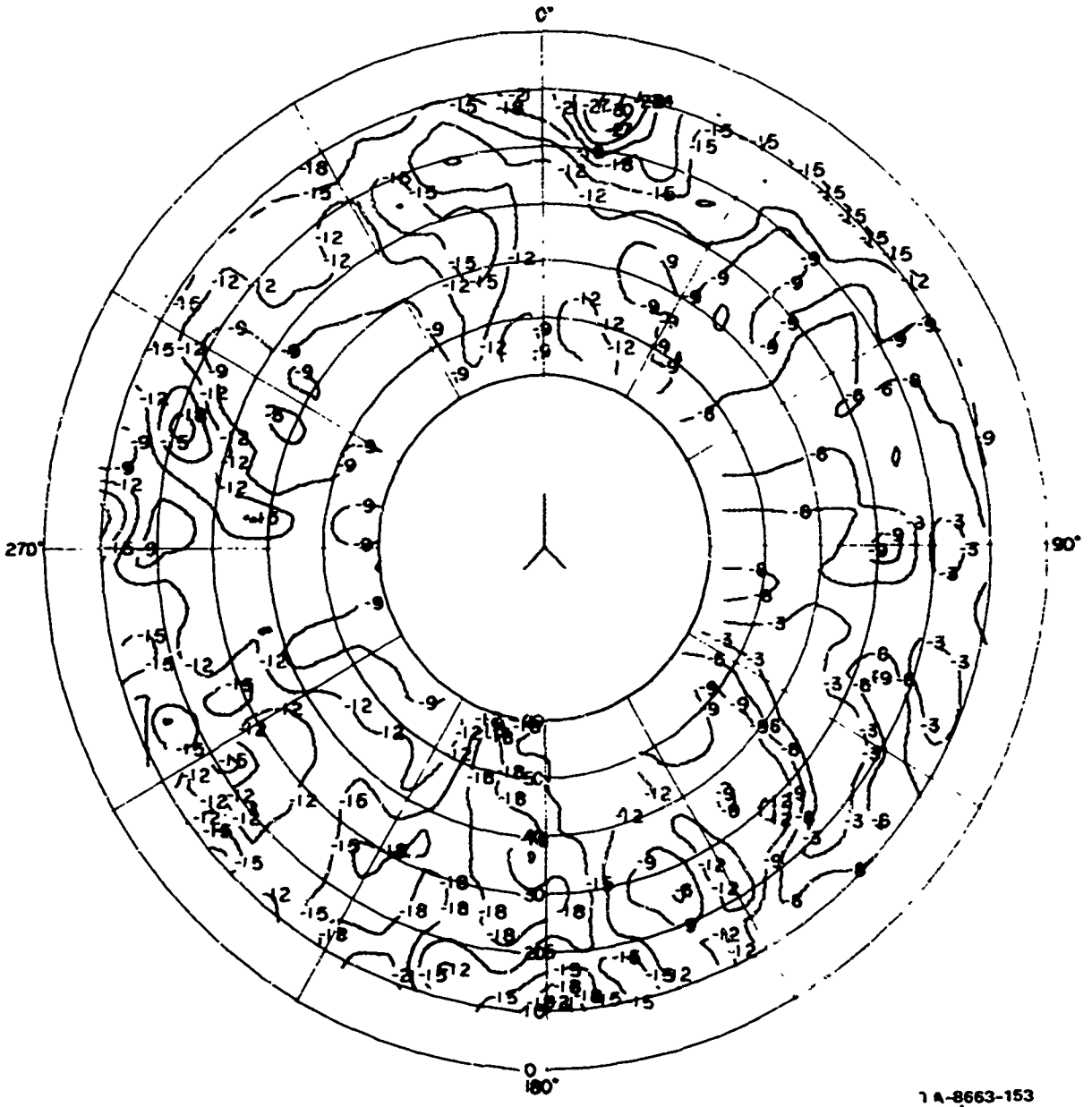

FIGURE B-12 MEASURED PATTERN OF 30° SLANT-WIRE ANTENNA ON HILLTOP, E_ϕ AT 4 MHz

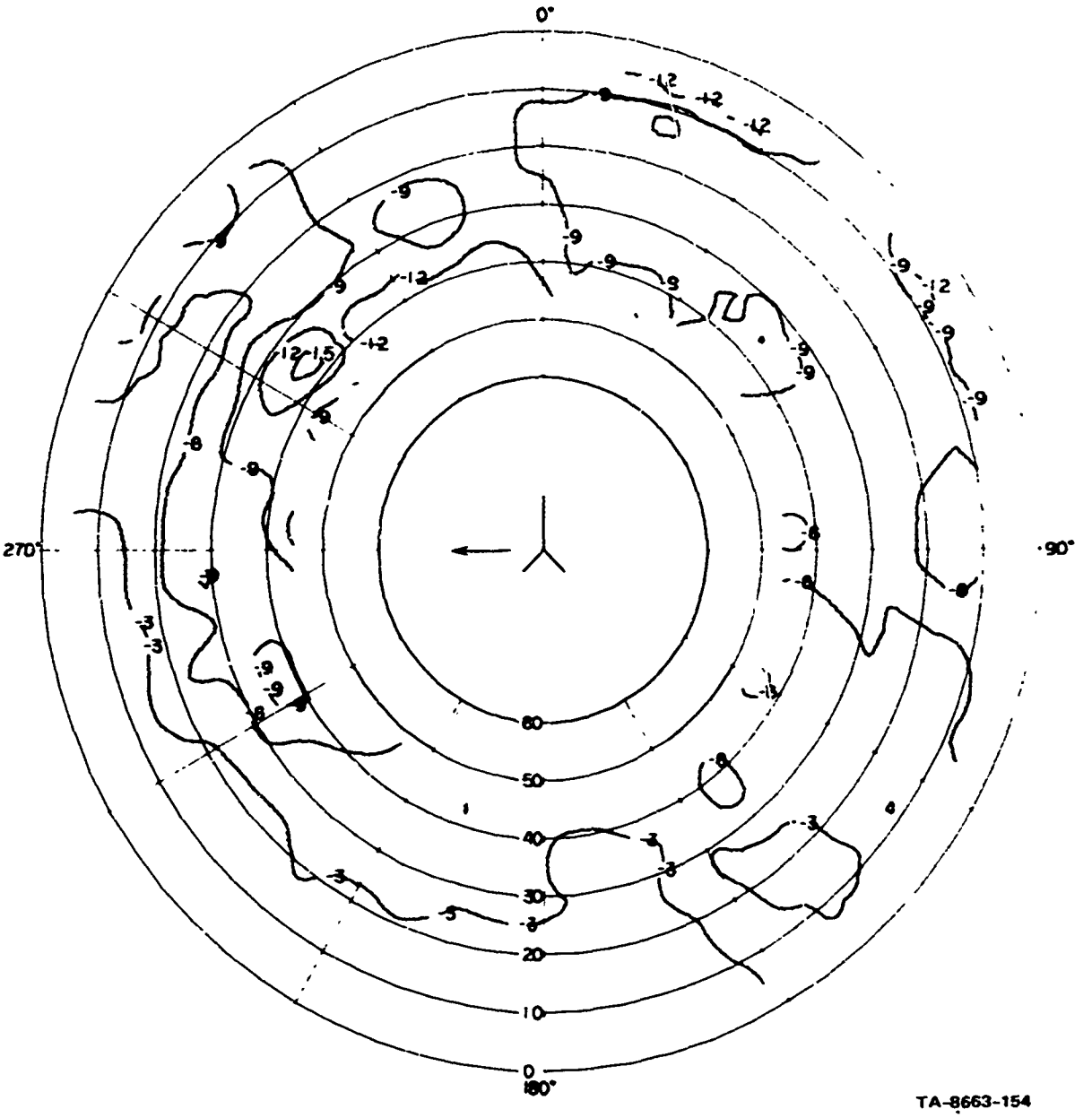

FIGURE B-13 MEASURED PATTERN OF 30° SLANT-WIRE ANTENNA ON HILLSIDE, E_θ AT 4 MHz

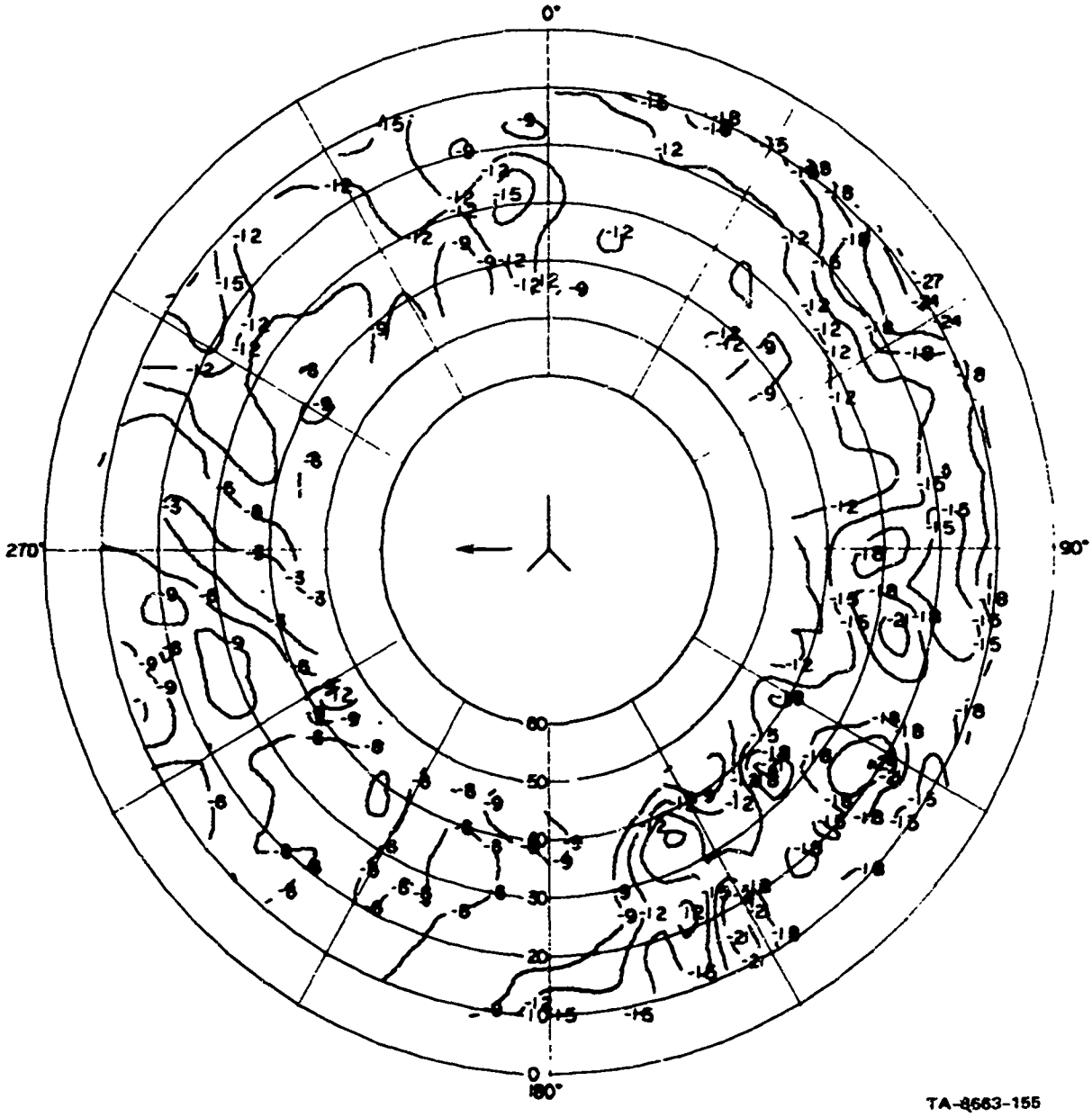

FIGURE B-14 MEASURED PATTERN OF 30° SLANT-WIRE ANTENNA ON HILLSIDE, E_ϕ AT 4 MHz

Appendix C

CONTOUR PLOTS OF THE MEASURED AND CALCULATED RADIATION PATTERNS OF DIPOLE ANTENNAS MEASURED IN THE TROPICAL FOREST IN THAILAND

Appendix C

CONTOUR PLOTS OF THE MEASURED AND CALCULATED RADIATION PATTERNS OF DIPOLE ANTENNAS MEASURED IN THE TROPICAL FOREST IN THAILAND

This appendix contains contour plots comparing the measured and calculated data from selected dipole antennas at Ban Mun Chit, Thailand, as discussed in Sec. IX of this report. The patterns for each antenna are presented in order of increasing frequency, with the E_θ (vertical polarization) response followed by the E_ϕ (horizontal polarization) response. The measured data are shown as solid lines and the calculated patterns are shown as dashed lines.

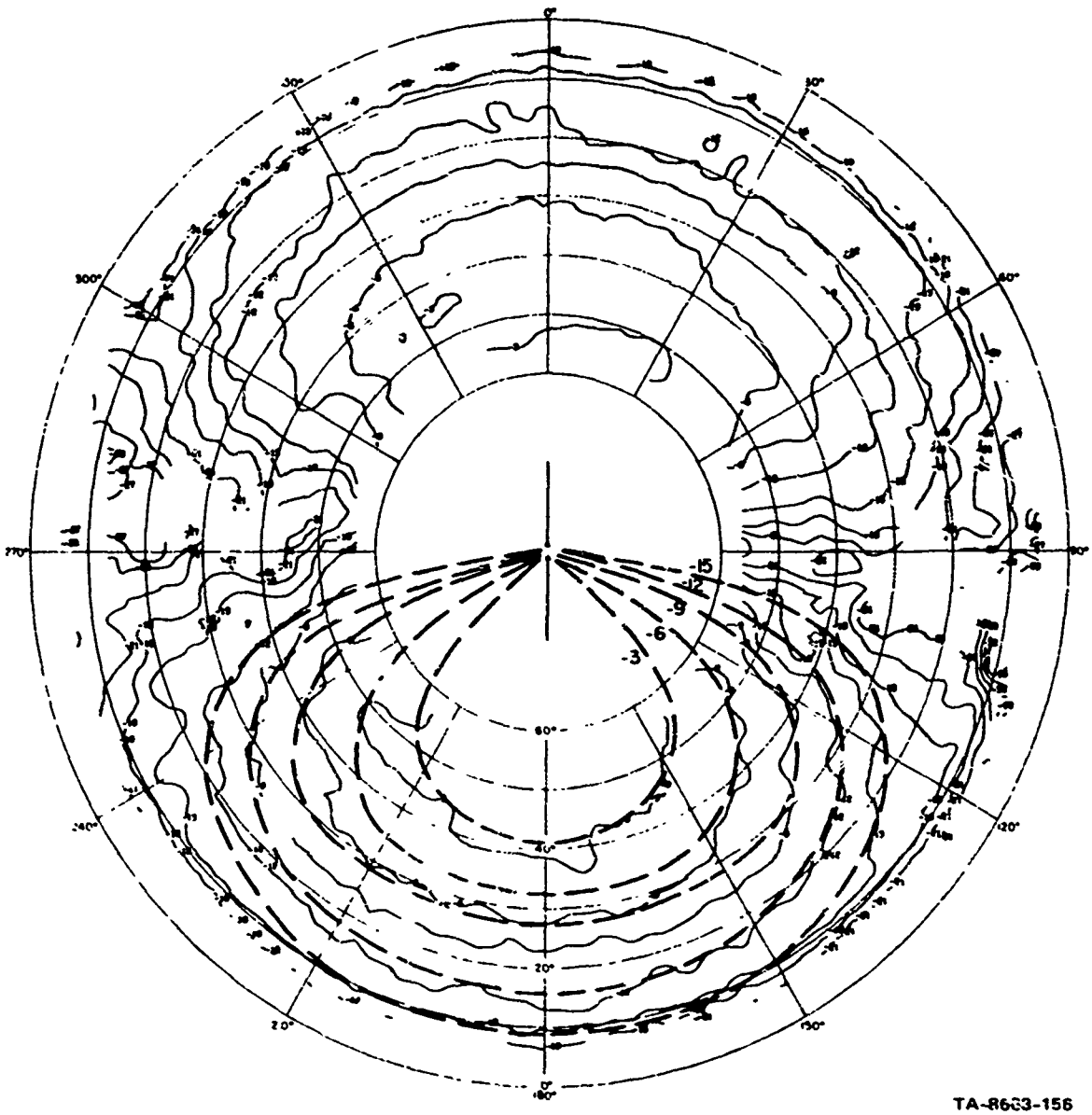

FIGURE C-1 CALCULATED AND MEASURED PATTERNS OF 6-MHz BALANCED DIPOLE OVER GROUND SCREEN IN CLEARING, E_θ AT 6 MHz

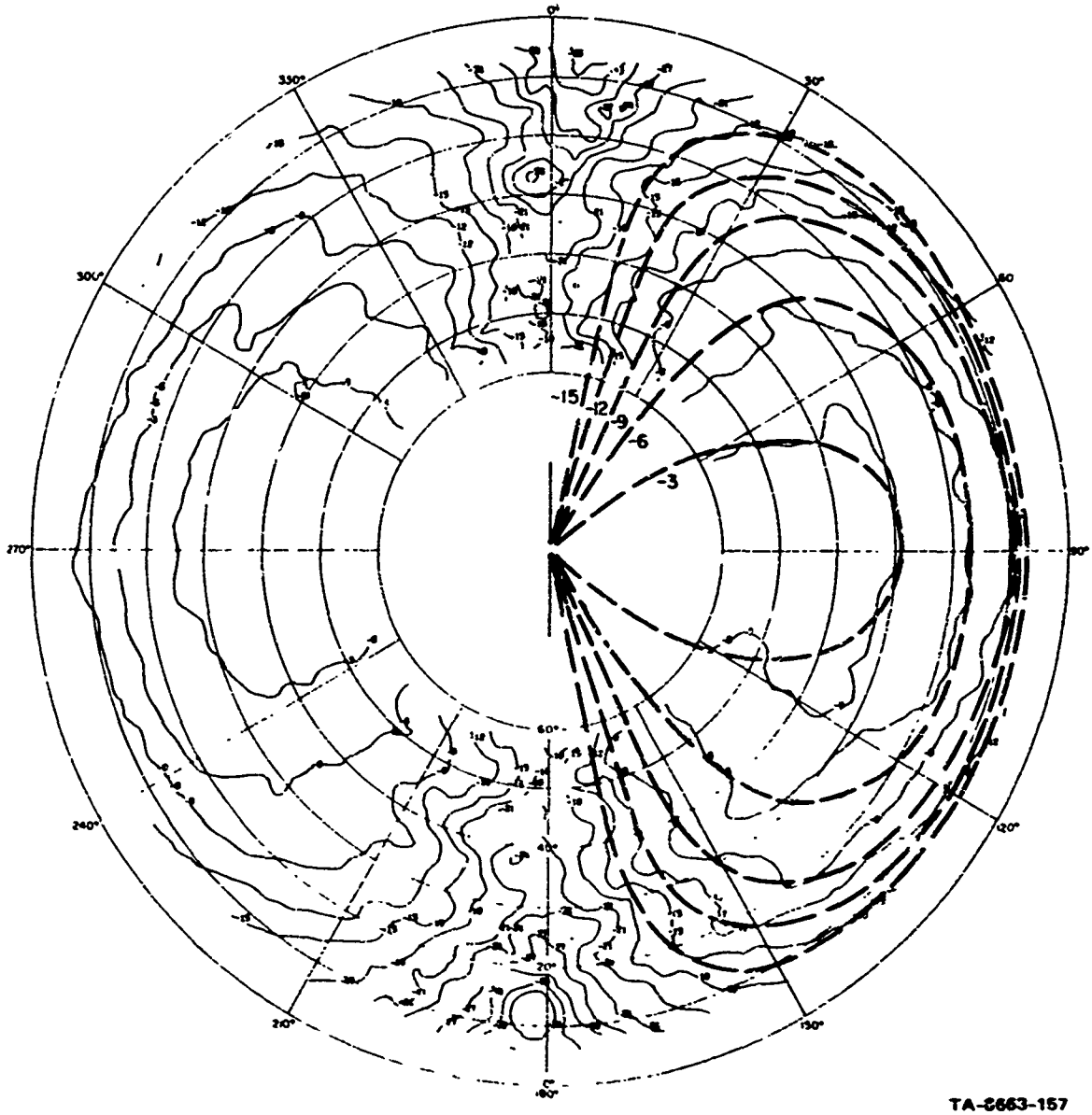

FIGURE C-2 CALCULATED AND MEASURED PATTERNS OF 6-MHz BALANCED DIPOLE OVER GROUND SCREEN IN CLEARING, E_ϕ AT 6 MHz

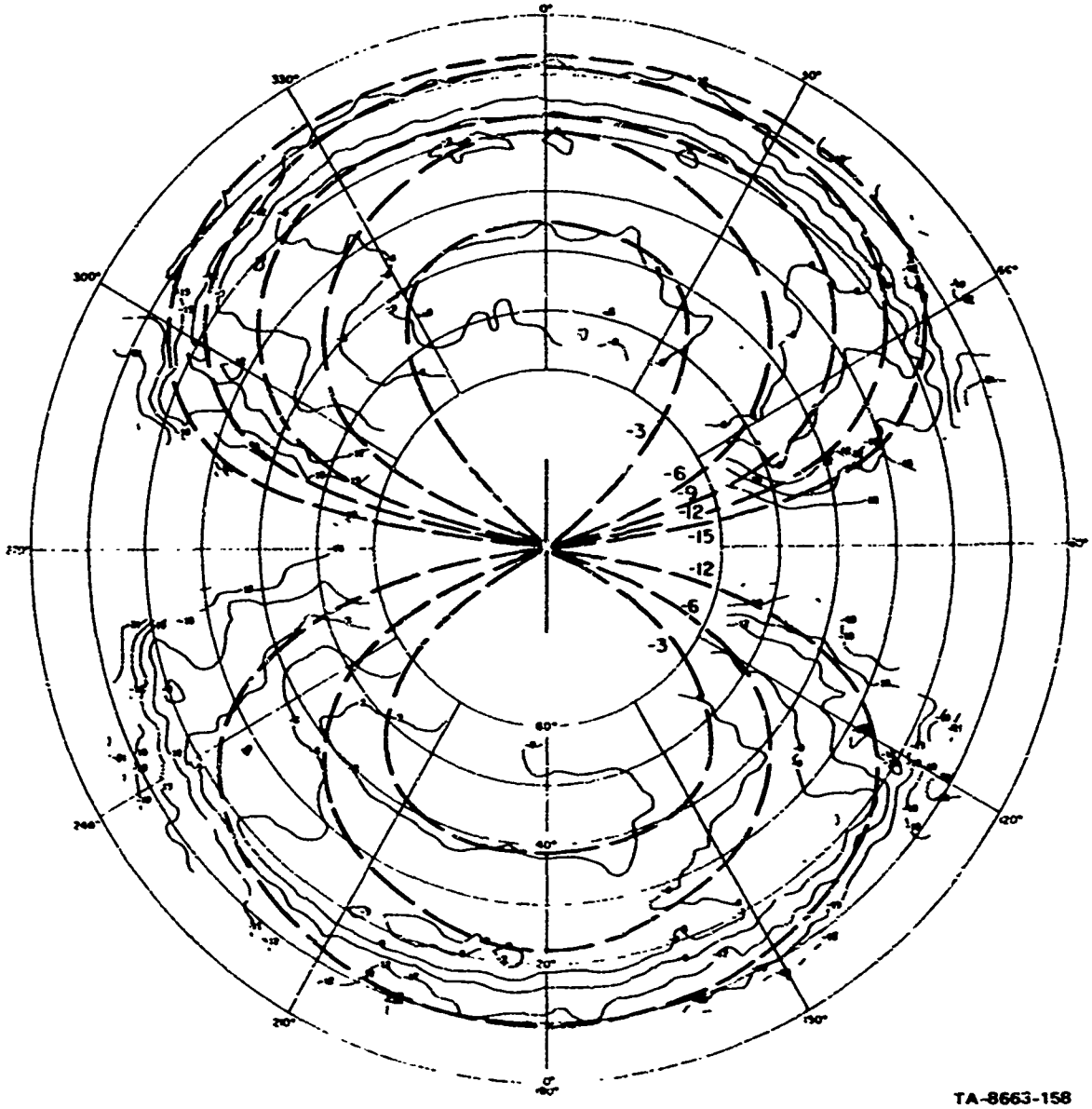

FIGURE C-3 CALCULATED AND MEASURED PATTERNS OF 6-MHz BALANCED DIPOLE IN CLEARING, E_θ AT 3 MHz

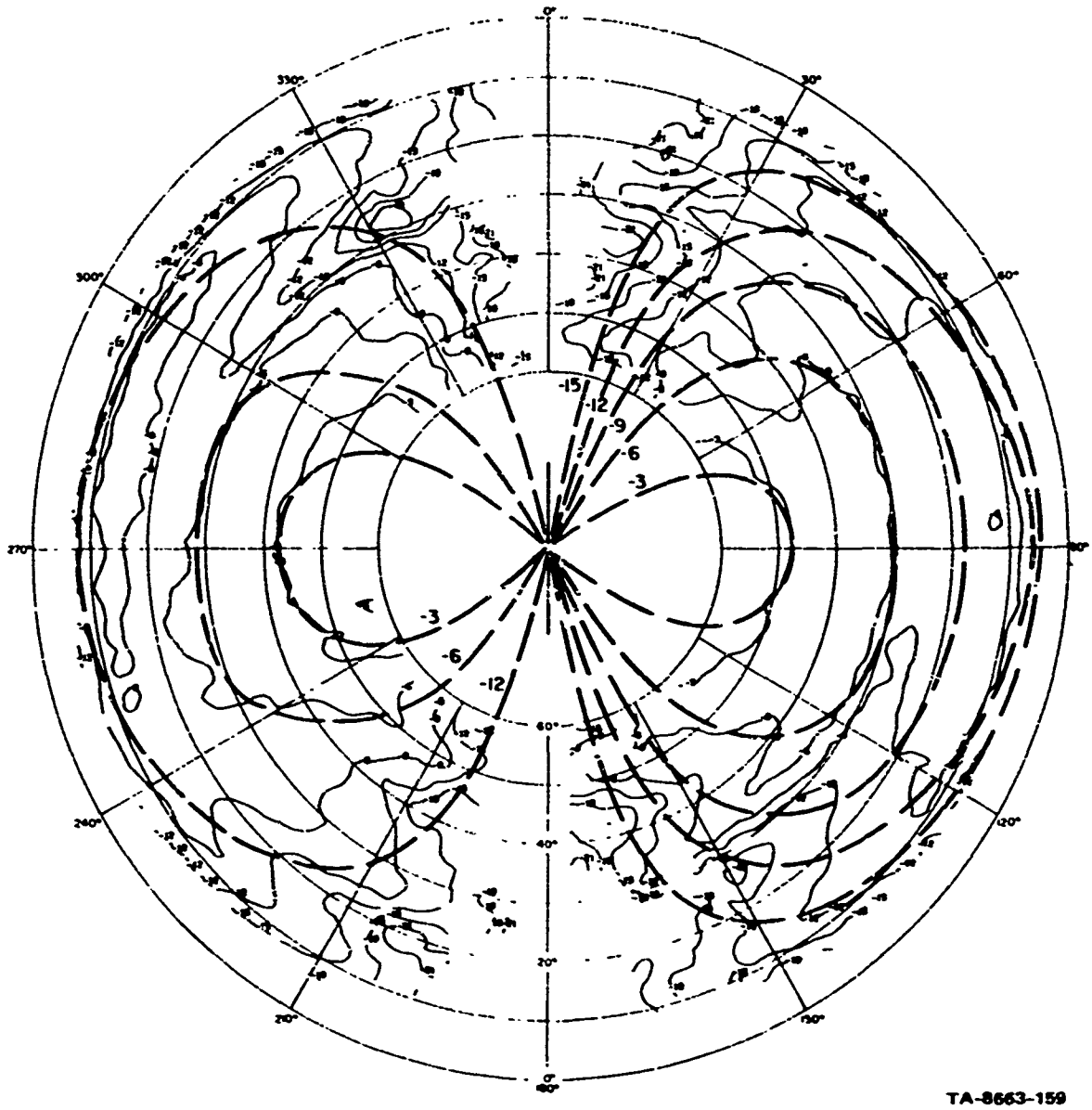

FIGURE C-4 CALCULATED AND MEASURED PATTERNS OF 6-MHz BALANCED DIPOLE IN CLEARING, E_ϕ AT 3 MHz

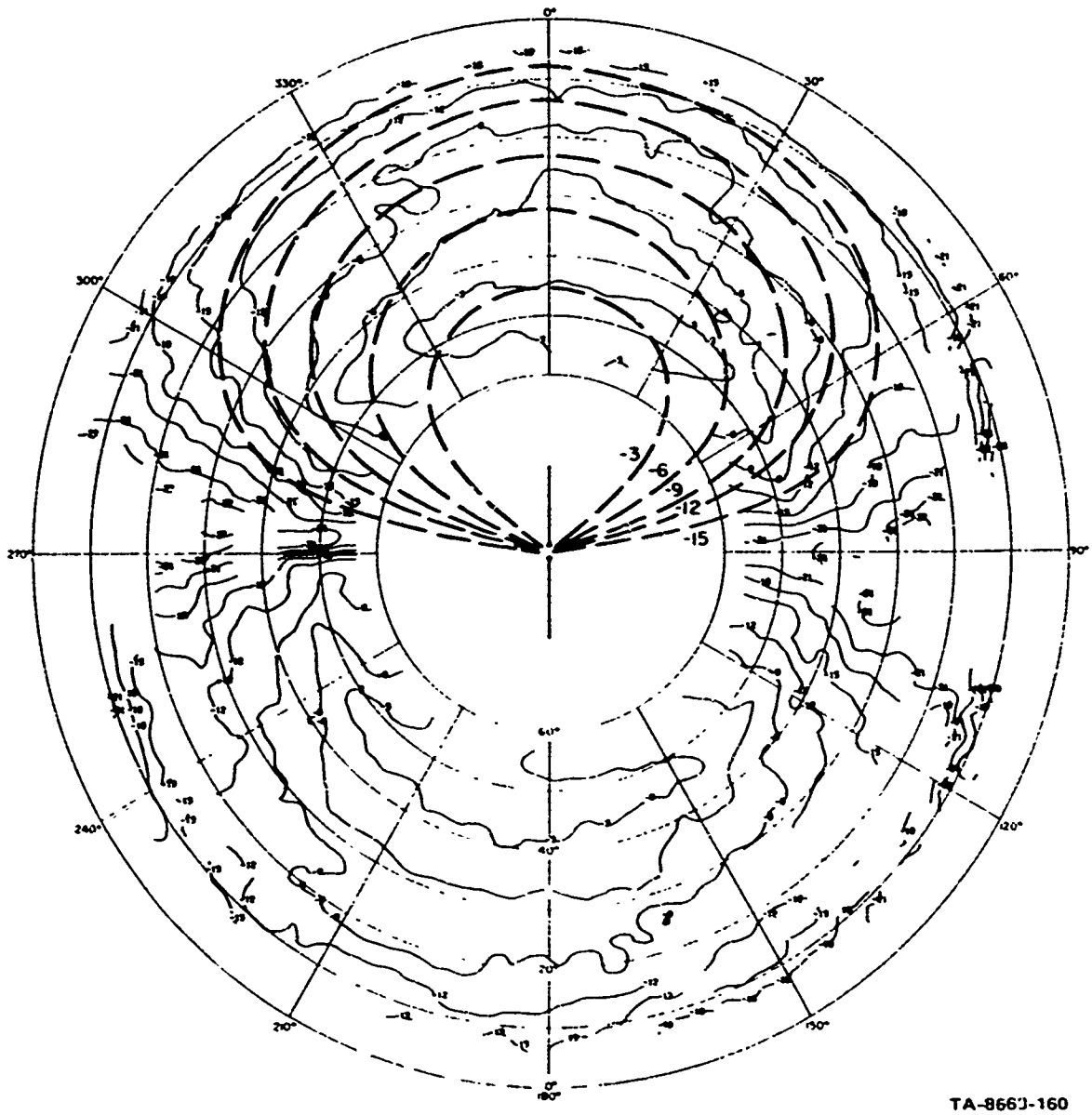

FIGURE C-5 CALCULATED AND MEASURED PATTERNS OF 6-MHz BALANCED DIPOLE IN CLEARING, E_θ AT 4 MHz

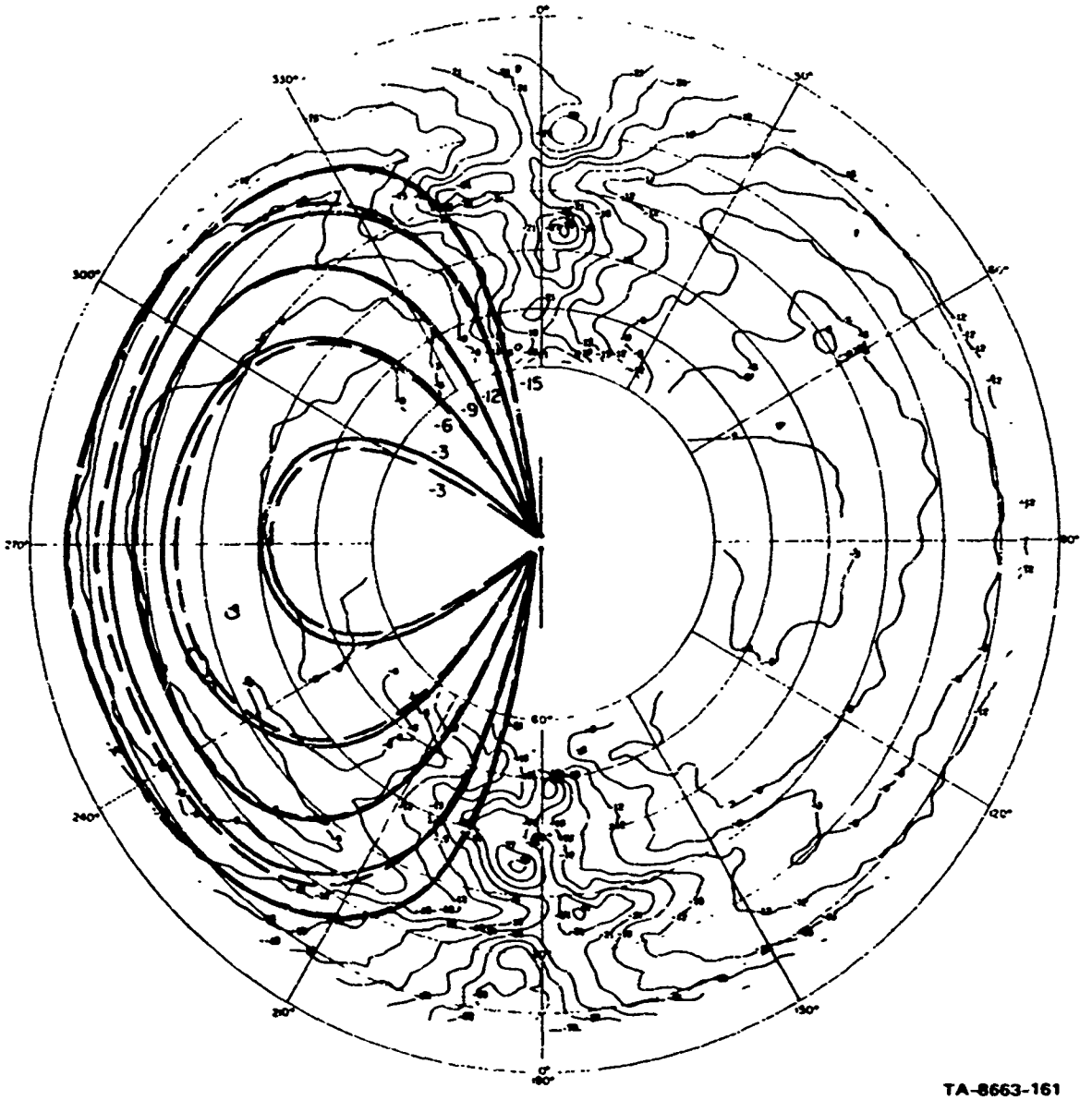

TA-8663-161

FIGURE C-6 CALCULATED AND MEASURED PATTERNS OF 6-MHz BALANCED DIPOLE IN CLEARING, E_ϕ AT 4 MHz

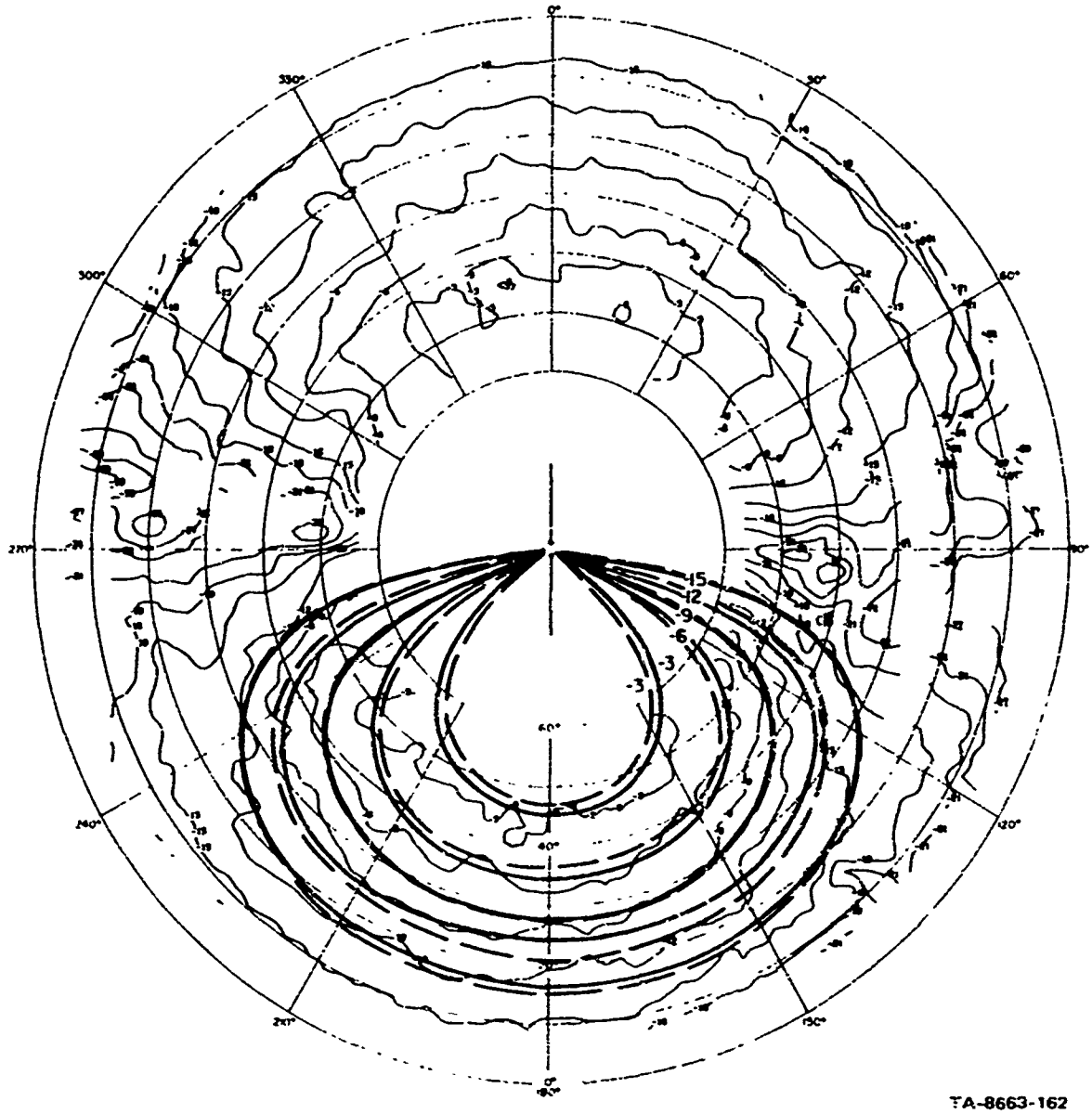

TA-8663-162

FIGURE C-7 CALCULATED AND MEASURED PATTERNS OF 6-MHz BALANCED DIPOLE IN CLEARING, E_θ AT 6 MHz

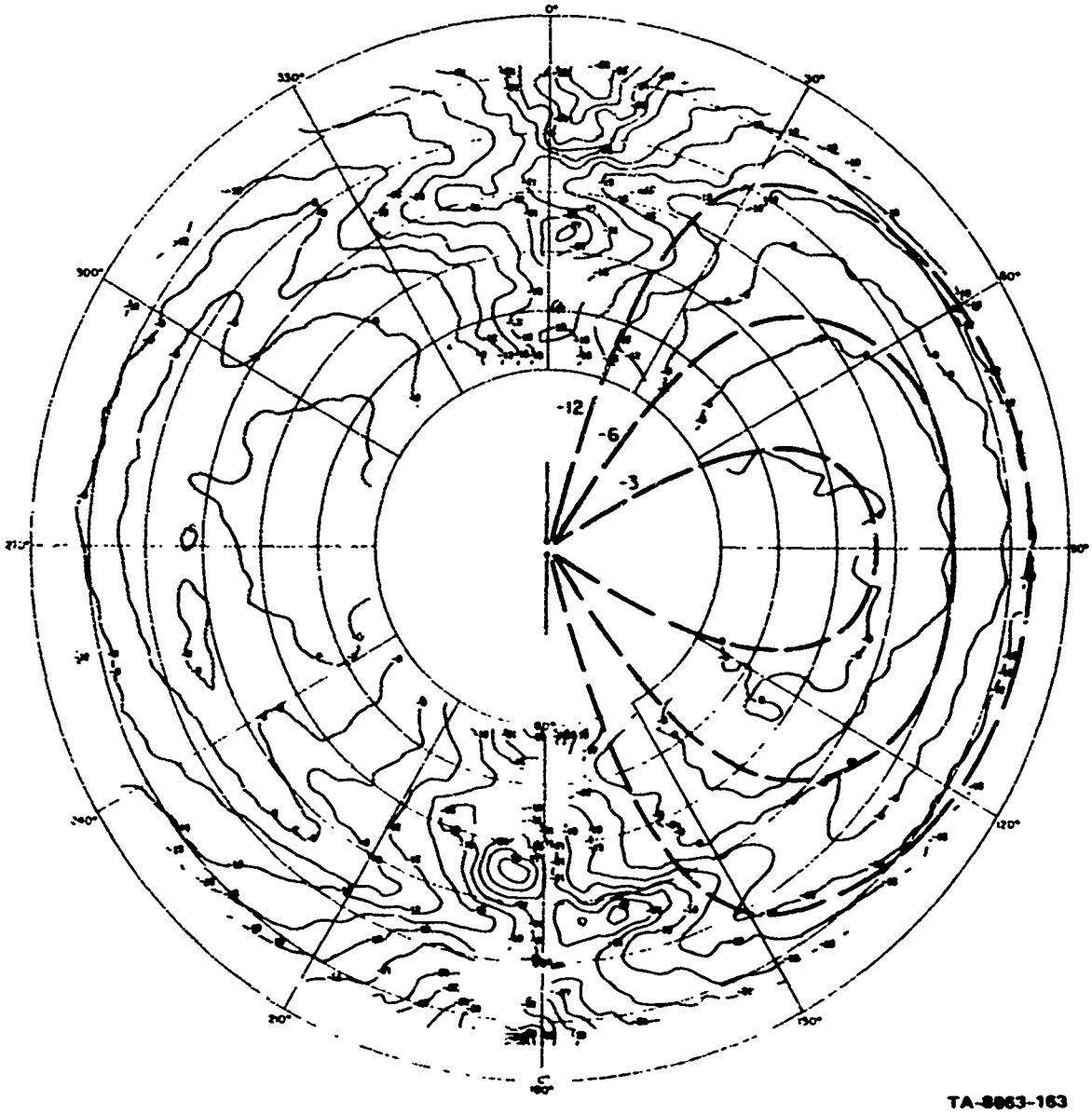

FIGURE C-8 CALCULATED AND MEASURED PATTERNS OF 6-MHz BALANCED DIPOLE IN CLEARING, E_ϕ AT 6 MHz

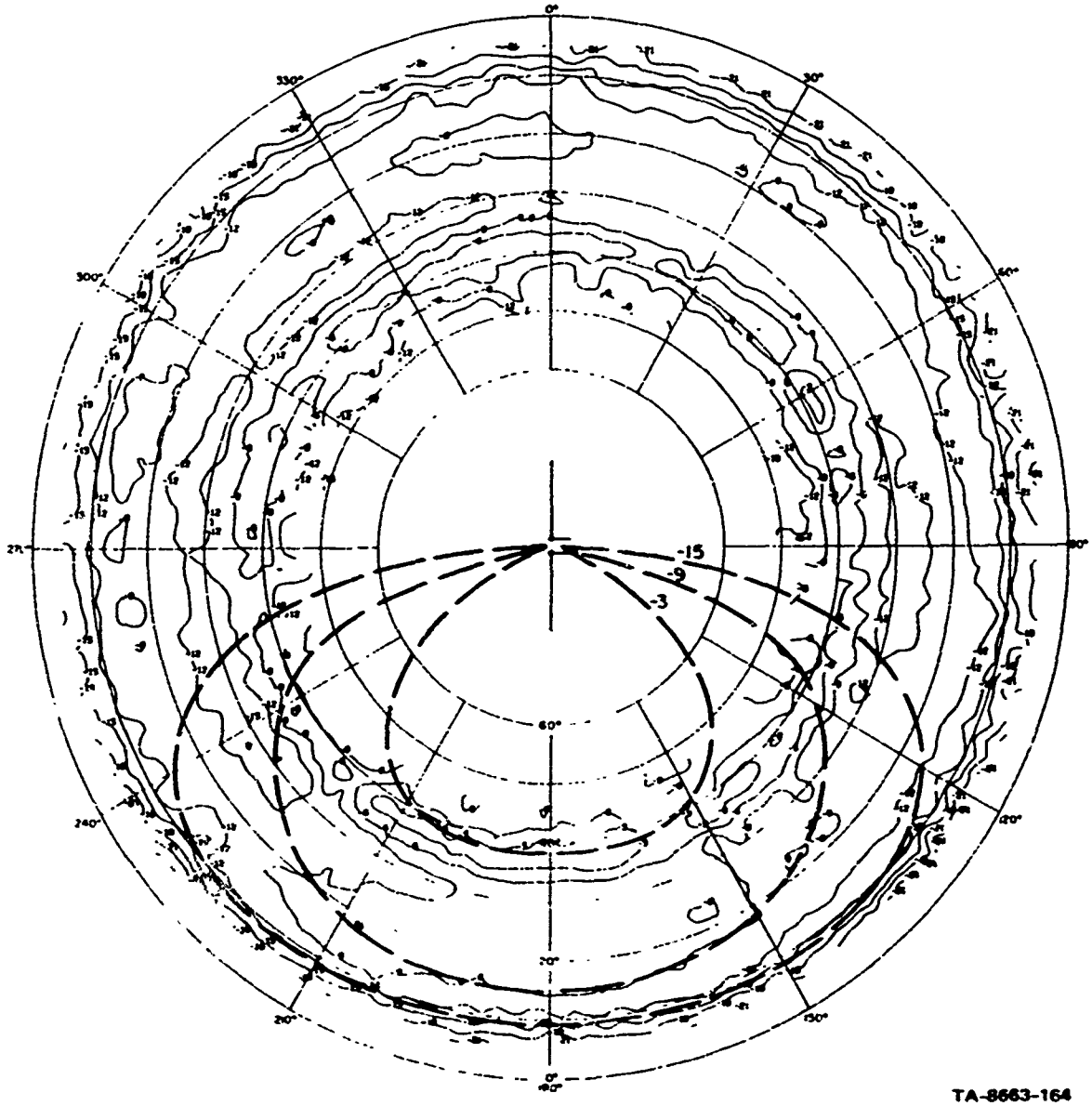

FIGURE C-3 CALCULATED AND MEASURED PATTERNS OF 6-MHz UNBALANCED DIPOLE IN CLEARING, E_θ AT 3 MHz

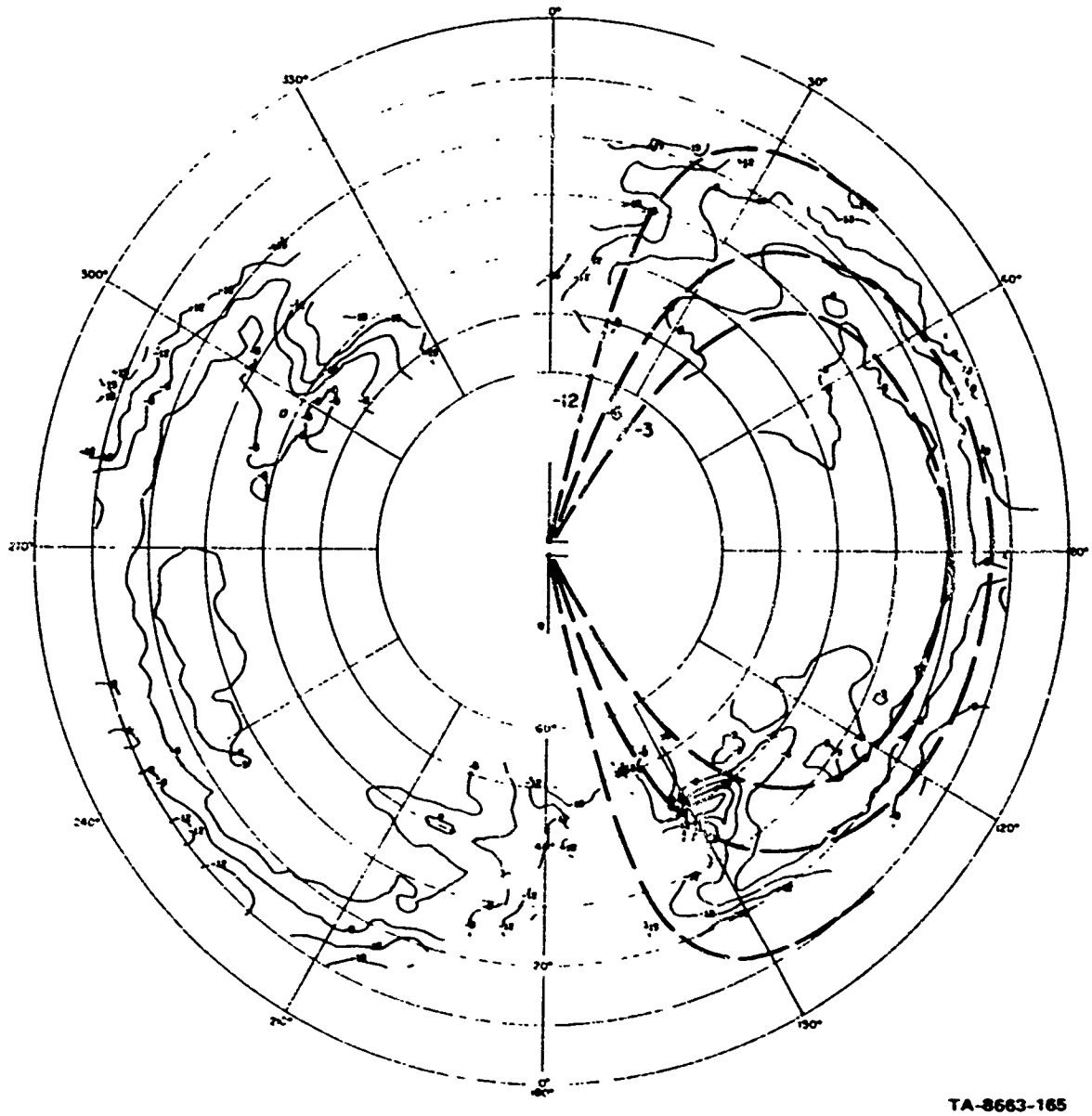

FIGURE C-10 CALCULATED AND MEASURED PATTERNS OF 6-MHz UNBALANCED DIPOLE IN CLEARING, E_ϕ AT 3 MHz

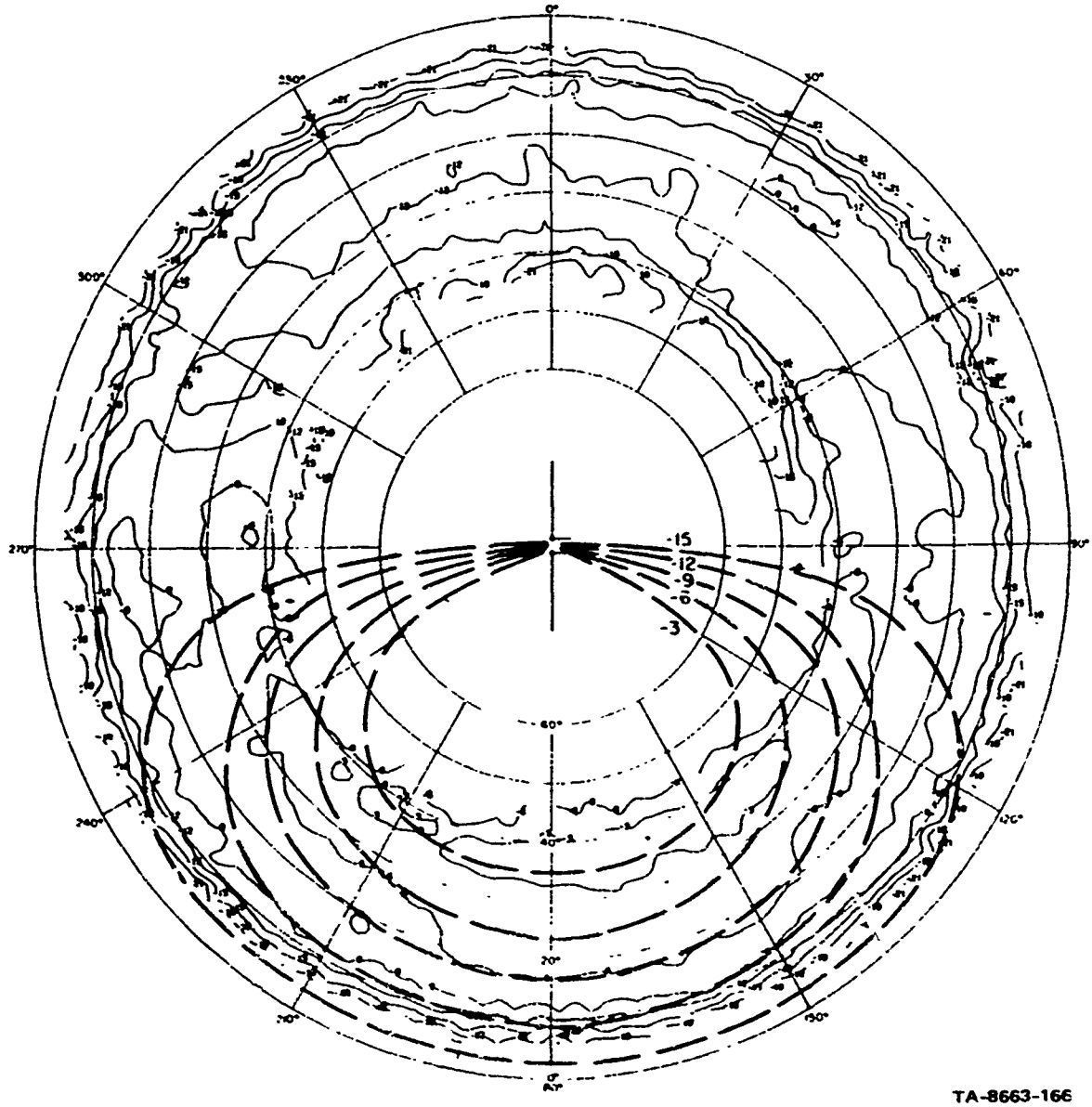

FIGURE C-11 CALCULATED AND MEASURED PATTERNS OF 6-MHz UNBALANCED DIPOLE IN CLEARING, E_θ AT 4 MHz

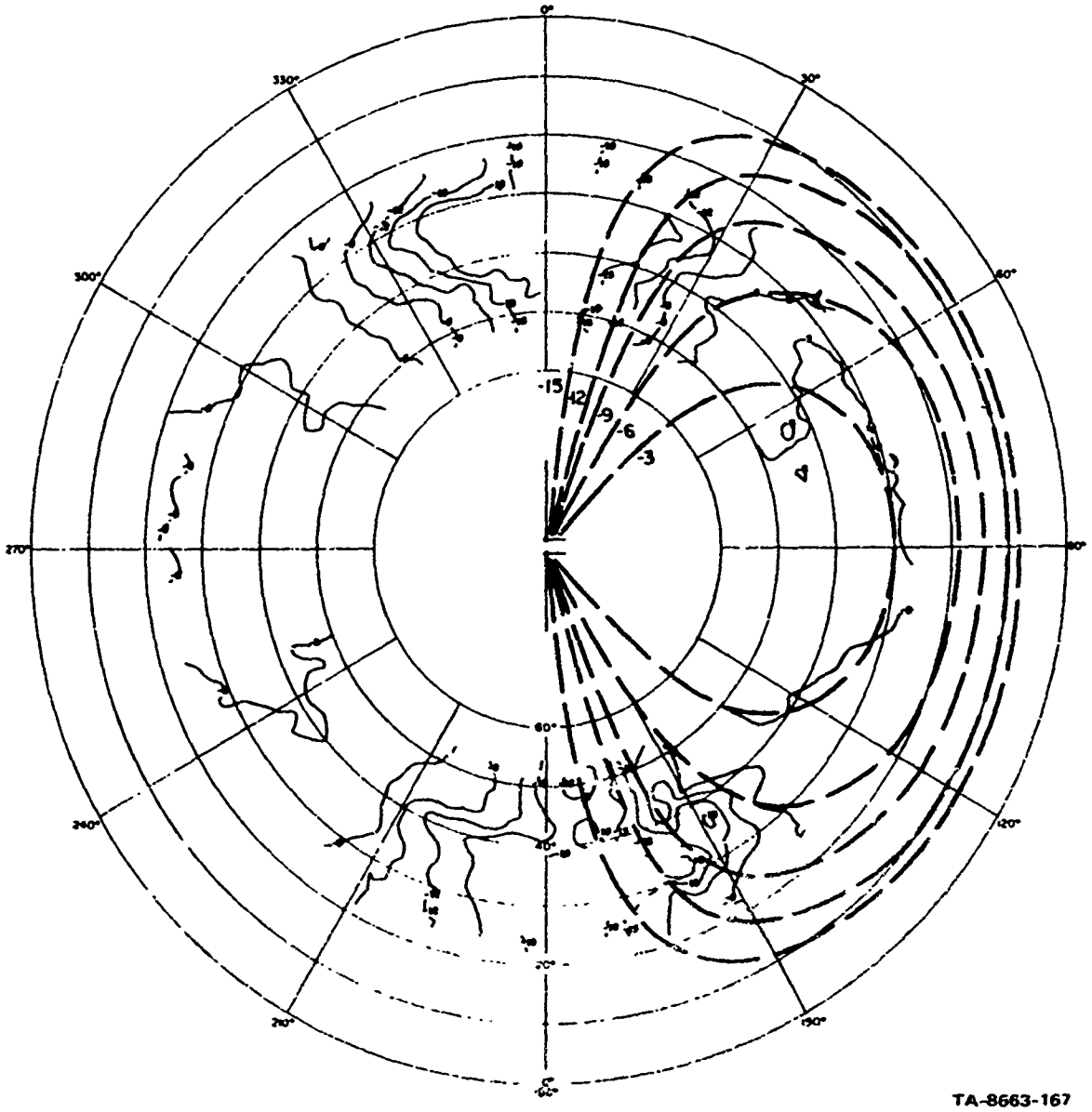

TA-8663-167

FIGURE C-12 CALCULATED AND MEASURED PATTERNS OF 6-MHz UNBALANCED DIPOLE IN CLEARING, E_ϕ AT 4 MHz

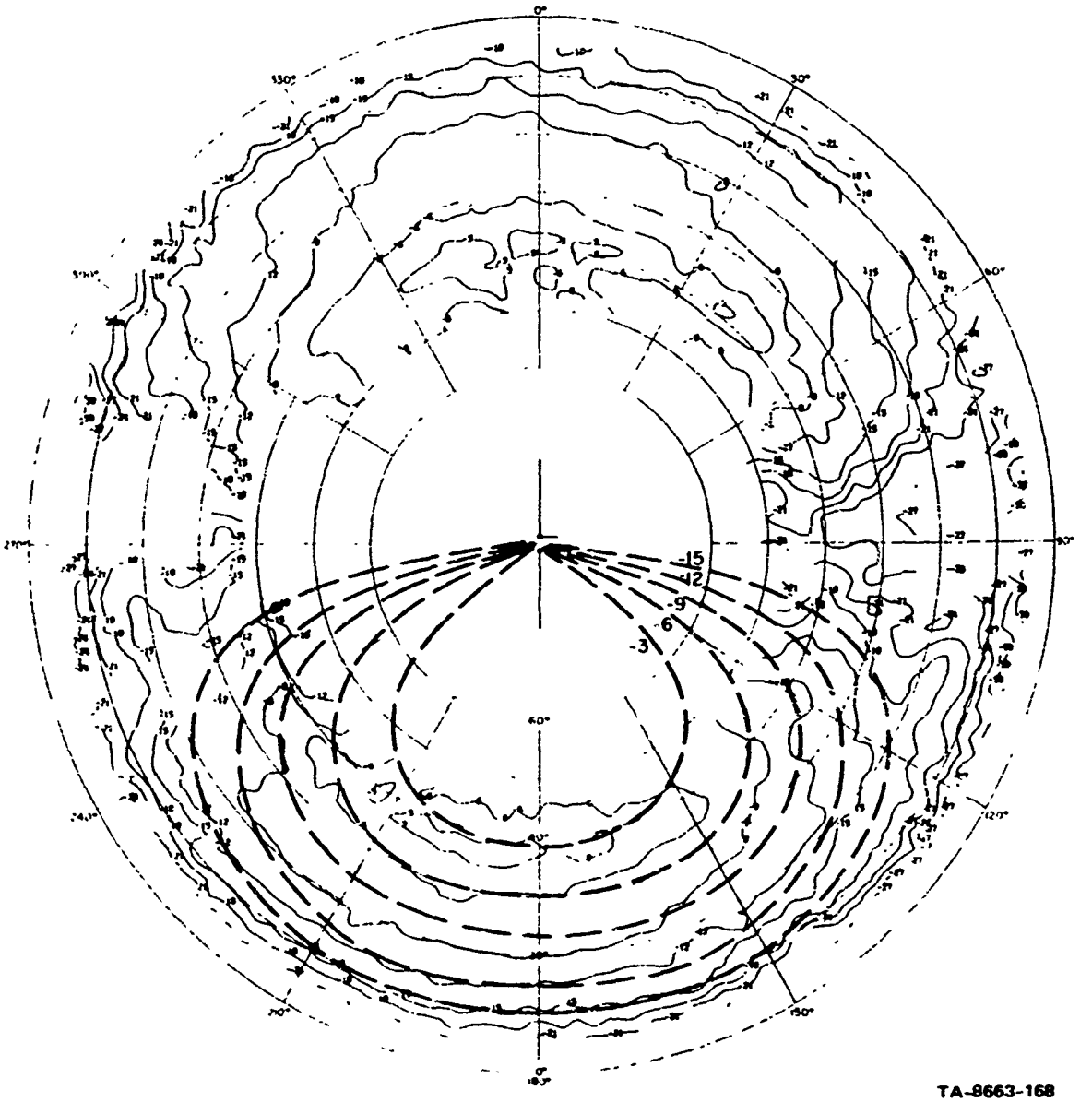

TA-8663-168

FIGURE C-13 CALCULATED AND MEASURED PATTERNS OF 6-MHz UNBALANCED DIPOLE IN CLEARING, E_θ AT 6 MHz

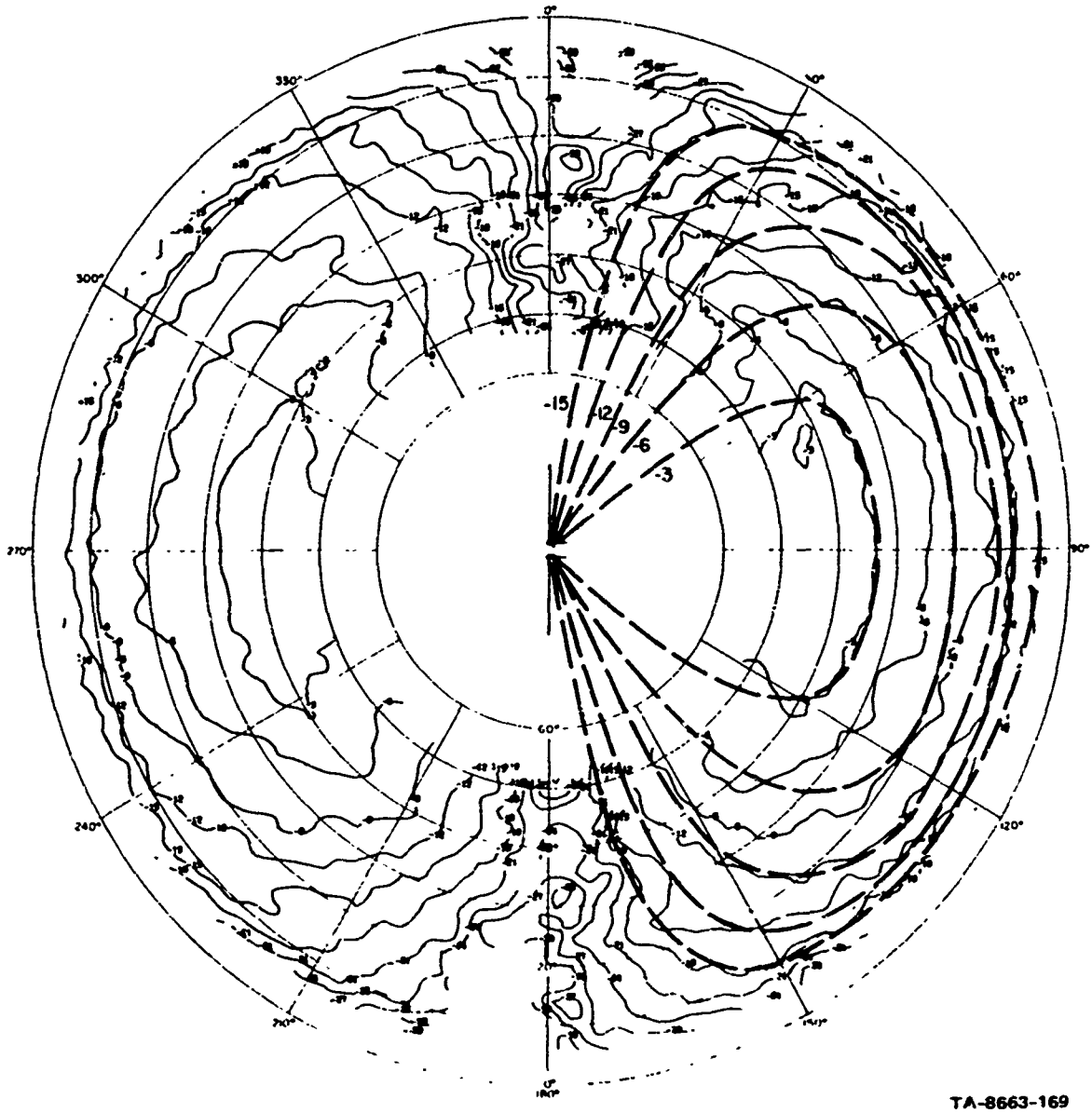

FIGURE C-14 CALCULATED AND MEASURED PATTERNS OF 6-MHz UNBALANCED DIPOLE IN CLEARING, E_ϕ AT 6 MHz

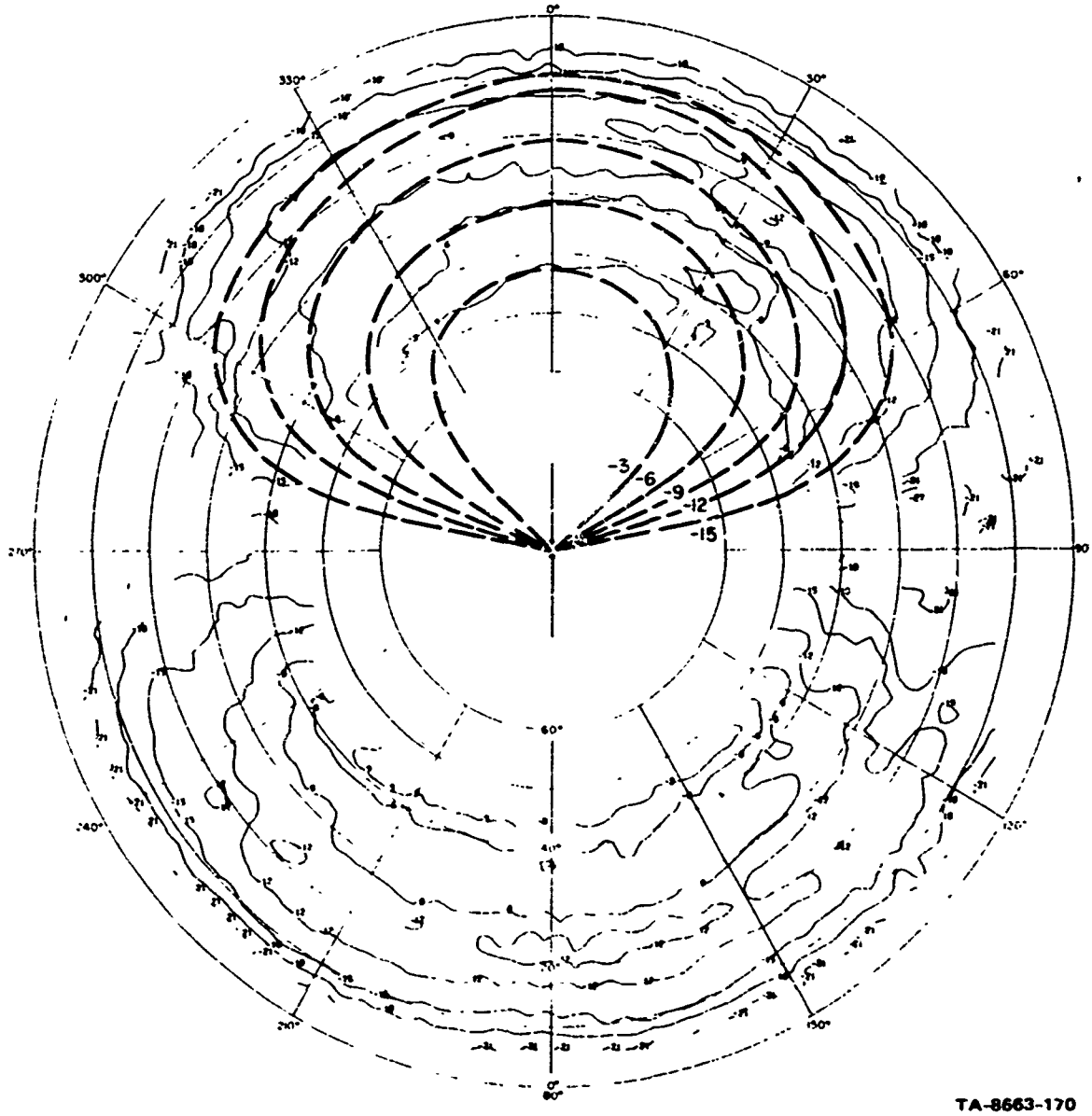

FIGURE C-15 CALCULATED AND MEASURED PATTERNS OF 6-MHz BALANCED DIPOLE IN FOREST, E_θ AT 6 MHz

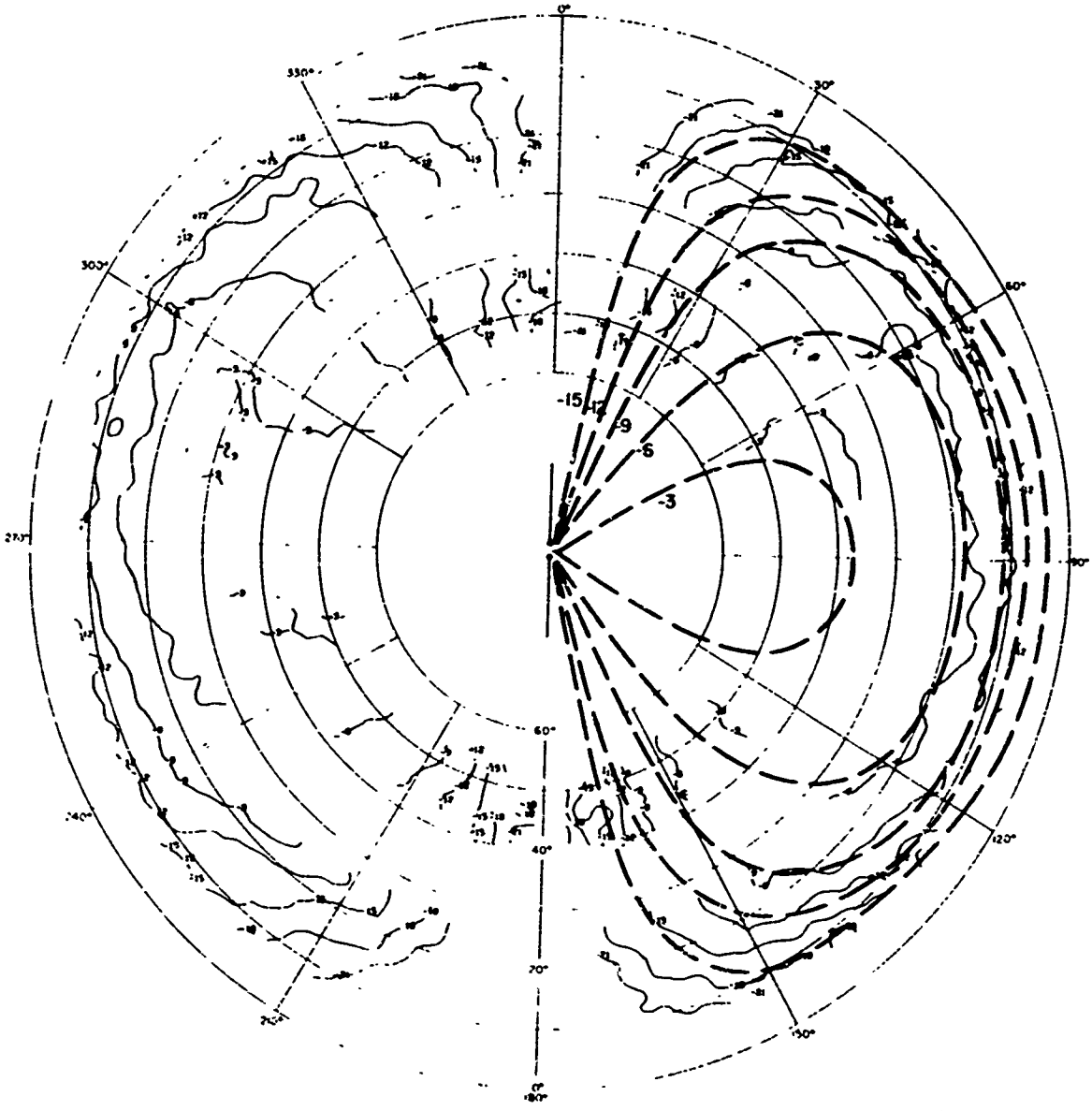

FIGURE C-16 CALCULATED AND MEASURED PATTERNS OF 6-MHz BALANCED DIPOLE IN FOREST, E_ϕ AT 6 MHz

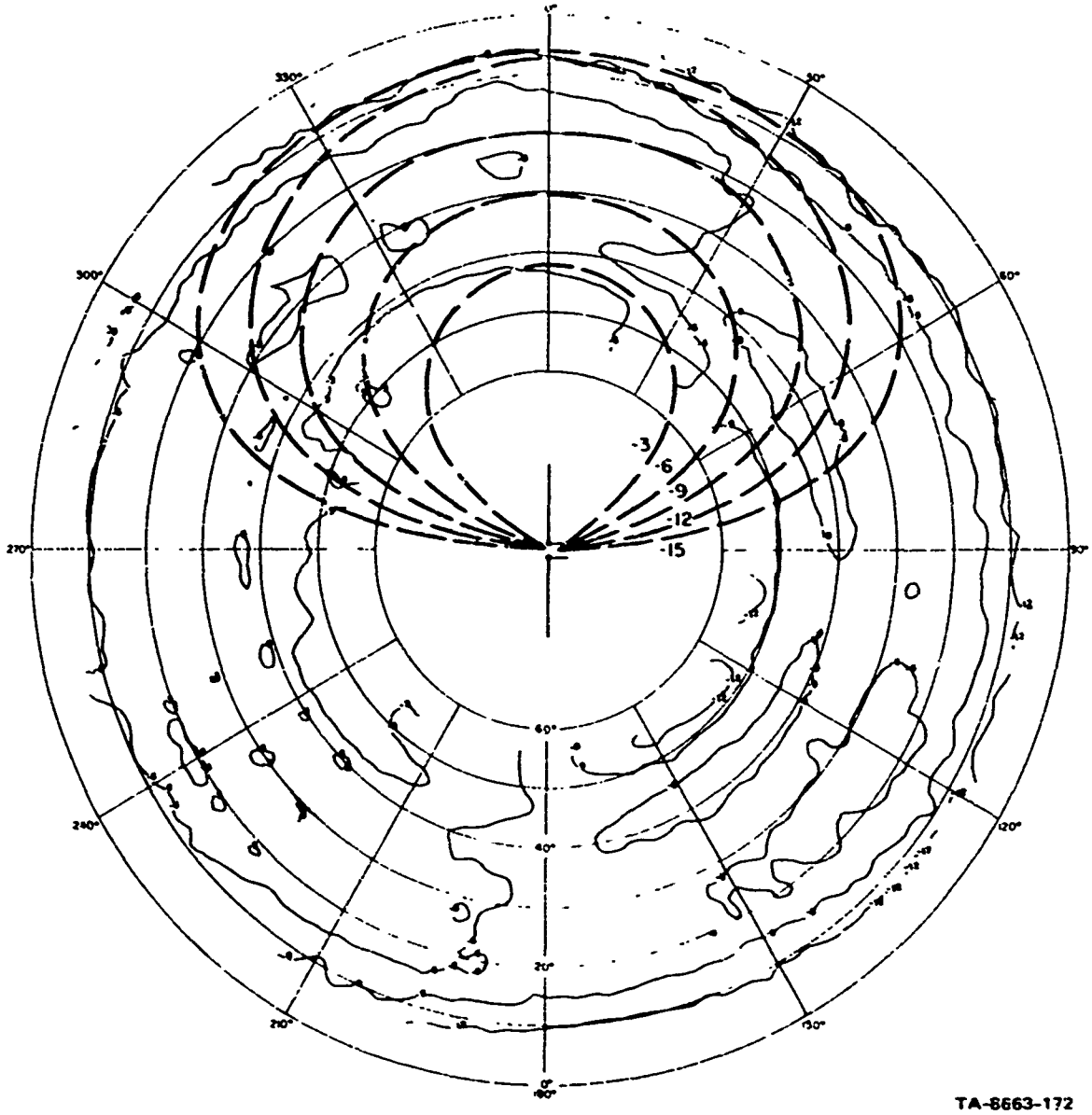

FIGURE C-17 CALCULATED AND MEASURED PATTERNS OF 6-MHz UNBALANCED DIPOLE IN FOREST, E_θ AT 3 MHz

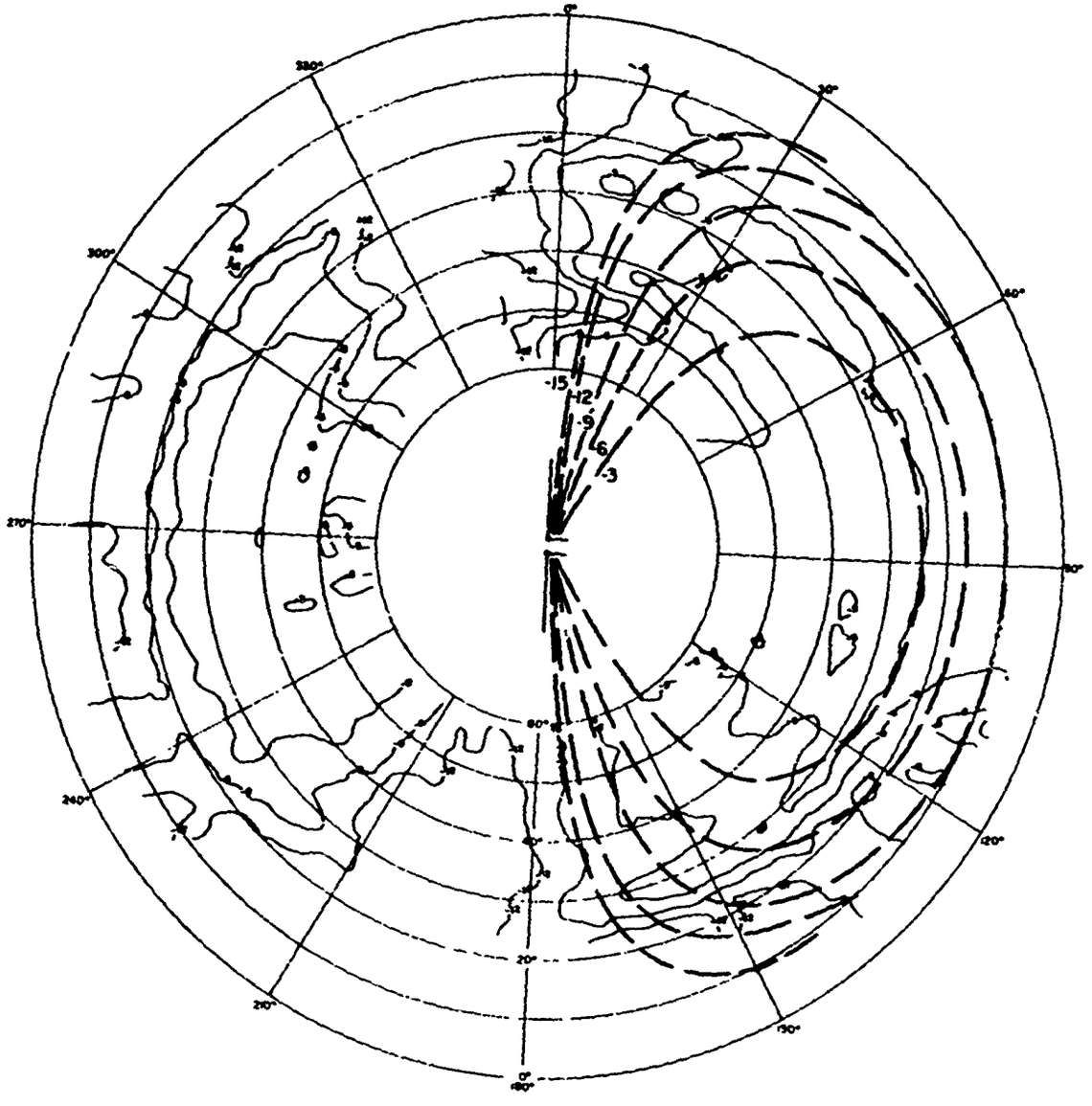

TA-8663-173

FIGURE C-18 CALCULATED AND MEASURED PATTERNS OF 6-MHz UNBALANCED DIPOLE IN FOREST, E_ϕ AT 3 MHz

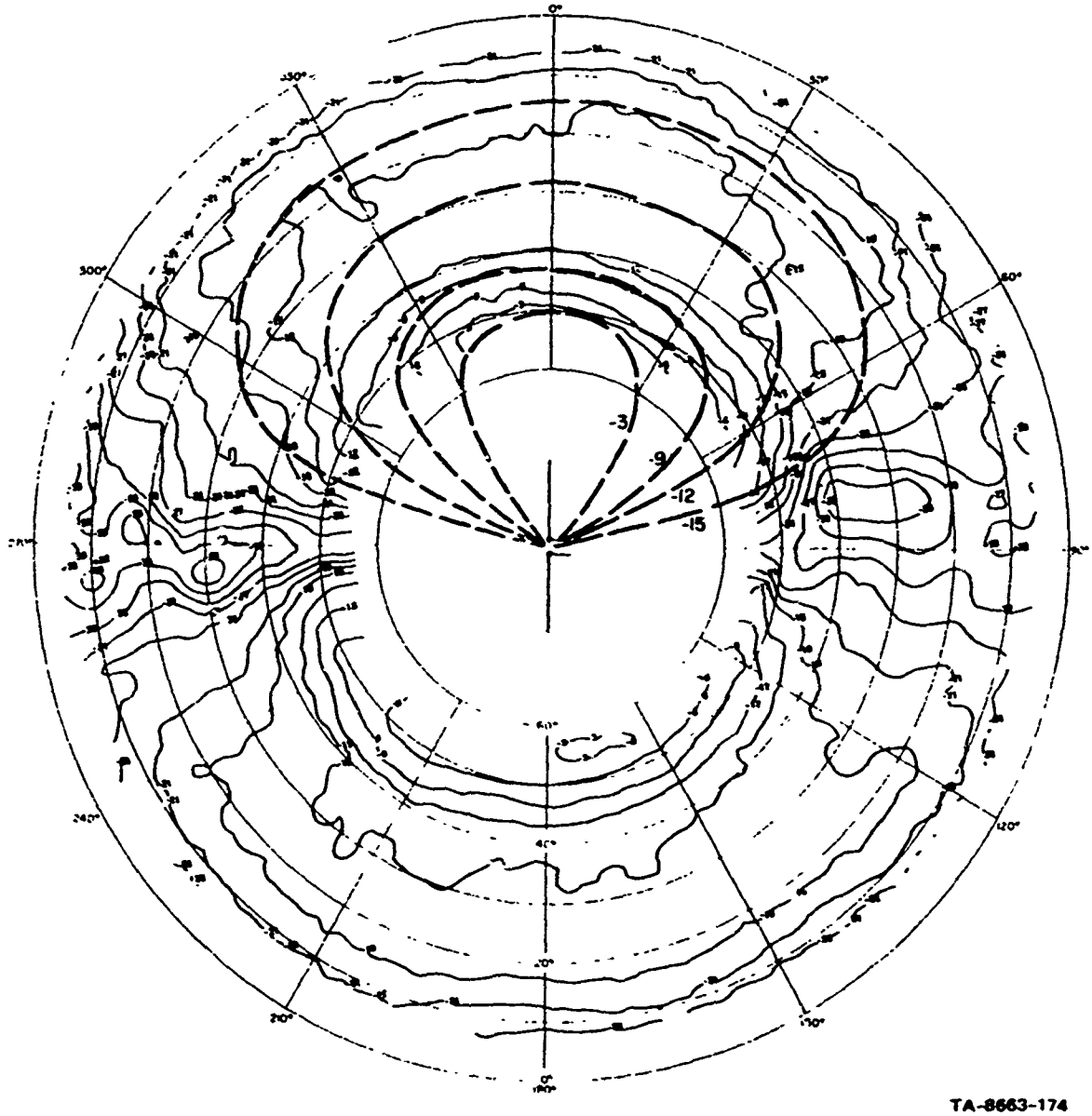

TA-8663-174

FIGURE C-19 CALCULATED AND MEASURED PATTERNS OF 6-MHz UNBALANCED DIPOLE IN FOREST, E_θ AT 6 MHz

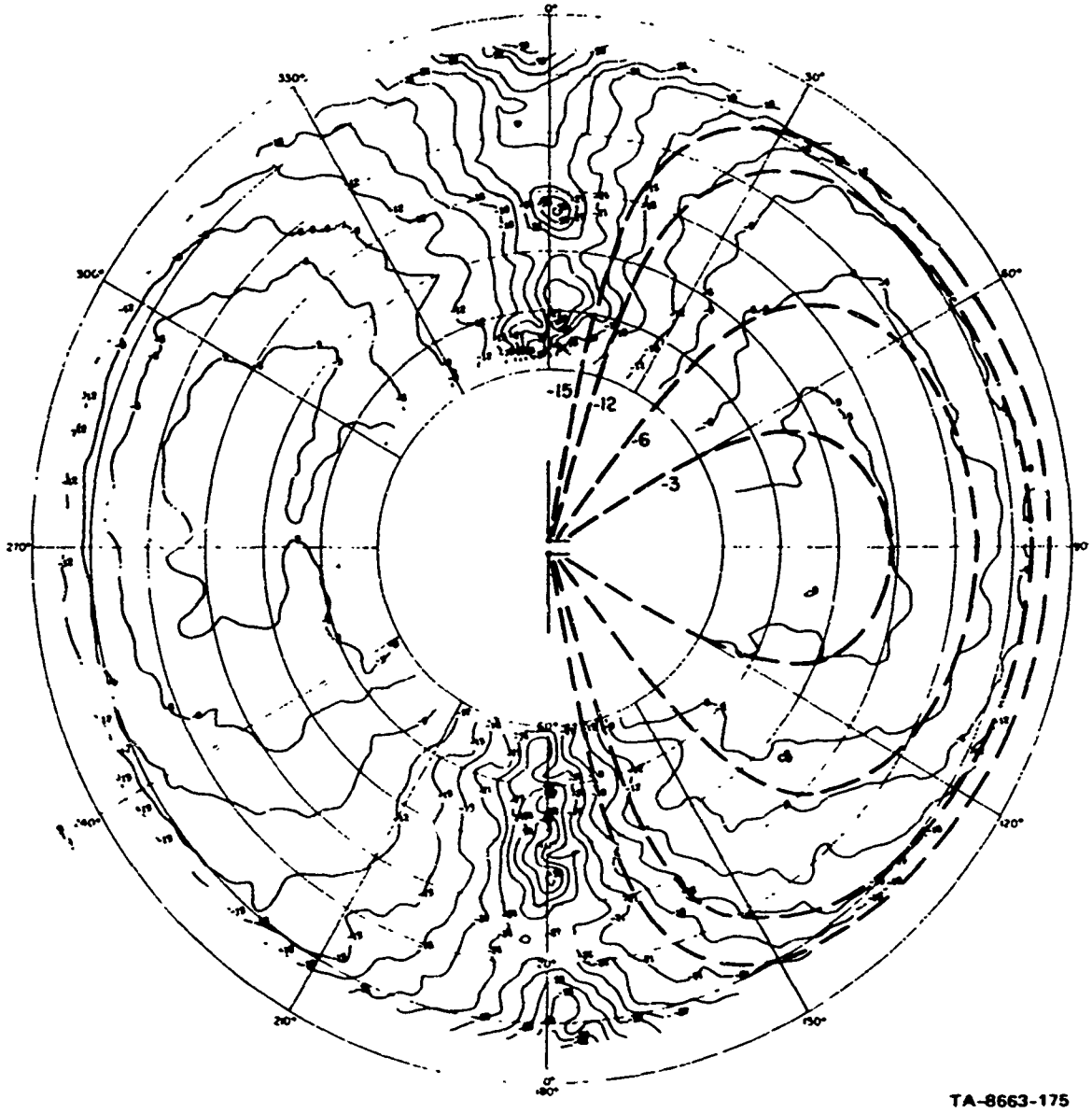

FIGURE C-20 CALCULATED AND MEASURED PATTERNS OF 6-MHz UNBALANCED DIPOLE IN FOREST, E_ϕ AT 6 MHz

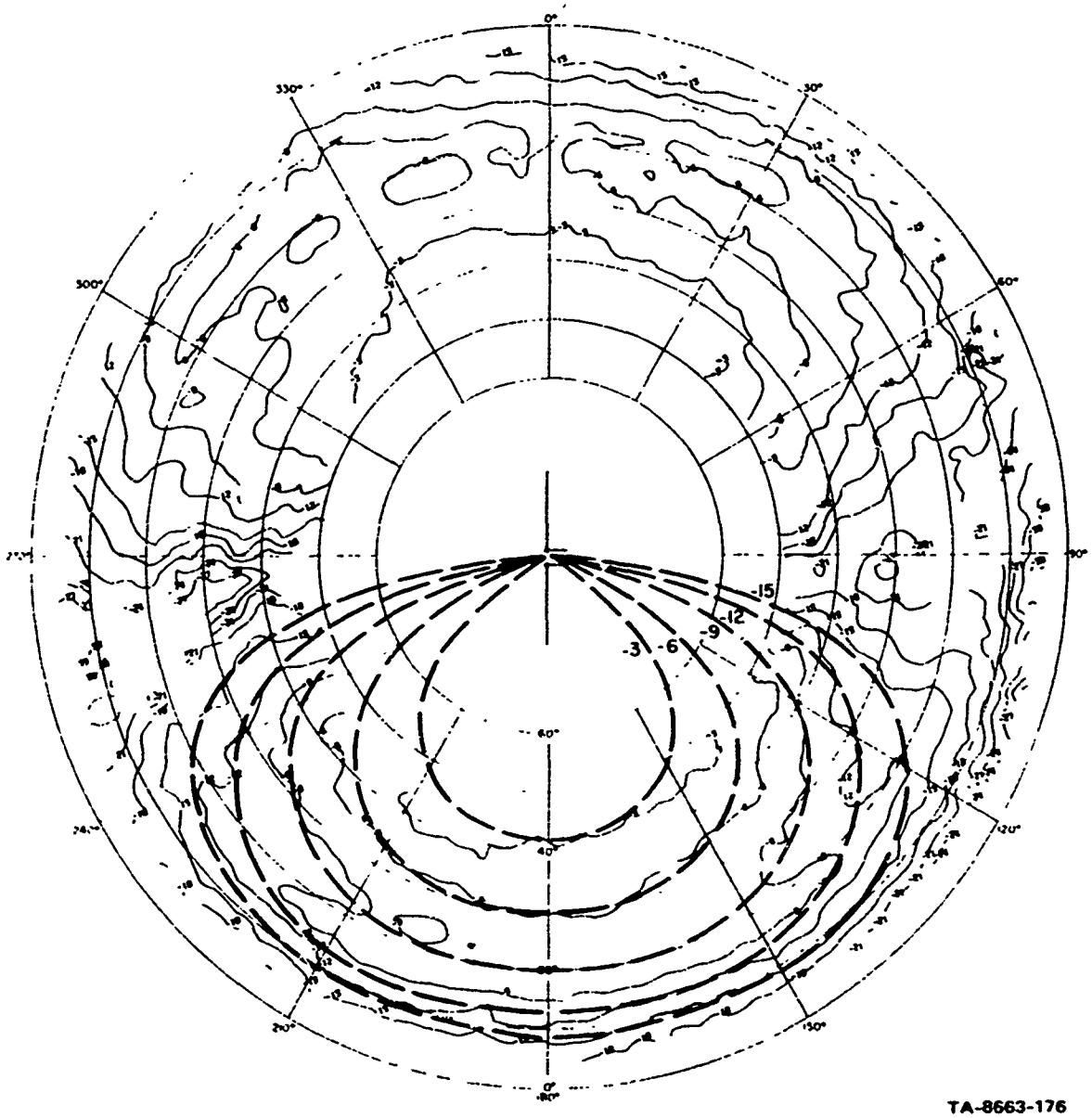

TA-8663-176

FIGURE C-21 CALCULATED AND MEASURED PATTERNS OF 16-FOOT-HIGH, 6-MHz UNBALANCED DIPOLE IN FOREST, E_θ AT 6 MHz

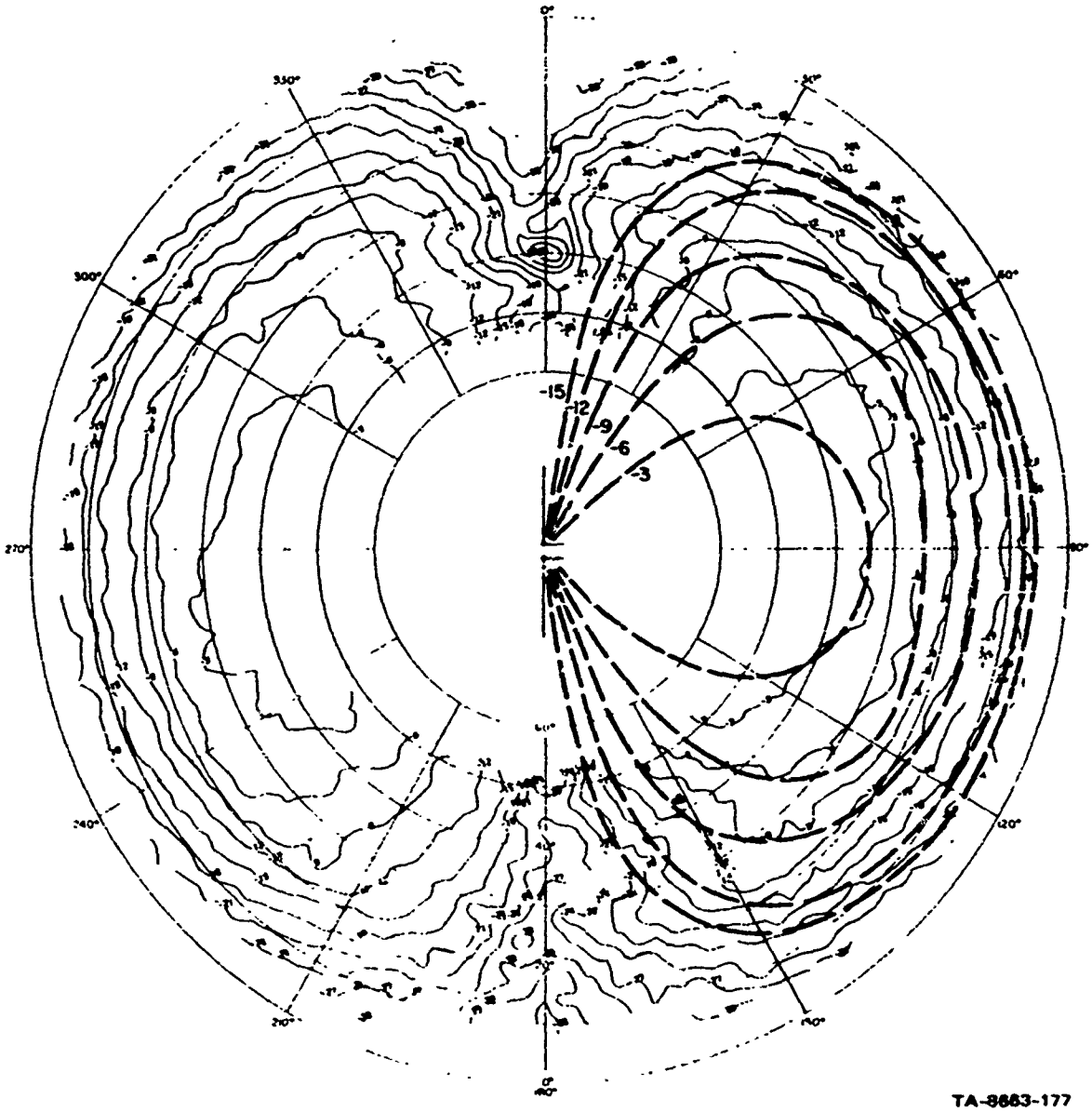

TA-8883-177

FIGURE C-22 CALCULATED AND MEASURED PATTERNS OF 16-FOOT-HIGH, 6-MHz UNBALANCED DIPOLE IN FOREST, E_ϕ AT 6 MHz

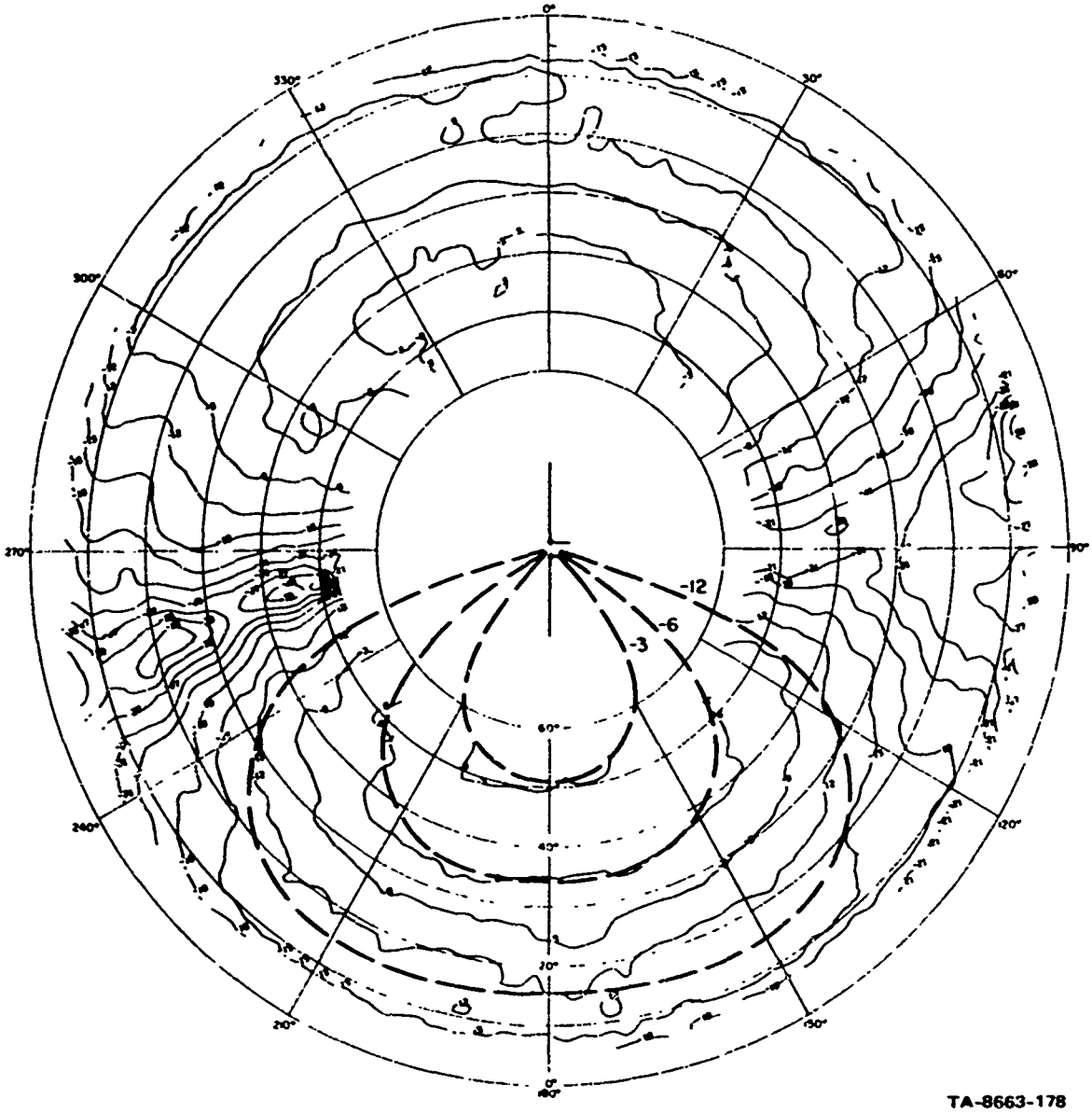

FIGURE C-23 CALCULATED AND MEASURED PATTERNS OF 8-FOOT-HIGH 6-MHz UNBALANCED DIPOLE IN FOREST, E_θ AT 6 MHz

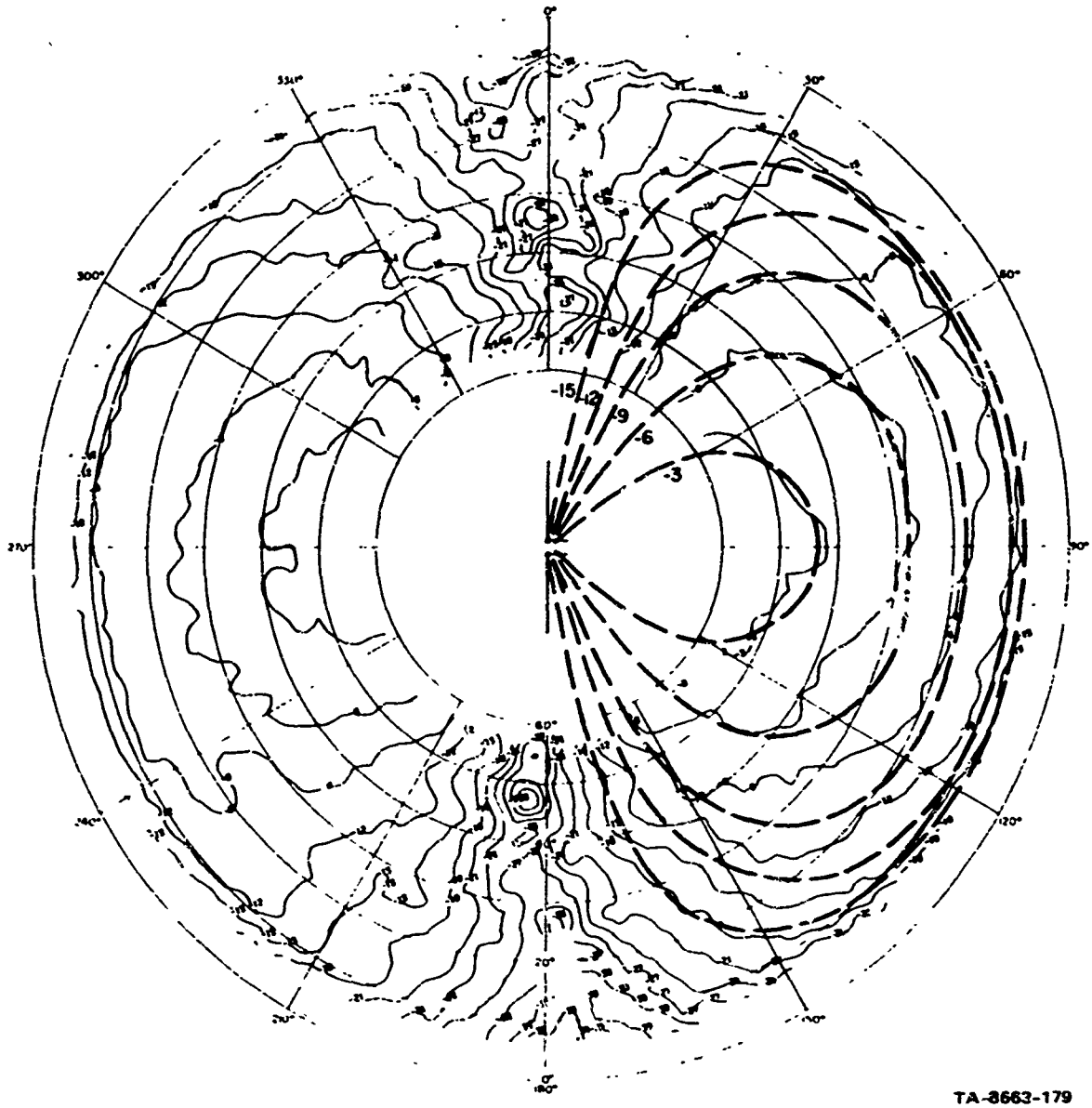

FIGURE C-24 CALCULATED AND MEASURED PATTERNS OF 8-FOOT-HIGH, 6-MHz UNBALANCED DIPOLE IN FOREST, E_ϕ AT 6 MHz

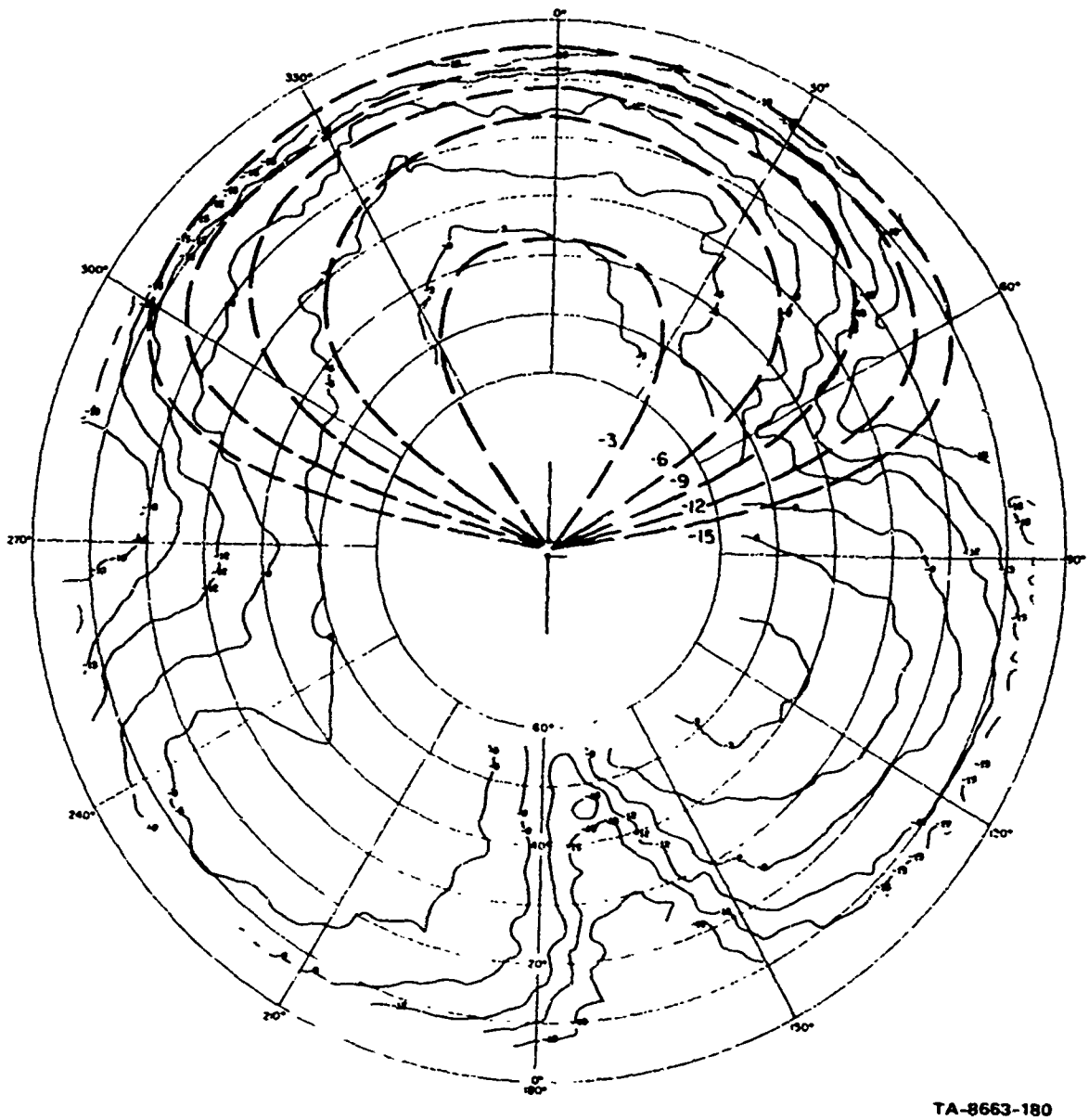

TA-8663-180

FIGURE C-25 CALCULATED AND MEASURED PATTERNS OF 2-FOOT-HIGH, 6-MHz UNBALANCED DIPOLE IN FOREST, E_θ AT 4 MHz

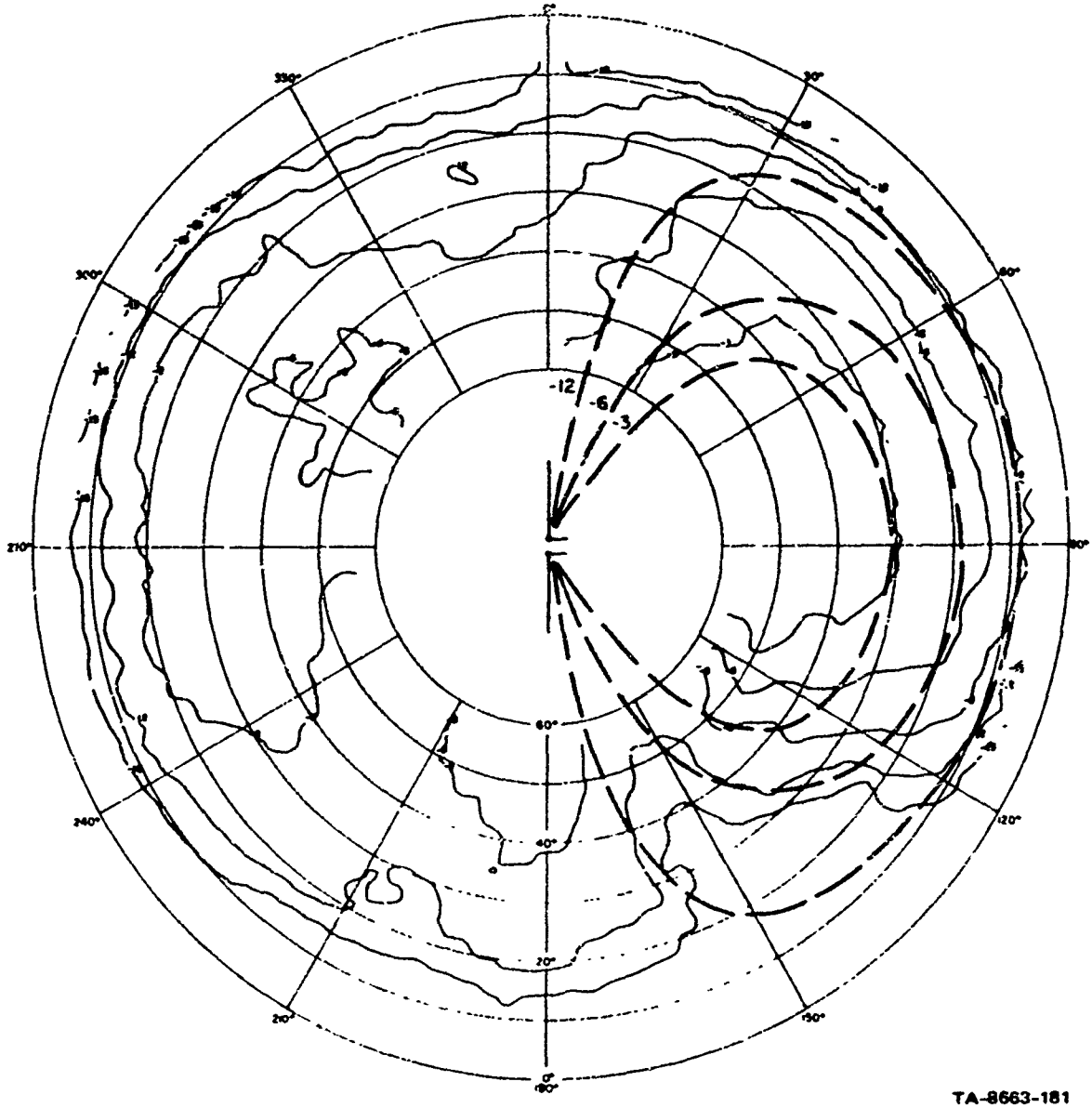

FIGURE C-26 CALCULATED AND MEASURED PATTERNS OF 2-FOOT-HIGH, 6-MHz UNBALANCED DIPOLE IN FOREST, E_ϕ AT 4 MHz

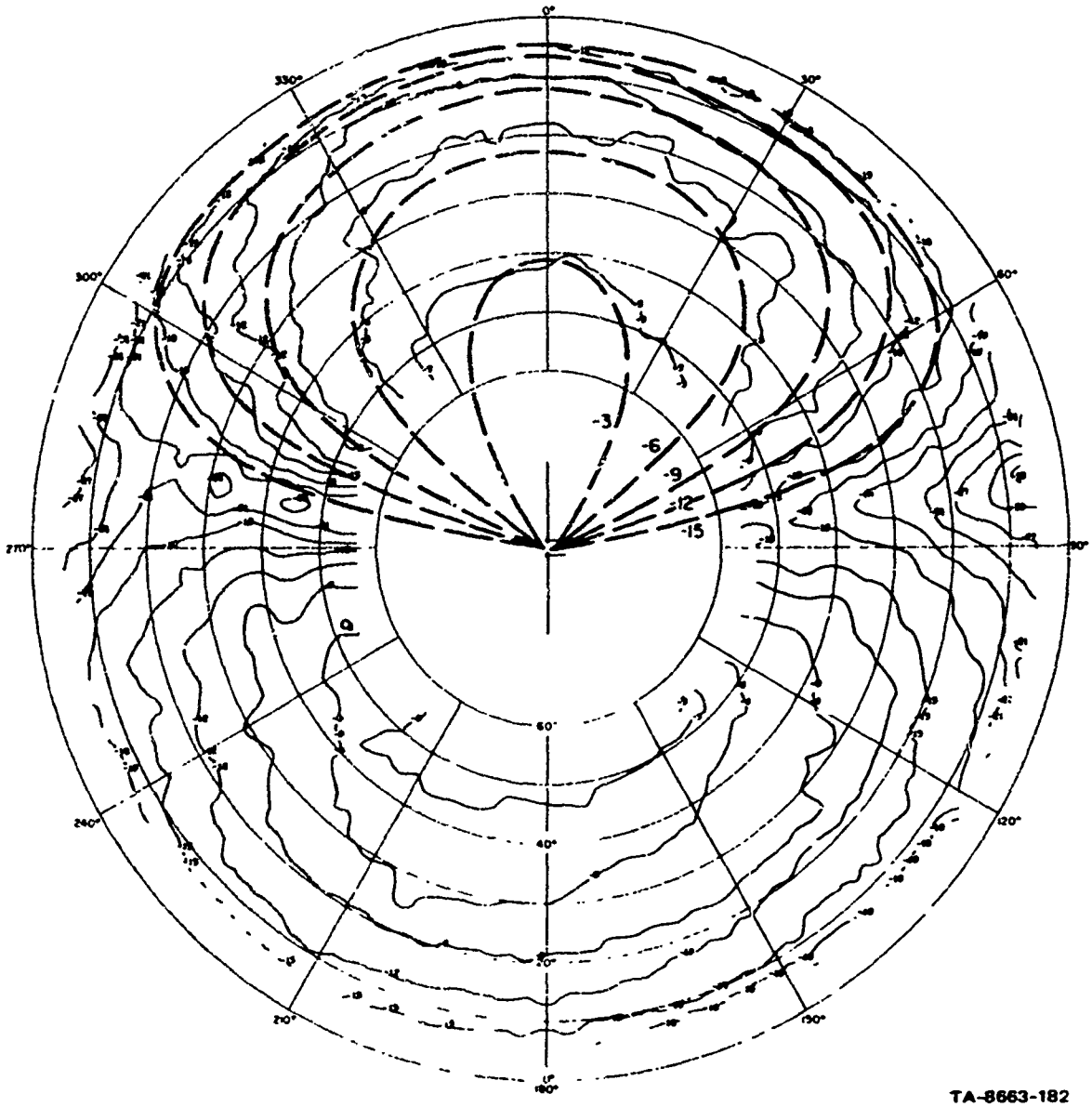

FIGURE C-27 CALCULATED AND MEASURED PATTERNS OF 2-FOOT-HIGH, 6-MHz UNBALANCED DIPOLE IN FOREST, E_θ AT 6 MHz

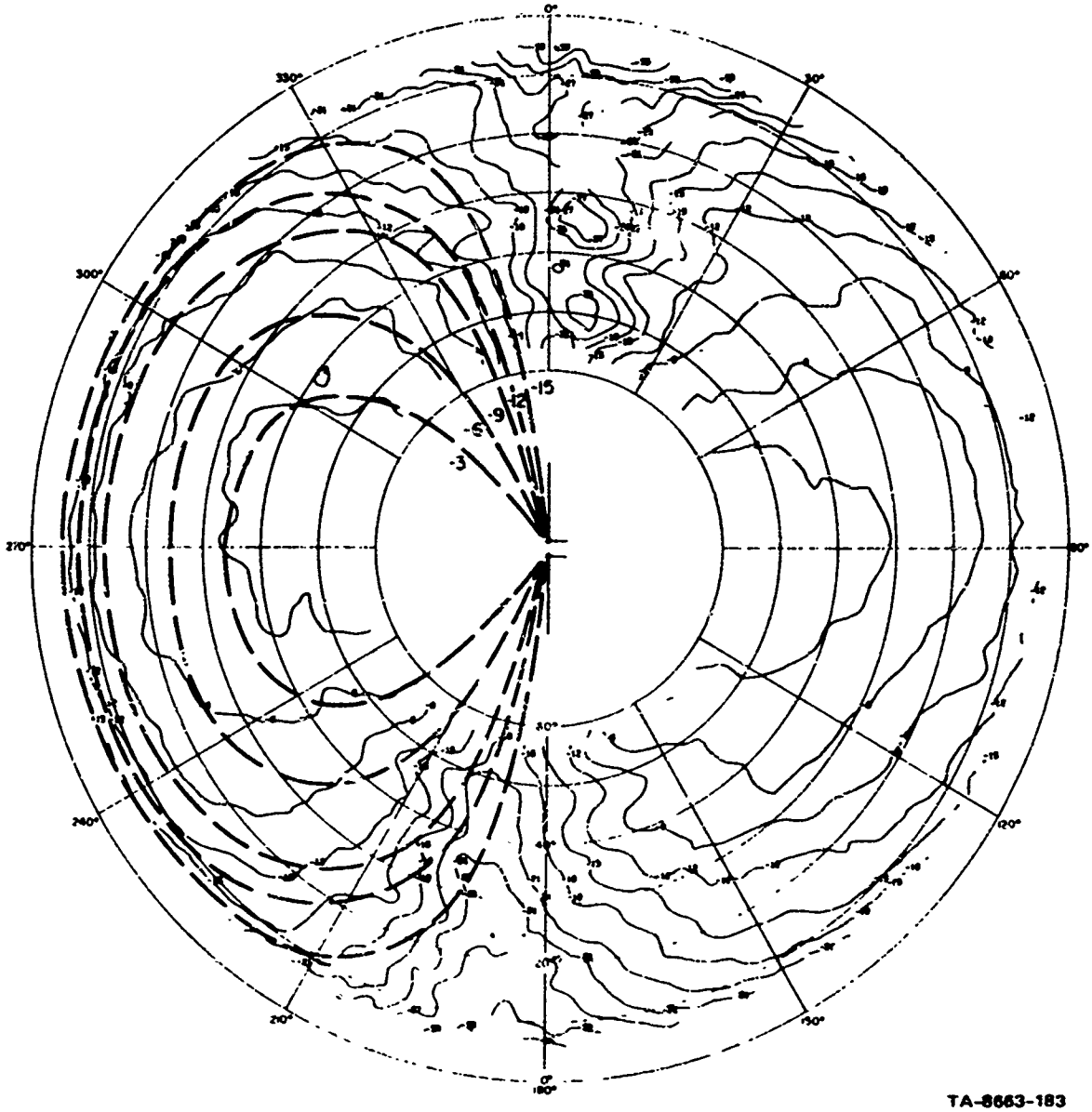

FIGURE C-28 CALCULATED AND MEASURED PATTERNS OF 2-FOOT-HIGH, 6-MHz UNBALANCED DIPOLE IN FOREST, E_ϕ AT 6 MHz

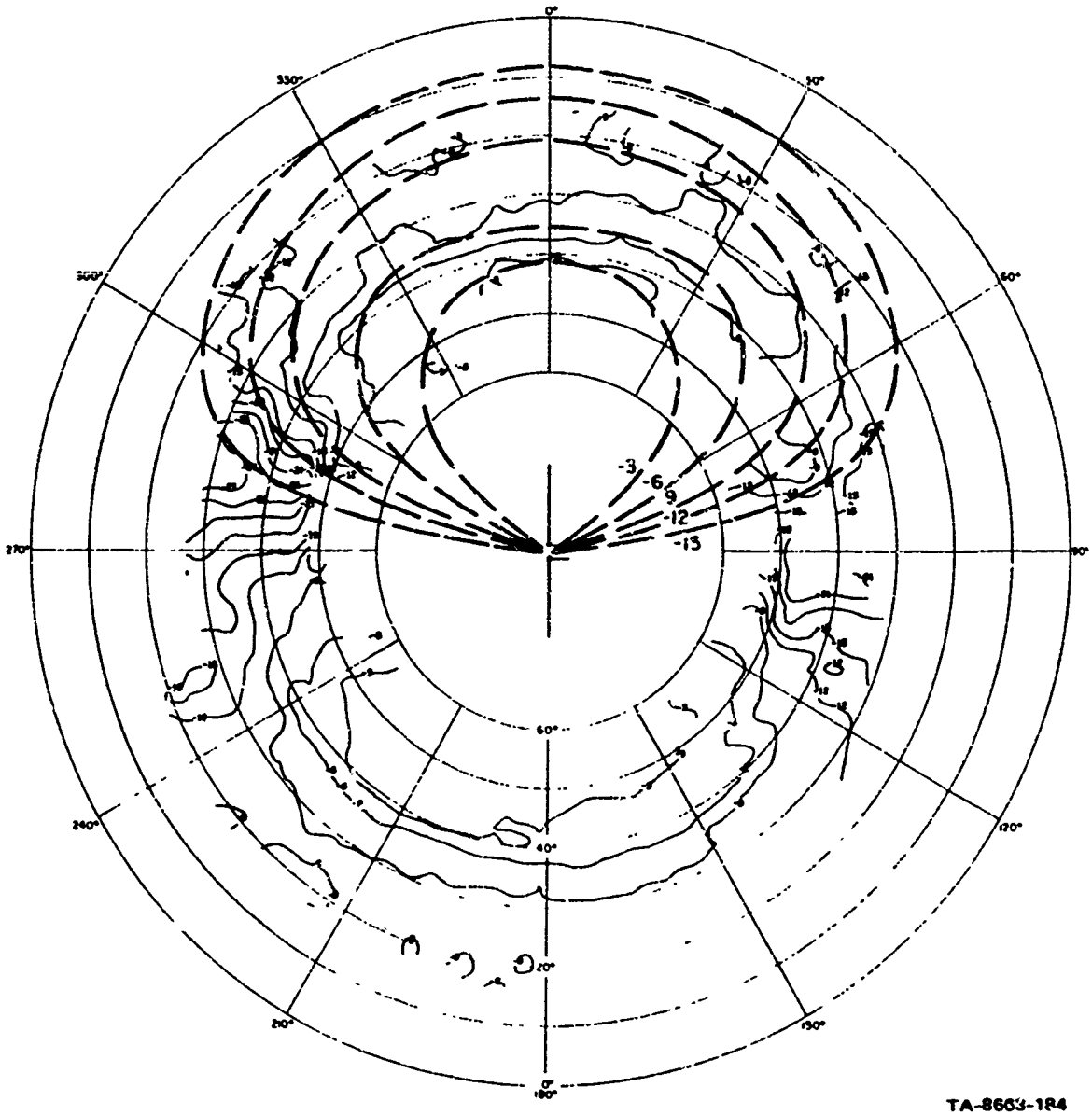

FIGURE C-29 CALCULATED AND MEASURED PATTERNS OF 23-FOOT-HIGH, 8-MHz UNBALANCED DIPOLE IN FOREST, E_θ AT 8 MHz

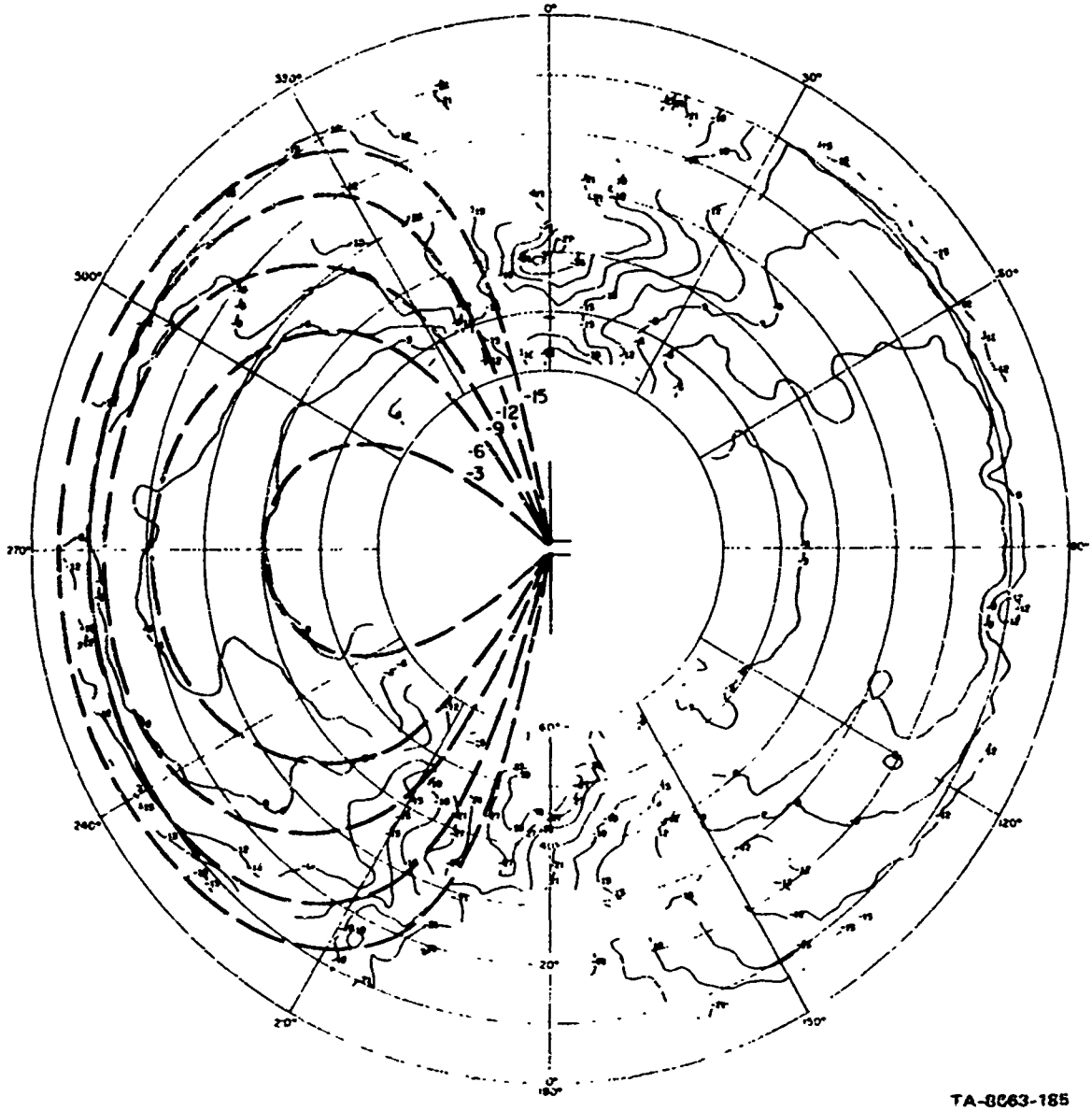

TA-8063-185

FIGURE C-30 CALCULATED AND MEASURED PATTERNS OF 23-FOOT-HIGH, 8-MHz UNBALANCED DIPOLE IN FOREST, E_ϕ AT 8 MHz

REFERENCES

1. J. Taylor, K. A. Posey, and G. H. Hagn, "Literature Survey Pertaining to Electrically Small Antennas, Propagation Through Vegetation, and Related Topics," Special Technical Report 17, Contract DA 36-039 AMC-00040(E), SRI Project 4240, Stanford Research Institute, Menlo Park, California (January 1966), AD-629 155.

2. W. A. Ray, "Full-Scale Pattern Measurement of Simple HF Field Antennas," Special Technical Report 10, Contract DA 36-039 AMC-00040(E), SRI Project 4240, Stanford Research Institute, Menlo Park, California (May 1966), AD-487 494.

3. W. A. Ray, G. E. Barker, and S. S. Martensen, "Full-Scale Pattern Measurements of Simple HF Field Antennas in a U.S. Conifer Forest," Special Technical Report 25, Contract DA 36-039 AMC-00040(E), SRI Project 4240, Stanford Research Institute, Menlo Park, California (February 1967), AD-653 185.

4. G. E. Barker and G. D. Koehrsen, "Full-Scale Pattern Measurements of Simple HF Antennas in a Tropical Forest in Thailand," Special Technical Report 35, Contract DA 36-039 AMC-00040(E), SRI Project 4240, Stanford Research Institute, Menlo Park, California (February 1968).

5. G. E. Barker and G. D. Koehrsen, "Full-Scale Pattern Measurements of Simple HF Field Antennas in Rough Terrain," Final Report--Volume I, Contract DAHC07-67-C-0144, SRI Project 6531, Stanford Research Institute, Menlo Park, California (January 1968).

6. J. Taylor, "A Note on the Computed Radiation Patterns of Dipole Antennas in Dense Vegetation," Special Technical Report 15, Contract DA 36-039 AMC-00049(E), SRI Project 4240, Stanford Research Institute, Menlo Park, California (February 1966), AD-487 495.

7. H. W. Parker and G. H. Hagn, "Feasibility Study of the Use of Open-Wire Transmission Lines, Capacitors, and Cavities to Measure the Electrical Properties of Vegetation," Special Technical Report 13, Contract DA 36-039 AMC-00040(E), SRI Project 4240, Stanford Research Institute, Menlo Park, California (August 1966), AD-489 294.

8. J. Taylor, Ching Chun Han, Chung Lien Tien, and G. Hagn, "Open-Wire Transmission Lines Applied to the Measurement of the Macroscopic Electrical Properties of a Forest Region," Special Technical Report 42, Contract DA 36-039 AMC-00040(E), SRI Project 4240, Stanford Research Institute, Menlo Park, California (August 1968).

9. H. W. Parker and W. Makarabhiromya, "Electric Constants Measured in Vegetation and in Earth at Five Sites in Thailand," Special Technical Report 43, Contract DA 36-039 AMC-00040(E), SRI Project 4240, Stanford Research Institute, Menlo Park, California (December 1967).

10. S. Pongpangan and D. V. Vanek, "Environmental Description of Stanford Research Institute Test Site at Ban Mun Chit, Thailand," Joint Thai-U.S. Military Research and Development Center, Bangkok, Thailand (in preparation).

11. Termpoon Kovattana, "Electrical Ground Constants of Central, Eastern, and Northeastern Thailand," Special Technical Report 29, Contract DA 36-039 AMC-00040(E), SRI Project 4240, Stanford Research Institute, Menlo Park, California (February 1967), AD-661 058.

12. N. E. Goldstein, H. W. Parker, and G. H. Hagn, "Three Techniques for Measurement of Ground Constants in the Presence of Vegetation," Special Technical Report 30, Contract DA 36-039 AMC-00040(E), SRI Project 4240, Stanford Research Institute, Menlo Park, California (March 1967), AD-672 496.

13. G. H. Hagn, E. L. Younker, and H. W. Parker, "Research-Engineering and Support for Tropical Communications," Semiannual Report 6, Covering the Period 1 October 1965 through 31 March 1966, Contract DA 36-039 AMC-00040(E), SRI Project 4240, Stanford Research Institute, Menlo Park, California (June 1966), AD-653 608.

14. E. L. Younker, G. H. Hagn, and H. W. Parker, "Research-Engineering and Support for Tropical Communications," Semiannual Report 7, Covering the Period 1 April through 30 September 1966, Contract DA 36-039 AMC-00040(E), SRI Project 4240, Stanford Research Institute, Menlo Park, California (September 1966), AD-653 615.

15. E. L. Younker, G. H. Hagn, and H. W. Parker, "Research-Engineering and Support for Tropical Communications," Semiannual Report 8, Covering the Period 1 October 1966 through 31 March 1967, Contract DA 36-039 AMC-00040(E), SRI Project 4240, Stanford Research Institute, Menlo Park, California (May 1967).

16. C. Barnes, "Xeledop Antenna Pattern Measuring Equipment, 2 to 50 Mc," Stanford Research Institute, Menlo Park, California (July 1965).

17. C. Barnes, "Transmitters Towed through Air Test Antenna's Radiation Pattern," Electronics, pp. 96-101 (October 18, 1965).

18. E. C. Hayden, "Radiolocation Systems," in Electromagnetics and Antennas, P. E. Mayes, Project Director, pp. 444-483 (University of Illinois, Urbana, Illinois, 1967).

19. G. H. Hagn, "Orientation of Linearly Polarized HF Antennas for Short-Path Communication via the Ionosphere near the Geomagnetic Equator," Research Memorandum 5 (Revised), Contract DA 36-039 AMC-00040(E), SRI Project 4240, Stanford Research Institute, Menlo Park, California (June 1964), AD-480 592.

20. G. H. Hagn, "Absorption of Ionospherically Propagated HF Radio Waves under Conditions where the Quasi-Transverse (QT) Approximation is Valid," Special Technical Report 9, Contract DA 36-039 AMC-00040 (E), SRI Project 4240, Stanford Research Institute, Menlo Park, California (September 1964), AD-480-588.

21. Lt. Cdr. Paibul Nacaskul, R.T.N., "Orientation Measurements in Thailand with HF Dipole Antennas for Tactical Communications," Special Technical Report 31, Contract DA 36-039 AMC-00040(E), SRI Project 4240, Stanford Research Institute, Menlo Park, California (June 1967).

22. D. J. Barnes, G. E. Barker, and G. H. Hagn, "Measured Impedances of Simple Field-Expedient Antennas in Open and Forested Terrain," Special Technical Report 6, Contract DA 36-039 AMC-00040(E), SRI Project 4240, Stanford Research Institute, Menlo Park, California (in preparation).

23. L. G. Sturgill and Staff, "Tropical Propagation Research," Final Report, Volume I, Contract DA 36-039 SC-90889, J&B Program 2860, Jansky and Bailey Engineering Department, Alexandria, Virginia (June 1966).

24. G. E. Barker and W. A. Hall, "Pattern Measurement and Modeling of Full-Scale VHF Antennas in a Thailand Tropical Forest," Special Technical Report 39, Contract DA 36-039 AMC-00040(E), SRI Project 4240, Stanford Research Institute, Menlo Park, California (in preparation).

25. G. E. Hagn and D. J. Barnes, "Sounder Measurements of the Relative Gain of HF Field-Expedient Antennas on Short Ground and Skywave Paths in Thailand," Special Technical Report 38, Contract DA 36-039 AMC-00040(E), SRI Project 4240, Stanford Research Institute, Menlo Park, California (in preparation).

26. S. A. Schelkunoff and H. T. Friis, Antennas, Theory and Practice, p. 301 (John Wiley and Sons, Inc., New York, 1952).

27. G. H. Hagn, H. W. Parker, and E. L. Younker, "Research-Engineering and Support for Tropical Communications," Semiannual Report 5, Covering the Period 1 April through 30 September 1965, Contract DA 36-039 AMC-00040(E), SRI Project 4240, Stanford Research Institute, Menlo Park, California (May 1966), AD-486 466.

28. G. H. Hagn, J. E. van der Laan, D. J. Lyons, and E. M. Kreinberg, "Ionospheric Sounder Measurement of Relative Gains and Bandwidths of Selected Field-Expedient Antennas for Skywave Propagation at Near-Vertical Incidence," Special Technical Report 18, Contract DA 36-039 AMC-00040(E), SRI Project 4240, Stanford Research Institute, Menlo Park, California (January 1966), AD-489 537.

29. F. E. Terman, Radio Engineer's Handbook, p. 791 (McGraw Hill Book Company, New York, New York, 1943).

30. F. E. Terman, Electronic and Radio Engineering, p. 808 (McGraw Hill Book Company, New York, New York, 1955.

31. G. H. Hagn, D. J. Barnes, J. W. Chapman, J. E. van der Laan, D. J. Lyons, and J. P. Muro, "Field Test of AN/GRA-93( ) HF Antenna Kit for Short-Path Skywave Communication in Thailand Forest Environment," Final Report II, Contract DA 28-043 AMC-02201(E), SRI Project 6183, Stanford Research Institute, Menlo Park, California (August 1967).